UNIVERSIDADE DE LISBOA
FACULDADE DE CIÊNCIAS

Sedimentary dynamics on the southern insular shelf of Madeira Island: insights from geophysical and sediment sampling data

" Documento Definitivo"

Doutoramento em Geologia

Geodinâmica Externa

Viviana Belvisi

Tese orientada por:

José Eduardo De Oliveira Madeira
Rui Manuel do Amaral Branco de Oliveira Quartau
Claudia Romagnoli

Documento especialmente elaborado para a obtenção do grau de doutor

2024

UNIVERSIDADE DE LISBOA

FACULDADE DE CIÊNCIAS

Sedimentary dynamics on the southern insular shelf of Madeira Island: insights from geophysical and sediment sampling data

Doutoramento em Geologia

Geodinâmica Externa

Viviana Belvisi

Tese orientada por:

José Eduardo De Oliveira Madeira

Rui Manuel do Amaral Branco de Oliveira Quartau

Claudia Romagnoli

Júri:

Presidente:

- Ana Cristina Costa Neves Dos Santos Azerêdo, Professora Catedrática e Presidente do Departamento de Geologia da Faculdade de Ciências da Universidade de Lisboa,

Vogais:

- Doutor Neil Charles Mitchell, Reader, School of Natural Sciences da University of Manchester;
- Doutor Óscar Manuel Fernandes Cerveira Ferreira, Professor Associado com Agregação, Faculdade de Ciências e Tecnologia da Universidade do Algarve;
- Doutor Rui Manuel do Amaral Branco de Oliveira Quartau, Investigador Auxiliar, Instituto Hidrográfico (orientador);
- Doutor Ana Maria Almeida Nobre Silva, Investigadora FCT nível Júnior, Faculdade de Ciências da Universidade de Lisboa.

Documento especialmente elaborado para a obtenção do grau de doutor

Financiada pela Fundação de Ciências e Tecnologia (FCT) com a bolsa número SFRH/BD/146942/2019

2024

ACKNOWLEDGEMENTS

I would like to express my sincere gratitude to my three supervisor Rui Quartau, José Madeira and Claudia Romagnoli for their continuous support and encouragements during this academic journey. The knowledge and enthusiasm transmitted have been fundamental to the completion of this thesis.

I would like to acknowledge the FTC for the financial support, and FCUL and IDL for embracing me as an integral member of their research groups. Additionally, I also wish to acknowledgment the Hydrographic Institute of the Portuguese Navy for providing me data and facilities. A special acknowledgment goes to all the researchers and technicians of the marine geology division. Here, I had the possibility to discuss my work and to explore diverse perspectives, thereby enhancing the constructive development of my ideas. I am also thankful to the University of Bologna for their collaboration as foreign hosting institution. I would like to thank you Dr. Rusu and Dr. Zhao for the modelling related to the wave regime and the associated sediment mobilization areas.

I am deeply thankful to Simone for each feedback, sparks, helps and all the moments of comparison and support, especially in occasion of every presentation. They were essential for me. Thank you to have been the best partner ever at all the congresses, summer schools and fieldworks.

Thanks to all new and long-standing friends, spending time with you it was therapeutic for me especially during stressful periods occurred these years. You all gave me joy, fun and light-heartedness.

Thank you, Lisbon. Here, this experience was wonderful. I have grown not only professionally but also personally in ways I would have never imagined. Now, I see things from a different point of view...like from a *miradouro,* at the sunset.

Last but not least, I would like to say a heartfelt thank you to my family. It was hard stay far away from home but you have never let me feel alone and I know that you all are proud of me. I am grateful for your unconditioned love; it makes me strong.

Finally, I am profoundly thankful for the unwavering support and encouragement from everyone mentioned and many others who have contributed in various ways to this work.

ABSTRACT

This work focuses on the sedimentary dynamics surrounding the southern shelf of Madeira Island (Atlantic Ocean) through the analysis of recent submarine clinoform bodies (SCBs) and bedforms using geophysical and sedimentological data. Geophysical data consist of multi-temporal bathymetries and seismic profiles. Bathymetries have been used to characterize the features from a morphological and morphometric point view. Seismic profiles have been used to investigate the architectures of SCBs. Sediment samples were used to characterize the sedimentary cover of the shelf and to understand sediment sources. The final aim of this work is to characterize the depositional and erosional features and to infer the processes behind their origin. Results allowed dividing the shelf in four sectors, which differ in terms of width and steepness, sedimentary cover, erosive and depositional features, and exposure to the energetic wave regime. The most exposed area is Sector 1. The shelf is very wide, has low gradients and the sedimentary cover is coarse. Sediments come mostly from cliff dismantling because stream discharge is low. SCBs are more extended, locally reaching the shelf edge and bedforms fields are oblique to the coastline. Sectors 2 and 3 are still influenced by the main wave regime but less. The shelf is narrower and steeper, and the sediment cover is fine. These areas are mainly influenced by stream discharge. SCBs are thicker but narrower in comparison to sector 1 and bedform fields are perpendicular to the coastline. Sector 4 is even narrower with higher gradients characterized by small and narrow SCBs and small perpendicular bedforms fields. The sediment is coarse but related to biogenic production except offshore the main streams where it is fine. The understanding of these shelf processes is relevant for the management of coastal risks, location of telecommunication cables and aquaculture infrastructures and the extraction of marine aggregates.

Keywords: Sedimentary dynamics, volcanic insular shelf, subaqueous clinoform bodies, bedforms, Madeira Island.

RESUMO

Neste trabalho analisa-se a dinâmica sedimentar na costa sul da ilha da Madeira, um edifício vulcânico localizado no Oceano Atlantico, através do estudo das estruturas erosivas e depositionais reconhecidas na sua plataforma insular. Particularmente, o trabalho está focado-se na caracterização e distribuição das corpos clinoformes submarinos (CCSs) e nos campos de formas de fundo (bedforms).

Os CCSs são elementos morfológicos comuns em todos os ambientes de deposição submarina, incluindo os vulcões insulares. Neste estudo, estudaram-se apenas os corpos clinoformes subaquáticos recentes que se começaram a formar há cerca de 6,5 mil anos, quando o nível do mar atingiu sua posição atual. Devido ao seu tamanho e localização na plataforma interna, podem ser considerados como corpos clinoformes à escala de deltas, apesar de terem diferentes terminologias na literatura científica. O seu perfil de equilíbrio é o resultado de múltiplos fatores, como suprimento de sedimentos, a sua granulometria, os processos de dispersão (por exemplo, regime de ondulação), o espaço de acomodação e a batimetria pré-existente. Os CCSs formam-se durante condições turbulentas, associadas a ondulação forte durante tempestades. Durante esses eventos, os sedimentos são transportados para o largo, por correntes de retorno ou correntes de elevada densidade, aliadas ao facto de a plataforma ter uma inclinação em direção ao largo. Uma vez terminada a influência da ondulação, o transporte também cessa e o sedimento deposita-se por efeito de avalanchas ou cascata. Dessa forma, os corpos clinoformes submarinos têm uma forma típica sigmoidal, com uma zona plana a levemente inclinada ("topeset" em inglês) onde ocorre a maior parte da erosão, uma zona íngreme onde a deposição predomina ("foreset" em inglês) e, finalmente, uma zona plana a levemente inclinada ("bottomset" em inglês) onde predomina a sedimentação pelágica.

Os ondas de areia (formas de fundo submarinas) são morfologias rítmicas formadas na interface entre o sedimento e a coluna de água sob o efeito de correntes unidirecionais ou bidirecionais. Elas resultam da interação entre processos sedimentares e erosivos que são ubíquos numa infinidade de ambientes geológicos, incluindo os flancos submarinos de ilhas vulcânicas. Essas formas de fundo podem formar-se em regimes de fluxo laminar ou turbulento, dependendo da relação de fase entre ondas na superfície dos fluxos e ondulações do sedimento no fundo. As ondas de areia em regime de fluxo laminar consistem em *ripples* e dunas. Estas formas migram em direção ao largo e a deposição ocorre no lado de sotavento. As formas de fundo em regime de fluxo turbulento incluem antidunas (comprimento de onda curto) e degraus cíclicos (comprimento de onda longo) que abrangem um contínuo de formas de fundo transitórias, que

estão ainda pouco estudadas. No entanto, um número crescente de estudos atribui aos degraus cíclicos um papel dominante na geração de formas de fundo numa variedade de ambientes marinhos. No entanto, um número crescente de estudos atribui aos degraus cíclicos um papel dominante na geração de ondas de areia numa variedade de ambientes marinhos. Elas são principalmente caracterizadas por uma deposição predominante no lado de barlavento e erosão no lado de sotavento, com migração em direção à costa. Essa evolução é devida à alternância entre regimes de fluxo laminar e turbulento, separados por um salto hidráulico no qual ocorre a variação do regime de fluxo. A sua origem está comumente relacionada a correntes de turbidez, um tipo de fluxo de densidade que pode ser desencadeado por diferentes mecanismos, como instabilidade gravítica, fluxos hiperpicnais e ondas de tempestade.

Este trabalho foi realizado com a interpretação de dados geofísicos e sedimentares, colhidos durante o último vinténio pelo Instituto Hidrográfico em várias campanhas oceanográficas. Os dados geofísicos consistem em batimetrias multifeixe multi-temporais e perfis de sísmica de reflexão ligeira do tipo Sparker. Foram também usadas dados de precipitação, que cobrem o período 2001-2020 em diferentes estações meteorológicas distribuídas pela ilha, fornecidos pelo Instituto Português do Mar e da Atmosfera. Usou-se também modelação SWAN ("Simulating WAves Nearshore") para obter a propagação da ondulação referente aos anos de 2013-2014 na plataforma insular e poder calcular as áreas onde os sedimentos são colocados em suspensão pela ação das ondas. A batimetria foi utilizada para caraterizar os CCSs e as formas de fundo de um ponto de vista morfológico e morfométrico. Os perfis sísmicos foram utilizados para investigar a arquitetura sedimentar dos CCSs, nomeadamente a morfologia interna, a espessura dos corpos sedimentares e a profundidade da superfície basal onde eles se desenvolvem. As amostras de sedimentos foram utilizadas para obter a distribuição da cobertura sedimentar na plataforma e inferir as fontes sedimentares. O objetivo final deste trabalho foi compreender os processos responsáveis por estas estruturas sedimentares e erosivas e e explicar os fatores que guiam e influenciam a variabilidade espacial dos CCSs e das ondas de areaia ao longo da plataforma insular sul da Madeira.

A ilha da Madeira representa o maior edifício do arquipélago, que do ponto de vista genético, inclui também as Ilhas Desertas e a Ilha do Porto Santo. As litologias aflorantes incluem essencialmente formações basálticas sob a forma de derrames e, em menor proporção, de depósitos piroclásticos, que podem apresentar graus de alteração variável (essencialmente em função da idade, mas localmente também condicionada pela altitude) o que condiciona a sua erodibilidade e a granulometria dos sedimentos produzidos. A ilha da Madeira caracteriza-se

por um forte relevo e um sistema de drenagem muito encaixado composto por ribeiras de regime torrencial capazes de erodir e transportar grandes volumes de sedimento. Durante eventos de intensa pluviosidade estas ribeiras adquirem grande poder erosivo e com os sedimentos produzidos descarregados na costa podendo formar correntes hiperpicnais ao entrar no mar. . Devido a sua posição geográfica, a Ilha da Madeira, está frequentemente sujeita a tempestades, que podem envolver eventos catastróficos como a última "flash flood" ocorrida no dia 20 de Fevereiro de 2010.

Considerando as características da região emersa, tais como as bacias hidrográficas e morfologia litoral, bem como as características da plataforma insular (largura e declive, cobertura sedimentar, estruturas erosivas e deposicionais e exposição ao regime de perturbação marítima) a área de estudo foi dividida em quatro setores diferentes. A área mais exposta à ondulação é o Setor 1 localizado a Oeste. Neste setor, a plataforma é larga, tem um declive baixo e os sedimentos são grosseiros. A fonte de alimentação dominante é o desmantelamento das arribas, enquanto a descarga fluvial é subsidiária. Os CCSs são mais extensos, alcançando localmente o bordo da plataforma e os campos de formas de fundo são oblíquos à linha de costa. Para Este, os Setores 2 e 3 ainda são influenciados pelo regime de ondas principal, embora menos intensamente. A plataforma torna-se mais estreita e íngreme, e os sedimentos são finos. Estas áreas são principalmente influenciadas pela descarga fluvial. Os CCSs são mais espessas, mas ocupam uma área menor relativamente ao setor 1, e os campos de formas de fundo são perpendiculares à linha costeira. No extremo Este da plataforma sul, o Setor 4 é ainda mais estreito, com gradientes altos e caracterizado por CCSs pequenos e estreitos e campos de ondas de areia pequenos e perpendiculares à costa. Os sedimentos são grosseiros e com importante componente biogénica, exceto em frente à foz dos principais cursos de água, onde são predominantemente finos e de origem terrígena.

Compreender os processos envolvidos na plataforma da Ilha da Madeira é fundamental para mitigar o risco costeiro e garantir uma gestão sustentável dos recursos. Além disso, essas atividades são essenciais para a economia das ilhas, especialmente para aquelas que dependem do turismo e do desenvolvimento costeiro. Ao compreendermos melhor esses processos, podemos garantir que no posicionamento de cabos de telecomunicações, a prática da aquacultura e a extração de recursos como areia e agregados sejam realizados de forma responsável e sustentável, minimizando impactos negativos no meio ambiente e na comunidade local que encontra no mar uma fonte de rendimento.

Palavras chave: Dinâmica sedimentar, ondas de areia, plataforma vulcânica insular, corpos clinoformes submarinos, Ilha da Madeira.

TABLE OF CONTENTS

LIST OF FIGURES

antidunes (B) form in Froude-supercritical flow regime (Fr >1). (C) Cyclic steps differentiate by alternating Froude-subcritical and supercritical flow regime. HJ: hydraulic jump is where the transition from Froude-supercritical to subcritical flow occurs. Changes in flow parameters (e.g., flow thickness) creates bedforms that vary orders of magnitude in size. Wavelength to flow thickness ratio as shown for antidunes and cyclic steps is representative (from Slootman et al., 2019).

CHAPTER 3

Figure 3.1. (A) Geographic setting of Madeira Archipelago in the Eastern North Atlantic (from open-access EMODnet bathymetry). Azores-Gibraltar Fracture Zone (AGFZ) according to Geldmacher et al., (2000); PS: Porto Santo; De: Desertas Islands; Am: Ampère; Se: Seine; CP: Coral Patch; Or: Ormond Seamount. (B) Inset zoom of Madeira Island within the archipelago. M: Madeira.

Figure 3.2. Altimetry of Madeira Island. The valleys of Ribeira Brava and Ribeira de S. Vicente streams separates the west and east regions of the island (red dotted circle). Yellow triangles represent the highest peaks of the island, simple green dots represent the valleys where the headwaters of the two longest southern streams are located.

Figure 3.3. Main hydrographic basins and network drainage of Madeira Island. ID numbers indicate the main streams described in Table 3.1.

Figure 3.4. A) Distribution of average annual precipitation between 1961 and 1990 (from Atlas do Ambiente, 1995) and B) Rose chart of the main wave regime in the 1996 - 2002 period (from Fortes et al., 2006). Green dots represent the buoy location off Funchal (F) and Caniçal (C). Orange dots the RCM9 current metric stations while red dot ACDP location.

Figure 3.5. Simplified geological map of Madeira Island (adapted from Ramalho et al. 2015). CVI: Lower Volcanic Complex (1-Porto da Cruz Formation, 2-Lameiros Formation); CVM: Middle Volcanic Complex (1-Encumeada Formation, 2-Penha d'Águia Formation, 3- Curral das Freiras Formation); CVS: Upper Volcanic Complex (1-Lombos Formation, 2-Funchal Formation); dmm, dv, a: mass wasting deposits, colluvia and slope deposits, alluvial deposits, respectively.

Figure 3.6. Simplified sketch of the main lineaments in Madeira Island deduced from satellite imagery (Fonseca et al., 1998 a, b).

terminations on the blue surface. The maximum thickness of the progradation unit is indicated by a double red arrow. B) Methodology used for determining the clinoform rollover point (Wear et al., 1974).

Figure 4.6. Terminology of the observed features and related parameters adopted in the morphometric analysis. (A) Plan view of a channel head with bedforms incising the shelf (B) Profile view of section A-B drawn in (A), showing the measurements done. (C) Cross section shape and respective classifications. (D) Crestline shape in plan-view and respective classifications. Modified from Symons et al. (2016) and Normandeau et al. (2016).

Figure 4.7. Example of coastal elevation trend shown on the ArcGIS interface. The blue line represents the digitized cliff, which is then plotted on the graph.

CHAPTER 5

Figure 5.1. A) Map displaying the division of the southern insular shelf of Madeira Island into four sectors (the cross-shelf green lines are the sector borders) and the sediment production of each basin onshore. White dots represent the following locations: 1- Ponta do Pargo; 2- Calheta; 3- Cabo Girão; 4- Funchal; 5- Caniçal. Black bold lines represent the clinoform rollover. In sector 1, the dotted lines indicate the minimum extension of SCBs' topset in areas where the seismic data do not cross entirely the features.

Figure 5.1. B) Map displaying the division of the southern insular shelf of Madeira Island into four sectors (the cross-shelf green lines are the sector borders) and the outcropping lithologies in each basin onshore. The remaining caption is the same as Fig. 5.1.A.

Figure 5.2. Cliff height trend along the south coast of Madeira Island. In each sector, the coloured line represents the average.

Figure 5.2. (A) Map of the southern shelf of Madeira Island showing the mapped SCB topset width (or clinoform rollover) and the shelf edge. Black and red lines represent the position of clinoform rollover and shelf edge, respectively. Black and red dashed lines indicate the inferred position of the same features due to lack of seismic and multibeam data. Brown polygons represent nearshore rocky seafloor. (B) Graphs illustrate the area occupied by the SCBs topset (grey dashed area) relatively to the shelf width. Numbers indicate the minimum and maximum area of the shelf, in percentage, that the SCBs topsets occupy. Note that the x-axis (horizontal) scale varies between graphs.

Figure 5.3. Map of the westernmost region of sector 1. The SCBs are limited to the inner shelf, with their minimum topset width depicted by a dotted black line. Brown polygons represent the nearshore rocky seafloor. The outer shelf displays a predominant rocky seafloor.

Figure 5.4. Map of the thickness of the SCBs in sector 1 of the insular shelf of Madeira (see location on Fig. 5.1). Brown polygons delimit nearshore rocky seafloor. Thickness increases from orange to green and blue tones. Contours are spaced each 4 m. The two red lines represent the location of the seismic profiles of Figs. 5.6 and 5.7.

Figure 5.5. Sparker seismic profile perpendicular to the coast in the westernmost part of sector 1 (location in Fig. 5.5). Red arrows represent the reflections with downlap terminations on the bold orange line that represents the maximum flooding surface (MFS). MFS separates the prograding unit (above) from that with an aggradation trend (below). The aggradating unit presents reflections with onlap terminations (green arrows) towards the bold and dashed blue line, which is the acoustic basement surface.

Figure 5.6. Sparker seismic profile perpendicular to the coastline located in the easternmost part of sector 1 (location in Fig. 5.5). Symbology as in Fig. 5.6; R marks the rollover point.

Figure 5.7. Map of the thickness of the prograding bodies in sector 2 of the insular shelf of Madeira (see location in Fig. 5.1). Brown polygons delimit nearshore rocky seafloor. Thickness increases from orange to green and blue tones. Contours are spaced each 4 m. The red line locates the seismic profile of Fig. 5.9.

Figure 5.8. Sparker seismic profile perpendicular to the coastline in sector 2 (location in Fig. 5.8). Symbology as in Fig. 5.6 in chap. 5. R marks the rollover point.

Figure 5.9. Map of the thickness of the prograding bodies in sector 3 of the insular shelf of Madeira (see Fig. 5.1 for location). Brown polygons delimit nearshore rocky seafloor. Thicknesses increases from orange to green and blue tones. Contours are spaced each 4 m. The two red lines are the locations of the seismic profiles of Fig. 5.11 and 5.12.

Figure 5.10. Sparker seismic profile perpendicular to the coastline in sector 3 (location in Fig. 5.10). Symbology as in Fig.5.6. R marks the rollover point.

Figure 5.11. Sparker seismic profile perpendicular to the coastline in sector 3 (location at Fig. 5.10). Symbology as in Fig.5.6. R marks the rollover point.

Figure 6.2. Shaded relief bathymetry of bedform field 1 (caption and location as in Fig. 6.1) Contours spaced every 25 meters. The transversal profile (A-B) is shown in Suppl. Fig. 10.3 in the Appendix and the longitudinal profiles of bedforms 1a, 1b, and 1c are shown in Suppl. Fig. 10.4 in the Appendix. SCB R.: subaqueous clinoform body rollover.

Figure 6.3. 3D image of bedform field 1 (location in Fig. 6.1). Note the link between the subaerial drainage (streams), the channels on the shelf and the tributary gullies in the canyons beyond the shelf edge. Vertical exaggeration 2x.

Figure 6.4. Shaded relief bathymetry (caption as in Fig. 6.1) of bedform fields 3, 4 and 5 (location in Fig. 6.1). Contours spaced every 25 meters. The longitudinal profiles 3, 4a, 4b, 4c and 4d, 5a, 5b, 5c are shown in Suppl. Figs. 10.17 and 10.20 respectively, in the Appendix. The transversal profiles (A-B and C-D) are shown in Suppl. Figs. 10.18 and 10.21 in the Appendix. SCB R.: subaqueous clinoform body rollover.

Figure 6.5. 3D illustration of bedform fields 3, 4 and 5 (location on Fig. 6.1). Note the absence of a clear clinoform failure onshore the fan-shaped feature of field 4. Field 5 shows a fan-shaped feature related to the clinoform failure which much steeper slope than that of field 4. Vertical exaggeration 3x.

Figure 6.6. Shaded relief bathymetry (caption as in Fig. 6.1) of bedform fields 7 and 8 (location in Fig. 6.1). Contours spaced every 25 meters. The transversal profile (A-B) is shown in Suppl. Fig. 10.36 in the Appendix. The longitudinal profiles 7a, 7b, 8 are shown in Suppl. Fig. 10.37 in the Appendix.

Figure 6.7. 3D illustration of bedform fields 7 and 8 (location on Fig. 6.1). Field 7 shows a fan-shaped feature with channels developing on top. East of field 8, the possible retrogressive evolution of channels from the shelf edge up to the clinoform rollover (stages 1 to 3) has been indicated. Vertical exaggeration 3x.

Figure 6.8. Box plots of the main parameters (y-axis) measured for the four bedforms types I-II- III-IV(x-axis), (n=203). Numbers represent lower whisker (minimum), 25th quartiles, median, 75th quartiles and upper whisker (maximum).

Figure 6.9. Scatter plots showing possible relationships between the main morphological parameters of the bedforms developed perpendicular to the coastline. Each colour represents a bedform fields as indicated in Suppl. Fig. 10.53 in Appendix.

Figure 7.4. Annual average precipitation of the hydrographic basins. Relation of SCBs rollover depth and bedforms distribution on the southern shelf versus wave-induced bed stress. Red areas indicate locations where sediment is suspended by waves, whereas green areas represent sites where sediment remains unaffected by wave action. Brown polygons represent nearshore rocky seafloor.

LIST OF TABLES

The values with "†" are related to the larger SCBs observed in sector 4. CVS: Complexo Vulcânico Superior; CVM: Complexo Vulcânico Médio.

LIST OF SYMBOLS

A = boundary layer in equation 4.5

A = drainage basin area in equation 4.11

D = sediment grain size

e= math constant, 2.71

Fr = Freud number

f_w = wave friction factor

g = acceleration of gravity

h = flow depth

H_s = significant wave height in equation 4.1

H_m0 = significant wave mean height

k = wave number in equations 4.1 and 4.2

k = constant, 0.07, in equation 4.11

km = kilometre

kg = kilogram

K_s = roughness height

m = meter

Qs = long term sediment load

R = maximum relief from sea level

s = second

sin = trigonometric function

T0 = wave mean period

T_p = wave peak period

T = wave peak period in equations 4.3 and 4.6

T = basin-average temperature in equation 4.11

U = depth-averaged downstream flow velocity in equation 2.1

u_m = wave orbital speed

y = variable function

v = water kinematic viscosity

z = depth

α_3 = constant, 6.1 x 10^{-5}

α_4 = constant, 0.55

α_5 = constant, 1.12

λ = wavelength

s = ratio of grain to water density

Θ = main cardinal direction related to wave peak period

θ_{cr} = critical angle

π = math constant, 3.14

ρ_s = density of bulk sediment

ρ_w = water density

τ_w = wave induced shear stress at the seabed

τ_{cr} = sediments' threshold of motion

τ_{ratio} = relationship between τ_w and τ_{cr}

ϕ = phi related to sediment size

°C = Celsius degrees

CHAPTER 1 – INTRODUCTION

1.1 OVERVIEW

In the last decade, several manuscripts revealed the importance of insular shelves for understanding the development and morphological evolution of volcanic edifices and the constructive and destructive processes that act to model their morphology (Mitchell et al., 2012; Quartau et al., 2010, 2012, 2014; Romagnoli, 2013; Ramalho et al., 2013; Casalbore et al., 2015, 2016). The insular shelf is the area shaped by wave erosion during glacial-interglacial sea-level oscillations that extends from the coastline down to the shelf edge (Quartau et al., 2010). By studying its morphology, we can obtain important information about how volcanic edifices evolved in the Quaternary (Quartau et al., 2014). Moreover, the investigation provides insights about sediment dynamics on the insular shelf and how particles are transported from shallow to deep waters, according to a source-to-sink approach. This knowledge can be also useful to support coastal communities in improving the management of their natural and economic resources. Moreover, volcanic islands represent highly vulnerable environments to diverse hazards, such as storms, which can intensify coastal and fluvial erosion, and consequently trigger associated landslides. The compounded impact of these hazards can escalate significantly due to their simultaneous occurrence and magnitude, particularly when coupled with the effects of climate change (López-Saavedra & Martí, 2023).

This thesis has been produced as part of a Ph.D. project conducted at the Faculty of Science of Lisbon University in partnership with the Hydrographic Institute of the Portuguese Navy and the Biological, Geological and Environmental Science Department of Bologna University (Italy).

1.2 OBJECTIVES

This work entails a thorough analysis of the southern shelf of Madeira Island integrating offshore data with onshore information. Its aim is understanding the sedimentary dynamics on the southern shelf of Madeira Island through morphological and morphometric analysis of its erosive-depositional features through bathymetric, seismic, and sedimentary data interpretation. The data has been acquired by the Portuguese Navy and consist of Sparker seismic profiles, multibeam bathymetries and seabed sediment samples. They were collected

between 2002 to 2019 along the entire southern shelf extension, from the shallowest to the deepest parts.

The great availability of geophysical and sedimentological data and the absence of previous detailed studies on islands make Madeira Island shelf an ideal case study to investigate subaqueous clinoform bodies and bedforms, very frequently observed in similar setting (see chapter 2). Moreover, examining the morphology and the great spatial variability of these features is fundamental to improve the knowledge about the complex sedimentary dynamics on shelves surrounding oceanic islands such as Madeira. Madeira is an oceanic island of volcanic origin, vulnerable to rainy extreme events. It exhibits a topography characterized by varied erodible volcanic formations shaped by several torrential streams. The island's southern coast and submarine areas experience diverse wave exposures. Consequently, Madeira serves as a perfect example to observe and study how factors like wave exposure and stream contributions influence the shelf morphology of a large volcanic edifice (~740 km²).

The research activity was conducted with the following objectives:

- To analyze the submarine morphology of the southern shelf of Madeira Island by measuring the shelf width and slope.
- Better constrain the sedimentary dynamics from the characterization of the erosive-depositional features on the shelf, namely:
    - Bedform fields in order to understand how they form and develop.
    - Subaqueous clinofom bodies (SCBs) aiming at understanding the different factors (wave regime, sediment supply, inherited bathymetry) that influence their characteristics and spatial variability.

1.3 THESIS STRUCTURE

The thesis structure is as follows:

Chapter 2 – State of the art. It resumes the literature regarding the formation and evolution of insular shelves and the processes behind it. A general overview of how subaqueous clinoform bodies (SCBs) and subaqueous bedforms are formed and how their characteristics are used to describe and classify them is presented.

Chapter 3 – Geologic, oceanographic and climatic setting. The geographical and geological setting of Madeira Island on the Archipelago, as well as its geomorphology, volcano-

stratigraphy, main tectonic features, wave regime and climatic setting are described. Furthermore, a direct association with these descriptors and the associated natural hazards is highlighted.

Chapter 4 - Data and methods. Information regarding data typologies and acquisition and processing procedures as well as their integration is provided. Additionally, it explains the methodology employed to obtain the morphometric parameters of bedforms and clinoform bodies, as well as the interpretative approach adopted for the analysis of seismic profiles.

Chapter 5 – Spatial variability of subaqueous clinoform bodies (SCBs) on the southern insular shelf of Madeira Island. This chapter correspond partially to the manuscript I, prepared for future publication. It aims to characterize and understand the recent SCBs and their variability along the shelf in terms of thickness, topset width and rollover point depth. Additional figures can be found in the appendix, between pages 136 and 137.

Chapter 6 – Origins and controlling factors of bedforms formed by supercritical sediment density flows on the southern shelf of Madeira Island. This chapter correspond to manuscript II, and presents the morphological and morphometric analysis of bedforms fields on Madeira southern shelf. A classification was made and a model is proposed for the processes involved in their development and evolution. The detailed description of each bedform field including the profiles in which the sedimentary waves have been measured and their measurements can be found in the appendix on pages 140-194.

Chapter 7 – The contribution of sediment sources, shelf morphology and wave forcing to understand depositional and erosional features on the southern shelf of Madeira Island. An integration of the two previous topics, SCBs and bedforms, is presented. In this chapter, their characteristics and formation are discussed showing the importance of sediment supply, shelf morphology and wave regime to the production and transport of sediment along the shelf.

Chapter 8 – Conclusions. A resume of the main findings of this study, its limitations, and directions for future research is given.

The outcomes of this research will be published in scientific journals dealing with Marine Geology or Sedimentology. The titles of the scientific papers will be:

- Manuscript I: ***Factors controlling the spatial variability of subaqueous clinoform bodies (SCBs) on the southern insular shelf of Madeira Island***

- Manuscript II: ***Origins and controlling factors of bedforms formed by supercritical sediment density flows on the southern shelf of Madeira Island***

CHAPTER 2 – STATE OF THE ART

2.1 THE SHELVES OF VOLCANIC ISLANDS

Volcanic islands commonly represent the emerged tip of larger edifices that develops from the seafloor. The relatively flat submarine portion around the islands is called insular shelf and comprises the shallow-water zone down to the shelf edge, after which the depth and slope drastically increase (Quartau et al., 2010). Insular shelf morphology is mainly the result of the long-term interplay and competition between wave erosion and volcanic activity. Wave erosion is the most important factor acting as promoter of shelf enlargement while volcanic activity may act in the opposite direction (Ramalho et al., 2013; Quartau et al., 2015).

In principle, the initiation of a shelf starts during the first still-stand phase of sea level after the emergent phase of the island. In concomitance with reduced volcanic activity, wave abrasion starts to erode, flattening the edges of the island slope at or near sea level. Following, relative sea-level oscillations can change the level of erosion (Fig. 2.1). Thus, the shelf width and the position of its edge is the result of polycyclic wave erosion that acted during different glacial-interglacial sea-level oscillations through time (Trenhaile, 2000, 2001).

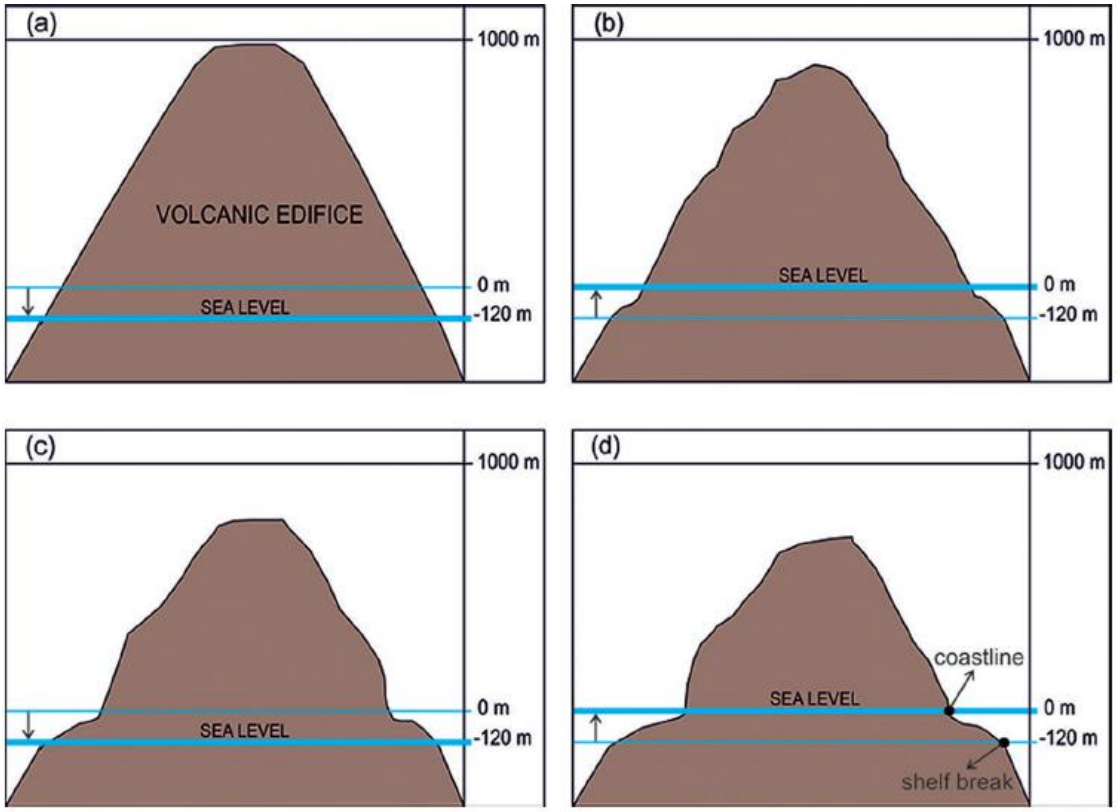

Figure 2. 1. Development of a shelf around a volcanic island across glacial-interglacial cycles and corresponding relative sea-level oscillations. Temporal scale increases from (a) to (d) (from Quartau et al., 2016).

It is widely accepted that these sea-level oscillations in the Quaternary are driven by the global climatic fluctuations linked to the variation of the Earth's orbit around the sun and the changes of its axis rotation (Milankovick, 1930). The last global (eustatic) sea-level fall reached its minimum level around 20 ka ago. In this period, called Last Glacial Maximum, the sea surface was approximately 120 m below the present-day level (Bintanja et al., 2005). The sea-level started raising at around 18 ka ago and reached the present level at around 6.5 ka, remaining in a quasi-stable still-stand stage since then (Patruno & Helland-Hansen, 2018).

At the local scale, however, other important factors influence the present-day shelf morphology (Fig. 2.2). These can be related to erosional, depositional, tectonic, isostatic and mass-wasting processes (Quartau et al., 2012; Ramalho et al., 2013). They act at different magnitude and scale, and for this reason, their relative contribution is difficult to infer (Quartau et al, 2010). Moreover, it should be noted that the existing shelf morphology could show ancient volcanic remnants that are no longer visible onshore and mostly reflects the imprint of geomorphological processes that took place during the late Quaternary period (Quartau et al., 2014; Ricchi et al., 2018).

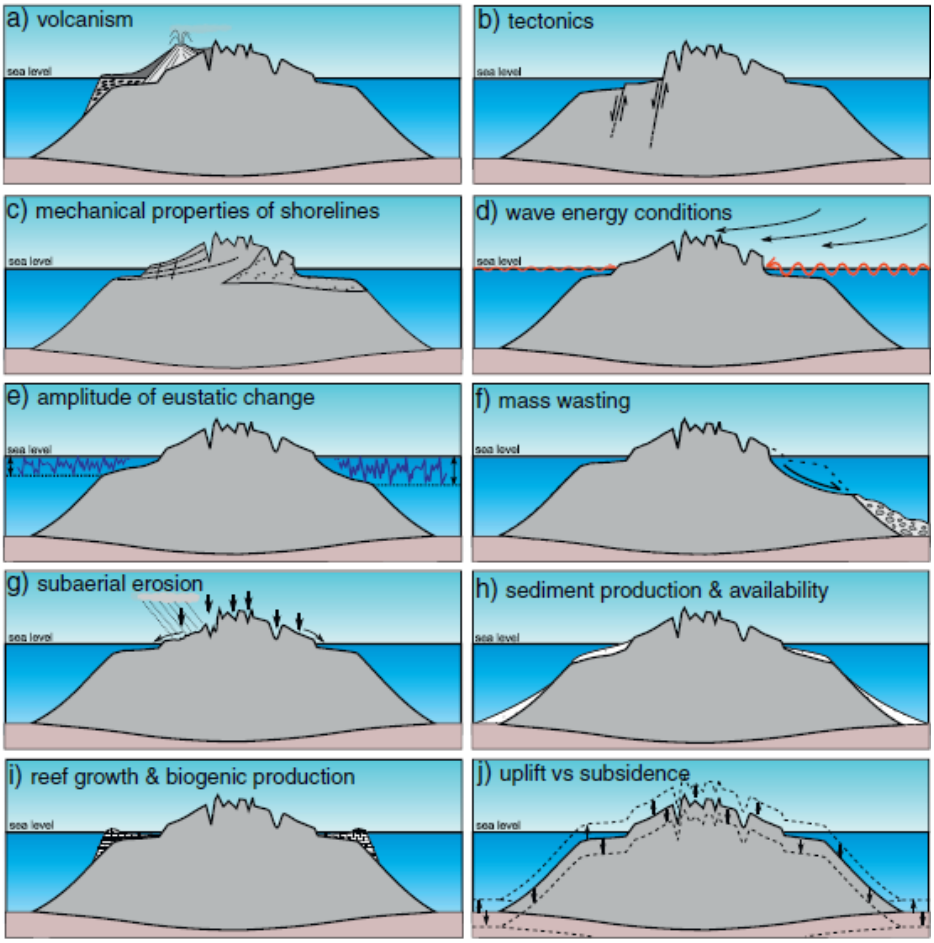

Figure 2. 2 Factors that control the morphology of a shelf of a volcanic island (from Ramalho et al., 2013).

2.2 DEPOSITIONAL AND EROSIVE FEATURES ON INSULAR SHELVES

On insular shelves, several depositional and erosive features are commonly observed. This environment frequently experiences energetic wave conditions especially in open-sea volcanic settings (Meireles et al., 2013). During these events, sediment on the shelf is remobilized and transported across- and along-shore according to the main wind and wave regimes. Wave- and wind-driven currents can transport sediments on the shelf forming ubiquitous morphological elements such as subaqueous clinoform bodies (SCBs) and bedforms. These features can give useful information about the sedimentary dynamics.

2.2.1 SUBAQUEOUS CLINOFORM BODIES

Subaqueous clinoform bodies (SCBs) are common morphological and depositional elements on many submarine environments, including insular volcanoes (Casalbore et al., 2018). They have a typical terraced shape in the bathymetry and their internal architecture is characterized by basin-ward inclined surfaces, called "clinoforms". As depicted in Fig. 2.3, each clinoform consists of gently dipping topset and bottomset connected by basin-ward inclined portions named foreset and, on the whole, by stacking units named "clinothems".

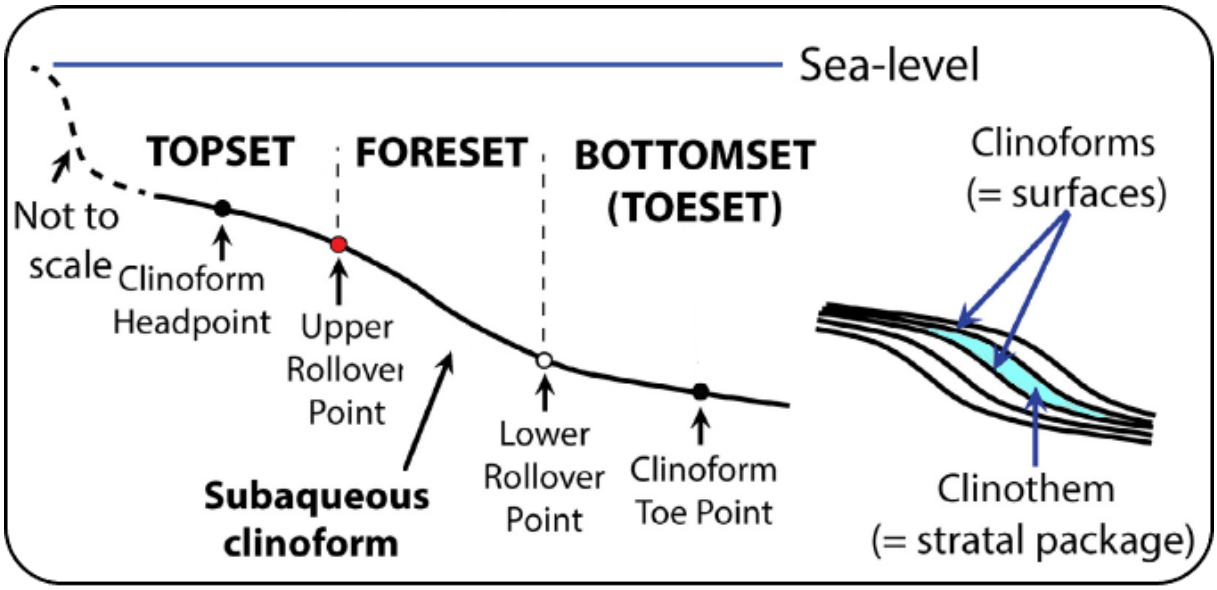

Figure 2. 3. Clinoform nomenclature. The topset is the gently dipping surface divided from the foreset, the inclined steeper part, by the upper rollover point. Offshore the foreset lies the bottomset, which is again a gentler surface that aligns the feature with the basal seabed (modified from García-Ramos & Zuschin., 2018).

They can be observed at different temporal and spatial scales (Fig. 2.4) and those that are restricted to the shelf (e.g., delta scale clinoforms; Patruno & Helland-Hansen, 2018), have been named with different terminologies such as "nearshore sand bodies" (Field and Roy, 1984),

"infralittoral prograding wedges" (Hernandez-Molina et al., 2000), "submerged depositional terraces" (Chiocci et al., 2004; Casalbore et al., 2016; Romagnoli et al., 2018), sandy clinoforms (Mitchell et al., 2012; Mitchell, 2012; Quartau et al., 2012) or "subaqueous clinoforms" (Medri et al., 2023). These authors agree on the interpretation that they have been formed during different sea-level still-stands, mostly related to glacio-eustatic variations and for this reason, their interpretation is useful to reconstruct ancient sea-level positions and/or the occurrence of subsequent vertical displacements of related coastal sectors.

The shallowest subaqueous clinoform bodies at the shelf scale started prograding ~6.5 ka ago, when sea-level reached the present-day position. In most cases, present-day SCBs have an upper rollover point located between the depths of 20 and 60 m depending on oceanographic conditions, and thicknesses of some meters up to 60 (Casalbore et al., 2017). They may prograde at rates ranging between 100-20000 m/ky (Patruno & Helland-Hansen, 2018).

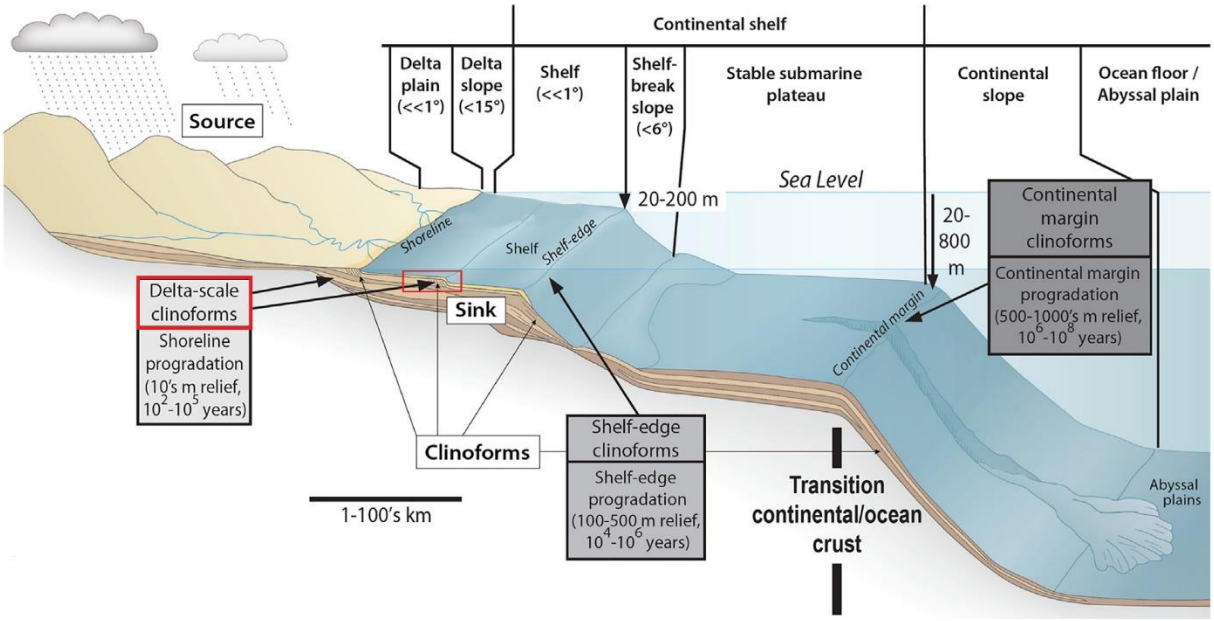

Figure 2. 4. SCBs temporal and spatial scale in a continental margin setting (modified from Patruno & Helland-Hansen., 2018).

However, their equilibrium profile is the result of multiple local factors such as sediment supply, grain-size, dispersal processes (e.g., wave climate), accommodation space and pre-existing bathymetry (Patruno & Helland-Hansen, 2018).

SCBs form during turbulent conditions, associated to energetic waves during storms (Chiocci & Romagnoli, 2004; Casalbore et al., 2017, Medri et al., 2023). Although these Authors agree that SCBs form during a higher wave energy regime when sand is transported from shallow environment and deposited down a slope into calmer environments, varied studies refer to slightly different mechanisms for their formation. For instance, Medri et al., (2023) hypothesize

that clinoforms are built by sandy wave-supported gravity flows. During storm, wave energy resuspends sediments. Near the seabed, a higher density layer forms which moves downslope by the effect of gravity over increasing shelf gradients. The sediments are then deposited by cascading when the wave energy is not able to maintain the flow and the shelf gradients increase. In this case, the geometry of the clinoforms reflects the pre-existing bathymetry. Other authors (Hernandez-Molina et al., 2000; Chiocci and Romagnoli, 2004, Casalbore et al., 2016, 2017; Romagnoli et al., 2018; Mitchell & Zhao, 2023) believe that their progradation is the result of wave-induced downwelling currents during high-energy storm events. These events, in fact, produce a high coastal set up that is balanced by opposite downwelling currents able to entrain and transport sediment offshore. Once wave influence ceases and gradients increase, sediments deposit by avalanching. In this way, the SCBs develop their typical shape; a flat and gentle area, the topset where transport and erosion occur; a steep gradient where deposition predominates and finally again a gentle gradient where pelagic sedimentation prevails (Fig. 2.5).

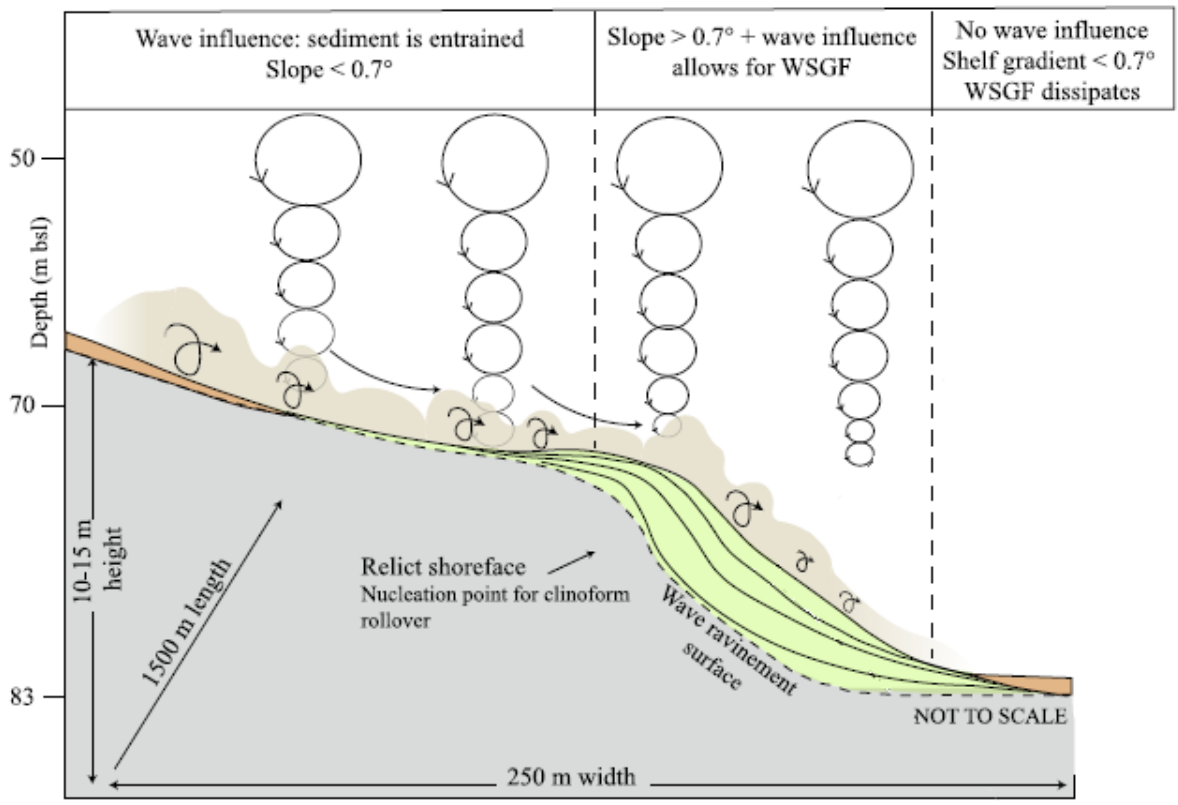

Figure 2. 5. Wave-supported current and clinoforms formation model (modified from Medri et al., 2023). WSGF: wave-supported gravity flow.

To assess the contribution of factors as sediment supply, wave regime and shelf morphology is essential to improve knowledge on clinoform generation and evolution. This is especially relevant since clinoforms are ubiquitous features and this knowledge can shed light on both

ancient and contemporary depositional environments. Furthermore, it has practical relevance in various industries, including energy exploration and the extraction of marine aggregates. SCBs not only exhibit a high potential for hosting hydrocarbon fluids, but they are also frequently dredged in insular regions where onshore resources for construction are scarce. A comprehensive understanding of clinoform characteristics also aids in the assessment of natural hazards like submarine landslides, which can trigger tsunamis and turbidity currents. Additionally, these deposits may play a protective role in mitigating coastal erosion, making this knowledge indispensable for effective coastal management.

2.2.2 SUBAQUEOUS BEDFORMS

Bedforms are quasi-rhythmic morphological patterns that develop as a result of the complex interplay between deposition and erosion processes acting in various geological settings. These include deltas, continental margins, canyons, submarine volcanic flanks, and carbonate platforms (Wynn et al., 2002; Symons et al., 2016; Slootman & Cartigny, 2020; Casalbore et al., 2021). Subaqueous bedforms form at the interface between sediment and the water column, under the influence of unidirectional and bidirectional currents. They arise as free instabilities where random perturbations in the near-flat bed are amplified into geomorphic patterns by the interaction of the driving flow, sediment transport and bedform evolution (Van Dijk et al., 2020).

Subaqueous bedforms are primarily categorized based on their orientation, wavelength, and height, as outlined by Ashley (1990). The morphometric characterization in cross-section and in plan-view implicate the measurement of wavelength, height, asymmetry, and lee- and stoss-slope angles (Fig. 2.6), moreover the crest and troughs serve as fundamental markers for these parameters while in plan-view to describe the crestal sinuosity and 3-D shape (Allen, 1982) and the bedforms migration.

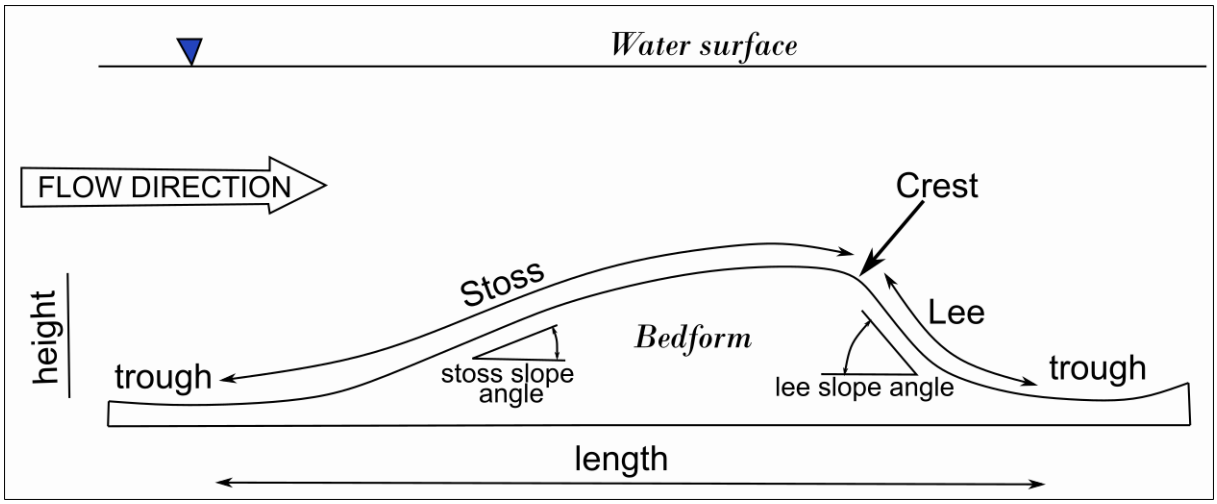

Figure 2. 6. Morphological elements of a bedform (modified from Cheel, R., 2016).

Laboratory experiments allowed categorizing and studying subaqueous bedforms. They have been classified and named according to characteristics of their shape and the forming flows. A unidirectional flow in a free-surface is defined as sub- or super-critical according to the Froude number (Cartigny et al., 2014). This number is adimensional and is given by the formula:

$$Fr = \frac{U}{\sqrt{gh}} \quad (2.1)$$

Where U is the depth-averaged downstream flow velocity, h the flow depth and g the acceleration of gravity. Such flows can be further characterized (Fig. 2.7) by: (i) a Reynolds number that distinguishes between turbulent and laminar flows (Robertson & Rouse, 1941); and (ii) the Vedernikov number, which distinguishes stable uniform flows from unstable non-uniform ones (Chow,1959; Koloseus & Davidian, 1966). Stability fields in Fig. 2.7 show the difference between the various bedforms types in relation to their formative flow. Below, key bedform types for this work are described in more detail.

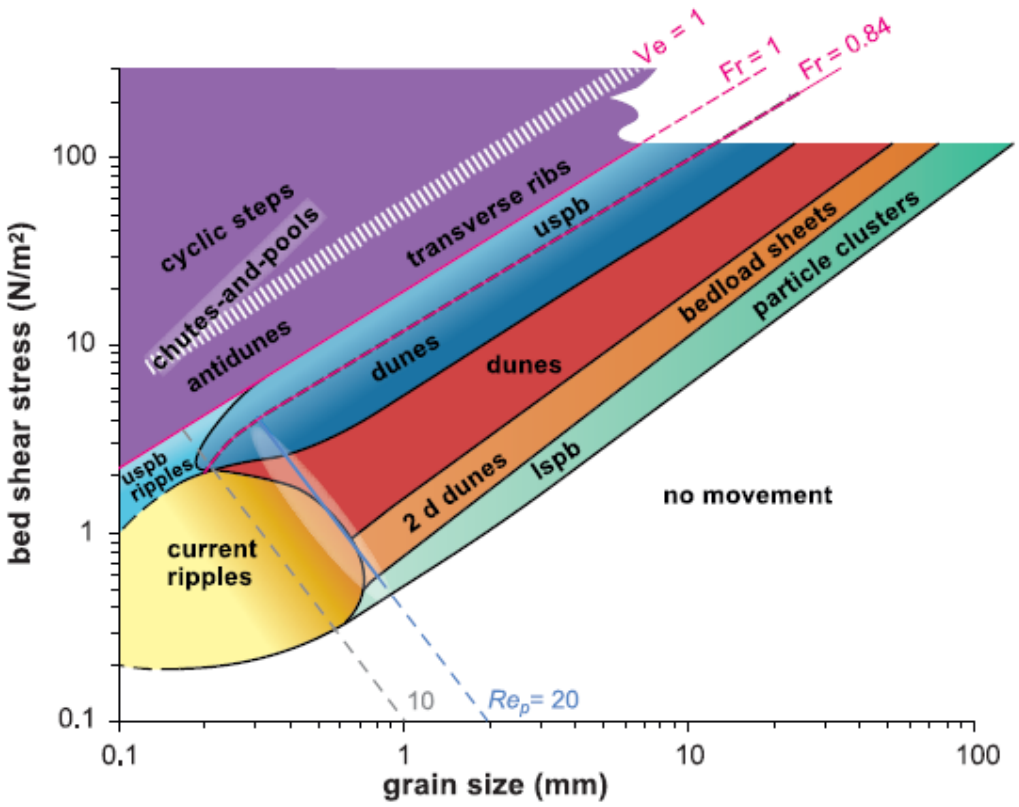

Figure 2.7. Stability fields diagram of bedforms types according to grain-size range under unidirectional flow. Colours indicate the increasing importance of grain roughness and/or formation and deterioration of bedforms. Dotted lines within stability fields indicate a gradual shift between various bed states, while solid lines signify a sudden transition. The stability areas of supercritical flow bedforms are based on Cartigny et al. (2014). The values of Froude and Vedernikov numbers are represented by the dashed pink lines and shaded zone, respectively, but may not align with shear stress values on the y-axis. The blue line designates the shear stress values associated with the threshold for the transition from ripples to dunes. The yellow to orange gradient highlights the area where ripples overlay dunes. The white oval marks the scale gap in bedform dimensions. Legend: lspb = lower stage plane bed; uspb = upper stage plane bed (from Van Dijk et al., 2020).

DUNE: Dunes are large bedforms forming in sub-critical conditions when the Froude number is below 1. They are stable in a wide range of sediment grain size (Fig. 2.7) (e.g. Kleinhans, 2001). They travel downstream and are characterized by erosion on the stoss side and deposition on the lee side (Fig. 2.8). In marine environments, they have been observed in both shallow and deep zones (Van Dijk et al., 2020). Dunes are flow-transverse bedforms, with regular wavelengths in the order of 1 to hundreds of meters, and heights between 0.1 and 10 m.

At Froude numbers greater than 1, a range of supercritical bedforms is generated by unidirectional flows (Fig. 2.7) that comprises antidunes and cyclic steps (Van Dijk et al., 2020).

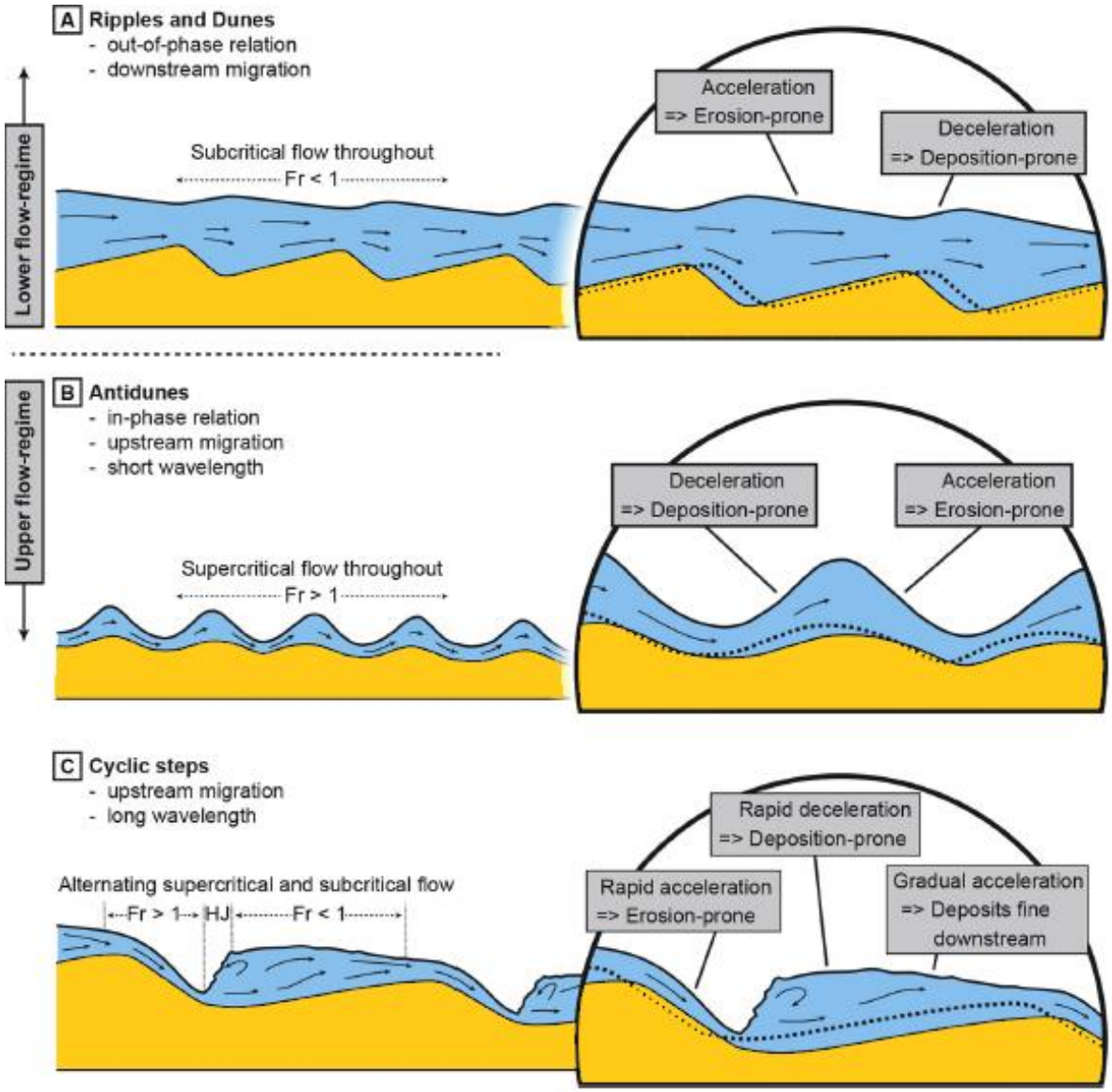

Figure 2. 8. Bedforms terminology for lower (A) and upper flow-regimes (B, C) and main differences. (A) Ripples and dunes form in Froude-subcritical flow regime (Fr <1) while antidunes (B) form in Froude-supercritical flow regime (Fr >1). (C) Cyclic steps differentiate by alternating Froude-subcritical and supercritical flow regime. HJ: hydraulic jump is where the transition from Froude-supercritical to subcritical flow occurs. Changes in flow parameters (e.g., flow thickness) creates bedforms that vary orders of magnitude in size. Wavelength to flow thickness ratio as shown for antidunes and cyclic steps is representative (from Slootman et al., 2019).

ANTIDUNES: Antidunes form when a series of surface waves are in-phase with the bed surface and may be stationary or translate both upstream and downstream. Typically, they are characterized by erosion on the lee side and deposition on the stoss side (Fig. 2.8). Antidunes can thus be characterized by their mode of movement (stationary, up- or downstream migrating) and wave instability, e.g. stable (stationary) vs. unstable (breaking waves). Stable antidunes appear to be generated as the first supercritical flow bedform once a Froude number is exceeded (Fig. 2.7). As Froude number increases, antidunes become unstable as sediment is deposited in

the region of decelerating flow on the upstream side of the bedform, giving rise to cyclic steps (Cartigny et al., 2014).

CYCLIC STEPS: If the Froude number further increases from a chute-and-pool sequence, alternating reaches with supercritical and subcritical conditions, cyclic steps form (Cartigny et al., 2014; Lang et al., 2020). This term was coined by Parker in 1996 outlining the typical characteristic defined by erosion on the lee side and accumulation on the stoss side, divided by a hydraulic jump that embodies the change of the flow conditions (Fig. 2.8). Cyclic steps have a wide range of wavelengths and heights depending on the characteristics of the forming flow and the initial bed-slope (Kostic et al., 2011; Cartigny et al., 2011). Cyclic steps in rivers are thus typically up to several meters in length, but under turbidity currents cyclic steps can be 100 m long. These larger cyclic steps have also been termed “sediment waves” and occur on delta slopes and the levees of submarine channels (Slootman & Cartigny, 2020).

In the literature, cyclic steps are occasionally confused with antidunes (West et al., 2019), because of the presumed morpho-dynamic analogy of the flow behavior (Fedele et al., 2016; Koller et al., 2017, 2019) in laboratory studies. This is also attributable to the absence of well-constrained forming conditions at present. Nonetheless, it has been noticed that wave breaking in experiments involving density flows leads to the transformation of antidunes into cyclic steps. This suggests that the forming conditions are not still well constrained. However, it has been observed how wave breaking in experiments with density flows cause antidunes to evolve into cyclic steps (Spinewine et al., 2009; Fedele et al., 2016) increasing the ratio of wavelength to flow thickness (see also Parker and Izumi, 2000; Kostic, 2011; Yokokawa et al., 2016) and a change in flow regime from dominantly Froude-supercritical over antidunes to a repeated alternation of Froude supercritical flow down the lee side and subcritical flow over the stoss side of cyclic steps. Due to their increasing recognition on submarine environment, recently Slootman and Cartigny (2020) proposed a further classification for cyclic steps. They have been divided into four categories according to the ratio of the bed aggradation rate and bedform migration. The four main types describe the most common features in nature. Thus, cyclic steps can be considered fully or partially depositional or fully or partially erosional.

Cyclic steps are important because they can significantly enhance sediment transport efficiency (Sun and Parker, 2005) and play a key role in the initiation and maintenance of submarine channels (Fildani et al., 2013; Hizzett et al., 2017).

CHAPTER 3 – GEOLOGIC, GEOMORPHOLOGIC, CLIMATIC AND OCEANOGRAPHIC SETTINGS OF MADEIRA

Madeira Island is the youngest and largest (737 km²) volcanic edifice of Madeira Archipelago (Fig. 3.1), having emerged between 7-5.6 Ma (Ramalho et al., 2015). It is located in the North-eastern Atlantic Ocean, about 850 km off the SW coast of the Iberian Peninsula and 650 km off the Moroccan coasts. Volcanism is characterized by low rates of magma supply and is likely still active. The latest dated event occurred at ~6 ka (Geldmacher and Hoernle, 2000; Geldmacher et al., 2000, 2006), although field observations suggest several other Holocene eruptions. Coeval chronicles describe the observation of a column of "fire" rising from the sea East of the island following the strongest earthquakes felt in Madeira on March 31, 1748 (Silva & Meneses, 1978). The description is compatible with a historical shallow submarine eruption (Brum da Silveira et al., 2010).

From a geological point of view, the archipelago also includes the islands of Porto Santo (43 km²) and Desertas Islets (14 km²), which form a triple radiated configuration (Fig. 3.1). Due to their configuration, Desertas Islets are considered the expression of one arm of a volcanic rift intersecting Madeira Island (the other arm) at an angle of ~110° and surrounded by the 200 m isobath (Klügel et al., 2009). The origin of the archipelago has been associated to a hotspot-track produced by a mantle plume within the slow-moving Nubian plate (about 1.2 cm/yr), moving towards the NE, represented by the alignment of Madeira and Porto Santo Islands, the seamounts Seine, Ampère, Coral Patch and Ormonde, and Serra de Monchique (Geldmacher et al., 2000; Fig. 3.1). An alternative interpretation considers that the magmatism in Madeira is the result of the interplay between a mantle plume and lithospheric fractures (Brum da Silveira et al., 2010).

The islands group is also part of the biogeographic region of Macaronesia that is formed by Selvagens Islets and the Archipelagos of Azores, Canaries and Cape Verde (Carracedo &Troll, 2020).

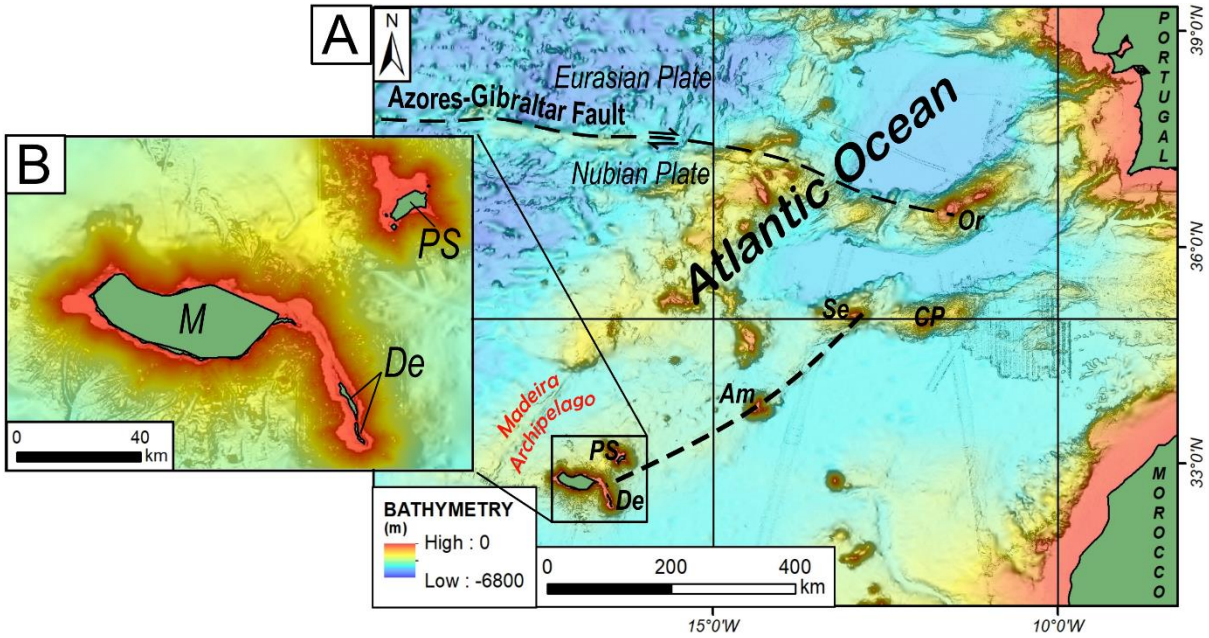

Figure 3.1. (A) Geographic setting of Madeira Archipelago in the Eastern North Atlantic (from open-access EMODnet bathymetry). Azores-Gibraltar Fracture Zone (AGFZ) according to Geldmacher et al., (2000); PS: Porto Santo; De: Desertas Islands; Am: Ampère; Se: Seine; CP: Coral Patch; Or: Ormond Seamount. (B) Inset zoom of Madeira Island within the archipelago. M: Madeira.

3.1. GEOMORPHOLOGY

Madeira Island has an elongated shape in the WNW-ESE direction, with a maximum length of 58 km and 23 km in width (along the N-S direction). It represents the emerged tip of a much larger shield-volcano that rises 6 km from the seafloor (Ramalho et al., 2015). The emergent part corresponds to 4,5 % of the volume of the volcanic edifice, estimated to be about 9000 km³ (Ribeiro & Ramalho, 2009). The island's maximum elevations are located at Pico Ruivo (1860 m a.s.l.), Pico das Torres (1853 m a.s.l.) and Pico Areeiro peaks (1810 m a.s.l.), and 25 % of area stands above 1000 m a.s.l. (Ribeiro, 1985; Fig. 3.2).

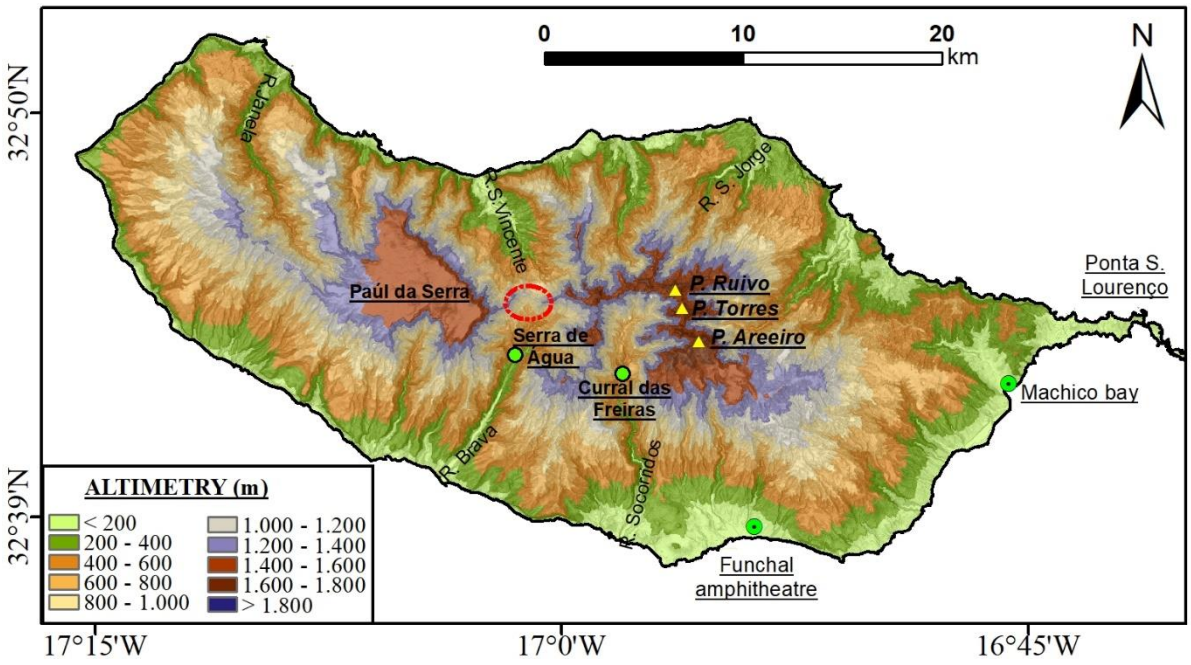

Figure 3. 2. Altimetry of Madeira Island. The valleys of Ribeira Brava and Ribeira de S. Vicente streams separates the west and east regions of the island (red dotted circle). Yellow triangles represent the highest peaks of the island, simple green dots represent the valleys where the headwaters of the two longest southern streams are located.

Conventionally, Madeira Island is divided in two main morphologic units, the "Maciço Vulcânico Central" and the "Litoral" (Ribeiro & Ramalho, 2009; Fig. 3.2).

The Central Volcanic Massif (Maciço Vulcânico Central) corresponds to the high ranges of the island. It is separated into a West and East region by Ribeira Brava and Ribeira de S. Vicente valleys (Fig. 3.2).

The West Massif is characterized by Paul da Serra Plateau standing between 1300 and 1500 m above sea level (Fig. 3.2). It is the result of Upper Pleistocene volcanism, but its morphology is smoothed by glacial erosion, possibly during the last glacial period, around 24-18 ky ago. This is evidenced by glacial deposits and morphologies such as till, moraines, U-shaped valleys, roches moutonées, and cirques or amphitheaters in the south edge of the plateau (Brum da Silveira et al., 2006). The West Massif is dominated by the highest peaks such as Pico Ruivo (1861 m), Pico das Torres (1851 m), and Pico do Areeiro (1811 m). The peaks are separated by deep fluvial valleys, the most important of which are Ribeira Brava (whose headwaters are located at Serra de Água depression), Ribeira dos Socorridos (Curral das Freiras), and Ribeira de S. Jorge (Fig. 3.2).

The Littoral area is mostly characterized by tall cliffs, especially on the north and west coasts, locally punctuated by littoral platforms (fajãs) of volcanic (lava deltas) or gravitative (landslides) nature. In the north, taller cliffs are the result of faster coastal retreat due to the

exposure to dominant winds and wave action and to large flank collapse episodes (Brum da Silveira et al., 2010; Quartau et al., 2018). In the southern littoral, the cliffs are only interrupted by the Funchal amphitheater, by Machico bay (Fig. 3.2) and by the mouth of major streams (see Table 3.1 and Fig. 3.3). The hydrographic network is well developed on both slopes, and it is constituted mainly by short and steep torrential streams that have a high erosional potential. The almost absence of river captures, and the poorly evolved valley slopes attest to the youth of the drainage system.

On the east, the narrow peninsula of S. Lourenço links Madeira with the Desertas islets at the -250 m bathymetric curve (Fig. 3.1).

Table 3. 1. Characteristics of the main hydrographic basins of Madeira Island by alphabetic order (adapted fromTeixeira, 2010). ID numbers refer to Fig. 3.3.

ID number/ Hydrographic basin/ stream	Hydrographic basin area (km^2)	Hydrographic basin perimeter (m)	Average altitude (m)	Average slope of the hydrographic basin (%)	Length of main stream (m)	Average slope of main stream (%)
1. Brava	41.225	31.869	755.02	74.11	13.643	11.29
2. Faial	49.939	31.688	712.49	72.17	14.526	10.27
3. Janela	51.092	44.565	843.15	53.21	21.987	7.11
4. João Gomes	12.750	22.82	847.74	45.19	10.220	12.94
5. Machico	24.528	24.967	394.84	42.81	12.384	8.36
6. Madalena	9.756	16.418	742.36	44.55	6.545	21.32
7. Ponta do Sol	19.339	25.013	836.92	55.67	11.842	13.22
8. Porto Novo	17.282	24.398	552.43	36.81	12.913	10.68
9. Santa Cruz	12.854	19.308	556.42	35.71	10.329	12.33
10. Santa Luzia	14.442	23.109	826.57	52.01	11.490	13.50
11. São João	14.64	24.21			11.51	
12. São Jorge	32.021	25.403	646.41	59.56	10.409	13.44
13. São Vicente	37.545	27.928	746.67	76.69	10.291	15.94
14. Seixal	14.056	21.569	875.02	74.55	10.472	14.93
15. Socorridos	38.691	35.285	796.86	74.84	16.766	9.74
16. Tabúa	8.862	16.831	684.27	62.13	7.604	19.76

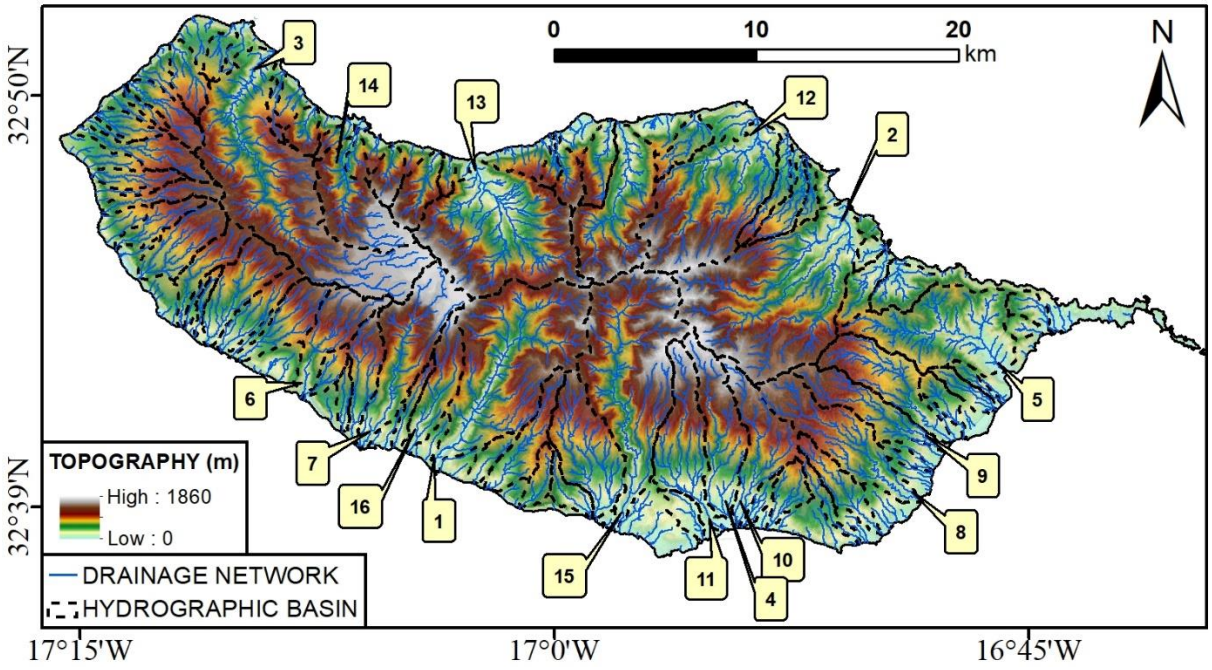

Figure 3.3. Main hydrographic basins and network drainage of Madeira Island. ID numbers indicate the main streams described in Table 3.1.

3.2. CLIMATE AND OCEANOGRAPHY

In this temperate region (> 30° N), the weather is predominantly influenced by the Azores Anticyclone. The relief of the island operates as a barrier to the prevalent NE trade winds, causing higher precipitation in the north-facing slopes (Prada et al., 2005).

The average annual precipitation is around 600-800 mm on the south coast and 1500-2000 mm on the north (Fig. 3.4A). Rainfall often concentrates in short periods making the island very prone to flash floods and subaerial landslides (Baioni, 2011).

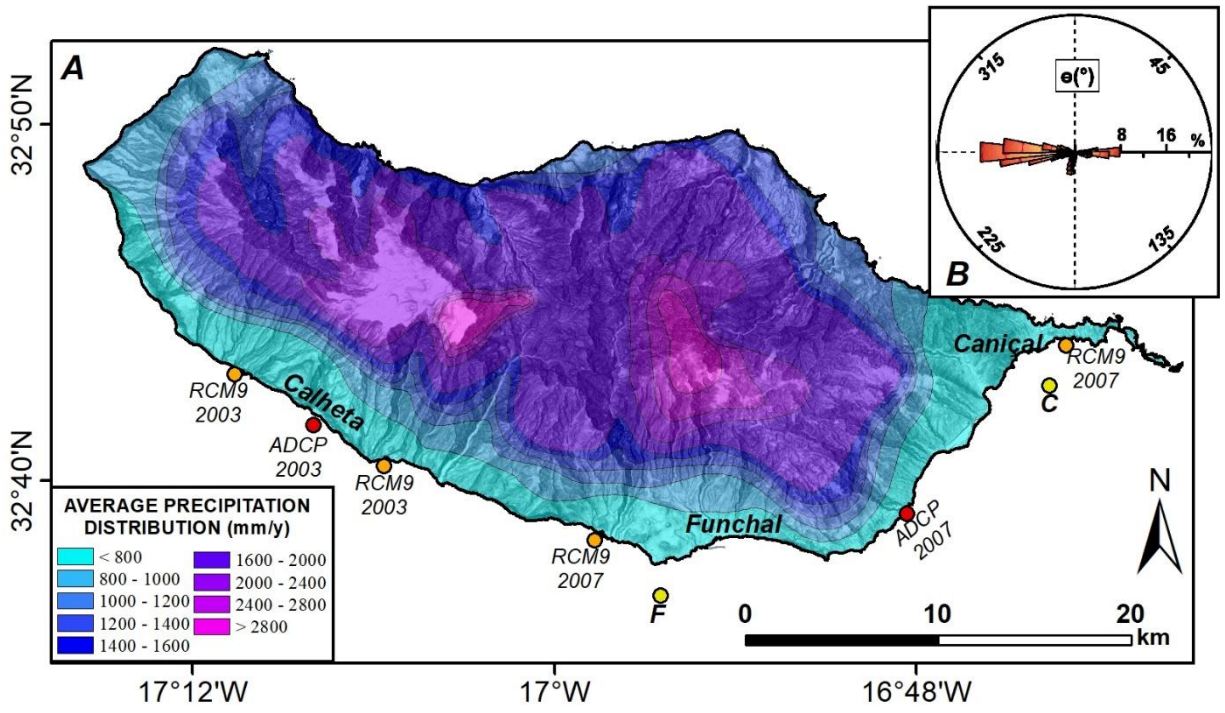

Figure 3.4. A) Distribution of average annual precipitation between 1961 and 1990 (from Atlas do Ambiente, 1995) and B) Rose chart of the main wave regime in the 1996 - 2002 period (from Fortes et al., 2006). Green dots represent the buoy location off Funchal (F) and Caniçal (C). Orange dots the RCM9 current metric stations while red dot ACDP location.

According to Rusu & Guedes Soares (2012), from 1997 to 2002, 96% of the waves hitting Madeira Archipelago had significant wave heights between 1 and 6 m and more than 50% come from the NNW, 27% from WNW, 19% from the NNE and only 3% from the SSW. However, the southern side of the island is influenced by wave propagation driven by refraction-diffraction processes. The tide regime is semi-diurnal, high and low tide occur simultaneously along the coast and with the same amplitude in the whole archipelago (Instituto Hidrográfico, 2001).

Oceanographic analysis was carried out by *Portuguese Hydrographic Institute* with data collected between November 1989 and December 2006 using *Datawell Waverider* buoys. They have defined the wave regime in the west and east parts of the south coast. Furthermore, average and seasonal wave regime (wave height, average and peak periods and the main direction related to peak time) are reported on Tables 3.2 and 3.4. They are related to Funchal and Caniçal offshore wave stations (green dots in Fig. 3.4A; Instituto Hidrográfico, 2007). Additionally, data collected on July 2003 and April 2007, respectively with *RCM9* and *RDI ADCP* (acoustic doppler current profilers, 600 Khz) instruments at 3 stations in 2003 and other 3 stations in 2007 (Fig. 3.4) gave information about currents at -20 m. Offshore Calheta, the total current (residual + tide component) and parallel to the coast is between 8 and 12 cm/s with NW-SE direction while the residual current is about 6 cm/s maintaining the same direction during fair-

weather conditions (Instituto Hidrográfico, 2003). Offshore Funchal, the transport velocity is between 7 and 14 cm/s with N-S direction and 7 to 20 cm/s with W-E direction. The residual bottom current is about 2 cm/s parallel to the bathymetry. Conversely, the residual bottom current offshore of Caniçal is mostly influenced by the tide regime and reaches 6-7 cm/s (Instituto Hidrográfico, 2007). Nevertheless, these measurements refer to a short-term period that cannot be used to represent the annual wave regime.

Table 3. 2. Average wave regime recorded to the south of Madeira Island (Instituto Hidrográfico, 2007).

	Funchal (average ± st. deviation)	***Caniçal*** (average ± st. deviation)
Hm0 (m - significant wave height)	0.85 ± 0.48	0.58 ± 0.32
T0 (s - mean period)	5.5 ± 1.1	4.5 ± 0.8
Tp (s - peak period)	9.9 ± 3.2	9.5 ± 3.8
Θ (main direction related to peak period)	W (51%) E (19%) S (16%)	S (39%) E (36%) SE (21%)

Table 3. 3. Seasonal wave regime surrounding the south of Madeira Island (Instituto Hidrográfico, 2007).

	Funchal				***Caniçal***			
	Summer		Winter		Summer		Winter	
	min	*max*	*min*	*max*	*min*	*max*	*min*	*max*
Hm0 (m)	<1	<3	0.8	<5	1	2.3	2	4
	mean	*max*	*mean*	*max*	*mean*	*max*	*mean*	*max*
T0 (s)	4	11	6	12	<4	10	4	8
Tp (s)	9	20	11	20	10	20	8	20
Θ (%main directions)	W (41.4%) E (23.8%) S (21.9%)		W (61.3%) E (14.1%)		S (44.1%) E (38.2%)		S (34%) E (33.4%) SE (29.8%)	

Just a few strong stormy events (considering wave-height >3 m) were recorded off the southern shore of the island during winter (November to March) coming mostly from the W and SW. Stormy events characterized by significant wave height of more than 6 m are tentatively estimated to have a return-around period >100 years (Instituto Hidrográfico, 2003).

3.3. VOLCANO-STRATIGRAPHY AND MAIN TECTONIC STRUCTURES

The volcano-stratigraphy used in the most recent geologic map of Madeira Island (Brum da Silveira et al., 2010a, b, c) divides the island evolution in three main stages (CVI, CVM, and CVS in Fig. 3.4), corresponding to different growth phases of the volcanic edifice. They are named: Lower (CVI – Complexo Vulcânico Inferior > 5.57 Ma), Middle (CVM – Complexo Vulcânico Intermédio 5.57 – 1.8 Ma) and Upper (CVS – Complexo Vulcânico Superior 1.8 – 0.007 Ma) Volcanic Complexes.

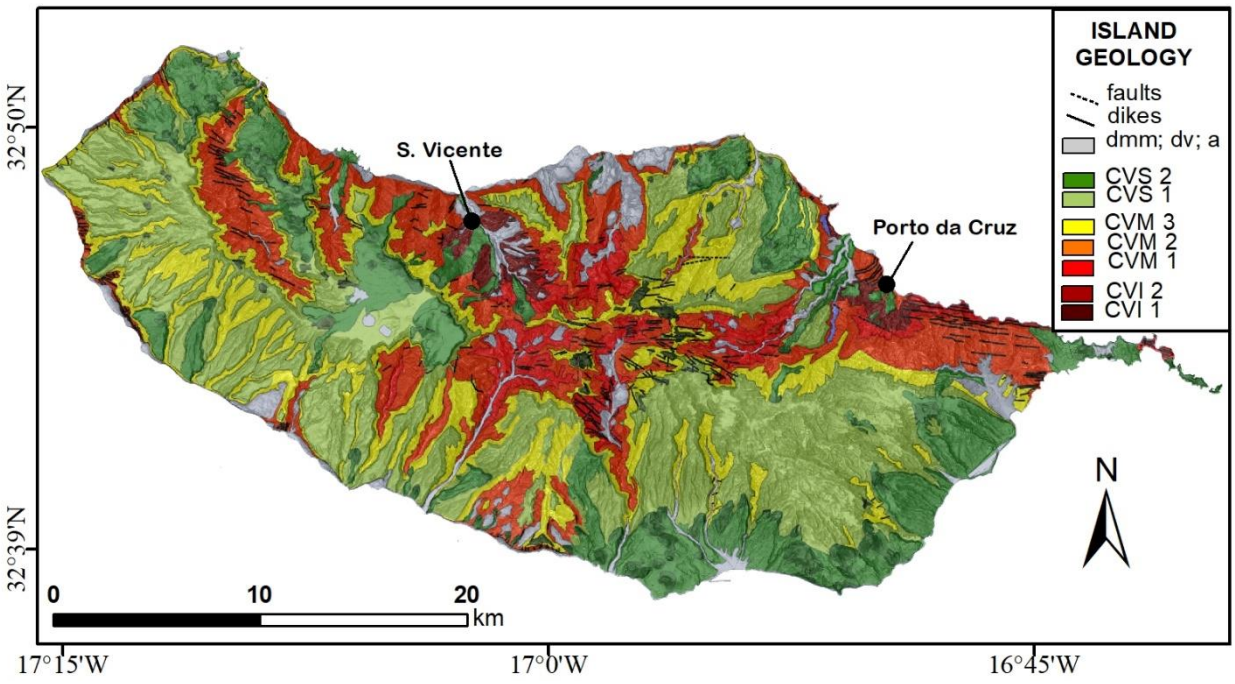

Figure 3. 5. Simplified geological map of Madeira Island (adapted from Ramalho et al. 2015). CVI: Lower Volcanic Complex (1-Porto da Cruz Formation, 2-Lameiros Formation); CVM: Middle Volcanic Complex (1-Encumeada Formation, 2-Penha d'Águia Formation, 3- Curral das Freiras Formation); CVS: Upper Volcanic Complex (1-Lombos Formation, 2-Funchal Formation); dmm, dv, a: mass wasting deposits, colluvia and slope deposits, alluvial deposits, respectively.

The Lower Volcanic Complex includes lithologies representing the oldest phase exposed above sea level, corresponding to the latest submarine and emergent phases. These rocks of mafic composition are so strongly weathered that a clear identification of volcanic products is not

possible, although they are interpreted as palagonitized submarine volcanic products (Brum da Silveira et al., 2010 a, b, c). This unit is intensely cut by dikes of all volcanic complexes. It is only exposed in two valleys (S. Vicente and Porto da Cruz) in the northern slope of the island.

The Middle Volcanic Complex corresponds to the construction of the subaerial shield volcano. This embodies the most important construction stage characterized by intense volcanism alternated with periods of reduced or absent activity, marked by two unconformities that divide the CVM into three units. These units crop out throughout the whole island and mostly on the slopes of the deepest valleys.

The Upper Volcanic Complex is related to the most recent volcanic activity (two units corresponding to the capping and post-erosional stages). Its formations are present through the whole island, mostly on the upper part of the interfluves (capping formations) and flowing into valleys or over sea-cliffs (post-erosional stage formations).

As indicated, the three main Volcanic Complexes are further divided into several units, separated by regional unconformities. The unit names derive from the local or area where the best-developed outcrops are displayed or by typical morphologies (e.g. Lombos Formation, referring to flat-topped interfluves). From the oldest to the youngest, the stratigraphic sequence is composed of the following units:

- The Porto da Cruz Formation is the older member of the Lower Complex. It comprises extremely weathered products of hydro-magmatic origin which are intensely intruded by dikes. Its rocks have a mafic composition, are strongly palagonized, and its internal structure is unclear due to intense weathering. This formation crops out inside the S. Vincente and Porto da Cruz valleys, up to the elevation of 700 m.

- The Lameiros Formation is the upper member of the Lower Complex. It is composed of a sequence of shallow-water calcareous marine sediments covered by coeval volcanic products (basaltic lava flows and block and ash flows). Together with the Porto da Cruz Formation, they reflect the final stage of the submarine phase of the volcanic edifice. This formation is exposed in the right bank of the valley of S. Vincente as isolated outcrops at about 320-430 m of elevation (Ramalho et al., 2015). The limited outcrop area is due to the cover by landslide and alluvial fan deposits of the lower half of the valley slope. The marine sediments are dominantly made up of conglomerates and microconglomerates, limestones and fossiliferous calcarenites. The fossiliferous content is compatible with a reef facies of a shallow open shelf. The marine sediments were covered by a basaltic lava flow and a

pyroclastic flow that produced peperitic interaction and caused deformation and metamorphism of the still soft sediment. The presence of this formation at those elevations supports the hypothesis that uplifting processes played a key role in the island emergence Ramalho et al. (2015).

- The Encumeada Formation is the lower unit of the Middle Complex. It crops out inside S. Vincente, Ribeira Brava and Serra de Água valleys, in the upstream half of the Boaventura valley (Ribeira do Porco), in Curral das Freiras depression, in the cliffs of the Faial / Ponta dos Clérigos region, in the Porto da Cruz area and at the base of the coastal cliffs. It is characterized by subaerial strombolian volcanic products of mafic composition, both explosive and effusive. They are strongly weathered and densely cut by dike swarms. This formation constitutes important paleo-reliefs in the Encumeada, Curral das Freiras, Fajã da Nogueira, and Faial areas where it reaches heights of up to 1600 m in elevation. This represents the first phase of the subaerial shield volcano construction.

- The Penha D'Águia formation, the second unit of the Middle Complex, is the most voluminous and expanded on the island. This unit corresponds to the period during which a huge volume of lava was extruded and includes effusive and explosive activity products of strombolian, hawaiian and phreatomagmatic nature. This formation crops out along the entire north coast, as patches in west cliffs and in the south and east coastal areas of the island up to Ponta de S. Lourenço. It is characterized by lava flow sequences or pyroclastic deposits locally cut by dyke swarms such as at Ponta de S. Lourenço and Jardim do Mar cliffs. Lahar, mudflow, and stream flow deposits are also interbedded within this formation. They correspond to the partial filling of valleys during intense erosional events.

- The Curral das Freiras Formation is the uppermost unit of the Middle Complex. It corresponds to the subaerial westward growth of the edifice. It is mainly present in the western coast and in the northern littoral. It is separated from the previous unit by a marked discordance as observed along the cliffs of Cabo Girão and Curral das Freiras slopes. It is typically composed of weakly weathered effusive products of hawaiian or strombolian subaerial activities. Moreover, phreato-magmatic products were also recognized. This unit marks the final period of the shield-building phase.

- The Lombos Formation is the lower unit of the Upper Complex and corresponds to the capping stage of the previous shield volcano configuration. It is formed by subaerial mafic products including lava flows and less abundant pyroclastic deposits and lahars. The main

vents display a fissural geometry and are preserved in areas such as Paul da Serra and eastern Maciço Central. The products of this formation cover the less dissected structural surfaces of the shield volcano or fill valleys where the shield volcano was already incised by a coeval drainage; they crop out in the upper parts of morphologies, and constitute flat interfluve tops, locally surrounding acute crests carved in older formations. Its weathering degree is variable, ranging from weak to intense, probably due to the conjugation of geochemical characteristics of the erupted materials and geographical position.

- The Funchal Formation is the upper unit of the Upper Volcanic Complex (CVS), and the youngest in Madeira. It corresponds to a post-erosive volcanic stage. Its products frequently cover young erosional morphologies such as fluvial valleys and sea cliffs. It comprises weakly weathered products of subaerial or littoral mafic activity (hawaiian, strombolian and surtseyan) and minor trachyte pumice fall-out pyroclastic deposits related to submarine plinian or phreato-plinian activity. Particularly, mafic subaerial products were identified from Porto Moniz to Ponta S. Lourenço, in flat areas such as Paul and S. António da Serra and in the south-side, from Câmara de Lobos to Machico. Surtseyan morphologies related to this formation are Ilhéu Mole and another cone in Porto Moniz area. Furthermore, surtseyan products were observed at Ilhéu do Farol and Praia Formosa. Its products fill the Funchal amphitheater (a flank collapse scar), where abundant hawaiian-strombolian cones still display a pristine morphology. The youngest dated eruption (6-7 ky; Geldmacher and Hoernle, 2000) corresponds to a hawaiian-strombolian event that occurred inside the valley of one of Ribeira de S. Vicente tributaries, whose pyroclasts covered the eastern part of the Paul da Serra plateau driven by winds from the north-east quadrant.

In Madeira Island, granular intrusive rocks and dykes were also observed. Granular intrusive rocks crop out in small areas in Voltas and Massapez streams at Porto da Cruz region. They are composed of gabbroic rocks and display some metasomatism. Intrusions of trachytic composition occur inside the valley of S. Vicente. The age of both the gabbro and trachyte intrusions has not been determined yet, but are probably related to the Lower or Middle Volcanic Complexes. Dyke swarms, marking the feeding volcanic rift areas of the shield volcano, are particularly abundant in Maciço Central and Ponta S. Lourenço areas. Their presence and orientation are connected to the evolution of the island. During the Lower and Middle Volcanic Complexes, the dyke systems have a dominant E-W direction, changing to an WNW-ESE to NW-SE during the capping and post-erosive phases. The dyke composition is

predominantly mafic, but occasional trachytic dykes occur in Boaventura and in S. Vincente valleys.

In the new geologic map (Brum da Silveira et al., 2010a, b), the sedimentary morphologies and products related to recent sedimentary and erosional processes are also mapped and described. These include:

- Alluvial products, characterized by fluvial heterogeneous gravel and coarse sand deposits. Their composition is related to the lithotypes cropping out in the area. Being the result of fluvial action, their characteristics depend to the importance of the stream. The larger alluvial valleys are those of Janela, S. Vicente, S. Jorge, and Faial streams in the north slope, and Brava, Socorridos, Santo António, Santa Luzia, João. Gomes, Porto Novo and Machico streams, in the south flank of the island.
- Beach deposits are present along the island littoral. Generally, sediment is composed of varied-sized gravel. The most important sand beaches are in the south-shore (Praia Formosa and Praínha) and in the north coast between Porto da Cruz promontory and Penha de Águia.
- Aeolian deposits are present in the central zone of Ponta S. Lourenço. They are constituted by fine sand with a light colour due to of dominant marine bioclast nature. These were dated by ^{14}C, amino acid epimerization, and U-Th dating methods (Goodfriend et al, 1996) yielding ages ranging from the Middle Pleistocene (200 - 300 ka) to the Holocene (8500 - 4500 BP).
- Landslide and mass-wasting deposits are widespread throughout the island on sea-cliffs and steep valley walls. The typology of the largest mass-wasting events includes rotational and translational landslides, while toppling and rock-fall smaller events are extremely common. Major flank collapses affected the north coast of Madeira in the Porto Moniz-Ponta de S. Jorge area (mega-landslide of S. Vicente Bay) and Porto da Cruz, and the south flank of the island from Cabo Girão to Machico (Funchal mega-landslide). These large subaerial scars have been correlated to impressive submarine landslide morphologies observed offshore these localities (Quartau et al., 2018; Fig. 3.7). Several large secondary landslides are found along the littoral of S. Vicente Bay. Smaller-scale deposits occur in Penha de Águia and Cabo Girão, Ribeira dos Socorridos, Curral das Freiras, Fajã do Marques, Boaventura and Fajã da Nogueira (rotational landslides) and São Jorge and Calheta Arc (translational landslides).
- Glacial and peri-glacial deposits are found in the higher regions of the island, such as periglacial deposits in Pico do Areeiro and Pico Ruivo, and glacial deposits and morphologies in Paul da Serra (moraines and till deposits).

Satellite imagery analysis of Madeira Island revealed three lineament families trending WNW-ESE, E-W and NNE-SSE (Fonseca et al., 1998 a, b; Fig. 3.6). The Seixal-Machico is the most important lineament in the island corresponding to a fault that extends for 38 km. It crosses the volcanic edifice in the E-W direction. It is well exposed at Quebrada Nova cliff on the west coast. This fault does not affect the younger sequences of the CVS. The island evolution was initially controlled by E-W to WNW-ESE oriented structures, mainly represented by major volcanic rift-zones marked by dike swarms. These structures controlled the elongated shape of the shield volcano. During the younger volcanic stage (CVS) there was a structural reorganization in the island, with the eruptions controlled and fed NW-SE trending structures widespread throughout the island, morphologically expressed by alignments of the CVS cones (Brum da Silveira et al., 2010c; Fig. 3.7).

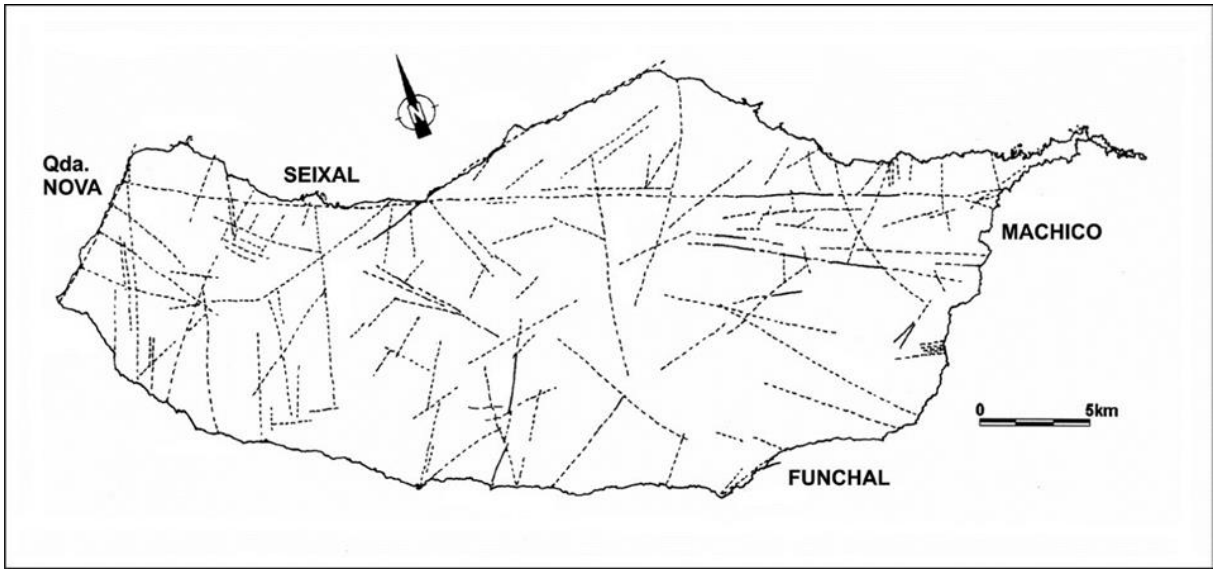

Figure 3. 6. Simplified sketch of the main lineaments in Madeira Island deduced from satellite imagery (Fonseca et al., 1998 a, b).

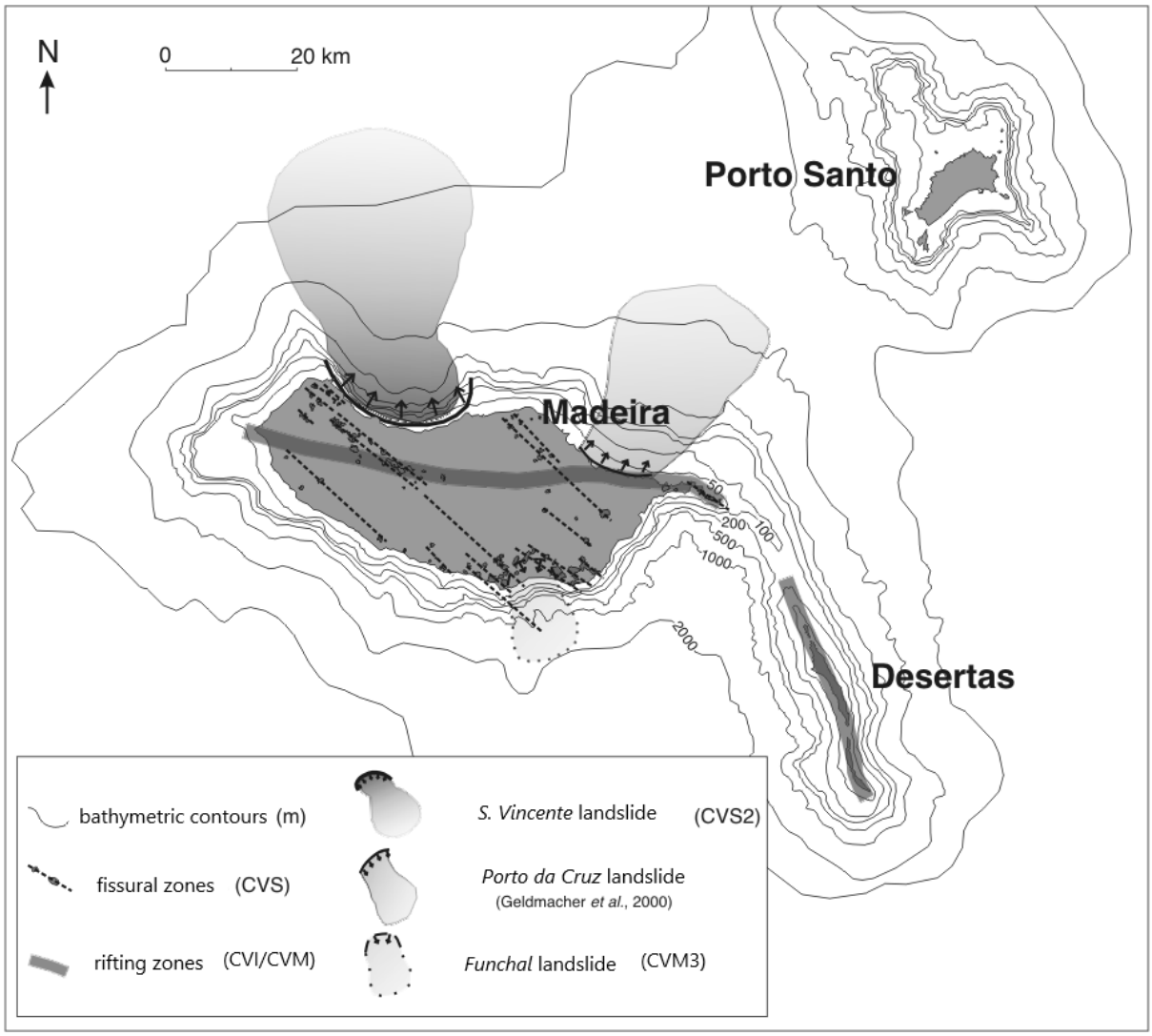

Figure 3.7. Main volcano-tectonic features of Madeira Island, main landslides and the bathymetric curves surrounding the Madeira-Desertas and Porto Santo group (modified from Brum da Silveira et al., 2010c).

3.4. GEOLOGICAL HAZARD

The island's morphology and climate regime make Madeira subjected to a series of potential geological hazards. These are mostly related to landslide processes and flooding. The latest is the most dangerous and recurrent risk affecting the island's communities (Brum da Silveira et al., 2010c).

Landslides

Landslide morphologies and deposits are present throughout the whole island. The most voluminous landslides are pre-historical and correspond to large flank collapses of the volcanic edifice (Brum da Silveira et al., 2010c; Quartau et al., 2018, Fig. 3.7). These include the S. Vicente, Porto da Cruz and Funchal collapses whose debris avalanches cover areas ranging

from 500 to 4000 km^2 (Quartau et al., 2018). The recent landslides affect mostly steep valley slopes cut on the older and intensely weathered stratigraphic units due to their extreme geotechnical weakness, or occur at tall and steep sea cliffs (Brum da Silveira et al., 2010c). Sea cliff collapses may additionally trigger local tsunamis, such as the one produced by the Cabo Girão landslide in 1930 that resulted in 19 fatalities in the nearby harbour of Câmara de Lobos (Omira et al., 2022).

Seismic events

The most intense seismic event occurred on the 31st of March, 1748, probably related to a submarine volcanic eruption off Ponta de S Lourenço (Silva & Meneses, 1945 in Brum da Silveira et al., 2010c). Since the volcanic edifice of Madeira is still active, future episodes like this are not excluded. However, seismic events are sporadic, usually located at sea, and characterized by very low magnitudes (Brum da Silveira et al., 2010c). Even though the intensity felt in the island is very low, they could trigger landslides in potentially unstable areas.

Volcanism

Geomorphological and geological observations indicate the occurrence of numerous Holocene to Upper Pleistocene eruptions in the island (Brum da Silveira et al., 2010c), which are corroborated by a radiocarbon age of 6-7 ka obtained for one of those events (Geldmacher et al., 2000). Furthermore, a historical account describes a column of "fire" rising from the sea following the strongest earthquake felt in Madeira in 1748 suggesting a near/shore submarine eruption.

Secondary volcanic manifestations are also observed on the island. They consist of concentrated emissions of CO_2 and small amounts of Radon ($_{222}Rn$). These exhalations were observed during tunneling works in the island. In some hydraulic galleries and road tunnels, such as in those of Fajã da Ama, Ribeira Grande and Fajã da Nogueira, water with temperatures higher than environment ones were also registered. All the above evidence supports the presence of an active volcanic system in Madeira.

Flooding

In Madeira flash-flooding events, transporting huge debris loads and flowing at high speeds towards the sea, are frequent (Brum da Silveira et al., 2010c). This is due to the morphology of the island characterized by very steep slopes and by very short streams, contributing to their torrential nature. Baioni (2011) revealed that only between 1941 and 1991, 46 of 56 total

damaging flash-floods occurred in the southern part of the island that is the most impacted by human activity. Besides the historical accounts, the geological record also presents evidence for the frequency of this type of deposits in the stratigraphy. An example is the downtown area of Funchal, built on a prehistoric debris fan. Most of the denser populated areas were subjected to catastrophic flooding events such as those of 1993 in Funchal, 1979 in Machico, and 1970 in Ribeira Brava. The floods represent the most dangerous and recurring hazard on the island (Baioni et al., 2011).

The latest catastrophic flood occurred on the 20th of February, 2010. During this event, at least 250 000 m^3 of debris were delivered into the central urban area of Funchal and more than 600 000 m^3 in Ribeira Brava area (Lira et al., 2013).

CHAPTER 4 – DATA AND METHODS

4.1 DATA

The data used in this work includes a Digital Terrain Model (DTM) of Madeira Island, the most recent geological map of Madeira (Brum da Silveira et al., 2010), multitemporal multibeam bathymetry, sparker seismic profiles and superficial sediment samples of the southern shelf. Additionally, the average annual precipitation from *Instituto do Ambiente* (Fig. 3.4; chap. 3); the dataset of daily accumulated precipitation from *Instituto Português do Mar e da Atmosfera* (IPMA), and the wave conditions around Madeira Island modelled with SWAN were also used. Below, a detailed description is given of the onshore and offshore data used.

4.1.1 ONSHORE DATA

Madeira Island DTM (Fig. 4.1) was published in 2018 and has been provided by *Infraestrutura Regional da Informação Geográfica of Madeira*. This DTM has cell size of 5 m and comprises elevations from 0 to 1840 m. The southern drainage basins and respective streams (Fig. 4.1) were delineated in the DTM of the island with several ArcGIS tools.

The geological map of the island has been georeferenced and the explanatory document provided by Brum da Silveira et al. (2010) was used to infer qualitatively the grade of erodibility of the outcropping formations.

The average annual precipitation (Fig. 3.4 chap. 3) from *Instituto do Ambiente* refers to data from 1961-1990. It was used to calculate the average precipitation for each Hydrographic basin (see sub-chap. 4.2.5).

The dataset of daily accumulated precipitation retrieved from *Instituto Português do Mar e da Atmosfera* (IPMA) obtained by 9 climatological weather stations on the southern slopes of Madeira Island (Fig. 4.1) covering the 2000-2020 period. These data were used to estimate the extreme rainfalls days that can lead to the occurrence of floodings (see sub-chap. 4.2.5).

4.1.2 OFFSHORE DATA

The main high-resolution multibeam bathymetry used in this study covers the southern shelf of Madeira Island from the coastline down to the depth of 175 m with a cell size of 4 m (from red to blue scale in Fig. 4.1). It was acquired on 2003 (SW part) and on 2007 (SE part) by *Instituto Hidrográfico*, the hydrographic office of the Portuguese Navy, onboard launches using a Simrad EM3000 echo-sounder and a DGPS system (Instituto Hidrográfico, 2003 and 2007). The

bathymetry covering the outer shelf down to 712 m (in grey colours in Fig. 4.1) was collected with Kongsberg EM710 system onboard R/V Gago Coutinho during 2013 and 2014 by *Instituto Hidrográfico*. It also has a cell size of 4 m. Further bathymetries were acquired in 2013 and 2019 by *Instituto Hidrográfico*. They have, respectively, cell sizes of 4 m (2013) and 1 m (2019). The 2013 bathymetry covers depths between 17 m and 300 m while the 2019 bathymetry goes from 13 m down to 198 m and only covers a small portion of the shelf (respectively red and blue polygons in Fig. 4.1). Their acquisition was carried out on board R/V *Gago Coutinho* with the Kongsberg EM 710 system. All the multibeam data was processed with CARIS-HIPS and tidal corrections were based on the Funchal tide gauge.

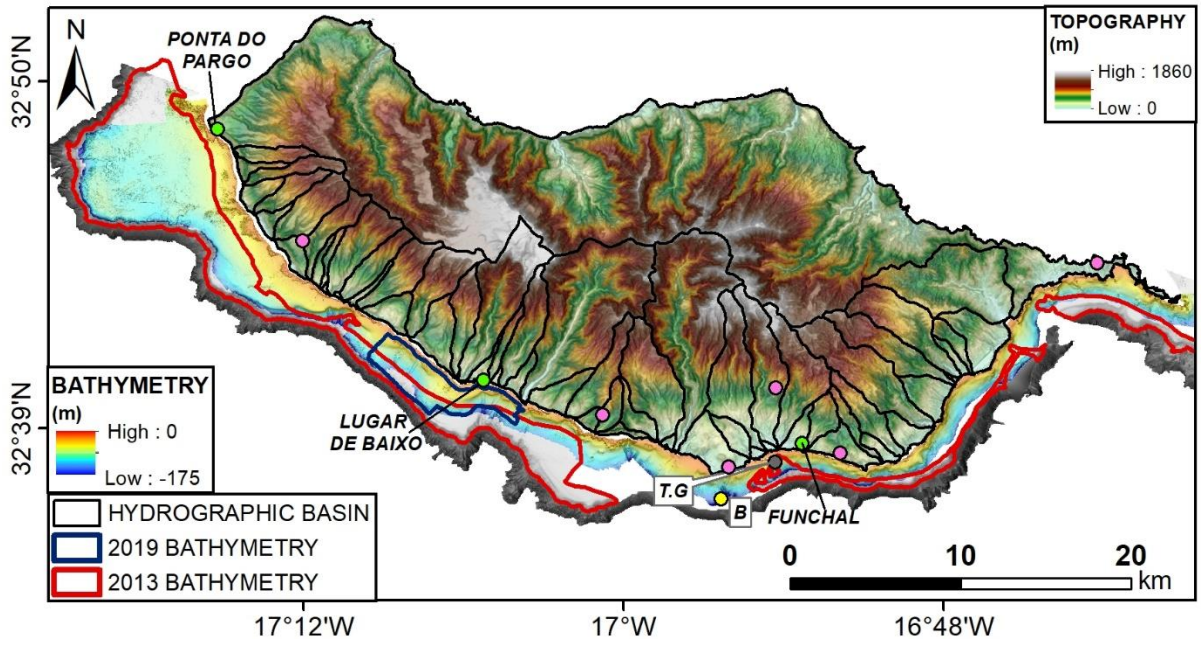

Figure 4. 1. Digital Terrain Model of Madeira Island and multibeam datasets of the southern shelf. The depth scale from red to blue refers to the 2003 and 2007 surveys. The shaded relief bathymetry in grey refers to the 2013 and 2014 bathymetries from the outer shelf to 712 m. Red polygons delimit the 2013 bathymetry and blue polygon delimits the one from 2019. Yellow dot represents Funchal wave buoy positioning (16.94° W, 32.62° N) and grey dot the tide gauge (16.92° W, 32.63° N) offshore Funchal. Green dots are the weather IPMA stations analyzed in detail, from the western to the east: Ponta do Pargo (17.26° W, 32.81° N), Lugar de Baixo (17.09° W, 32.68° N), Funchal Observatory (16.89° W, 32.65° N). Pink dots represent the locations of other weather IPMA stations not analyzed in detail. Black polygons enclose areas of the southern hydrographic basins delineated in this study. The offshore areas in white have no multibeam data.

The seismic profiles consist of 179 lines parallel and perpendicular to the coastline (Fig. 4.2). Perpendicular seismic profiles have variable lengths (from < 500 m to 1.5 km) and an average distance of 250 m (500 m of spacing if protected areas have been crossed during the acquisition). Seismic profiles were acquired with a Sparker system operating at 12 J, a frequency of 8 kHz, and an acquisition interval of 150 ms (Instituto Hidrográfico, 2003).

Sediment sampling was carried out by *Instituto Hidrográfico* in 2003 and 2007 onboard the launches *S. Roque* and NRP *Auriga* using a Smith-McIntyre grab sampler (Instituto

Hidrográfico, 2003, 2007). A total of 233 samples were collected on the southwestern shelf in 2002 and 175 samples on the southeastern shelf in 2007 from the coastline down to -500 m. Grain-size analyses were carried out at the sedimentological laboratory of Instituto Hidrográfico. The sediments were wet sieved with a 500 μm (1 Φ) mesh and the fractions retained were mechanically sieved using a set of sieves from 1 Φ (500 μm) to -5 Φ (31.5 mm) with an interval of 0.5 Φ. Particles finer than 1 Φ were measured by laser diffraction from 0.25 μm to 500 μm (12 Φ to 1 Φ). The grain-size statistical parameters were determined by the moment method (Folk, 1974, Instituto Hidrográfico, 2003 and 2007). These results were provided for my PhD thesis that I used to map the sediment distribution on the shelf and to calculate the critical shear stress necessary put sediments in motion. Finally, I used the sedimentological parameters (mode and the percentage of the fine fraction) to obtain the grain-size distribution on the entire shelf using the "*natural neighbor*" interpolation tool in ArcGIS (see section 4.1.4).

The total inorganic carbon and the total organic carbon (TIC and TOC) content of 117 samples (75 from the SW and 42 from the SE) used in this study were also carried out at the sedimentological laboratory of *Instituto Hidrográfico*. They were determined by Non-Dispersive Infra-Red detection (NDIR) using a Skalar PrimacsSNC-100 analyser (Skalar Analytical BV, Breda, The Netherlands). For the analysis, the sediment was first pulverised using a Retsch Ball Planetary Mill, model PM 100. Calcium carbonate ($CaCO_3$) contents were calculated from the TIC values multiplying them by 8.33 (Verardo et al., 1990).

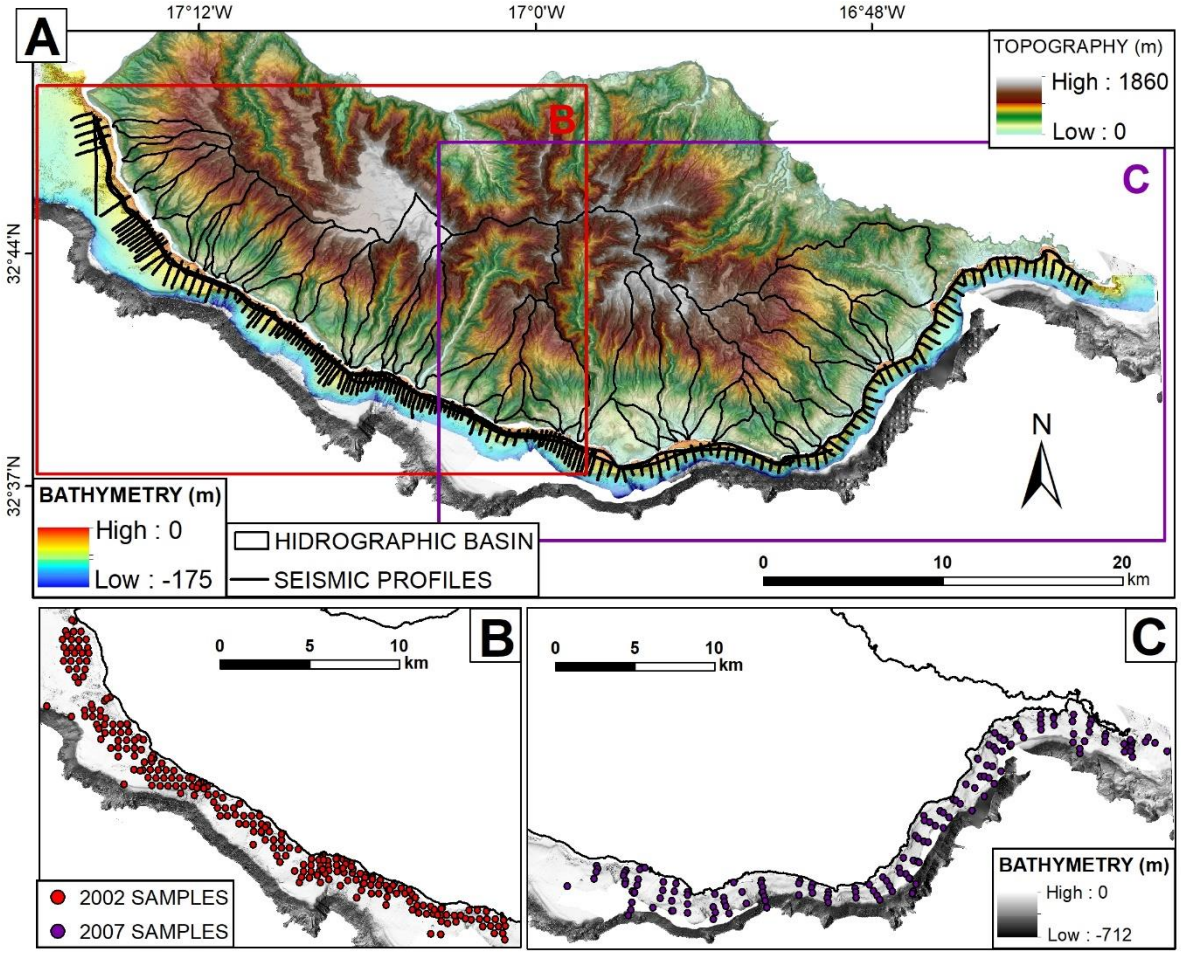

Figure 4. 2. (A) Seismic profiles and sediment sampling distribution used in this work. B) and C) are respectively zooms of the western and eastern shelf. Within each, the black lines indicate the coastline.

4.1.3 WAVE PROPAGATION MODELLING

Wave conditions around Madeira Island, were simulated in a four-level wave modelling system exclusively based on the 41.31A version of the SWAN model (*Simulating Waves Nearshore*, Booij et al., 1999). The initial computational domain (Level I) covered the entire North Atlantic region without considering any boundary conditions as in previous studies (e.g., Gonçalves et al., 2020; Rusu, 2022). The following domains were nested, focusing on the Madeira coastal environment and enhancing spatial resolution closer to the shore. Table 4.1 provides details about the physics and input parameters used for the wave model simulation at each level. Simulations were conducted using data from January 1, 2013, to December 31, 2014, a period characterized by recurrent extreme storms impacting the western European coasts (Fig. 3.3). The validation of this wave modelling system was carried out by Rusu (2023). This data was used on the calculations presented in section 4.1.4.

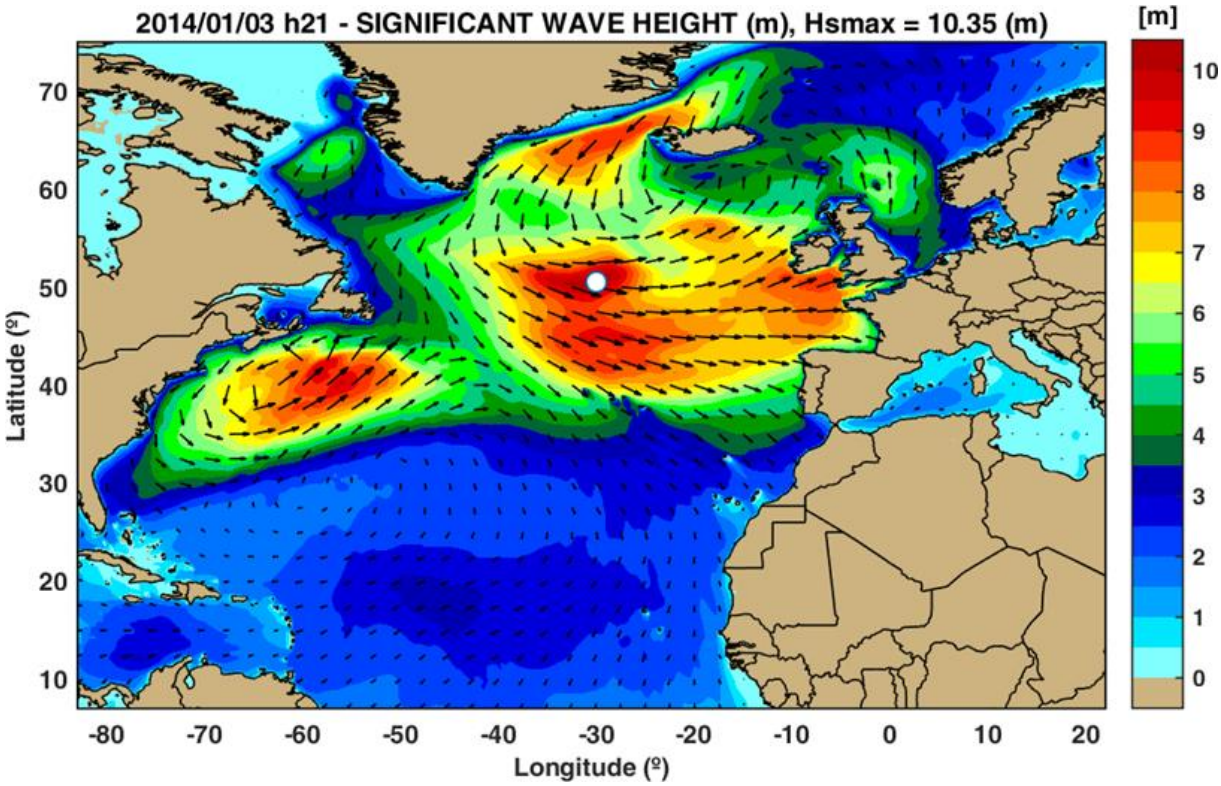

Figure 4. 3. The significant wave height fields simulated for the North Atlantic area during cyclone Christina in January 2014.

Table 4. 1. Physics and inputs considered in the SWAN model simulations.

Input and process	**Level I**	**Level II**	**Level III**	**Level IV**
Computational grid resolution (°) $\Delta x \times \Delta y$	0.5°×0.5°	0.1°×0.1°	0.02°×0.02°	0.004°×0.004°
Number of grid points	211×137	111×91	66×51	176×101
Origin (longitude/latitude)	83° W / 7° S	20° W / 26° N	17.4° W / 32°N	17.3°W / 32.55°N
Wind forcing / spatial and temporal resolution	ERA5 (Hersbach et al., 2020)/ 0.25°×0.25° - 3 hours			
Ice fields / spatial and temporal resolution	ERA5 / 0.25°×0.25° - daily	-	-	-
Boundary conditions	-	from Level I	from Level II	from Level III
Computational mode / Time step	Non-stationary / 15 min			
Numerical scheme	Second-order upwind scheme (default)	Second-order upwind scheme (default)	First-order scheme backward space, backward time	First-order scheme backward space, backward time

Bottom friction	-	Activated	Activated	Activated
Quadruplet nonlinear interactions	Activated	Activated	Activated	Activated
Wind input and whitecapping	ST6 (Rogers et al, 2012)	Westhuysen formulation (Van der Westhuysen et al., 2007)	Westhuysen formulation	Westhuysen formulation
Depth-induced wave breaking	-	Activated	Activated	Activated

4.1.4 DEFINITION OF AREAS WITH MOBILE AND IMMOBILE SEDIMENT UNDER EXTREME WAVE REGIME

Wave-induced shear stress calculations generally followed the procedure of Zhao et al. (2022) using $\tau_{ratio} = \tau_w / \tau_{cr}$ to justify if the shear stress working at the seabed induced by waves τ_w exceeded shelf sediments' threshold of motion τ_{cr}. Shelf sediments were interpreted as mobile or erosive when $\tau_{ratio} \geq 1$, and quiescent or depositional when $\tau_{ratio} < 1$. Wave properties of the 95th percentile of significant wave height H_s (m) and wave peak period T (s) were derived from three hourly Simulating Waves Nearshore (SWAN) modal output for a two-year period (1 January 2013 to 31 December 2014). Wave orbital speed u_m (m/s) at depth z was calculated following linear wave theory (Komar and Miller, 1973):

$$u_m = \frac{\pi H_s}{T sinh(kz)} \quad (4.1)$$

wave number k (1/m) was estimated using the empirical relations of Hunt (1979):

$$(kz)^2 = y^2 + \frac{y}{1 + 0.666y + 0.355y^2 + 0.161y^3 + 0.0632y^4 + 0.0218y^5 + 0.00654y^6} \quad (4.2)$$

$$y = 4.03\frac{z}{T^2} \quad (4.3)$$

Soulsby (1997) deduced that wave induced shear stresses at the seabed τ_w could be calculated using the following expression:

$$\tau_w = 0.5\rho_w f_w {u_m}^2 \quad (4.4)$$

where ρ_w is sea water density (1025 kg/m^3) while the wave friction factor f_w could be obtained from:

$$f_w = 0.237(\frac{A}{Ks})^{-0.52} \text{ (4.5)}$$

Nielsen (1992) proposed that water particle semi-excursion at the top of the boundary layer A and Nikuradse roughness height K_s could be estimated using

$$A = \frac{u_m T}{2\pi} \text{ (4.6)}$$

$$K_s = 2.5D \text{ (4.7)}$$

Where D is the sediment grain size.

Shelf sediments' threshold of motion τ_{cr} was calculated from Soulsby (1997):

$$\tau_{cr} = \theta_{cr} g(\rho_s - \rho_w)D \text{ (4.8)}$$

$$\theta_{cr} = \frac{0.3}{1 + 1.2D_*} + 0.055(1 - \exp(-0.02D_*)) \text{ (4.9)}$$

$$D^* = (\frac{g(s-1)}{v^2})^{1/3} D \text{ (4.10)}$$

where ρ_s is the density of bulk sediment (1800 kg/m^3), s is the ratio of grain to water density (1.8 for marine sediments) and v is the water kinematic viscosity (1.36*10^{-6} m^2/s). The density value of bulk sediment is based on measurements using ITRAX on marine sediment from Faial Island shelf with similar grain sizes to Madeira shelf (Valente, 2020).

The above modelling was calculated for each grid node (cell size 0.0001°) in MATLAB and then interpolated over the entire southern shelf using the Inverse Distance Weighted (IDW) interpolation tool in ESRI ArcGIS. In order to better visualize the shelf sediment being mobile or quiescent on the sea bed under wave actions, we coloured the shelf area to blue (erosive) and green (depositional) respectively, based upon their relative stress. These results were used in the interpretation of the factors that are controlling the formation of the SCBs and bedforms.

4.2 METHODS

Different approaches were used to measure and calculate the morphological and morphometric characteristics of the depositional and erosive features, as well as the estimation of the sediment production of the hydrographic basins. The following subsections describe the methodologies and the approaches used to characterize the morphological features object of this work.

4.2.1. DRAINAGE NETWORK AND SHELF WIDTH AND SLOPE

Defining a watershed (and streams) on a Digital Terrain Model (DTM) involves identifying the boundaries of the area that drains into a specific outlet point or stream. On ArcGIS, the procedure used the following steps:

1. **Flow Direction Calculation** to calculate the direction of water flow across the terrain surface. This tool assigns a flow direction value to each cell in the DTM, indicating the direction that water would flow downhill from that cell.
2. ***"Flow Accumulation"*** tool to apply to the flow direction raster to obtain the total contributing area or cells that drain one specific outlet point or stream in the DTM. The accumulated flow of water for each cell in the DTM corresponds to the main streams.
3. **Watershed Delineation** using the "basin" tool, to delineate watersheds based on the flow accumulation raster identifying the boundaries where flow converges.

After delineating the drainage network across the entire island (see Fig. 3.3 in chap. 3), only the major hydrographic basins situated on the southern side of Madeira were considered for this study. These selected basins are indicated by black outlined polygons, as shown in Fig. 4.1.

The shelf width and slope were computed using Global Mapper software. Multiple segments along the shelf were delineated at a cross-shelf interval of 200 meters (Fig. 4.4A). For each segment, a line parallel to the surface was digitized with Global Mapper using a tool (Path profile/Line of sight) that provides the shelf's width and slope (Fig. 4.4B).

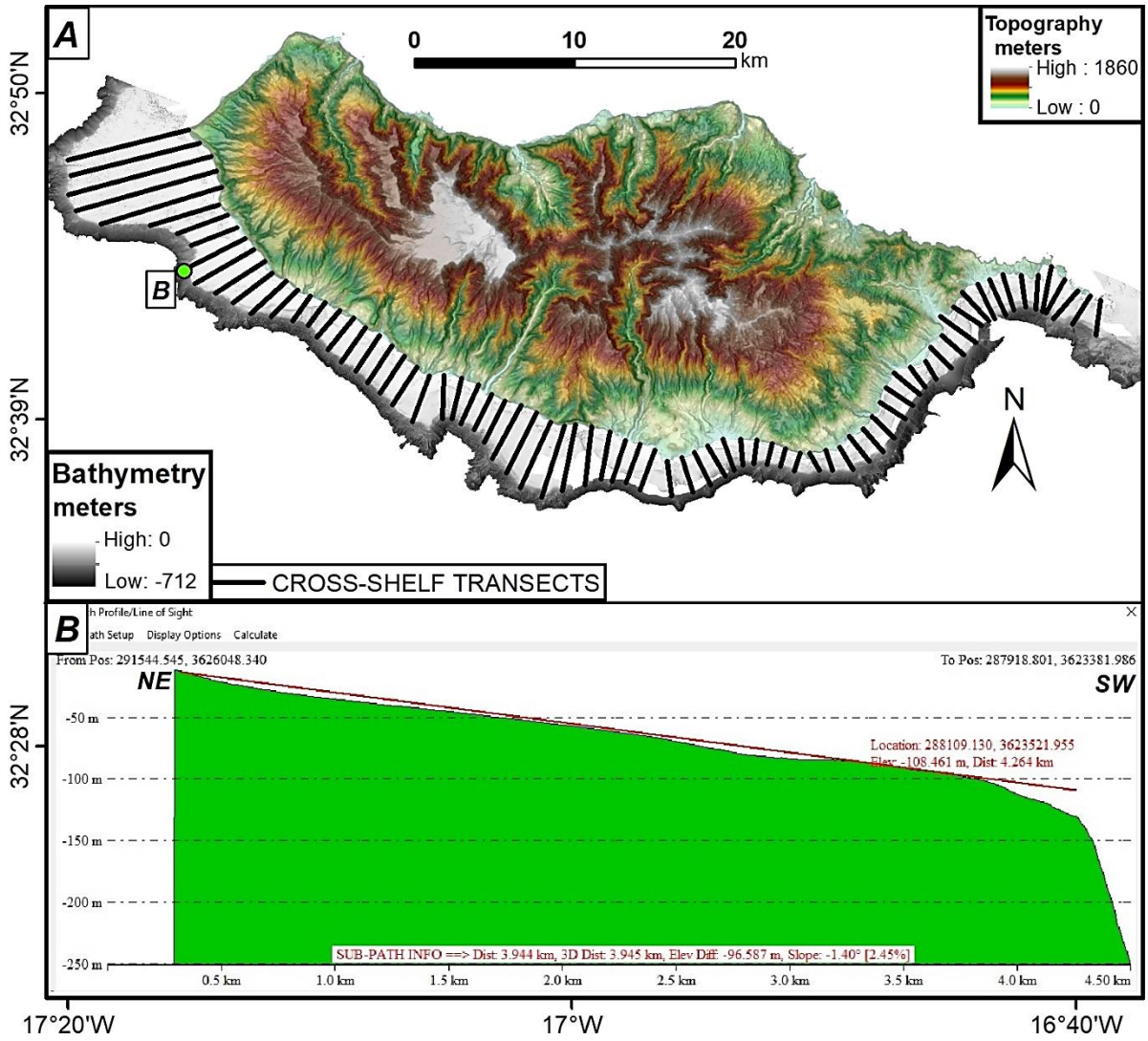

Figure 4.4. A) Transects for the measurements of the width and slopes of the southern insular shelf of Madeira (interspacing of 200 m). B) Example of Global Mapper interface for the measurements of the width and slopes.

4.2.2. SUBAQUEOUS CLINOFORMS BODIES (SCBs) CHARACTERIZATION

The analysis was carried out based on multibeam bathymetry, information from sediment samples, and interpretation of seismic profiles. The seismic processing and the analysis of seismic data was carried out with TEI DELPH SEISMIC. Seismic processing involved the remotion/attenuation of the multiple reflections, application of high/low filters to improve the reflection visualization and the remotion of the water column. The exportation of the depth of interpreted reflections and the thickness of the upper seismic unit in each seismic profile was carried out assuming a sound sediment velocity of 1759 m/s. This average velocity was used because the average sediment grain-size covering Madeira shelf is 2 ± 1 ϕ (medium-fine sand) and according to a database of sound sediment velocity, samples with similar grain-sizes have this velocity (Hamilton et al., 1982). Mapping of the clinoform rollover on the multibeam

bathymetry was done in ArcGIS and Global Mapper. The final presentation with graphs showing the results of the measurements and the interpretation of the seismic profiles were made using Grapher10 and Inkscape. Maps of distribution of sediment grain-size variation and thicknesses were created using Natural Neighbour algorithm in ArcGIS.

The study of the SCBs on the southern shelf of Madeira followed different steps:

I. Mapping of the clinoform rollover on the multibeam bathymetry and seismic profiles. This point represents the topset-to-foreset transition on the clinoform surface (Fig. 4.5). Its mapping on the multibeam bathymetry was carried out using ArcGIS and Global Mapper by searching for the first seaward significant gradient change on the sedimentary seafloor. Determination of the rollover point in the seismic profiles was based on the Wear et al. (1974)'s approach. The methodology consists of drawing two lines, one parallel to the topset and another parallel to the foreset and finding the bisector between the two. The rollover point is located on the intersection of the bisector with the clinoform surface (see Fig. 4.5 B). Interpolation of the results allowed drawing a continuous line of the rollover point alongshore. This also allowed determining the topset width by measuring the distance between the coastline and the rollover point.

II. Individualizing on the seismic profiles the uppermost seismic unit, that normally corresponds to a progradational clinoform laying on a (commonly retrogradational) lower seismic unit. Using the same approach as Mitchum et al., (1977a, b), I interpreted the upper seismic unit as the most recent clinoform, formed in the last 6.5 ka when sea was already at its present level, and the lower one as a clinoform built during the transgression after the last glaciation. The seismic reflection separating them is the maximum flooding surface (Fig. 4.5A). I measured the thickness of the recent clinoform (doubled arrowed red line in Fig. 4.5A) to create a thickness distribution map.

III. Mapping the characteristics (depth and slope) of the inherited topography, i.e., the basal surface underlying the most recent clinoform (orange line in Fig. 4.5 A). When previous (lower) clinoforms are absent, it can correspond to the acoustic basement (blue line in Fig. 4.5A). The depth of the inherited topography was then interpolated on ArcGIS to produce areal maps of this feature. Slope values have been determined through manual measurement using the tool (Path

profile/Line of sight) in Global Mapper along each profile to calculate the average gradient of this surface.

IV. Finally, relationships between measured clinoform characteristics were observed using scatter plots and the values of the resulting R^2. The SCBs characteristics considered were topset width, rollover depth, thickness, and sediment grain-size at the rollover point. Subsequently, the SCBs characteristics have been analysed considering: (i) the shelf bathymetry, (ii) the inherited topography, (iii) sediment supply and (iv) sediment threshold of motion, to discuss to which extent these factors control the clinoform bodies development along the insular shelf.

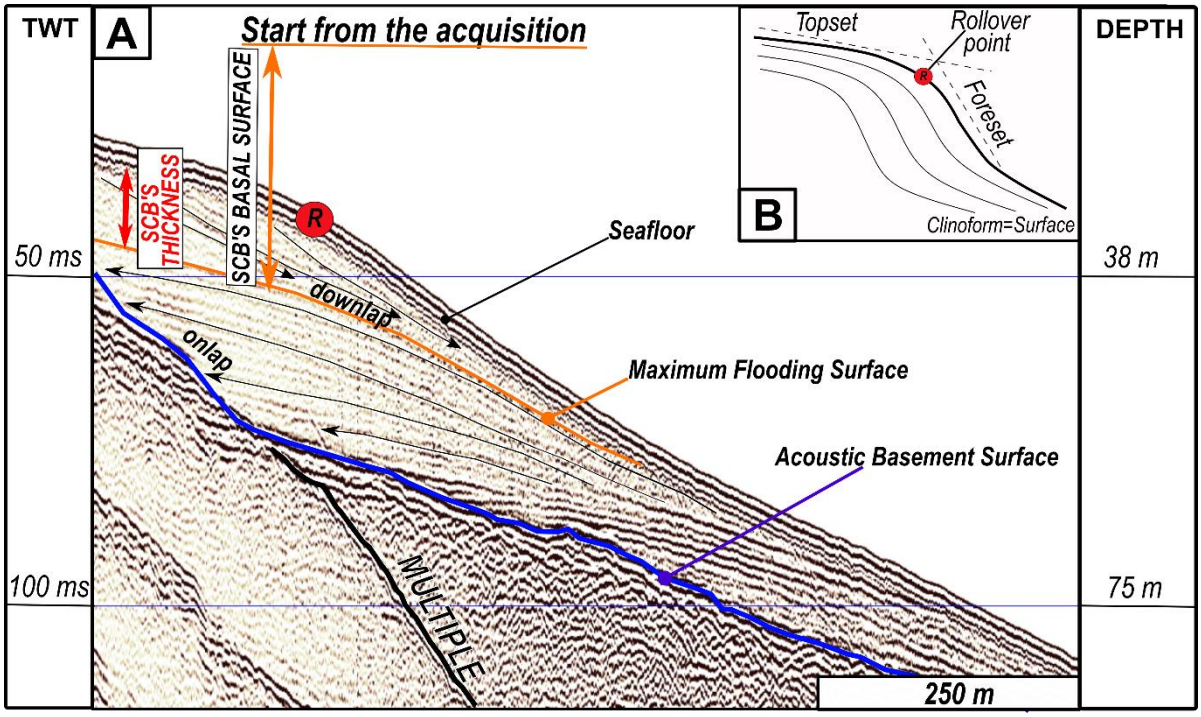

Figure 4.5. A) Example of the seismo-stratigraphic approach used for the interpretation of the seismic profiles (Mitchum et al., 1977a,b). Coloured lines represent the main significant seismic reflections: the blue one represents the acoustic basement surface; the orange line represents the maximum flooding surface (MFS) which marks the passage from retrogressive to progradational units. This recent unit is characterized by basinward accumulation of sediment and downlap terminations above the orange maximum flooding surface. The lower and older unit is made by upward and retrogradational sediment accumulation and shows onlap terminations on the blue surface. The maximum thickness of the progradation unit is indicated by a double red arrow. B) Methodology used for determining the clinoform rollover point (Wear et al., 1974).

4.2.3. BEDFORM FIELDS CHARACTERIZATION

This section details the work done to describe the bedforms that develop parallel to the shelf slope, constituting the main bedform fields that I mapped. On these, several morphological properties of the coastal-shelf system were also mapped and described, such as the type of coast

(cliffs or stream mouths), nearshore nature (rocky or sedimentary), cross- and long-shore extension of the bedform fields and slopes, and whether they occur confined within channels or not. Additionally, four areas of bedforms oblique to the shelf slope were described less extensively.

For each bedform area, several representative along-slope profiles were made to characterize the bedforms. For each profile, 13 characteristics were recorded according to the methodologies proposed by Symons et al. (2016) and Normandeau et al. (2016) (Fig. 4.6 and Table 4.2): (i) wavelength, (ii) wave depth, (iii) wave height, (iv) aspect ratio, (v) stoss-side length, (vi) stoss-side slope, (vii) lee-side length, (viii) lee-side slope, (ix) asymmetry, (x) bedform slope, (xi) general slope, (xii) cross-section shape and (xiii) crestline shape. The measurements were used for creating box and scatter plots with the bedforms characteristics and assess relationships between them.

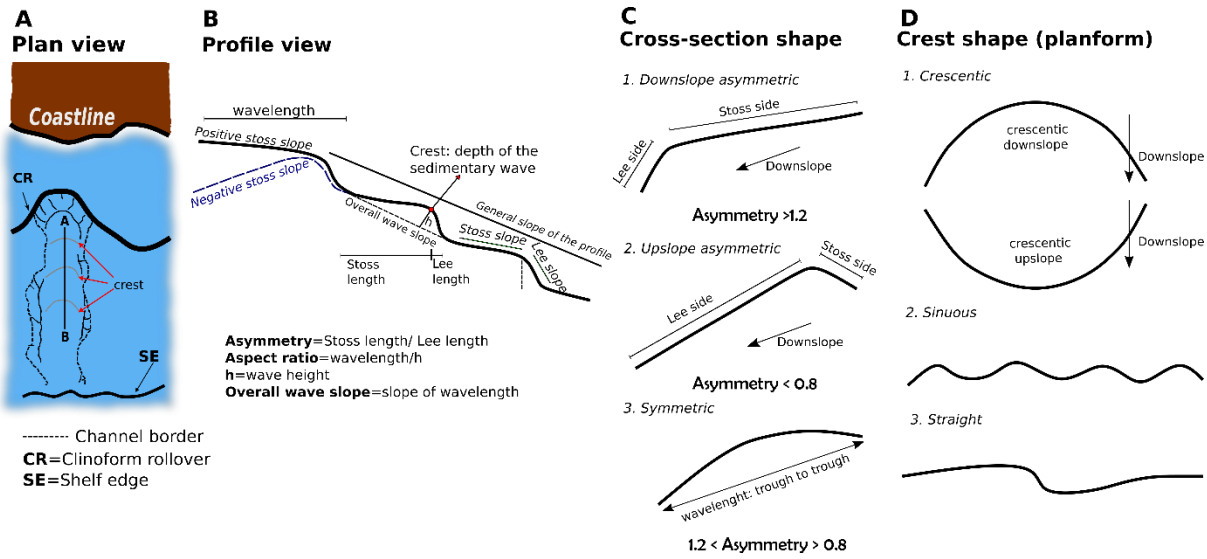

Figure 4. 6. Terminology of the observed features and related parameters adopted in the morphometric analysis. (A) Plan view of a channel head with bedforms incising the shelf (B) Profile view of section A-B drawn in (A), showing the measurements done. (C) Cross section shape and respective classifications. (D) Crestline shape in plan-view and respective classifications. Modified from Symons et al. (2016) and Normandeau et al. (2016).

Table 4. 2. Description of the main parameters measured on the bedforms.

Parameter	Unit	Description
1. Wavelength	m	Horizontal length between the two troughs
2. Wave depth	m	Depth of wave crest
3. Wave-height	m	Shortest distance between the crest and a line joining the two troughs

4. Aspect ratio	-	Ratio between wavelength and wave-height of a bedform
5. Stoss side length	m	Length of the stoss side
6. Stoss side slope	(°)	Slope of the stoss side
7. Lee side length	m	Length of the lee side
8. Lee side slope	(°)	Slope of the lee side
9. Asymmetry	-	Ratio between stoss-side length and lee-side length
10. Bedform slope	(°)	Slope of the bedform measured between the two consecutive troughs
11. General slope	(°)	General slope of the profile
12. Cross section shape	-	Shape of bedform in profile view. It can be symmetric, upslope asymmetric (stoss side much shorter than lee side), downslope asymmetric (stoss side much longer than lee side)
13. Crestline shape	-	Shape of bedform in plan-view. It can be straight, sinuous and crescentic downslope or crescentic upslope.

4.2.4. ANALYSIS OF PRECIPITATION DATA

From the dataset cited in section 4.1.1, only 3 stations (Funchal/Observatório, Ponta do Pargo and Lugar de Baixo, Fig. 4.1) had more than 80% of complete precipitation records and for this reason were chosen to analyze using the approach of Ramos et al. (2018). Only the winter months (October to March) were taken in consideration, since the intense rainfalls occur mainly in this season (Baioni, 2011) disregarding values below 1 mm/day. For these stations I calculated the number of the extreme precipitation days, i.e., days with precipitation over the 95^{th} percentile. The values of the 95th percentiles can be considered as indicative of extreme rainfall events, which have the potential to lead to flooding events (Ramos et al., 2018).

4.2.5. QUANTITATIVE ESTIMATION OF THE HYDRIC EROSION, AVERAGE BASIN PRECIPITATION, AND CLIFF HEIGHT ALONG THE COASTLINE

The quantitative contribution of sediments from the hydrographic basins was calculated using equation 4.11 proposed by Syvitski et al. (2003). It allows estimating the long-term flux of sediment from river basins to the coast, knowing the geographic location and some basin

characteristics. It considers the relief, basin area and the basin-averaged temperature. The equation adopts different coefficient values according to the main hemispheric climate regions (Polar, Temperate and Tropics) and is as follows:

$$Qs = \alpha_3 A^{\alpha 4} R^{\alpha 5} e^{kT} \quad (4.11)$$

Qs is long term sediment load (kg/s); A is drainage basin area (km^2), R is the maximum relief from sea level to the highest point of the basin (m), T is the basin-average temperature (°C). Madeira is located on a northern temperate environment (latitude > 30° N, T > 0 °C) and, according to Table 4 of Syvitski et al. (2003), the values of the constants on those areas are:

$$\alpha_3 = 6.1 \times 10^{-5}$$

$$\alpha_4 = 0.55$$

$$\alpha_5 = 1.12$$

$$k = 0.07$$

$$T = 9.9\ °C$$

The areas of the hydrographic basins were obtained using different tools in ArcGIS to defined the drainage network and relative watersheds (see section 4.1.1). These areas, together with the DTM of Madeira Island, were used to calculate the average and the maximum relief of each hydrographic basin, using the “slope analysis” tool in ArcGIS software. This tool calculates the steepness or gradient of the terrain surface at each location within a raster dataset representing elevation. Qs was calculated twice using the average and the maximum relief and then converted to m^3/s using the value of 1800 kg/m³ that is assumed as the density of sediments described in section 4.1.4. Subsequently, the values were converted to m^3/year. The calculation of average annual precipitation for each basin involved the ArcGIS "extract by mask" tool. This tool extracted the values from the average annual precipitation raster (referenced in Fig. 3.4 of chap. 3) based on the boundaries defined by the area of each hydrographic basin (Fig. 4.2), allowed the calculation of an average of that data.

The coast height along the southern shelf was digitized on the DTM and plotted to an elevation/distance graph showing the height trend along the southern coast (Fig. 4.7).

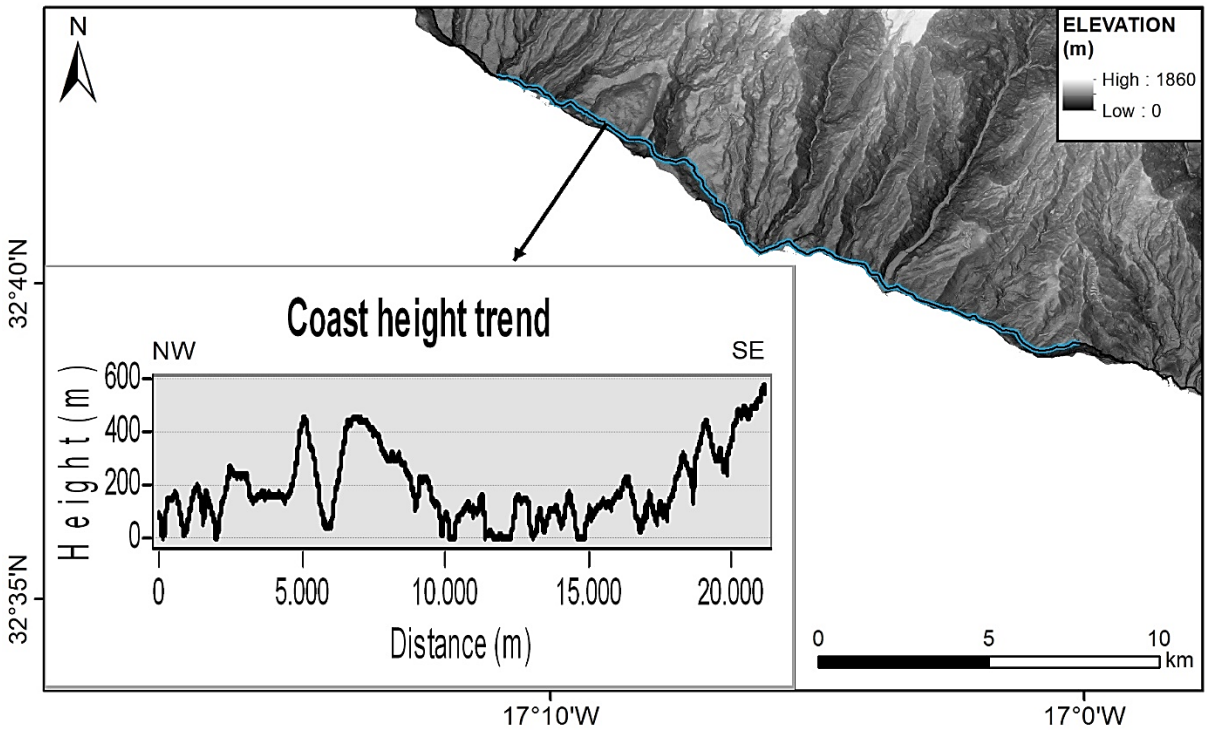

Figure 4. 7. Example of coastal elevation trend shown on the ArcGIS interface. The blue line represents the digitized cliff top, which is then plotted on the graph.

CHAPTER 5. SPATIAL VARIABILITY OF SUBAQUEOUS CLINOFORM BODIES ON THE SOUTHERN MADEIRA ISLAND SHELF

5.1. INTRODUCTION

This chapter shows the mapping and characterization of the subaqueous clinoform bodies (SCBs) along the entire southern shelf of Madeira Island based on multibeam bathymetry, seismic profiles, and sediment grain-size data. The aim is to provide a detailed description of SCBs variability in terms of extension and lateral continuity, rollover point depth, internal structure, and thickness to understand the main factors that influence their spatial variability. I also looked qualitatively at differences in sediment supply, grain-size, inherited bathymetry, and hydrodynamics to understand the influence of these factors on the spatial and geometrical variability of the observed deposits. Additional figures related to this chapter can be found in the supplementary material in Appendix. These results will be prepared to submit as a manuscript to an ISI journal.

5.2. RESULTS

The southern shelf of Madeira Island (Fig. 5.1) extends for ~75 km in length, comprising an area of ~210 km². Morphologically, it is possible to identify from west to east: (i) a wider shelf west of Calheta (3 to 9 km wide); (ii) an area between Calheta and Funchal with intermediate widths (2 to 5 km in width) and (iii) a narrower area east of Funchal (1 and 2 km in width). However, it appears to be more reasonable a subdivision of the shelf in four sectors when the grain-size of its sedimentary cover (Phi mode) and the related onshore features are integrated (Figs. 5.1A, 5.1B, 5.2 and Table 5.1):

- SECTOR 1 extends from Ponta do Pargo to Calheta (see white dots numbered 1 and 2 in Fig. 5.1). This is the widest sector of the southern Madeira shelf, with widths normally above 3 km, reaching 9 km in the widest part. The coast is predominantly composed of high cliffs with an average height of ~330 m (Fig. 5.2). The hydrographic basins that flow into this sector have relatively small areas (5.5 ± 3 km^2, Table 5.2) and include plio-pleistocene volcanic units, mostly CVM 3 and CVS 1, some of which are moderately weathered (CVM 3). According to equation 4.11 (see chap. 4), sediment production in a hydrographic basin can be estimated by considering basic information such as area, maximum altitude, and temperature, and then multiplying these values by coefficients specific to the regional area

(polar, temperate, tropics). Based on this equation, these basins have the capacity to generate approximately 5,200-23,000 m^3 of sediment annually (Table 5.2). However, the nearshore seafloor mainly displays rocky outcrops which result from cliff failures and only coarser sediments (medium to coarse sand) are found offshore these rocky outcrops.

- SECTOR 2 is comprised between Calheta and Cabo Girão (numbers 2 and 3 in Fig. 5.1). This sector has intermediate widths, normally above 2 km, reaching almost 5 km in the widest part. The coast is still high, with average values ~190 m but intensely dissected by streams. Their hydrographic basins are larger than in sector 1 (around 8 ± 5 km^2, with the exception of the largest one, Ribeira Brava, which is 41 km^2) and insists on plio-pleistocene volcanic units mostly belonging to CVM 2 and CVM 3. The largest hydrographic basins also include CVM 1 (Rib. da Ponta do Sol and Rib. Brava). These lithologies are intensely to moderately weathered. Based on equation 4.11, these basins have the potential to produce 8100 – 43000 m^3 of sediment per year (excluding Ribeira Brava that produces 68350 m^3/y). The nearshore seafloor has fewer rocky outcrops than that of sector 1 but there are still deposits that result from cliff failures; the best example of which is Cabo Girão. Next to these landslide deposits, coarser sediments predominate (medium to coarse sand), but on the remaining parts of this sector the sediments are generally much finer (fine to very fine sand).

- SECTOR 3 has a limited area that extends from Cabo Girão to Funchal (numbers 3 and 4 in Fig. 5.1). This shelf area is narrower than that of sector 2, ranging from slightly more than 3 km in the west and progressively narrowing toward the east, where it reaches 1 km. The coast is predominantly composed of low cliffs with average heights of 80 m (Fig. 5.2). The hydrographic basins draining to this area are large (11 ± 6 km^2) and may discharge considerable volumes of sediments into this sector. The hydrographic basin size average also does not include the largest one, Ribeira dos Socorridos, which reaches 38 km^2 in area. They include plio-pleistocenic volcanic products (CVM 3, CVS 1 and CVS 2), which are mostly less weathered with the exception of Ribeira dos Socorridos and some small basins near Cabo Girão that cross older and more weathered products (CVM 1). These basins can produce ~3500-41200 m^3 of sediment per year. Ribeira dos Socorridos stands out by being capable of producing 73500 m^3 of sediment per year. In terms of grain size, this sector is characterized by a finer fraction than sector 2, where only fine to very fine sands prevail.

- SECTOR 4 corresponds to the southeasternmost part of the island and includes the area between Funchal and Caniçal (see white dots number 4 and 5 in Fig. 5.1). This is the narrowest shelf sector, normally less than 2 km, and just 1 km wide in the narrowest part. This stretch of coast is predominantly composed of low cliffs with average heights of ~ 65 m (Fig. 5.2) and hydrographic basins similar in size respect to sector 3 (10 ± 6 km^2 on average). According to equation 4.11, these hydrographic basins can produce volumes of sediments up to ~35900 m^3 of sediment per year. In this sector, the outcropping lithologies are volcanic products from CVS and CVM 3, which are mostly less weathered, except on Machico hydrographic basin where CVM 2 also outcrops. The grain size is very similar to sector 1, where medium to coarse sands prevail, with only finer sediments at the nearshore offshore the largest hydrographic basins (fine to very fine sand).

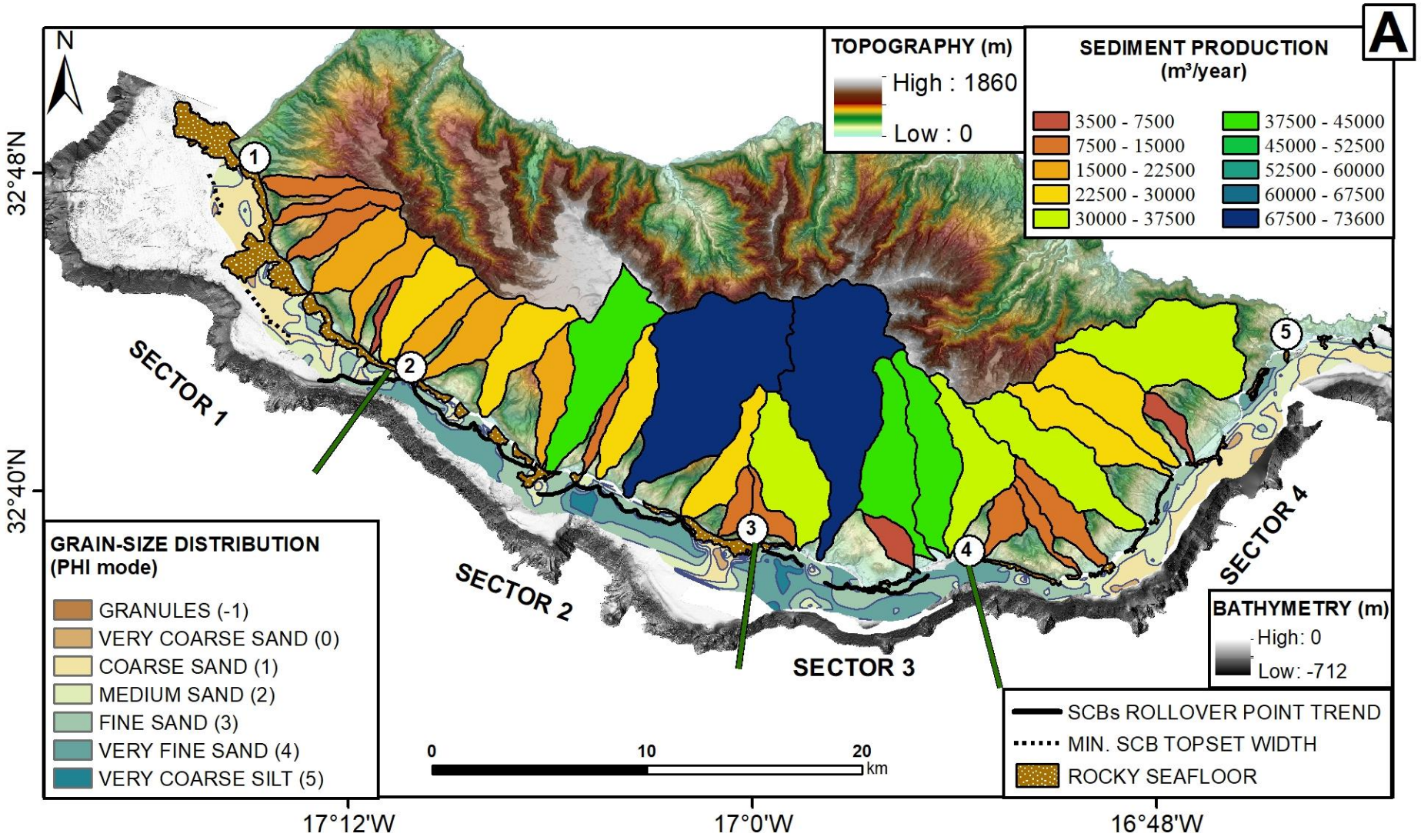

Figure 5.1. A) Map displaying the division of the southern insular shelf of Madeira Island into four sectors (the cross-shelf green lines are the sector borders) and the sediment production of each basin onshore. White dots represent the following locations: 1- Ponta do Pargo; 2- Calheta; 3- Cabo Girão; 4- Funchal; 5- Caniçal. Black bold lines represent the clinoform rollover. In sector 1, the dotted lines indicate the minimum extension of SCBs' topset in areas where the seismic data do not cross entirely the features. Brown polygons delimit the nearshore rocky seafloor.

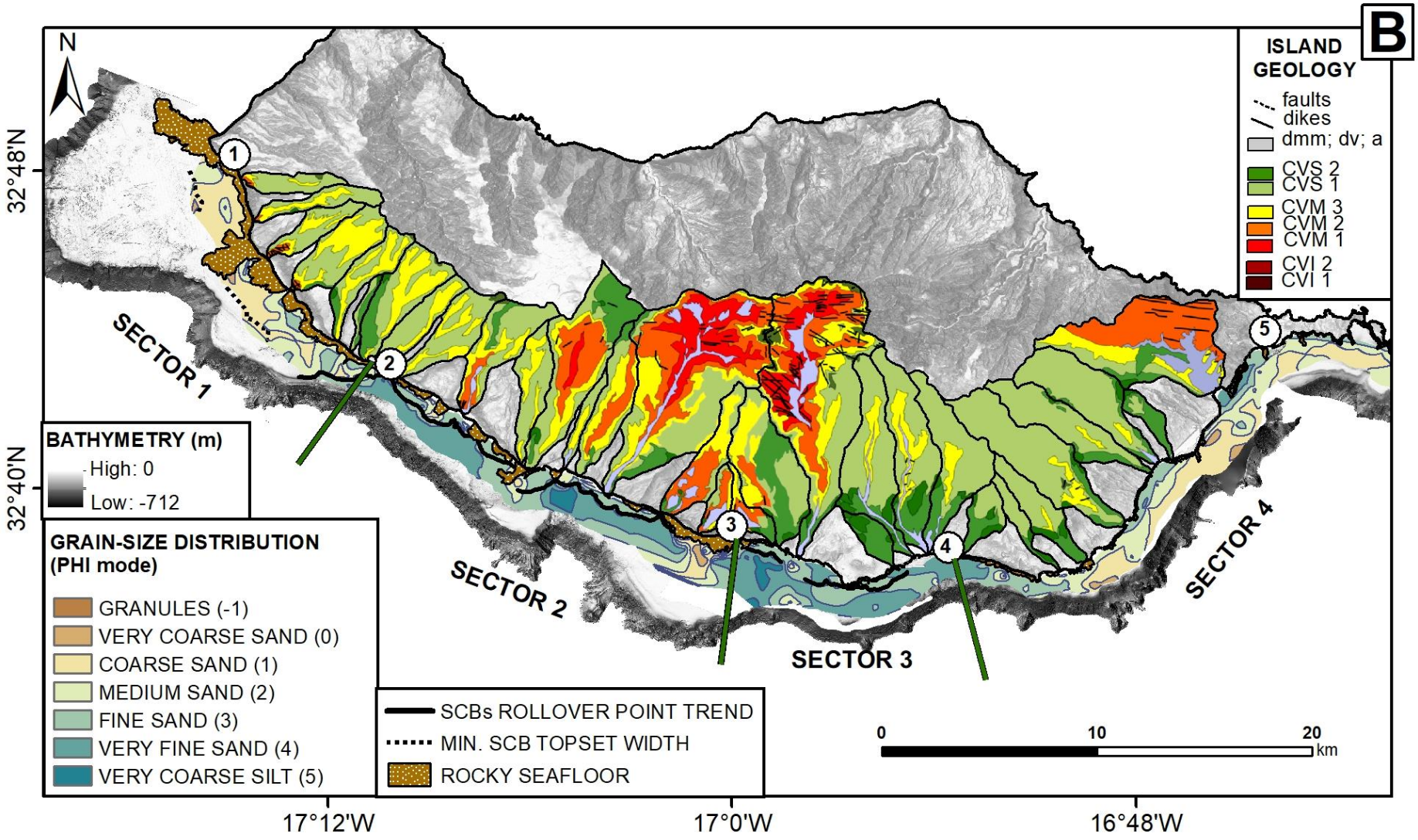

Figure 5.1.B) Map displaying the division of the southern insular shelf of Madeira Island into four sectors (the cross-shelf green lines are the sector borders) and the outcropping lithologies in each basin onshore. The remaining caption is the same as figure 5.1.A.

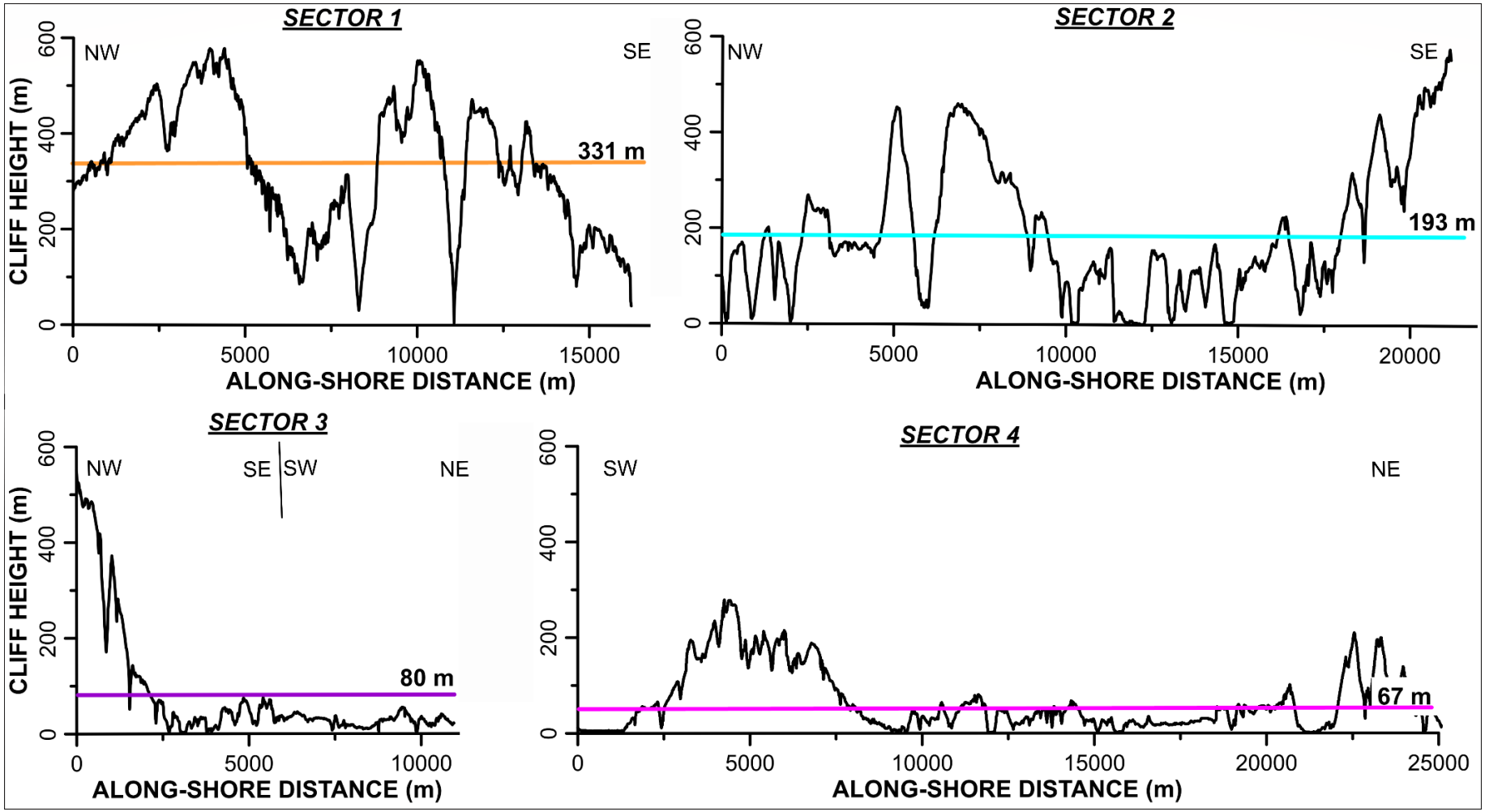

Figure 5.2. Cliff height trend along the south coast of Madeira Island. In each sector, the coloured line represents the average.

Table 5. 1 Characteristics of the hydrographic basins flowing to the south of Madeira and sediment production based on equation 4.11. Legend ID: identification number; SEC: sector; AN. AV. PREC: annual average precipitation; AV. ALT: average altitude; MAX ALT.: maximum altitude; SED. LOAD MAX: sediment load considering maximum altitude; SED. LOAD AV: sediment load considering average altitude.

ID	NAME	SEC	AREA	AN. AV. PREC.	AV. ALT.	MAX ALT.	SED. LOAD MAX	SED. LOAD AV.
N°	Ribeira	-	(km^2)	(mm/y)	(m)	(m)	(m^3/y)	(m^3/y)
1	DOS CAMBIOS	1	3,62	1200-1300	747,19	1130	11450,08	7204,49
2	DOS MARINHEIROS	1	4,2	1200-1300	903,77	1314	14712,44	9674,82
3	DAS GALINHAS	1	4,52	1200-1300	756,58	1262	14641,43	8254,95
4	SECA	1	8,73	1200-1300	798,44	1314	22001,66	12593,32
5	FUNDA	1	6,22	1200-1300	763,95	1297	17994,86	9946,91
6	DA IGREJA	1	1,34	1000-1200	535,49	920	5265,27	2871,97
7	DE S. BARTOLOMEO	1	10,11	1200-1400	689,37	1263	22816,85	11581,12
8	DA CALHETA	2	5,82	1200-1400	585,94	1296	17333,89	7124,82
9	DA ATOUGUIA	2	7,77	1200-1400	771,11	1416	22438,47	11359,85
10	DA MADALENA	2	9,75	1200-1400	923,32	1424	25583,18	15747,73
11	DE SANTIAGO	2	6,72	1200-1400	757,36	1416	20716,43	10278,80
12	DA PONTA DO SOL	2	19,33	1400-1600	953,1	1618	43008,50	23775,71
13	DA CAIXA	2	2,2	1200-1300	586,79	1191	9234,74	4179,30
14	DA TABUA	2	8,86	1400-1600	719,5	1569	27055,60	11298,84
15	BRAVA	2	41,22	1400-1600	787,85	1687	68351,68	29133,79
16	DO CAMPANARIO	2	7,73	1200-1300	688,95	1435	22711,39	9984,81
17	DA QUINTA GRANDE	2	2,82	1000-1100	596,08	938	8101,68	4875,83
18	DA CALDEIRA	3	3,1	1000-1200	410,71	951	8667,26	3384,38
19	DO VIGARIO	3	15,45	1200-1300	661,53	1410	32591,70	13963,59
20	DOS SOCORRIDOS	3	38,69	1400-1600	930,88	1859	73594,12	33916,51
21	SECO	3	3,01	< 800-900	194,45	437	3569,62	1441,28
22	DE SÃO JOÃO	3	14,54	1400-1600	743,02	1759	40381,18	15381,61
23	DE STA. LUZIA	3	14,44	1400-1600	817,36	1800	41279,84	17050,45
24	DE SÃO JOÃO GOMES	3	12,99	1400-1600	842,43	1593	33965,47	16640,02
25	DE SÃO GONÇALO	4	3,83	1200-1300	497,11	931	9507,23	4708,22
26	DA ABEGOARIA	4	2,65	1200-1300	550,9	932	7773,24	4313,78
27	DO CANIÇO	4	6,07	1200-1300	539,91	1100	14763,33	6653,11
28	DO PORTO NOVO	4	17,28	1400-1500	782,09	1455	35902,65	17912,96
29	DA BOAVENTURA	4	10,57	1200-1400	764,13	1365	25507,08	13318,63
30	DE STA. CRUZ	4	12,85	1200-1400	670,77	1298	26843,26	12815,34
31	DO MORENO	4	2,6	1000-1100	425,87	751	6039,81	3199,61
32	DOS MACHICO	4	24,58	1200-1300	406,65	1081	31244,65	10452,45

Table 5. 2. Average and deviation standard of the morphological characteristic used for the division in sectors of the Madeira southern shelf. The values with "*" do not include the largest hydrographic basins (Ribeira Brava and Ribeira dos Socorridos).

	SECTOR 1 (average ± standard dev.)	**SECTOR 2 (average ± standard dev.)**	**SECTOR 3 (average ± standard dev.)**	**SECTOR 4 (average ± standard dev.)**
Hydrographic basin size (km²)	5.5 ± 3	8 ± 5*	11 ± 6*	10 ± 7
Sediment production (m³/y)	15554 ± 6117	21798 ± 10365*	26742 ± 16416*	19698 ± 11573
Cliff height (m)	331 ± 132	193 ±137	80 ± 122	66 ± 64
Shelf slope (°)	1.45 ± 1.1	3.8 ± 0.1	6.4 ± 1.3	6.4 ± 0.8
Min and max shelf width (km)	1.8 – 9.5	1.6 – 4.5	1.5 – 2.5	0.9 – 2.3
Φ granulometric distribution (mode)	1 ± 0.5	2.6 ± 1	3 ± 0.3	1.4 ± 0.8

5.2.1. MORPHOLOGICAL AND SEISMO-STRATIGRAPHIC CHARACTERISTICS OF THE SCBs

Morphology of SCBs

The southern insular shelf of Madeira Island shows subaqueous clinoform bodies (SCBs) along its whole extension whose rollover depth varies along the shelf, apart from areas with rocky outcrops (see Table 5.3). However, SCBs in Sector 4 are very small and restricted to the shallower areas. Due to the partial seismic coverage in this sector, only two profiles were used to obtain the values reported in Table 5.3. This prevented reconstructing the distribution of the SCBs thickness and of its basal surface (depth and gradient) in Sector 4.

Table 5. 3. Summary of the SCBs characteristics in the different sectors of Madeira's southern shelf.

	Topset width (m)	**Percentage of shelf area occupied (%)**	**Thickness (m)**	**Rollover point depth (m)**	**Foreset steepness (°)**	**Basal surface's depth (m)**	**Basal surface's slope (°)**
	min - max average	min – max average	min - max average	min - max average	min - max average	min - max average	min - max average
SECTOR 1	680 / 2390 1917 ± 417	> 14 / 89 48 ± 22	1 / 38 9 ± 6	30 / 80 60 ± 15	1 / 15 2 ± 1.3	20 / 100 57 ± 11	(-1) / 8 1.2 ± 0.7
SECTOR 2	175 / 1150 628 ± 250	14 / 45 23 ± 8	1 / 32 15 ± 7	15 / 45 38 ± 5	6 / 18 9 ± 4	20 / 100 50 ± 14	2 / 14 2.8 ± 1
SECTOR 3	130 / 1090 576 ± 240	8 / 48 25 ± 10	1 / 20 10 ± 4	15 / 36 27 ± 4	3 / 7 6 ± 2.2	20 / 90 44 ± 12	2 / 11 2.6 ± 1
SECTOR 4	80 /360 224 ± 62	3 / 19 12 ± 4	9-13 11 ± 2	14 /34 22 ± 5	8 / 22 15 ± 7	/	/

In the context of the shelf extension, the SCBs topsets vary considerably alongshore on the four sectors. On Fig. 5.3 the percentage of the topset width relative to the overall shelf width is

presented. However, areas where the SCBs have retreated due to erosive headwall channels or failure scars are not representative of the topset width because they result from mass-wasting rather than hydrodynamics. and were excluded from the measurements. In Sector 1, where the shelf reaches the largest width (over 8 km, see graph 1 in Fig. 5.3), the partial bathymetric coverage prevented the determination of the total extension of the SCBs. However, as one can see from the shaded relief bathymetry, rocky outcrops dominate the outer shelf on the northwestern area (Fig. 5.4), so the visible topset occupies at least 14-21% of the shelf area, but does not extend beyond the middle of the shelf. Moving southeast on sector 1, the clinoform topset width increases and occupies almost all the shelf near sector 2 (up to 89%, graph 3 in Fig. 5.3). The SCBs topset in Sector 2 occupies a larger shelf area (32-42%) in the western side (graph 4 in Fig. 5.3), decreasing towards the east (11-33%, graph 5 in Fig. 5.3). The topset width in Sector 3 is less than 33% of the shelf and shows the same trend, narrowing to the east (graphs 6 and 7 in Fig. 5.3). In Sector 4, the shelf is very narrow and the SCBs are restricted to the nearshore part of the shelf. The largest example of a SCBs in this sector is in the eastern part. Here, the SCB has a small topset width and occupies only a little part of the shelf area (< 13%, graph 8 in Fig. 5.3).

The thickness and the seismic structure of the SCBs are described in the following sections.

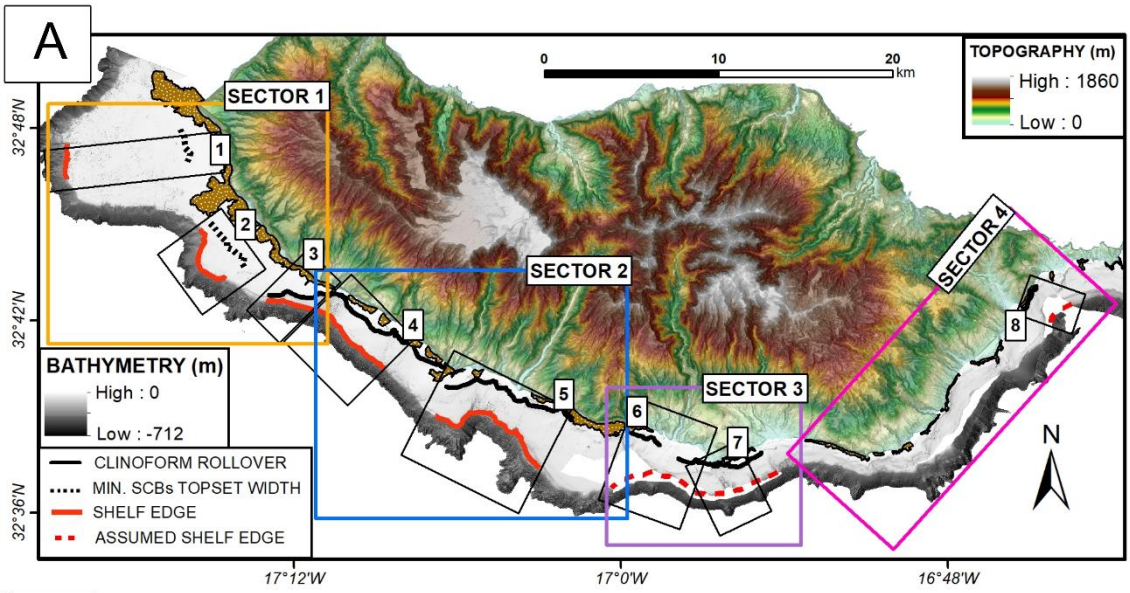
A
SECTOR 1
SECTOR 2
SECTOR 3
SECTOR 4
1
2
3
4
5
6
7
8
0
10
20
km
TOPOGRAPHY (m)
High : 1860
Low : 0
BATHYMETRY (m)
High : 0
Low : -712
CLINOFORM ROLLOVER
MIN. SCBs TOPSET WIDTH
SHELF EDGE
ASSUMED SHELF EDGE
N
32°48'N
32°42'N
32°36'N
17°12'W
17°0'W
16°48'W

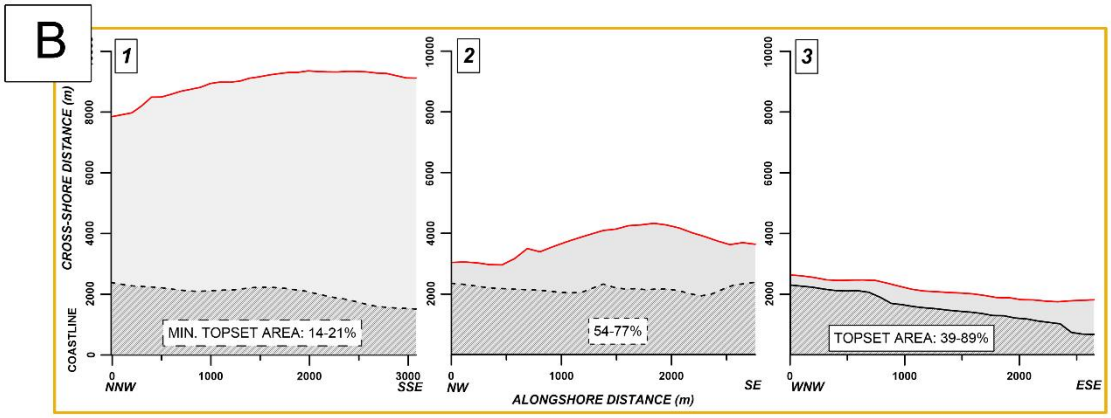
B
1
2
3
CROSS-SHORE DISTANCE (m)
COASTLINE
MIN. TOPSET AREA: 14-21%
54-77%
TOPSET AREA: 39-89%
NNW
SSE
NW
SE
WNW
ESE
ALONGSHORE DISTANCE (m)

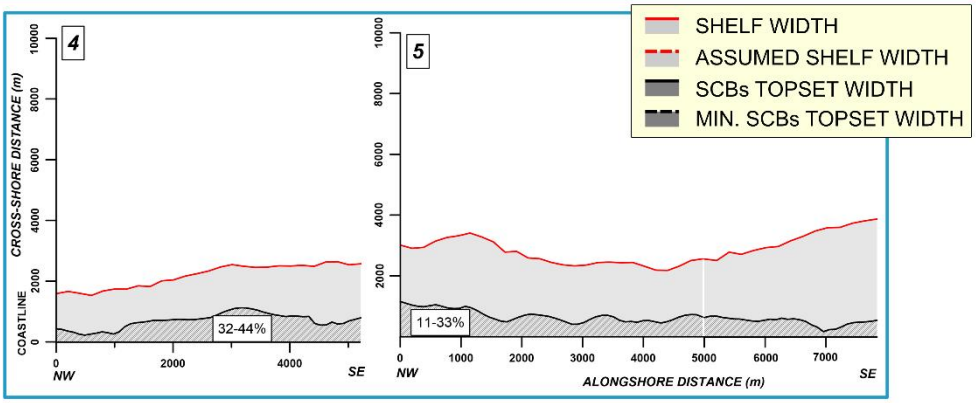
4
5
CROSS-SHORE DISTANCE (m)
COASTLINE
32-44%
11-33%
NW
SE
ALONGSHORE DISTANCE (m)
SHELF WIDTH
ASSUMED SHELF WIDTH
SCBs TOPSET WIDTH
MIN. SCBs TOPSET WIDTH

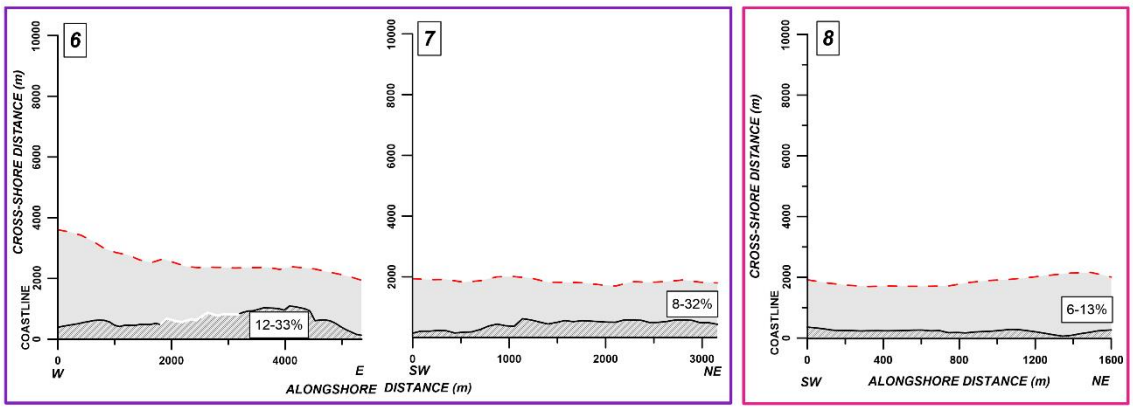
6
7
8
CROSS-SHORE DISTANCE (m)
COASTLINE
12-33%
8-32%
6-13%
W
E
SW
NE
ALONGSHORE DISTANCE (m)

Figure 5.3. (A) Map of the southern shelf of Madeira Island showing the mapped SCB topset width (or clinoform rollover) and the shelf edge. Black and red lines represent the position of clinoform rollover and shelf edge, respectively. Black and red dashed lines indicate the inferred position of the same features due to lack of seismic and multibeam data. Brown polygons represent nearshore rocky seafloor. (B) Graphs illustrate the area occupied by the SCBs topset (grey dashed area) relatively to the shelf width. Numbers indicate the minimum and maximum area of the shelf, in percentage, that the SCBs topsets occupy. Note that the x-axis (horizontal) scale varies between graphs.

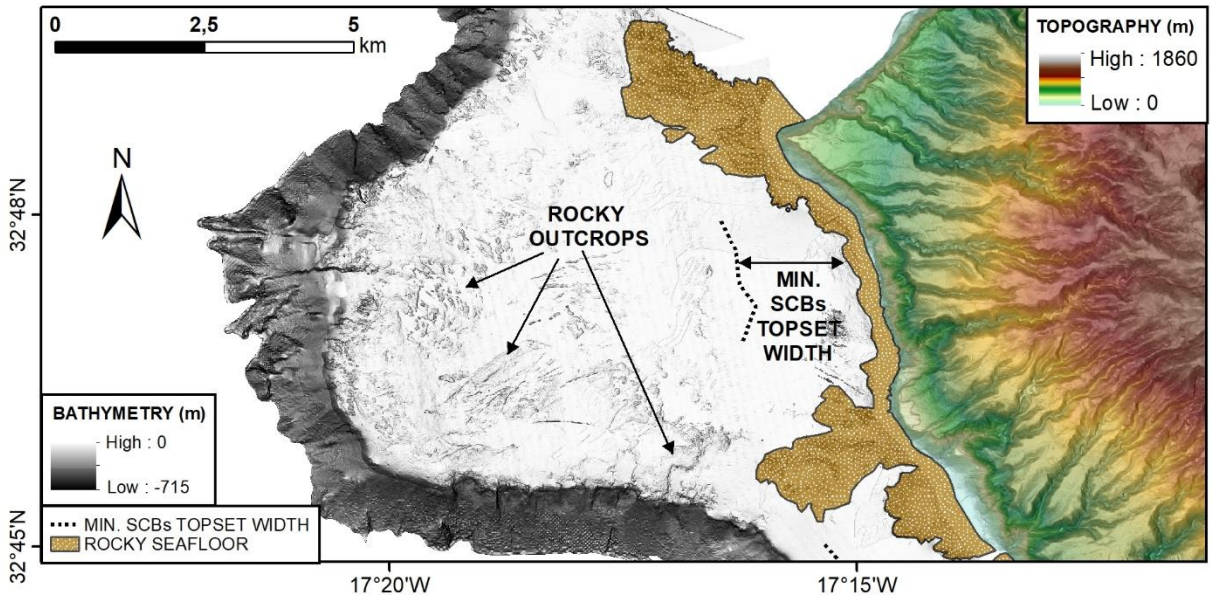

Figure 5.4. Map of the westernmost region of sector 1. The SCBs are limited to the inner shelf, with their minimum topset width depicted by a dotted black line. Brown polygons represent the nearshore rocky seafloor. The outer shelf displays a predominant rocky seafloor.

Seismic structure of SCBs

SECTOR 1

In this shelf sector, the structure of the clinoform bodies was not fully mapped because, in the network adopted during the survey, the seismic profiles do not cover their entire extension. The exception is the easternmost part of this sector where the topset width was fully mapped (see Fig. 5.5). Here, the topset width decreases from ~2 to 1 km eastwards (rollover depth between 80 and 45 m, see graph 3 of Fig. 5.3B) and the grain size (Fig. 5.1) is generally finer (fine to medium sand) than the westernmost part (coarse sand). This eastern area marks a change in the SCBs characteristics. West of this zone, thickness values are generally lower than 6-8 m, except for the northwest most body that reaches 18 m. From the bathymetry this thicker body ends on the mid-shelf (Fig. 5.5) and the seismic data shows low-angle internal reflections (1°- 2.5°) that downlap over an even smoother surface with an aggradational pattern (Fig. 5.6). Moving eastward, the SCBs topset width starts to coincide with the shelf edge, where the shelf gets narrower. Here, the SCB shows steeper internal reflections (5°-16°) that develop also on a steeper pre-existing bathymetry (see Fig. 5.7).

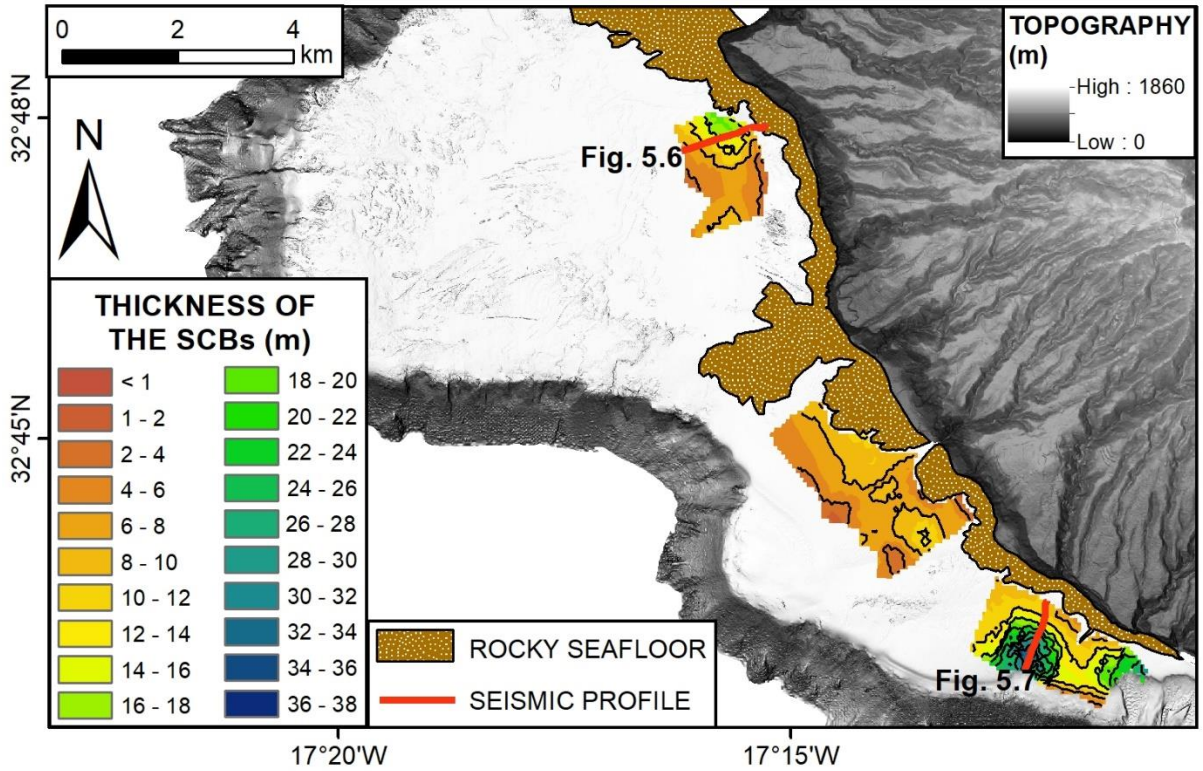

Figure 5.5. Map of the thickness of the SCBs in sector 1 of the insular shelf of Madeira (see location on Fig. 5.1). Brown polygons delimit nearshore rocky seafloor. Thickness increases from orange to green and blue tones. Contours are spaced each 4 m. The two red lines represent the location of the seismic profiles of Figs. 5.6 and 5.7.

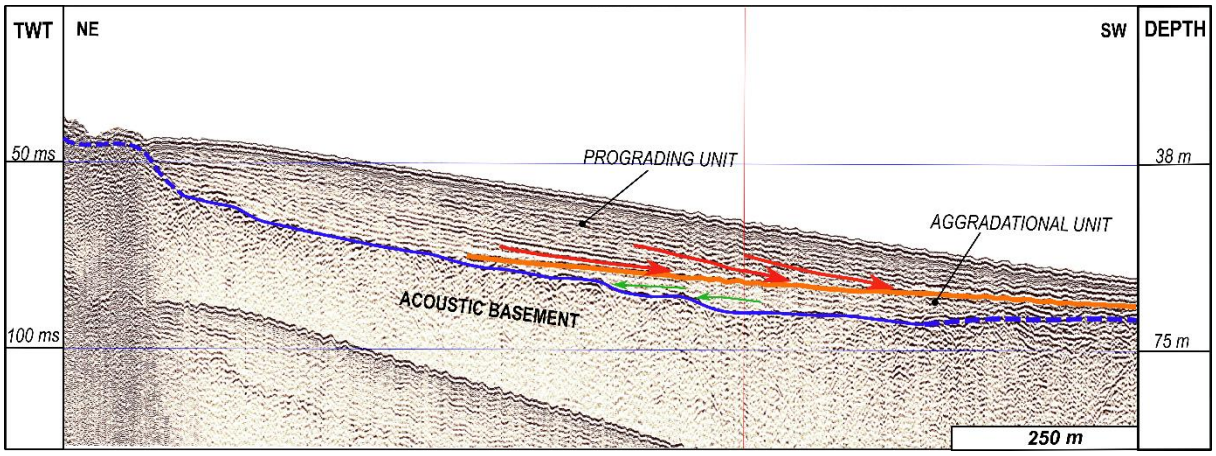

Figure 5.6. Sparker seismic profile perpendicular to the coast in the westernmost part of sector 1 (location in Fig. 5.5). Red arrows represent the reflections with downlap terminations on the bold orange line that represents the maximum flooding surface (MFS). MFS separates the prograding unit (above) from that with an aggradation trend (below). The aggradating unit presents reflections with onlap terminations (green arrows) towards the bold and dashed blue line, which is the acoustic basement surface.

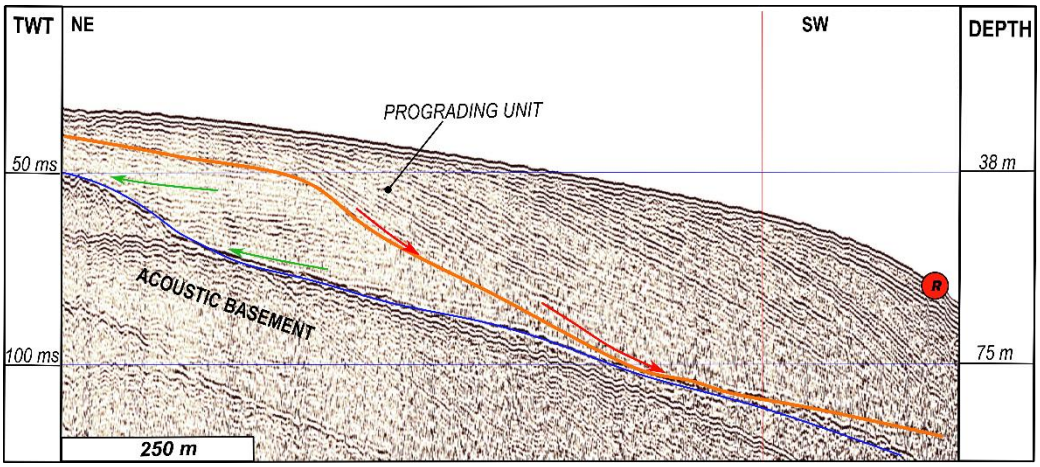

Figure 5.7. Sparker seismic profile perpendicular to the coastline located in the easternmost part of sector 1 (location in Fig. 5.5). Symbology as in Fig. 5.6; R marks the rollover point.

SECTOR 2

In this sector, SCBs show variable thicknesses with the largest depocenters being 18 to 32 m-thick, and normally thicker offshore the largest hydrographic basins such as Ribeira Brava. The SCBs topset is on average 630 m in width (average rollover depth of 38 m). In the easternmost part, the seismic profile (Fig. 5.9) is an example of the seismic characteristics of the upper progradational unit in sector 2. This SCB has sigmoidal-oblique configuration with steep foresets (~12°). It completely overlays an underlying aggradational unit lying on the acoustic basement.

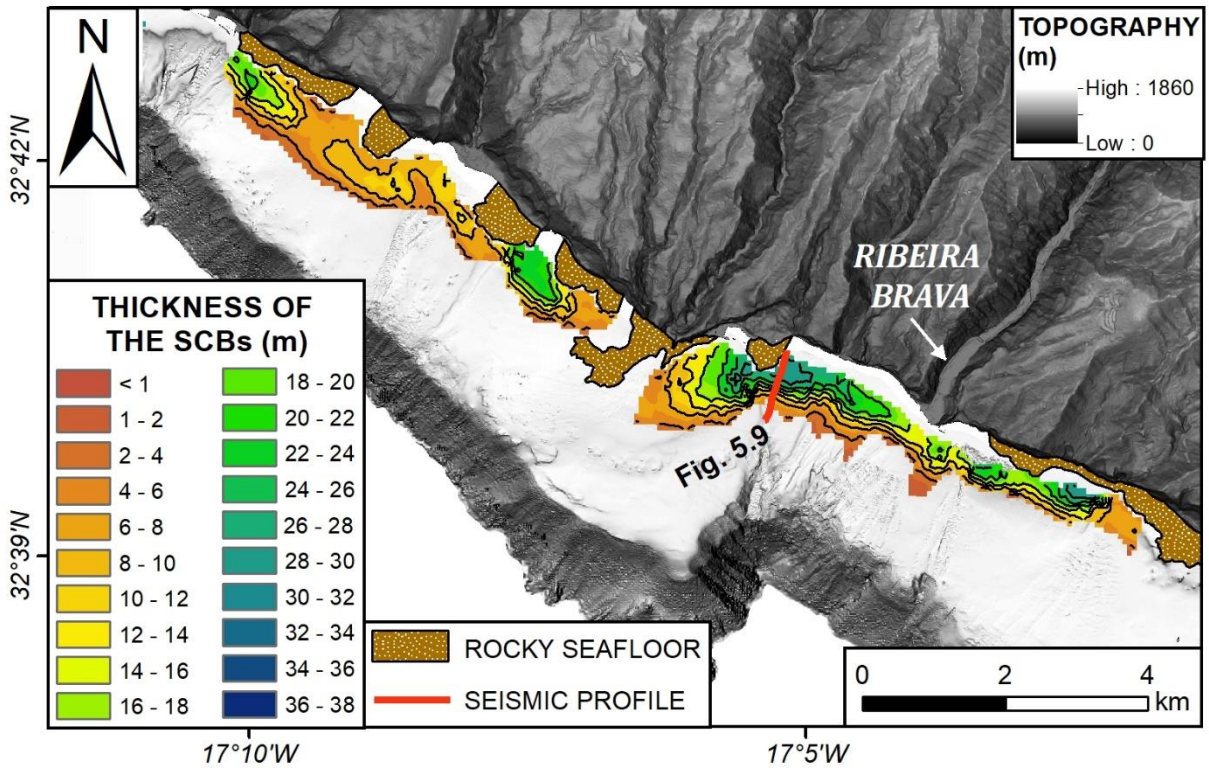

Figure 5.8. Map of the thickness of the prograding bodies in sector 2 of the insular shelf of Madeira (see location in Fig. 5.1). Brown polygons delimit nearshore rocky seafloor. Thickness increases from orange to green and blue tones. Contours are spaced each 4 m. The red line locates the seismic profile of Fig. 5.9.

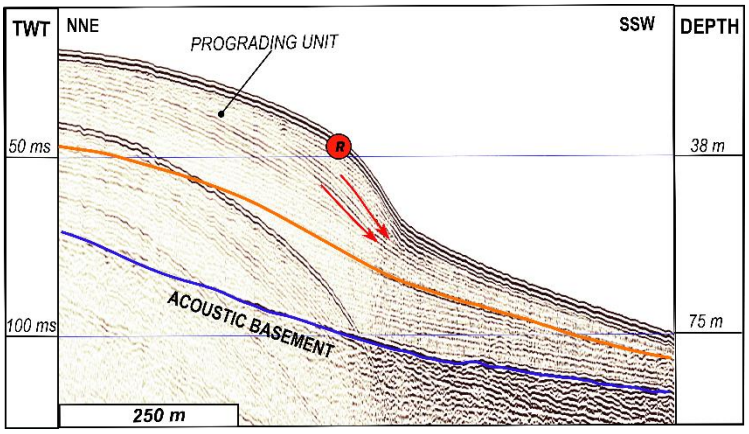

Figure 5.9. Sparker seismic profile perpendicular to the coastline in sector 2 (location in Fig. 5.8). Symbology as in Fig. 5.6 in chap. 5. R marks the rollover point.

SECTOR 3

On this sector, the SCBs are better developed between Cabo Girão and Funchal where they can reach thicknesses close to 20 m (Fig. 5.10) at both sides of Ribeira dos Socorridos and thickness within 14-16 m off Funchal. Here, the SCB's topset is on average ~570 m in width (average rollover depth of 27 m). To the east of Ribeira dos Socorridos, the seismic profile (Fig. 5.11) shows a prograding unit with oblique clinoforms, with foresets 3°- 4° steep. It develops above

a very thin aggradational unit and partly on the acoustic basement. To the west of Funchal, the upper prograding body (Fig. 5.12) has internal architecture with oblique geometry and the foresets are steeper (4°-7°) than those of Fig. 5.11. An old prograding body is recognized underneath (Fig. 5.12).

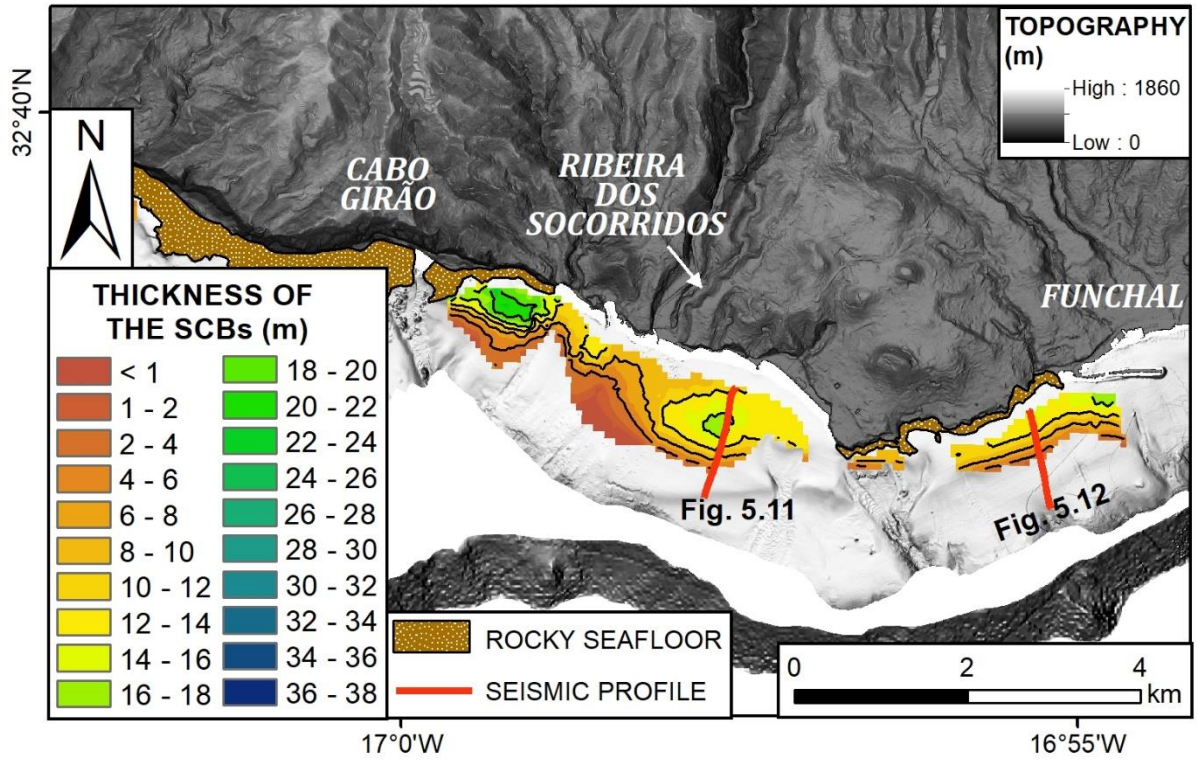

Figure 5.10. Map of the thickness of the prograding bodies in sector 3 of the insular shelf of Madeira (see Fig. 5.1 for location). Brown polygons delimit nearshore rocky seafloor. Thicknesses increases from orange to green and blue tones. Contours are spaced each 4 m. The two red lines are the locations of the seismic profiles of Fig. 5.11 and 5.12.

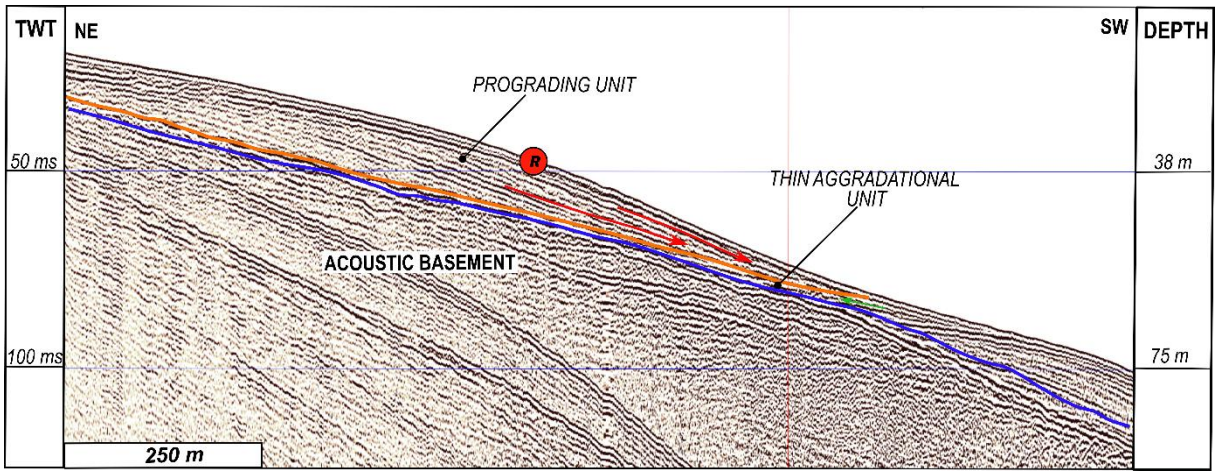

Figure 5.11. Sparker seismic profile perpendicular to the coastline in sector 3 (location in Fig. 5.10). Symbology as in Fig.5.6. R marks the rollover point.

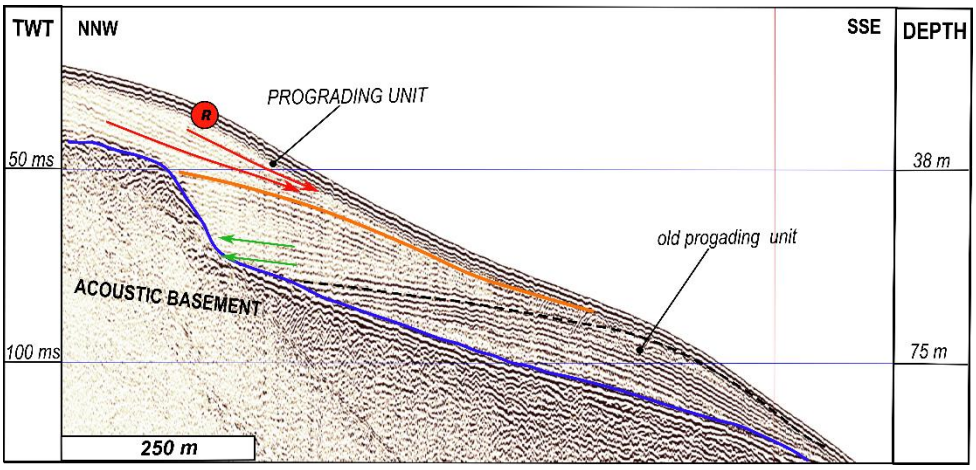

Figure 5.12. Sparker seismic profile perpendicular to the coastline in sector 3 (location at Fig. 5.10). Symbology as in Fig.5.6. R marks the rollover point.

SECTOR 4

In this sector, the SCBs are offshore the largest hydrographic basins but too narrow to be mapped with the seismic profiles and therefore the characteristics presented in Table 5.2 refer only to the few places where these could be obtained from the bathymetry (Fig. 5.13, RECENT SCBs). In these places the SCBs topset is around 220 m in width (average rollover depths of 22 ± 5 m). One seismic profile crossing the SCBs in this sector is represented in Fig. 5.14.

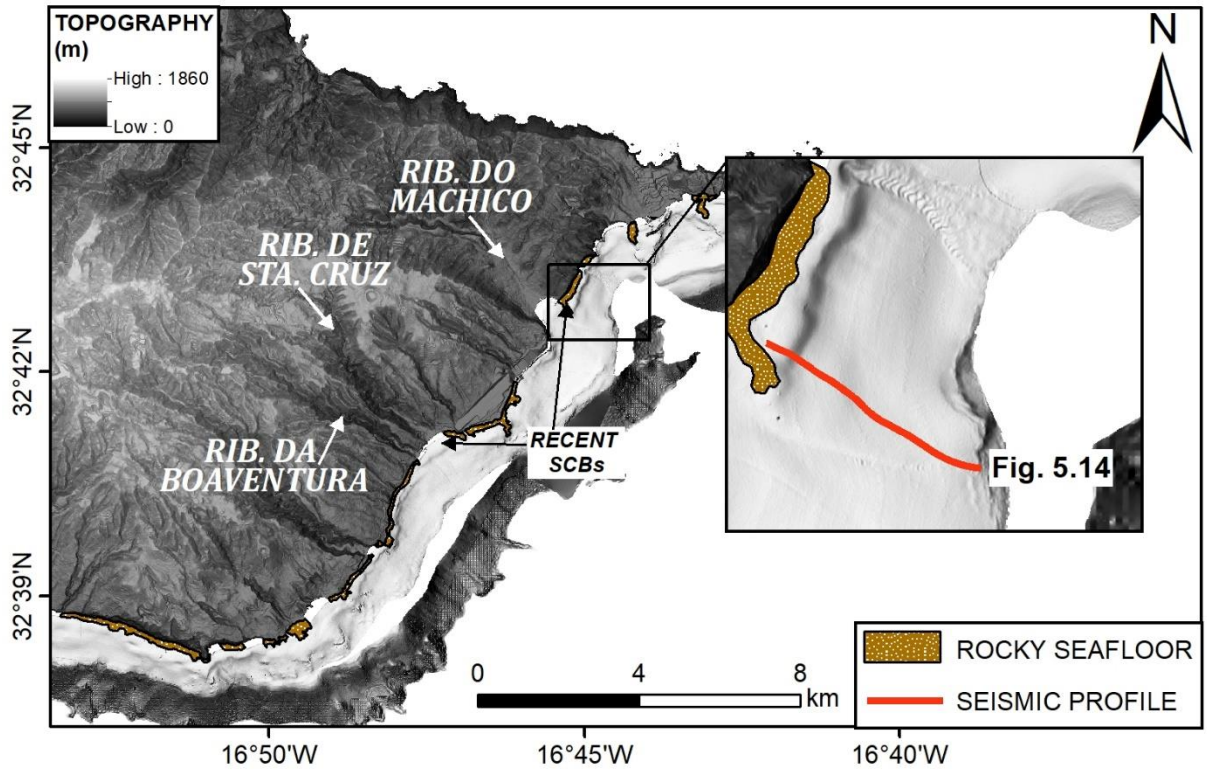

Figure 5.13. Easternmost part of sector 4 (see location in Fig 5.1) and location of the seismic profile crossing the SCB in Fig. 5.14. Brown polygons delimit the nearshore rocky seafloor.

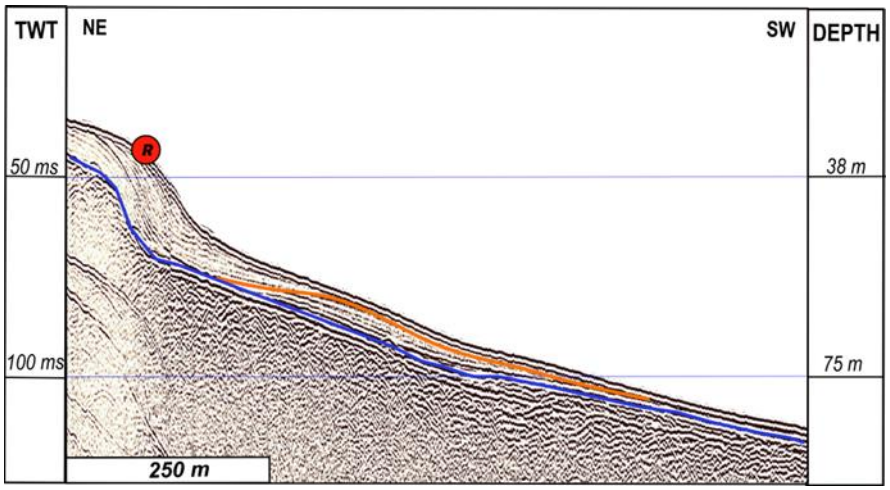

Figure 5.14. Sparker seismic profile perpendicular to the coastline in sector 4 (location in Fig. 5.13). Symbology as in Fig. 5.6. R marks the rollover point.

5.2.2. DISTRIBUTION OF WAVE HEIGHT AND SEDIMENT THRESHOLD OF MOTION

According to the 95th percentiles (Fig. 5.15) of the waves hitting the Madeira southern coast for the period 2013-2014, sector 1 is directly exposed to the highest waves (Hs 2 – 3.2 m), that come mostly from W and NW. Sectors 2 and 3 are still influenced by moderate waves (Hs up to 1.5 m) that decrease nearshore and towards east to 1 m. Sector 4 is sheltered from the highest waves coming from W and NW, and only hit from small waves (0.5 to 1 m) coming from the E.

The τ-ratio can be seen in Fig. 5.16 and shows the division between sediments that are put in motion by the 95th percentiles of waves hitting this coast and where sediment is quiescent with these wave characteristics.

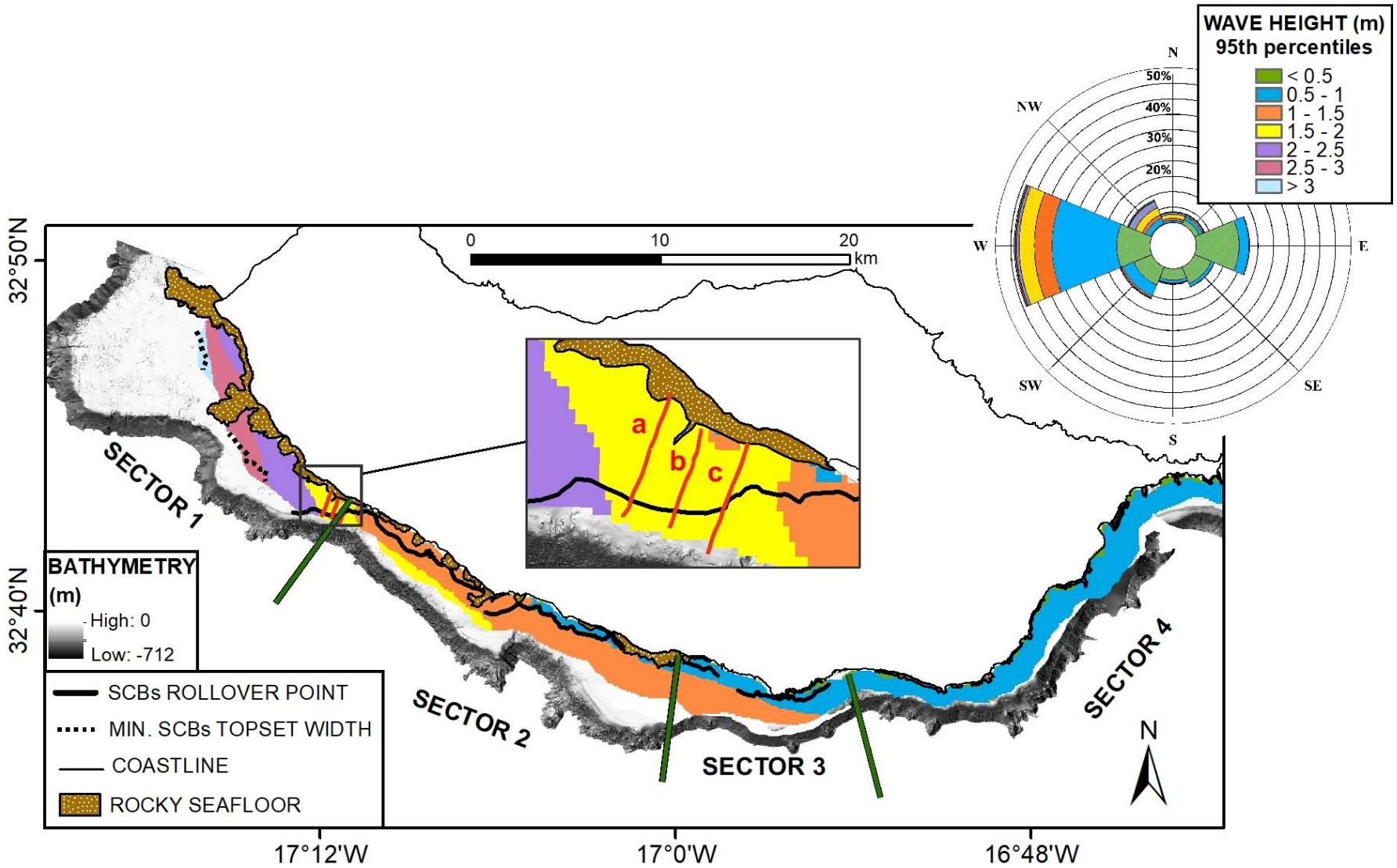

Figure 5. 15. Result of SWAN wave height distribution along Madeira's southern coast during adverse wave conditions (95th percentile) for the period 2013-2014. The inset displays the area of the seismic profiles shown in Fig. 5.18. On top, the rose chart shows the main wave heights and directions. Brown polygons delimit the nearshore rocky seafloor.

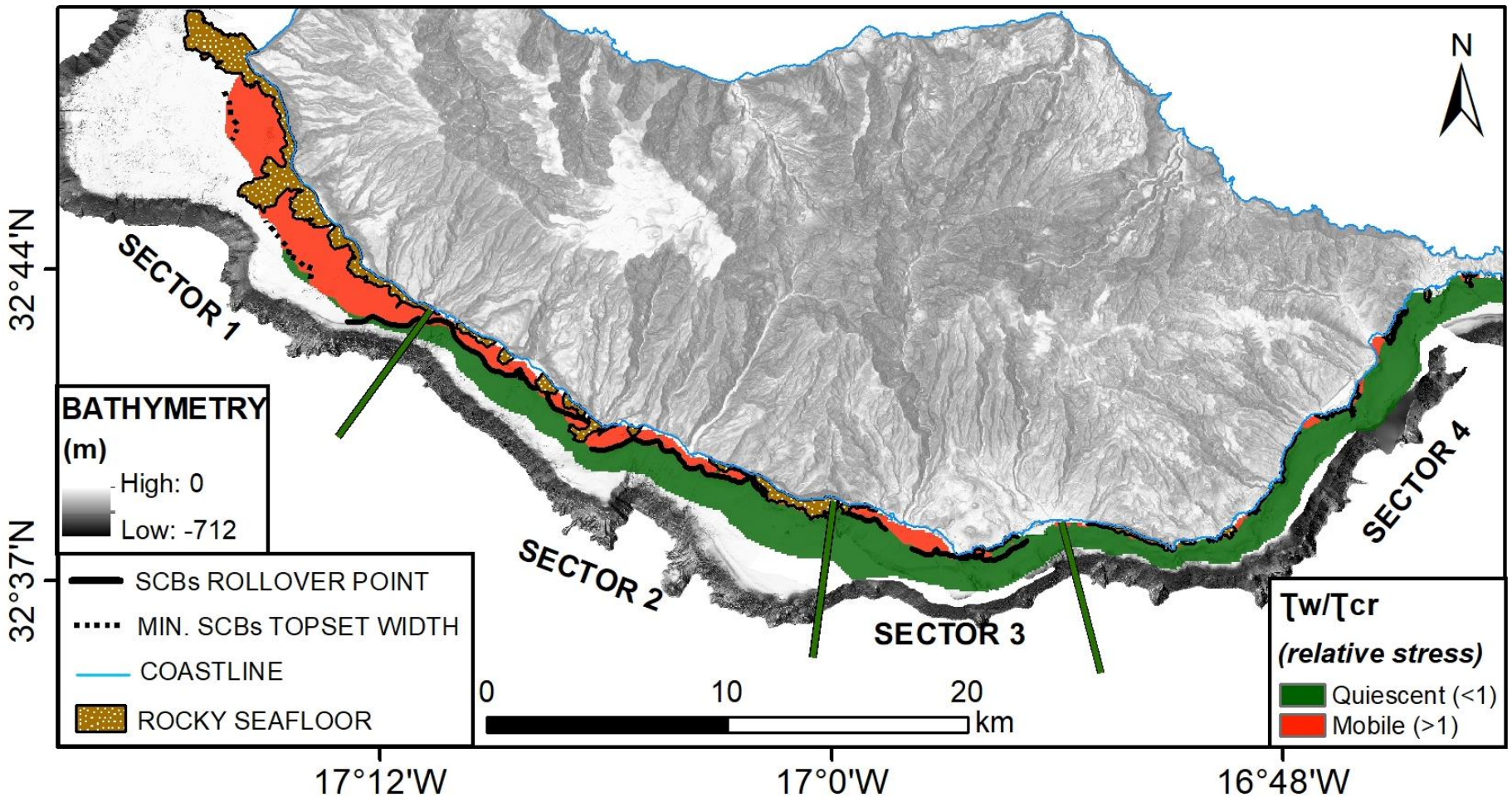

Figure 5. 16. Shaded-relief of Madeira Island and distribution model of the sediment threshold of motion based on the 95th percentile of waves for the period 2013-2014. The red colour represents the areas where the sediment is mobilized, while in the green areas the sediment is not mobilized. The transition between mobile and quiescent sediment fits fairly well with the SCBs rollover point trend (black bold line). Brown polygons delimit the nearshore rocky seafloor.

It also shows that the transition between the mobile and quiescent sediment coincides almost entirely with the SCBs rollover in the eastern part of sector 1, the entire sector 2, the western part of sector 3 and where the biggest SCBs are present in sector 4. In addition, the rollover location on sector 2 marks very well the transition from fine to very fine sands (topset to foreset transition) (see Fig. 5.1 to compare).

5.2.3. RELATIONSHIPS BETWEEN SCBs MORPHOLOGICAL PROPERTIES

The relationships among the clinoform morphological characteristics were analysed using scatter plots and the related R^2 considering values between 0 and 0.4 as inexistent or weak correlation; the values between 0.4 and 0.6 as a moderate correlation. Finally, the values comprise between 0.6 and 0.8 as strong correlated. The relations between rollover point depth and sediment grain-size, and between SCBs basal surface slope and thickness are weak, or not correlated at all (Fig. 5.17, R^2 in plots I, III, IV). Conversely, between the rollover point depth and the basal surface depth there is a strong positive correlation (Fig. 5.17, plot II). The SCBs thickness has no correlation or weak correlation with sediment grain-size and with basal surface slope (Fig. 5.17, plots V and VI). Between the basal surface depth and slope, no correlation was observed (Fig. 5.17, plot VIII).

The inherited topography represents the basal surface (or pre-existing bathymetry) on which the SCBs have developed. It corresponds to the volcanic basement or to previous depositional units (if present). The basal surface depth of the SCBs in sectors 1, 2 and 3 can be seen in Suppl. Fig. 10.1 and the slope of that surface in Suppl. Fig. 10.2 (in Appendix). In general, there is a relationship between the slope of the inherited bathymetry and the topset width (Fig. 5.17, plot IX). Accordingly, on sector 1 the slope is the lowest and this is where the topset width is wider. On sector 2 and the western part of sector 3, the slope gradients of the inherited topography are higher and the topset widths are shorter than in sector 1 (values in Table 5.2). On the eastern part of sector 3 and in sector 4, the slope of the inherited topography was not measured but from the bathymetry it is possible to see that SCBs are small with narrow topsets, and the slope of the inherited bathymetry must be high because the shelf is very narrow. The topset width also shows weak relationship with the grain-size (Fig. 5.17, plot X) but a strong correlation with the rollover point depth (Fig. 5.17, plot XI).

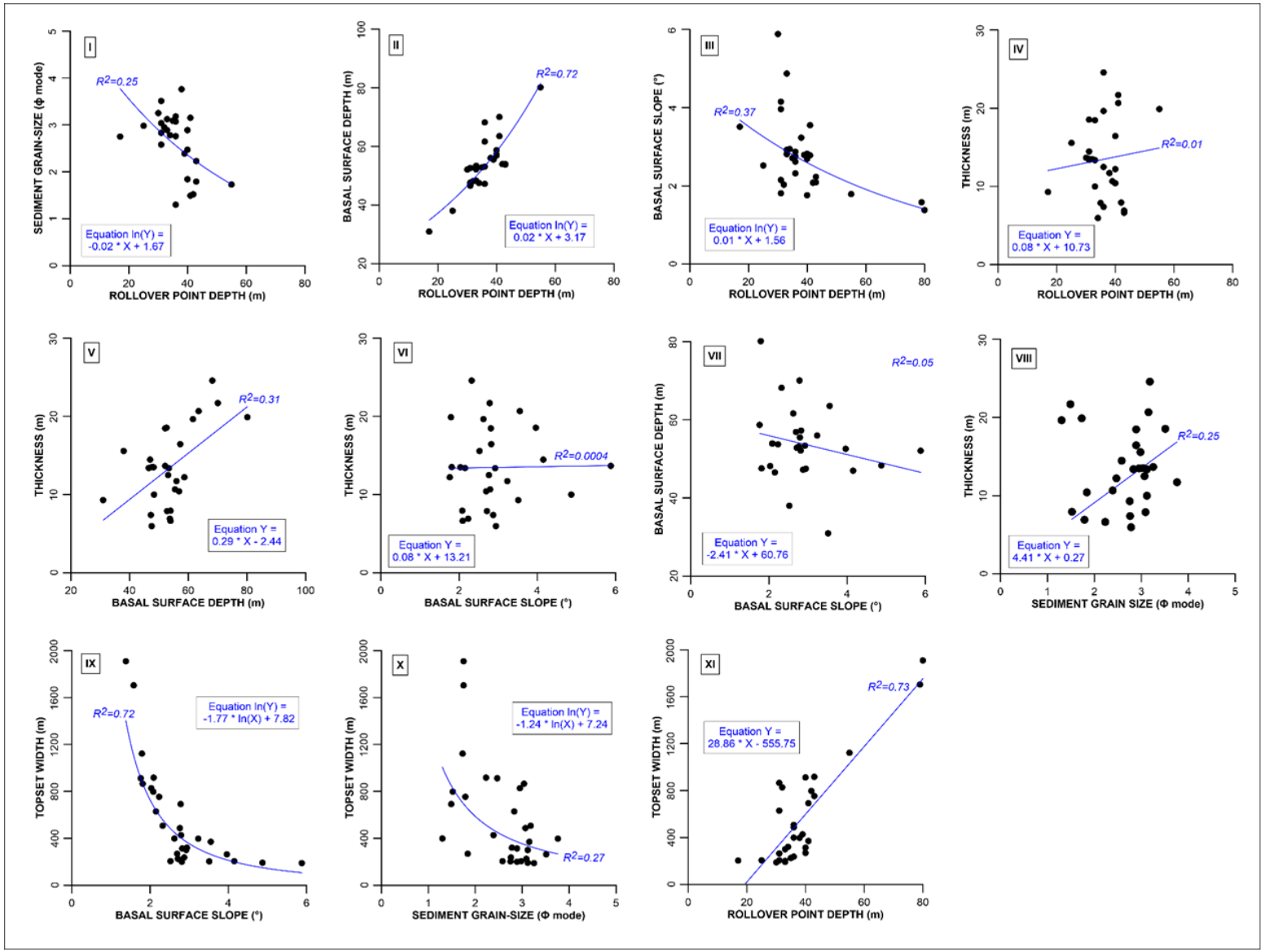

Figure 5. 17. Scatter plots showing the correlation of various parameters of the SCBs analysed for this study.

5.3 DISCUSSION

The morphology of the southern shelf of Madeira Island is the result of different factors that influence it, such as, its age of formation, the exposure to wave regime, pre-existing bathymetry, and sediment supply from the drainage network and cliff dismantling. Those contributions reflect in the SCBs spatial variability. The geophysical and sedimentary data available allowed the analysis of the morphological characteristics of the recent SCBs from the southern shelf of Madeira Island, evidencing which factors have more influence in the development of these features. In the following sections their role is discussed.

5.3.1. THE INFLUENCE OF WAVE ENERGY

One of the most important factors controlling the SCBs spatial variability in Madeira shelf seems to be the wave regime. In fact, there an almost perfect coincidence in sector 2 and in the western part of sector 3 between the clinoform rollover and the τ ratio mapping which suggests that wave action has a strong influence. The clinoform rollover (the topset to foreset transition) separates the zone where sediments are mostly in motion (onshore the rollover) because they are entrained by wave action and associated currents and transported from a zone outside the wave influence, offshore the rollover, where deposition prevails (Medri et. al., 2023; Mitchell, 2012; Mitchell et al., 2012). The τ ratio calculation which represent the shear-stress produced by the wave action (see chap. 4) is based on the wave characteristics (95^{th} percentile of H_s and T_p, significative wave height and peak period) and the mean grain-size of the seabed sediments. The mentioned coincidence fits well with what other authors have claimed in the past, that the clinoform rollover depth is mostly related to the 5^{th} or 10^{th} percentile of the wave height (Mitchell, 2012; Mitchell et al., 2012, Walsh et al., 2004).

In what concerns the area occupied by the SCBs on the shelf, there is a tendency for the clinoforms to become progressively narrower eastwards. In Sector 1, the topset width corresponds to more than 50% of the shelf width, whilst on sectors 2 and 3 it represents normally less than one third of the shelf width and on sector 4 it represents less than 10%. From west to the east the wave exposure also changes (decreasing wave heights and periods). This fits well with the modelling by Swenson et al. (2005) that showed that an increase in wave height will increase the topset width and decrease the foreset gradient. In fact, well-developed subaqueous deltas are normally located in energetic marine environments. If the system is too energetic, it could eventually affect the entire shelf and the resulting shear stresses can destroy

the subaqueous delta geometry (Swenson et al., 2005). That is what appears to be happening in the eastern part of sector 1 where no clinoform rollover can be discerned from the bathymetry. The τ ratio calculation does not coincides so well with the clinoform rollover on sector 1. The limit between mobile and quiescent sediments is shoreward the rollover in the east part of this sector, and in the west, it was not possible to map the rollover due to the lack of seismic data. In the eastern part of sector 3 and sector 4, only in some places it was possible to map the clinoform rollover but the τ ratio mapping shows that the sediment is quiescent on most of the shelf. This means that most likely, on these areas, other factors are influencing the SCBs position.

5.3.2. THE INFLUENCE OF ACCOMMODATION SPACE (AND INHERITED TOPOGRAPHY)

In most of the analysed seismic profiles it is possible to observe how the progradation of the recent SCBs occurs above a surface which is a previous aggradational unit or an erosional volcanic basement. The shelf width, as well as the physiography of the pre-existing bathymetry in terms of slope and depth, significantly influence the formation and shape of the sedimentary deposits lying above (Ainsworth et al., 2020; Burgess et al., 2008; Ulicny et al., 2002). It is commonly accepted that high pre-existing gradients produce thicker sand bodies but these prograde shorter distances (small topset widths) and vice versa. This is exactly what it is observed along the southern coast of Madeira where shelf width decreases eastwards (and consequently pre-existing bathymetry becomes narrower) from a maximum of 9 km to a minimum of 1 km and so, the topset width. Two extreme situations are observed on sector 1, where apparently the topset width coincides with the shelf break or the rollover is absent, and on the eastern sector 3 and sector 4, where the topset width is so narrow that could only be mapped in some places due to lack of nearshore data. The best example of how the inherited topography controls clinoform development lies in the transition from sector 1 to sector 2. In a relatively small alongshore area, topset width changes from 2.5 to 1 km and the wave exposure here is similar. Here, the controlling factor is most likely the shelf width (or pre-existing bathymetry) as shown in Fig. 5.18, which tends to form thicker and narrower bodies.

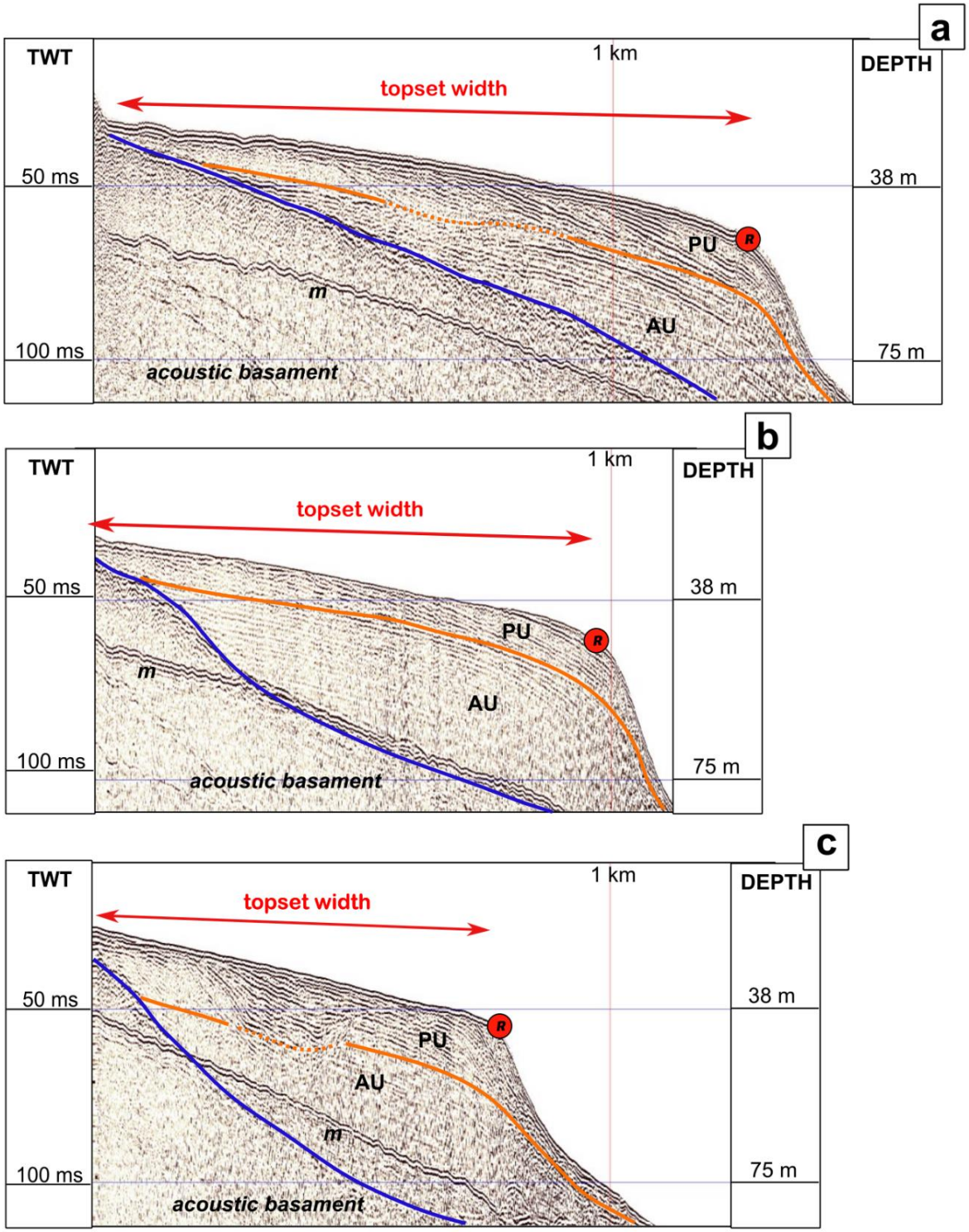

Figure 5. 18. Seismic profiles in the eastern part of sector 1 showing different topset widths in concordance with the inherited topography. Their location is shown in Fig. 5.15. Symbology as in Fig.5.6. R marks the rollover point position.

The occurrence of uplift or subsidence is another significant aspect influencing the accommodation space on the shelf. Nonetheless, along the coast, the absence of subaerial and submarine marine terraces, as documented on Santa Maria Island, Azores (Ricchi et al., 2018), and at Salina, in the Aeolian Islands (Lucchi et al., 2019), suggests that vertical movements induced by volcano-tectonic processes were not significant in the past 7,000 years. In fact, the island must be either stable or slowly subsiding, because there are no markers for uplift (Ramalho et al., 2010), such as submarine lavas or sediments, in the younger volcanic sequences cropping out above sea level.

According to Zhang et al. (2019), a shelf can be classified as either accommodation-dominated or supply-dominated based on the characteristics of its SCBs deposits. In the earlier case, SCBs do not extend to the shelf edge and exhibit a step-backward morphology, with the most recent deposits found in the shallowest areas of the shelf. Conversely, a supply-dominated system is distinguished by recent SCBs that reach the shelf edge, with their rollover points position coinciding with the shelf edge. Observations on the southern shelf of Madeira indicate a predominantly accommodation-dominated system, except for the region between sectors 1 and 2, where SCBs almost reach the shelf edge.

5.3.3 THE INFLUENCE OF SEDIMENT SUPPLY (AND GRAIN-SIZE DISTRIBUTION IN THE INNER SHELF)

The superficial sedimentary cover of the southern shelf of Madeira Island is inherently related to its sources and apparently also influences the SCB's geometry.

Sector 1 is mostly covered by coarse and medium sands which are found offshore high cliffs (up to ~ 550 m high), and, in general, close to landslide deposits and other rocky outcrops on the shelf (brown polygons in Figs. 5.1, 5.4 and 5.8 for example). In this sector, sediment production from hydrographic basins is the lowest; these basins are relatively small, have low gradients, and are installed in the younger and less weathered volcanic units (CVM3, CVS 1-2) and CVS2, yellow and green colours in Fig. 5.1B). Therefore, it appears that, in this part of the shelf, sediment results mainly from cliff dismantling. In addition, this sector is the most exposed to the wave regime that could originate strong along-shore currents, transporting finer sediments to the east, leaving the coarser sediment behind as previously suggested by Rodrigues et al. (2004). The reduced thickness of the deposits and the larger topset widths is also consistent with a more energetic environment. According to Swenson et al. (2005), high sediment advection will result in wide subaqueous delta clinoforms.

Sector 2 is mostly covered by fine and very fine sand, where the corresponding hydrographic basins are larger, including the largest stream, Ribeira Brava. These basins cross highly weathered and more likely erodible formations (CVM 1-2 units, see red to yellow colours in Fig. 5.1 B). The coastline is characterized by lower cliffs than sector 1 (average of 291 m), intercalated by several stream outlets. The SCBs have medium topset widths and show the thickest deposits of Madeira shelf. In addition, the topset to foreset transition (rollover) is marked by a change of fine to very fine sands. Given these characteristics, it seems that shelf sediments result mainly from the outflow of streams and that the larger sediment supply is also responsible for the ticker deposits on this sector.

Sector 3 is very similar to the previous one in terms of sediment grain-size and SCBs characteristics in its western part. Towards the east topset widths became very narrow and unable to be mapped due to the lack of nearshore coverage. The coast has even lower cliffs (average less than 100 m) and the remnants of a recent lava delta. This sector is characterized by smaller hydrographic basins with respect to the previous sector, despite still being large. They cross mainly lithologies corresponding to Pleistocene units (CVS 1 and 2 in Fig. 5.1 B), except for Ribeira dos Socorridos, where older and more weathered lithologies outcrop (CVM 1-3). It looks like on the western part of this sector the shelf sediments result mainly from stream discharge while towards the east this source is probably decreasing because SCBs tend to be smaller. However, their small size towards the east is probably more likely to due to less energetic environment since the τ ratio predicts very small to no SCBs.

Sector 4 is formed by very small SCBs that are restricted to the nearshore where seafloor sediment is composed of fine and very fine sands. The SCBs width on this sector has been measured offshore the largest hydrographic basins which can deliver more sediment, explaining why they are thicker (9-13 m). However, as one moves offshore, sediment becomes coarser (medium to coarse sands), probably linked to the presence of bioclastic material, i.e., carbonated skeletal organism particles (see chapter 7). This sector is characterized by hydrographic basins that produce less sediment than those from sectors 2 and 3. The small size of the SCBs is probably related to lower sediment production and to being more protected from wave energy as the τ ratio suggests. This is consistent with the modelling of Swenson et al. (2005) that showed that a decrease in advection will generate smaller topset widths.

5.3.4. PROCESS OF FORMATION

From the previous discussion wave energy appears to be the most important factor in controlling SCB's morphology and spatial variability, seconded by inherited topography and lastly by sediment supply. Whether SCBs are formed by wave-supported gravity flows as suggested by Mitchell (2012) and Medri et al. (2023) or by wave-generated downwelling currents as suggested by Hernández-Molina et al. (2000), Chiocci & Romagnoli (2004), Quartau et al. (2012) and Innocentini et al., (2022), the τ ratio calculation predicts considerably well the clinoform rollover position (or topset width). Hyperpycnal outflow caused by extreme rainfall it is not providing any control on topset width since sectors 2, 3 and 4 have greater outflows than sector 1 but show narrower topset widths. It does provide, however, a control on grain-size with sectors 2 and 3 showing the more productive hydrographic basins and the finer grain-sizes. The topset width is apparently controlled by the gradient of the inherited bathymetry and that is the reason why on the western side of sector 1 topset widths coincide with the shelf edge when the τ ratio calculation predicts them to be narrower.

Based on these findings, we provide a model of clinoform development at the Madeira southern shelf (Fig. 5.19):

- Type I SCBs - They have very large topset widths and low thickness. Sometimes, they do not even show clinoform geometry, i.e., they are just tabular bodies that end on the shelf edge. This results from the action of stronger wave energy and very low gradients of the inherited bathymetry. Sediment supply comes mostly from cliff erosion, and the sediment is coarse.
- Type II SCBs - They have intermediate topset widths that occupy ~¼ of the shelf width and are thicker. This results from the action of intermediate wave energy and intermediate gradients of the inherited bathymetry. Sediment supply comes mostly from stream discharge, and sediment is fine.
- Type III SCBs - They have the smallest topset widths that occupy ≤1/10 of the shelf width. This results from the action of low wave energy and high gradients of the inherited bathymetry. Sediment supply comes mostly from stream discharge, and sediment is fine.

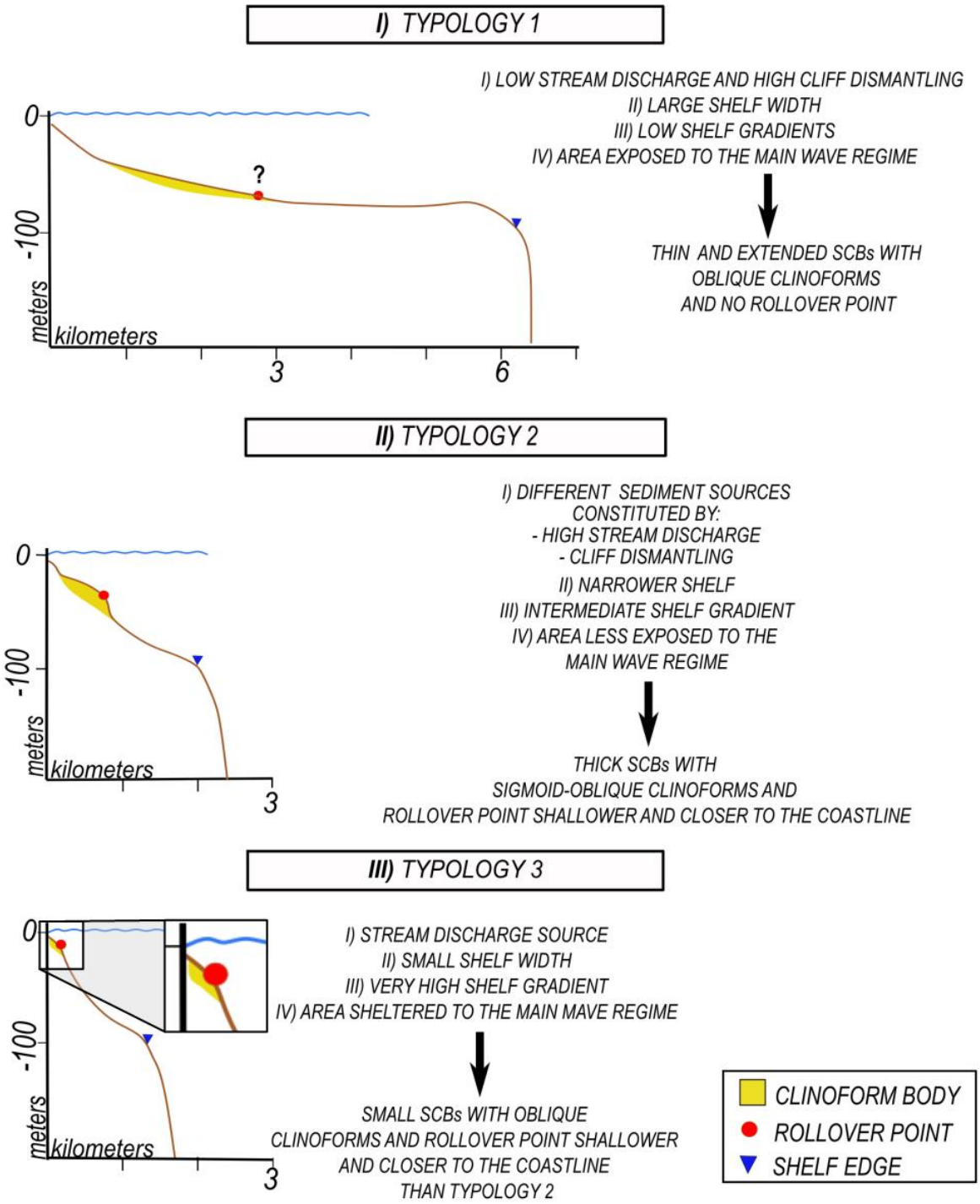

Figure 5. 19. Sketches of the different SCBs growth patterns observed, highlighting the factors influencing their variability in the southern shelf of Madeira Island. SCBs are the yellow polygons, the position of the clinoform rollover point is represented by red dots; shelf edges are depicted as blue triangles.

5.4. CONCLUSIONS

Subaqueous clinoform bodies are common depositional features within insular volcanic shelves. On the southern submarine shelf of Madeira Island these features show great variability in terms of extension, thickness, internal structure, and rollover point depths. These characteristics can be related to three main factors: wave exposure, morphology of the inherited bathymetry and sediment supply. Higher waves will cause the sediment to be transported and deposited more offshore, creating SCBs more extended in width. The inherited bathymetry is defined by the depth and slope of the basal surface on which the SCBs are developed. Both parameters determine the accommodation space available for the sediment accumulation, which is reflected in the external and inner geometry of the SCBs. Thus, when the basement is shallower but has low gradients (i.e. in Sector 1), the SCBs are thin and eventually no rollover point will form, instead higher gradients will promote the formation of thicker bodies characterized by a clear and laterally continuous rollover point (i.e. Sectors 2 and 3). However, when the gradients are too high and the shelf is narrow, the clinoform bodies are small and are restricted to the shallowest parts (i.e. sector 4). The sediment supply on the insular shelf is mainly provided by stream discharges and cliff dismantling. The sediment load discharged to the coast is higher where the streams have more erosive capacity and cut through more erodible and weathered formations. Indeed, within each sector, distinct grain-size mode distributions are observed. These variations can be attributed to factors such as the primary feeding source, specific characteristics of the hydrographic basins, and the nature, texture, and degree of weathering of lithologies cropping out in the area.

Overall, the southern Madeira shelf can be considered as an accommodation-dominated system despite its significant sediment production. This might be unexpected for an island experiencing frequent heavy rainfall and possessing such a well-developed drainage network. Due to its large shelf dimension (~ 740 km²), the amount of sediment generated is insufficient to properly fill the entire shelf extension. Consequently, the recent SCBs are mostly confined to the inner part of the shelf occupying only a small portion of it.

CHAPTER 6: ORIGINS AND CONTROLLING FACTORS OF BEDFORMS FORMED BY SUPERCRITICAL SEDIMENT DENSITY FLOWS ON THE SOUTHERN SHELF OF MADEIRA ISLAND

6.1. INTRODUCTION

This chapter presents and discusses the findings concerning the bedform fields observed on the southern shelf of Madeira Island. It is organized according to the draft prepared for manuscript II (see subchapter 1.3). Detailed maps, graphs, and measurements for each bedform field are provided in the supplementary material in Appendix, between pages 140 and 194.

Large scale bedforms have been widely recognized in submarine volcanic island flanks, mostly on their deeper parts (Wynn et al., 2000a, 2000b; Masson et al., 2008; Leat et al., 2010; Hoffmann et al., 2011; Casalbore et al., 2014; Mazuel et al., 2016; Pope et al., 2018; Quartau et al., 2018, Santos et al., 2019; Casalbore et al, 2021). However, only a few studies have shown small scale bedforms on volcanic islands shelves, and these were confined to channels cutting the upper slope (Casalbore et al. 2010, 2017, 2021, Clare et al., 2018). There is only one study describing small-scale bedforms on insular shelves, at La Réunion Island (Babonneau et al., 2013). In this Thesis, the first systematic study of sediment waves found on volcanic islands shelves is presented.

Madeira Island is a tall and rainy island, incised by a drainage network with a powerful erosive capacity (Lira et al., 2013) and displaying a well-developed shelf (Quartau et al., 2018). Therefore, it has the ideal conditions to improve our understanding on the generation of these features on island shelves because there is: (i) available multibeam bathymetry and sedimentological data collected during the last 20 years, (ii) a marked variability of the size of hydrographic basins and hence the amount of sediment discharge onto the shelf (iii) morphologic variability along the coastline, i.e., tall cliffs faced by shelf sediment starved areas, alternating with low interfluve coastlines where streams discharge sediments and, (iv) variable shelf morphologies (in terms of width and slope) and sediment types. This available information allowed performing a morphological and morphometric characterization of the bedform fields recognized in the southern shelf of Madeira Island and an analysis of their evolution based on multi-temporal bathymetric data (2002-2013-2019). This contributed to better understand the triggers of sediment density flows, their timing, and the type of hazards expectable on this type of settings. This awareness has important implications because these flows can damage infrastructures such as submarine communication cables and aquaculture structures (Pope et

al., 2018). They can also affect marine aggregate dredging activities and trigger submarine landslides which in turn can produce small tsunamis that may impact the neighbouring coastlines (Omira et al., 2022).

6.2. RESULTS

The majority of bedform fields are located within the shelf region spanning from Jardim do Mar to Funchal (fields 1 to 8 in Fig. 6.1). Many bedforms fields occur downslope of scars incising the clinoform rollover. Ten bedform fields oriented perpendicular to the coastline were mapped (blue circles in Fig. 6.1). Bedforms mostly have asymmetrical cross-section shape but different wave height, wavelengths, slopes and asymmetry. According to their location (type of adjacent coastline, link or not to hydrographic basin) and morphologies (channelized or fan-shaped features) were grouped in four main classes (see Table 6.1 and subchapters 6.2.1., 6.2.2., 6.2.3. and 6.2.4.). A further type of bedforms, developed obliquely to the shelf slope, is described in subchapter 6.2.5.; related observations are located in some areas of the shelf and delimited by red boxes in Fig. 6.1. A thorough description of each bedform field can be found in the Appendix between pages 140 and 194.

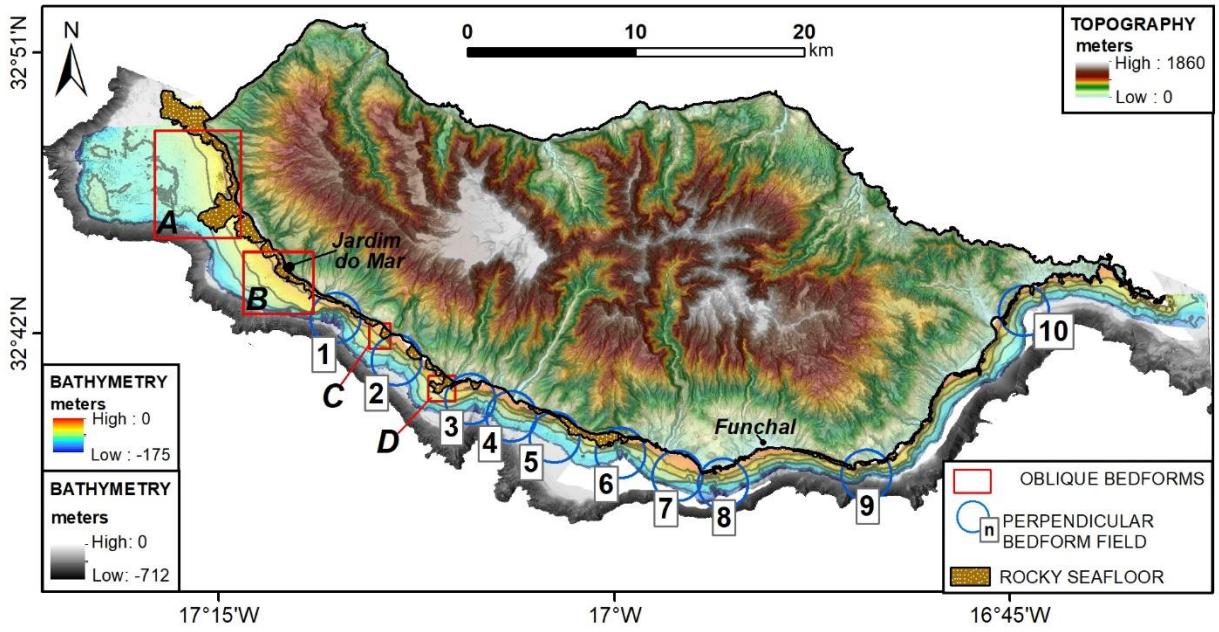

Figure 6.1. Map of the bedform fields recognized in the southern shelf of Madeira Island. The numbered blue circles identify each bedform field perpendicular to the coastline. Red rectangles mark the areas where bedforms that are oblique to the coastline were also recognized, identified A to D. Brown polygons represent nearshore rocky seafloor. The two bathymetries are from 2002 (coloured scale) and 2014 (grey tone scale). Contours are each 25 m.

Table 6.1. Synthesis of the main bedform fields and their characteristics.

	Bedforms fields linked to hydrographic basins		Bedforms fields not linked to hydrographic basins	
	Channelized features (Type I)	Fan-shaped features (Type II)	Channelized features (Type III)	Fan-shaped features (Type IV)
ID number	1, 2, 3, 4	4, 5, 7	6, 8, 9	10
Min and max. hydrographic basin area (km²)	1 - 10	4.5 - 41	-	-
Onshore morphology	stream outlets		tall cliffs / lava deltas	
Clinoform rollover steepness (°)	6 - 23	8 - 11	7 - 15	16
Incision of shelf edge by the erosive channel (m)	less than 1 to > 50	-	less than 1 to ~40	-
Elevation of fan features (m)	-	5 to ~ 10	-	6
Channel or fan-shape feature steepness (°)	4.7 - 13	4.5 - 7	4 - 11	6.8 – 4.2
Plan-view bedform crest shape	crescentic	mostly sinuous	crescentic	sinuous / crescentic
BEDFORM PARAMETERS **(average ± dev. standard)**				
Wavelength (m)	39.6 ± 9.6	71.9 ± 16.7	35.6 ± 11.6	33.7 ± 5.7
Wave-height (m)	2.2 ± 0.8	3.7 ± 0.9	2.4 ± 0.5	1.5 ± 0.3
Stoss-side slope (°)	3.3 ± 1.6	1.7 ± 1.2	-0.7 ± 1.4	-1.04 ± 1.1
Lee-side slope (°)	9.2 ± 2.8	12.7 ± 2.8	10 ± 1.5	10.4 ± 1.4
Bedform slope (°)	4.2 ± 0.9	4.2 ± 0.8	4.2 ± 0.6	5.1 ± 0.7
Asymmetry	1.2 ± 0.5	2.3 ± 0.8	1.3 ± 0.7	1.2 ± 0.5
Cross-section shape	Downslope asymmetric			

6.2.1. BEDFORMS INSIDE CHANNELS LOCATED OFFSHORE STREAM MOUTHS (TYPE I)

These bedforms occur on fields 1 to 4 (Figs. 6.2, 6.3, 6.4 and 6.5) and are found within channels that occur offshore one or more stream outlets. The headwalls of the channels correspond to scars on the clinoform rollover and occur at distances between 180 and 700 m from the coastline and at depths between 20 and 40 m. All the channels extend to the shelf break, and some are connected to canyon headwalls by tributary gullies on the upper slope (Figs. 6.3 and 6.5). On those cases, narrowing of the shelf width is observed due to retrogressive erosion of the canyon headwalls. Near the shelf edge, the channels are linear, usually present U-shaped cross sections

and large vertical incisions (that can reach >50 meters in the wider channels; see Suppl. Fig. 10.3 in Appendix). The vertical incision of the channels decreases upslope, and some develop dendritic patterns (e.g. Fig. 6.2). The bedforms inside the channels are mostly crescentic downslope in plan-view and, sometimes, they do not start at the channel heads but at greater depths.

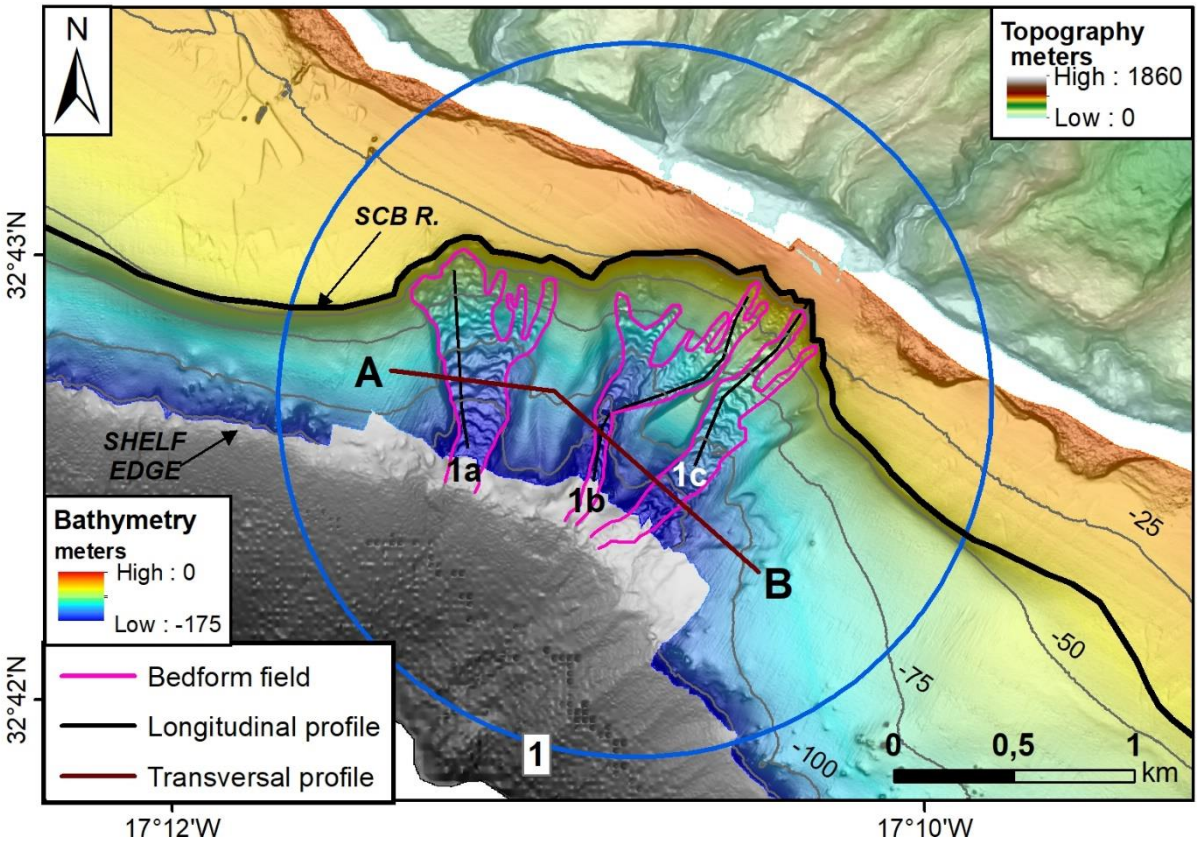

Figure 6.2. Shaded relief bathymetry of bedform field 1 (caption and location as in Fig. 6.1) Contours spaced every 25 meters. The transversal profile (A-B) is shown in Suppl. Fig. 10.3 in the Appendix and the longitudinal profiles of bedforms 1a, 1b, and 1c are shown in Suppl. Fig. 10.4 in the Appendix. SCB R.: subaqueous clinoform body rollover.

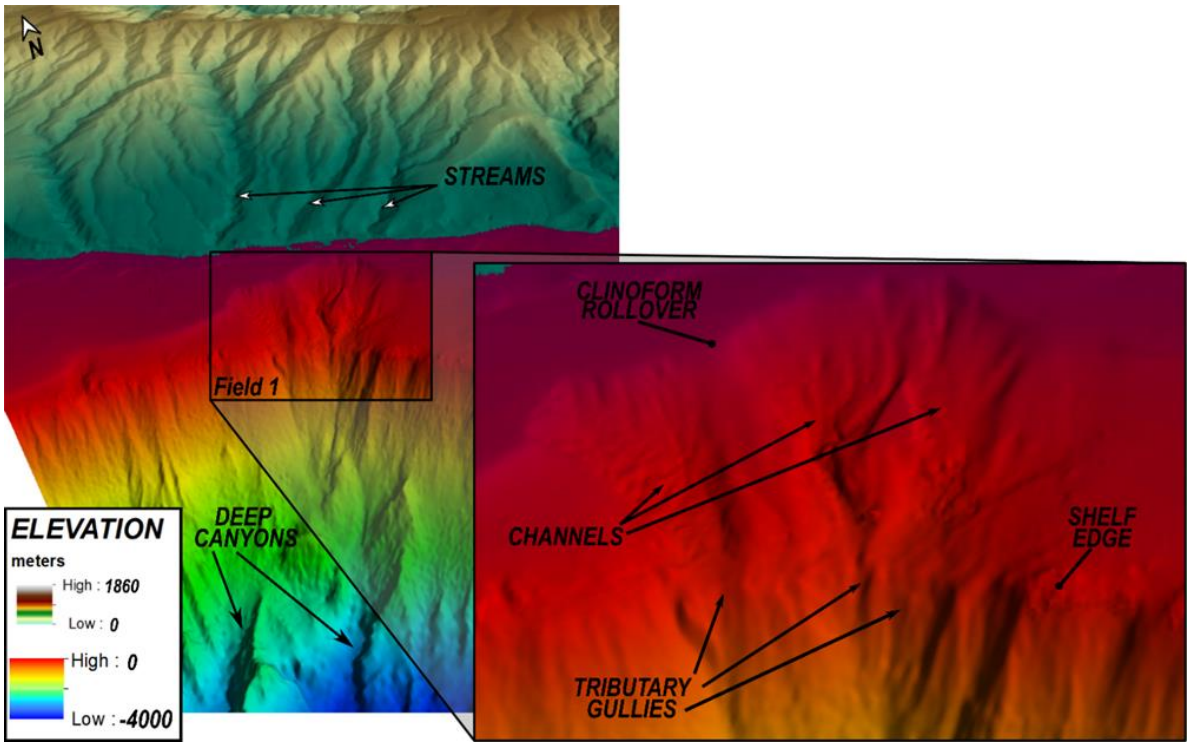

Figure 6.3. 3D image of bedform field 1 (location in Fig. 6.1). Note the link between the subaerial drainage (streams), the channels on the shelf and the tributary gullies in the canyons beyond the shelf edge. Vertical exaggeration 2x.

6.2.2. BEDFORMS ON TOP OF FAN-SHAPED AREAS LOCATED OFFSHORE STREAMS MOUTHS (TYPE II)

These bedforms develop on top of positive relief areas (up to 10 m above surrounding areas) that have a fan-shaped morphology, widening downslope (fields 4, 5 and 7 in Fig. 6.1). These areas may have headwalls corresponding to scars in the clinoform rollover (profiles 4a, 4b and 4d of field 4 and field 5 located in Figs 6.4 and 6.5) or can start offshore the clinoform rollover without any clear scar (profile 4c in bedform field 4 located in Figs. 6.4 and 6.5). The bedforms here are mostly sinuous in plan-view. In one case, the fan-shaped morphology is laterally delimited by smaller channels where crescentic sediment waves are observed (bedform field 7 located in Figs 6.6 and 6.7).

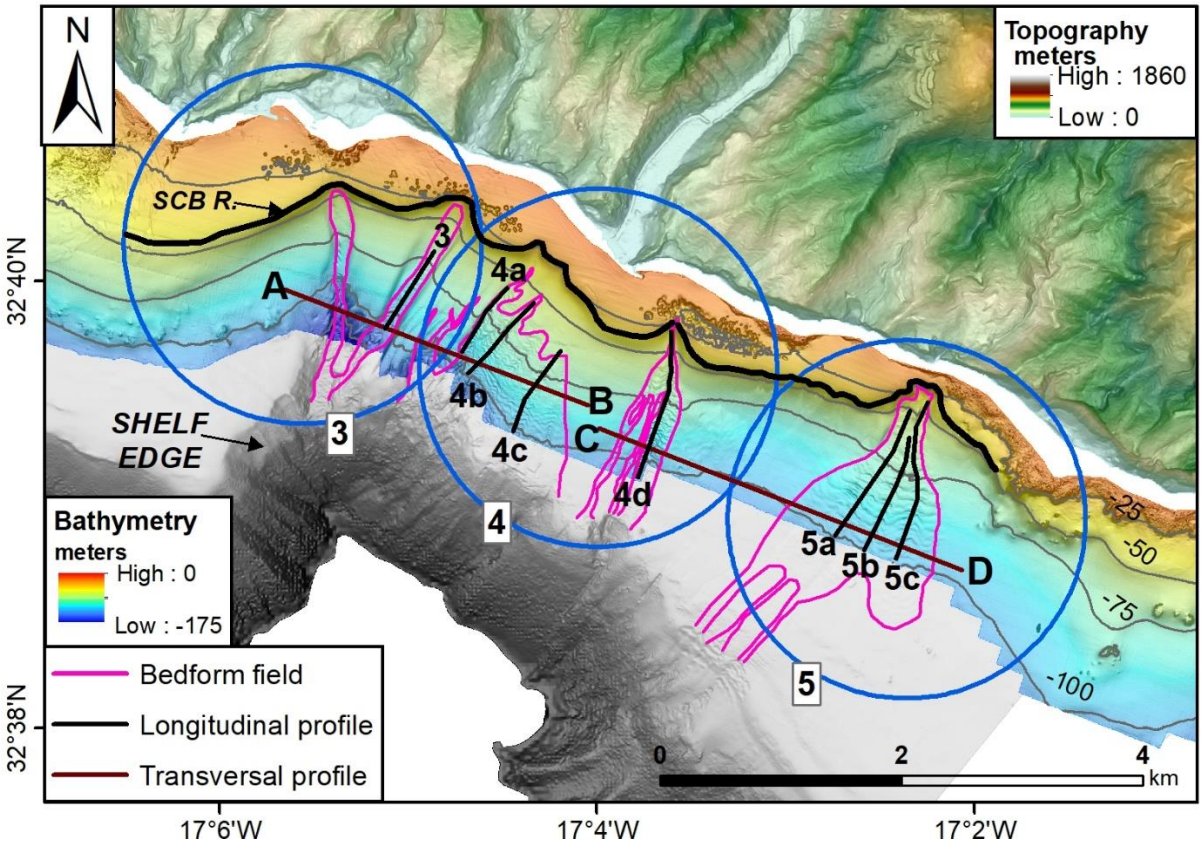

Figure 6.4. Shaded relief bathymetry (caption as in Fig. 6.1) of bedform fields 3, 4 and 5 (location in Fig. 6.1). Contours spaced every 25 meters. The longitudinal profiles 3, 4a, 4b, 4c and 4d, 5a, 5b, 5c are shown in Suppl. Figs. 10.18 and 10.21 respectively, in the Appendix. The transversal profiles (A-B and C-D) are shown in Suppl. Figs. 10.19 and 10.22 in the Appendix. SCB R.: subaqueous clinoform body rollover.

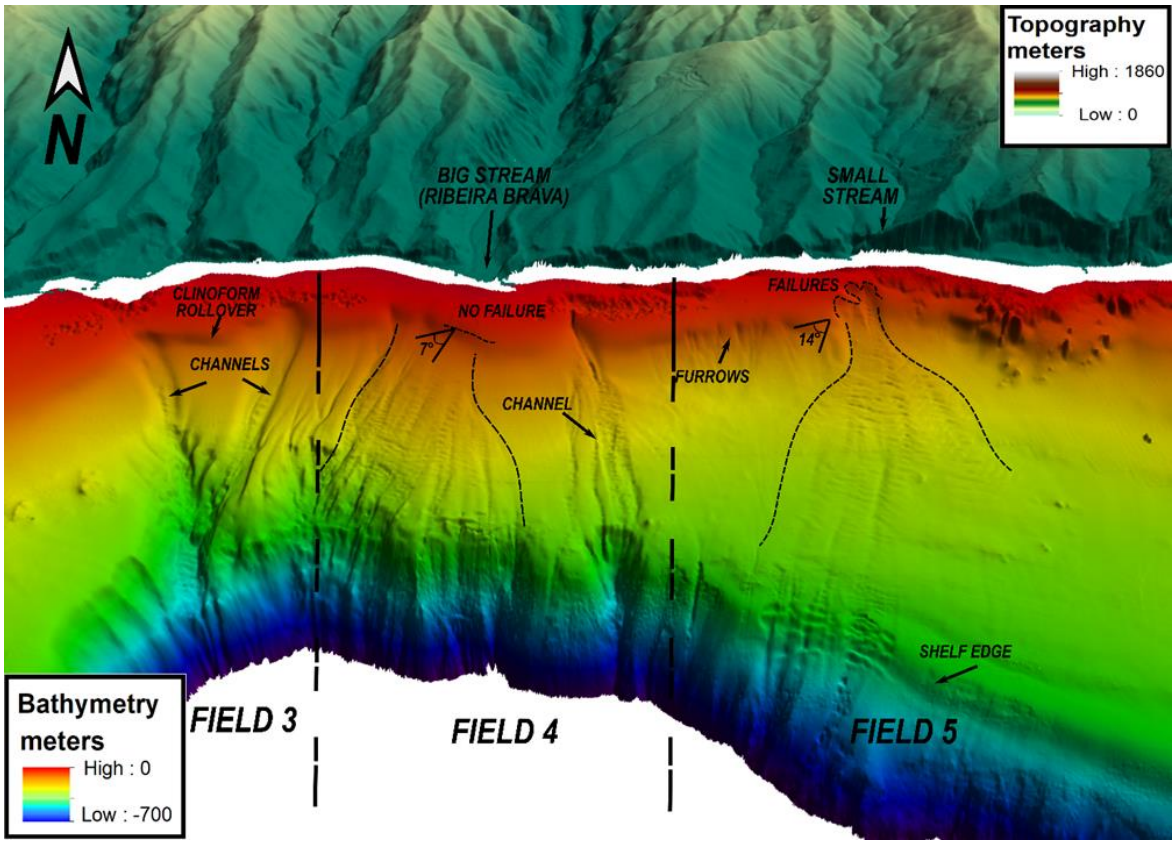

Figure 6.5. 3D illustration of bedform fields 3, 4 and 5 (location on Fig. 6.1). Note the absence of a clear clinoform failure onshore the fan-shaped feature of field 4. Field 5 shows a fan-shaped feature related to the clinoform failure which much steeper slope than that of field 4. Vertical exaggeration 3x.

6.2.3. BEDFORMS INSIDE CHANNELS WITHOUT LINK TO ONSHORE STREAM MOUTHS (TYPE III)

These bedforms occur inside channels that also initiate nearshore as scars in the clinoform rollover. However, these scars are not generally related to streams mouths, and the related coastal area is either composed of tall cliffs or lava deltas (fields6, 8 and 9in Figs. 6.1 and 6.6). Both the channels and the bedforms of Type III have similar morphologies to Type I. East of bedform field 8, very narrow channels (some with incipient bedforms) cutting the shelf break with headwalls at varying depths were also observed (Fig. 6.7). Some of these headwalls reach further upslope and incise the clinoform rollover.

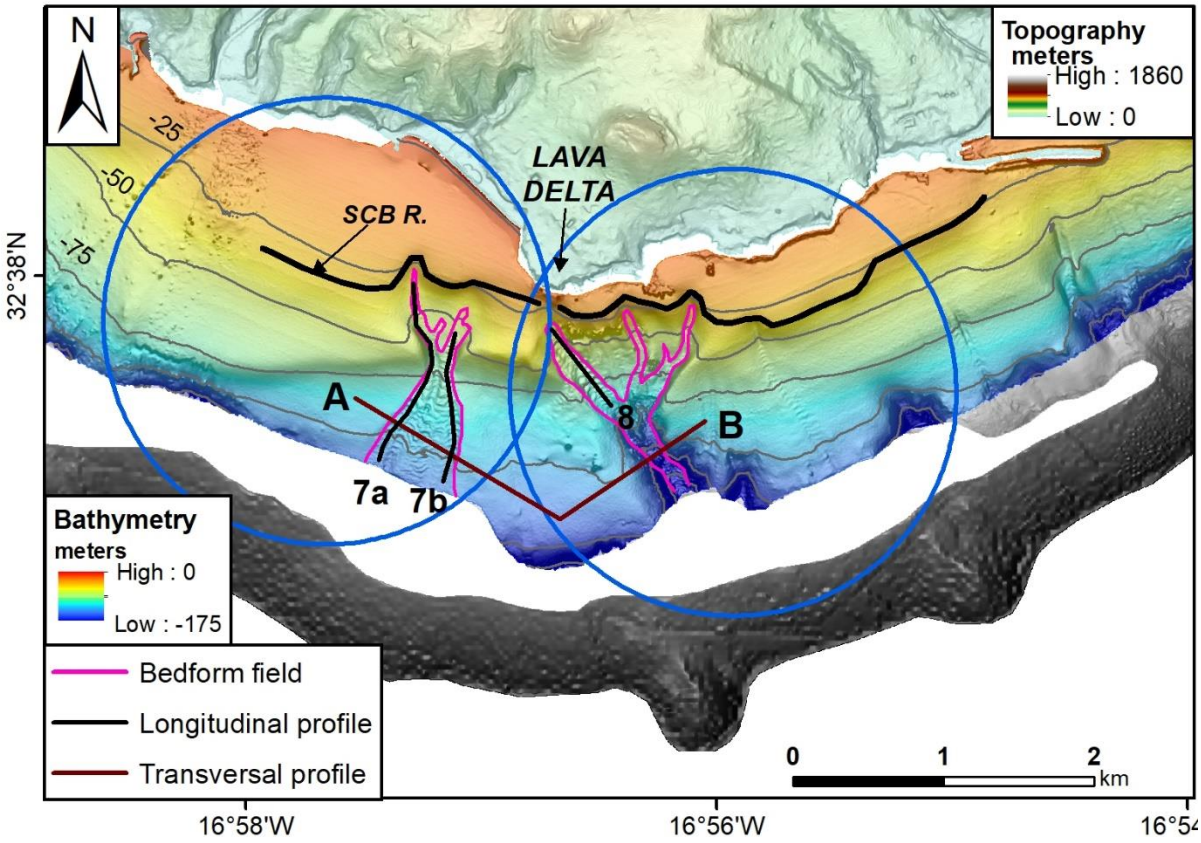

Figure 6.6. Shaded relief bathymetry (caption as in Fig. 6.1) of bedform fields 7 and 8 (location in Fig. 6.1). Contours spaced every 25 meters. The transversal profile (A-B) is shown in Suppl. Fig. 10.37 in the Appendix. The longitudinal profiles 7a, 7b, 8 are shown in Suppl. Fig. 10.38 in the Appendix.

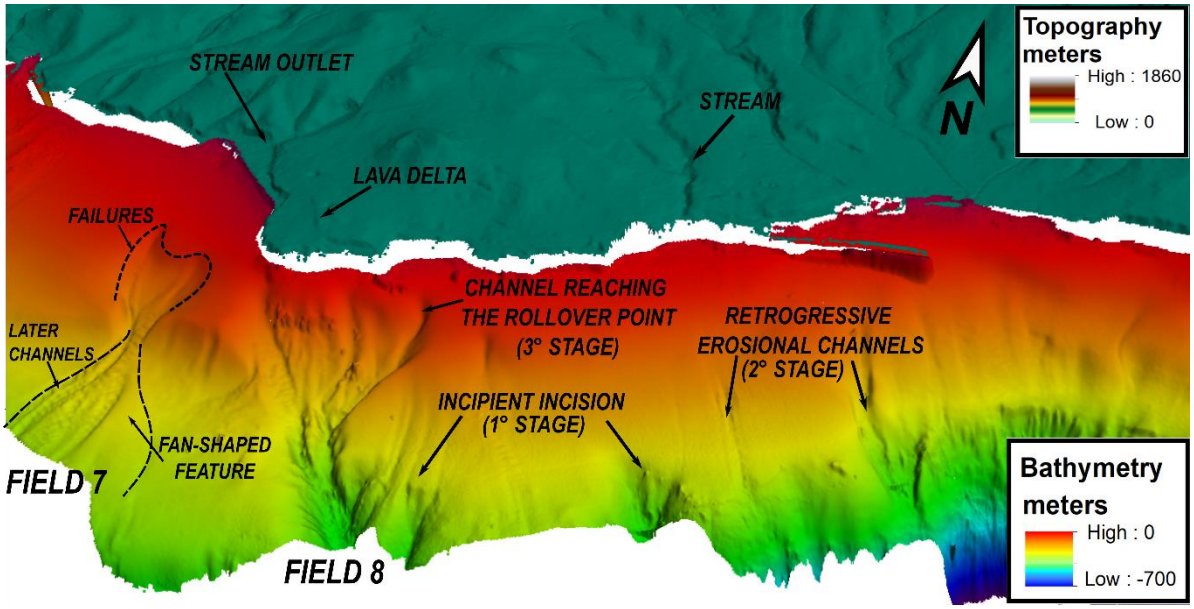

Figure 6.7. 3D illustration of bedform fields 7 and 8 (location on Fig. 6.1). Field 7 shows a fan-shaped feature with channels developing on top. East of field 8, the possible retrogressive evolution of channels from the shelf edge up to the clinoform rollover (stages 1 to 3) has been indicated. Vertical exaggeration 3x.

6.2.4. BEDFORMS ON TOP OF FAN-SHAPED AREAS WITHOUT A LINK TO ONSHORE STREAM MOUTHS (TYPE IV)

Only one bedform field of this type (field 10 in Fig. 6.1 and in Suppl. Fig. 10.46 in Appendix) was found and shares similarities to Type II bedforms. The fan-shaped area occurs offshore a tall cliff coastline and immediately downslope of a scar in the clinoform rollover.

6.2.5. BEDFORMS OCCURRING OBLIQUELY TO THE SHELF SLOPE (TYPE V)

These bedforms occur mainly west of bedform field 1, although small areas also exist between fields 1 and 2 and between fields 2 and 3 (red rectangles in Fig. 6.1). Here, bedforms develop obliquely to the shelf slope, so they have gentle slopes (<2º). They are reported and described in the Appendix (Suppl. Figs. 10.51, 10.52,10.53, 10.54 and Suppl. Table 10.22)

6.2.6. STATISTICAL ANALYSIS OF BEDFORMS

The main morphometric parameters of the bedforms (see Fig. 4.5) have been measured and a statistical analysis has been carried out for each type. Generally, bedforms of types I to IV are typically asymmetric downslope, with steeper lee slopes and gentler stoss slopes (Figs. 6.8 A-F). They occur on basal slopes dipping between 3.7° and 7.8° and the bedforms themselves dip between 0.4° and 7.9° (average 4°-5°, see Table 6.1). They have wave heights between 0.4 m and 6.2 m (averaging 2-3 m) and wave lengths between 17 m and 126 m (averaging 30-40 m).

Regarding the differences, Type I and Type III bedforms have very similar characteristics and are clearly distinct from Type II and IV. In general, Type II bedforms rest on gently dipping basal slopes, have smaller lee and stoss slopes (and consequently are less steep), are more asymmetric and have larger wave lengths in comparison to type I. Type IV are the smallest bedforms and overall, rest on steeper slopes.

Bedforms type V are larger and more varied in sizes, with wavelengths between 30 and 100 m and wave heights between 1 and 8 m. The crest-lines are linear to sinuous and are normally longer than 100 m (see Suppl. Figs. 10.51, 10.52, 10.53, 10.54 and Suppl. Table 10.22 in the Appendix).

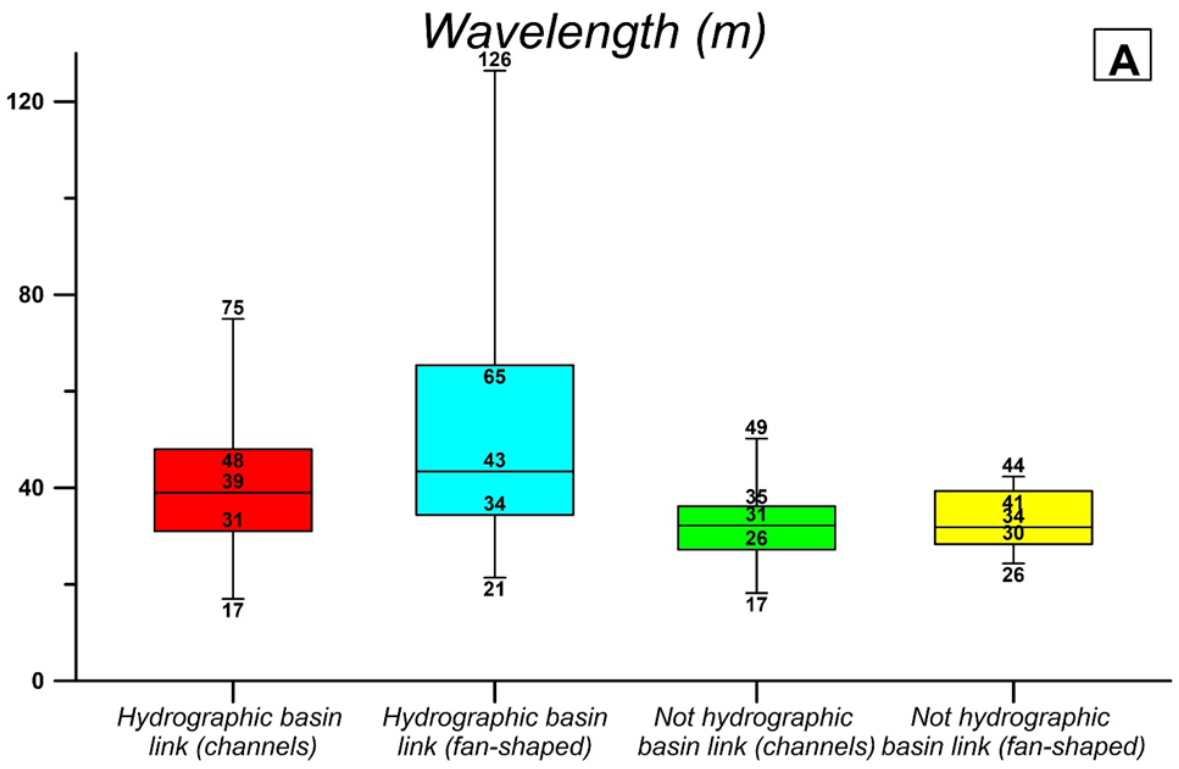
Wavelength (m)
A
120
80
40
0
126
75
65
48
43
39
34
31
21
17
49
44
35
41
31
34
26
30
17
26
Hydrographic basin link (channels)
Hydrographic basin link (fan-shaped)
Not hydrographic basin link (channels)
Not hydrographic basin link (fan-shaped)

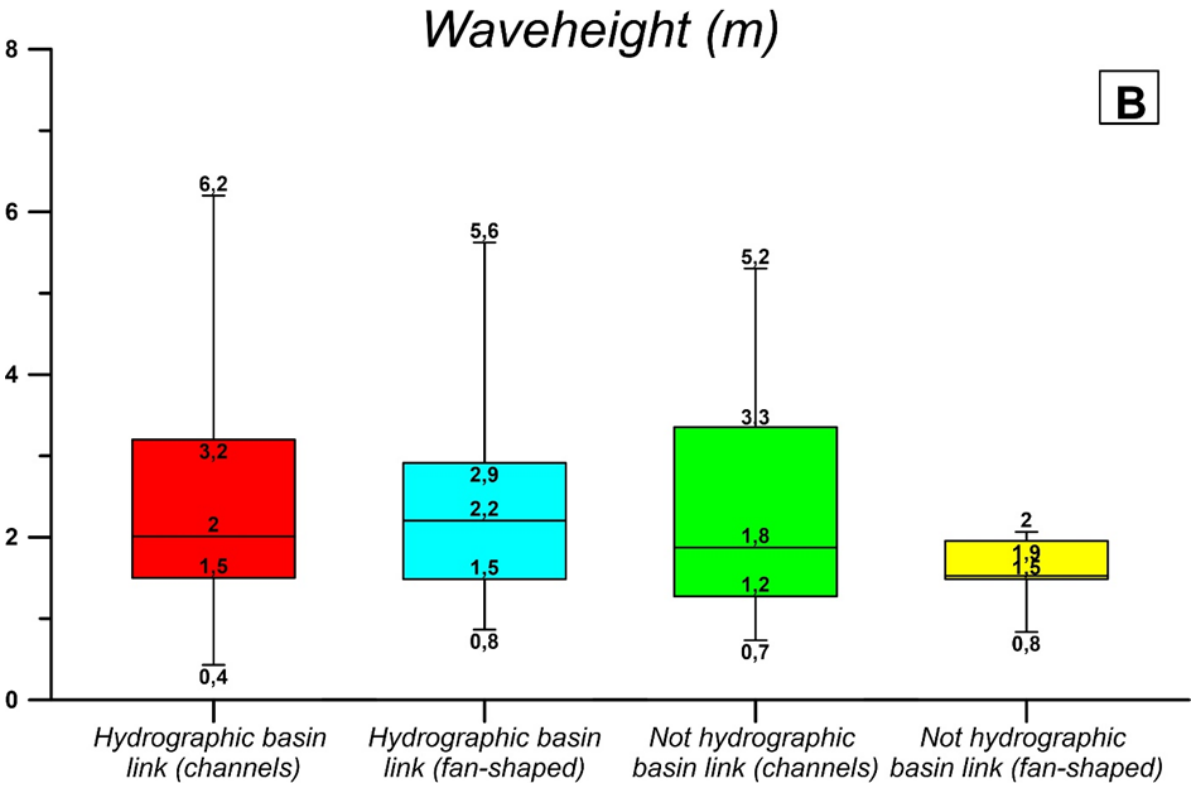
Waveheight (m)
B
8
6
4
2
0
6,2
5,6
5,2
3,2
2,9
3,3
2,2
2
1,8
1,5
1,5
1,2
0,4
0,8
0,7
0,8
Hydrographic basin link (channels)
Hydrographic basin link (fan-shaped)
Not hydrographic basin link (channels)
Not hydrographic basin link (fan-shaped)

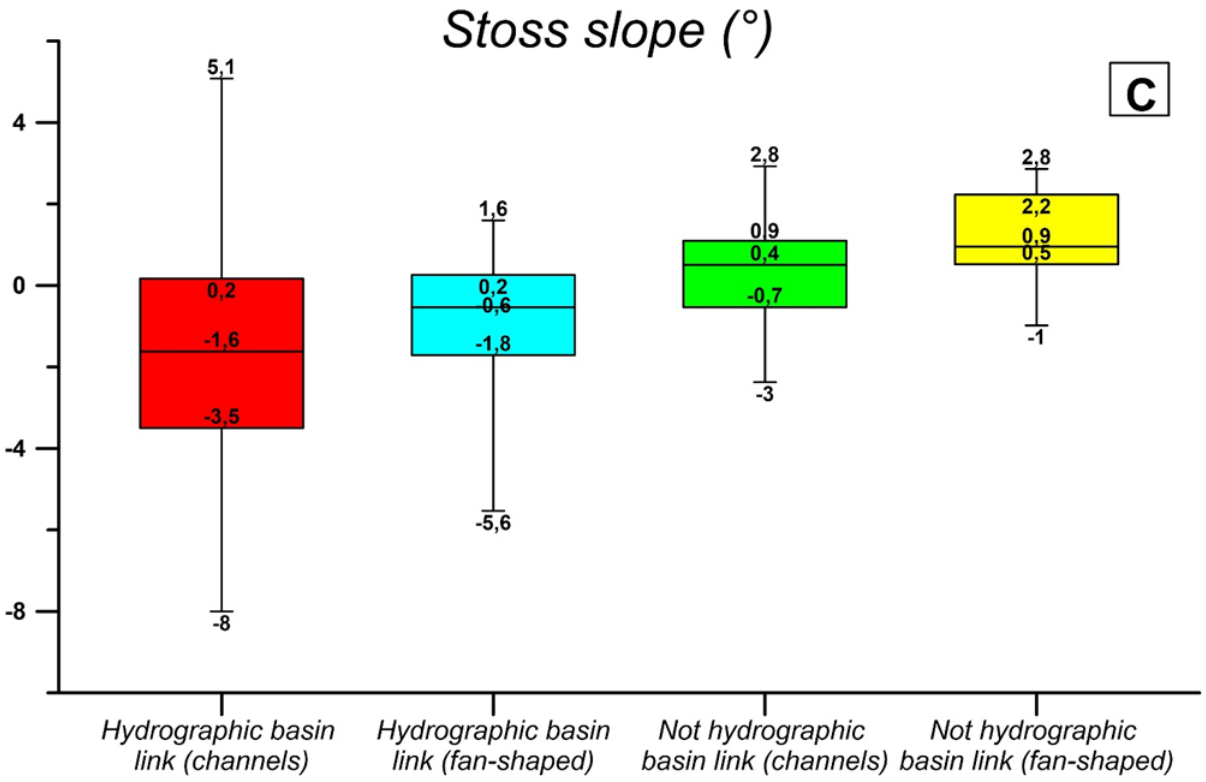
Stoss slope (°)
C
5,1
0,2
-1,6
-3,5
-8
1,6
0,2
0,6
-1,8
-5,6
2,8
0,9
0,4
-0,7
-3
2,8
2,2
0,9
0,5
-1
4
0
-4
-8
Hydrographic basin link (channels)
Hydrographic basin link (fan-shaped)
Not hydrographic basin link (channels)
Not hydrographic basin link (fan-shaped)

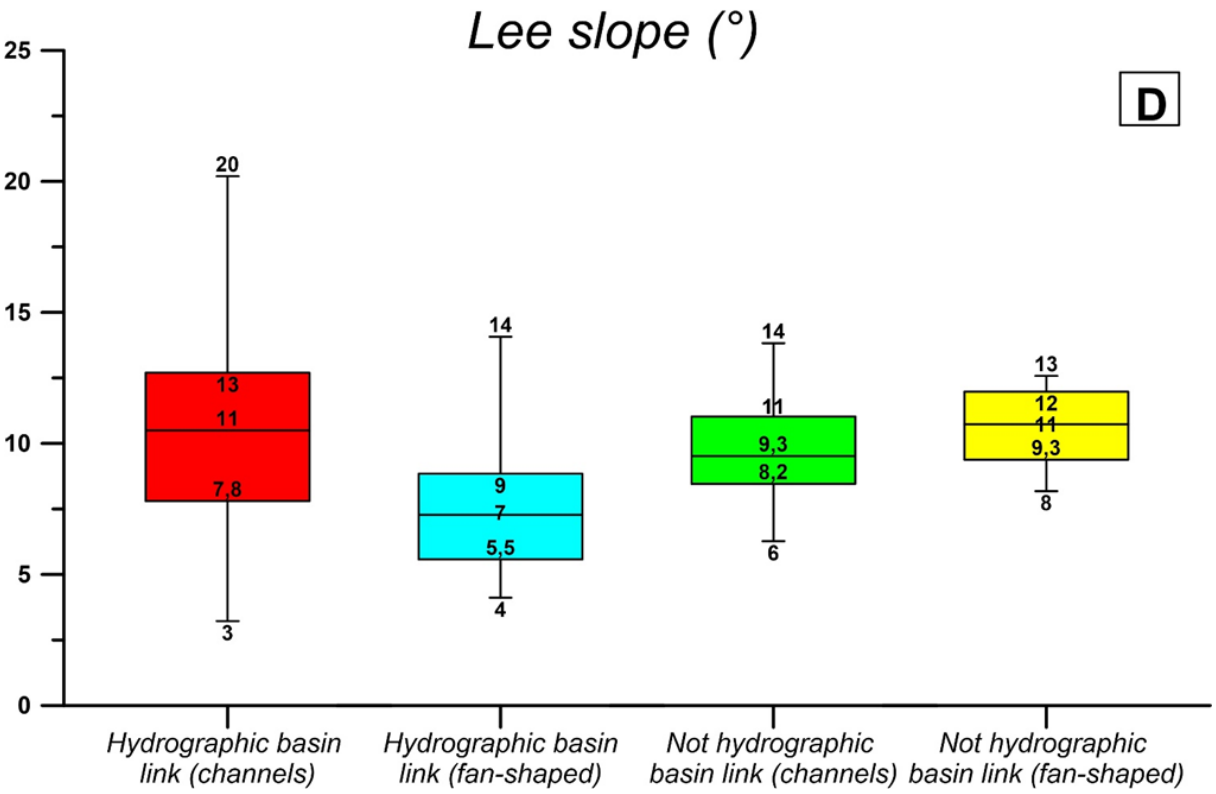
Lee slope (°)
D
20
13
11
7,8
3
14
9
7
5,5
4
14
11
9,3
8,2
6
13
12
11
9,3
8
25
20
15
10
5
0
Hydrographic basin link (channels)
Hydrographic basin link (fan-shaped)
Not hydrographic basin link (channels)
Not hydrographic basin link (fan-shaped)

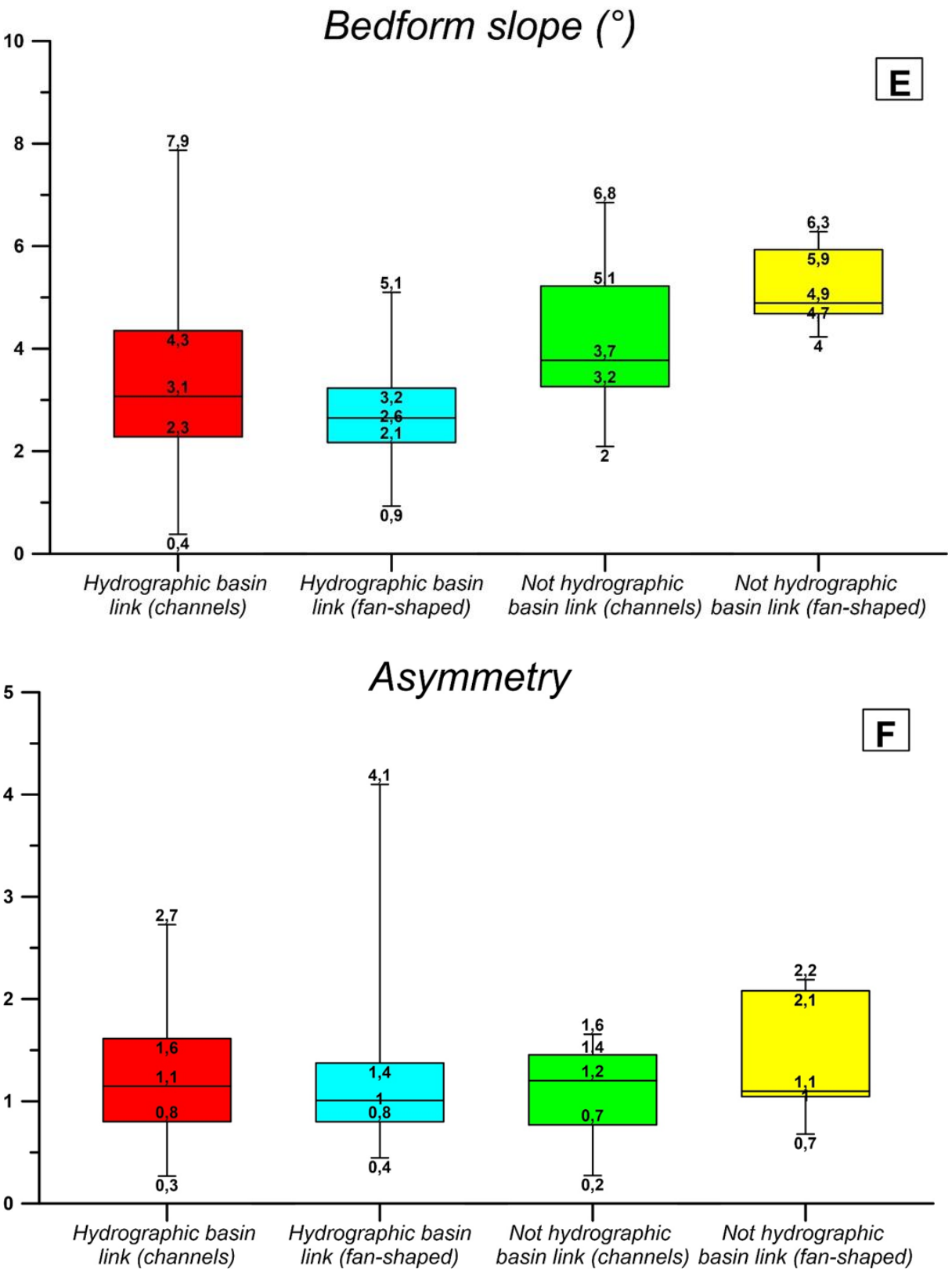

Figure 6.8. Box plots of the main parameters (y-axis) measured for the four bedforms types I-II- III-IV(x-axis), (n=203). Numbers represent lower whisker (minimum), 25th quartiles, median, 75th quartiles and upper whisker (maximum).

The scatter plots did not reveal any clear relationship between the main parameters (Figs. 6.9 A-L), R^2 is always below 0.30. However, visually there appears to be some correlation between lee slope and aspect ratio (Fig. 6.9D), wave height and lee slope (Fig. 6.9F), and wave height and wavelength (Fig. 6.9H). Some parameters seem also to have some decreasing trend with distance from the shore (Figs. 6.9 K-L).

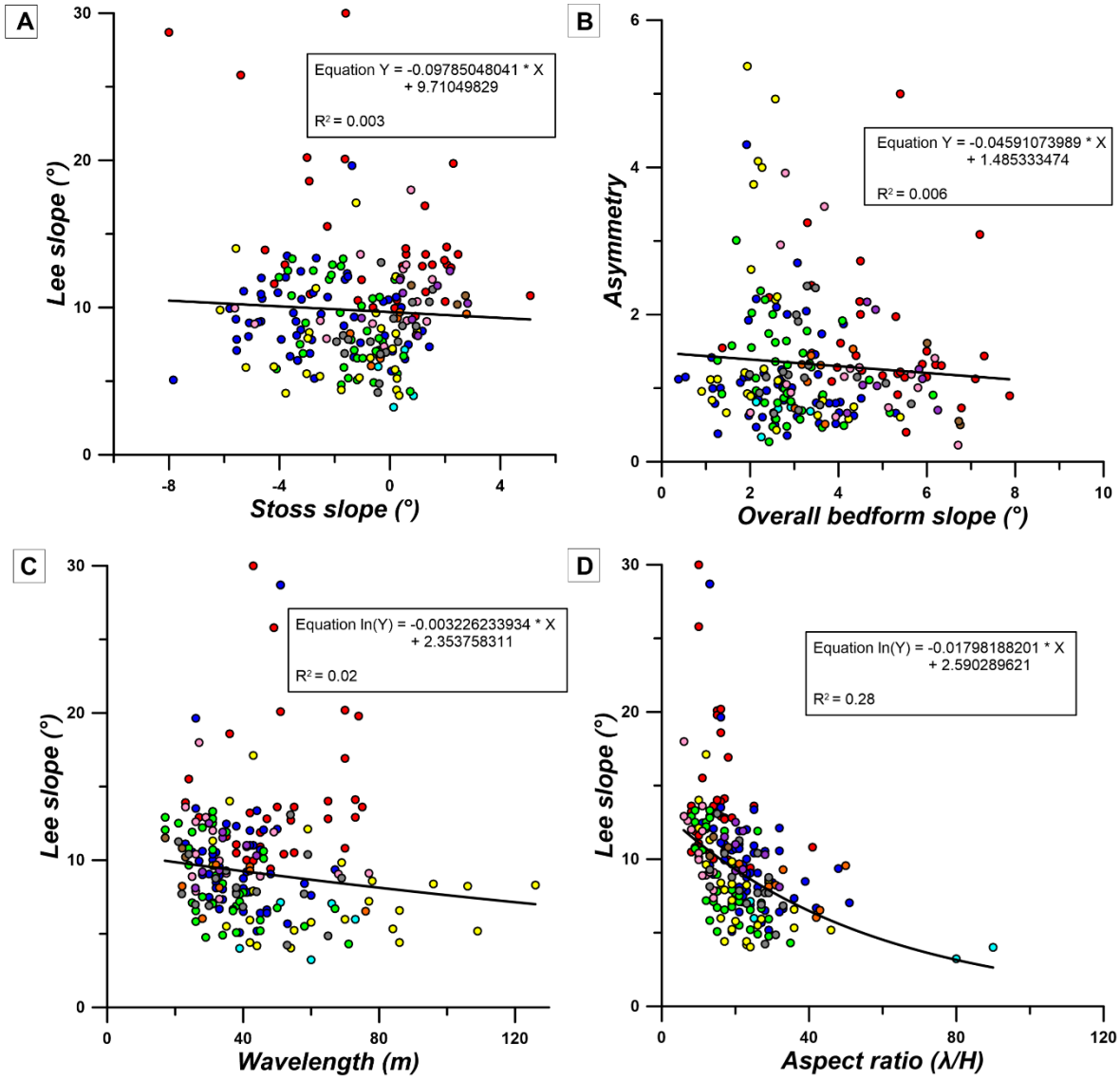

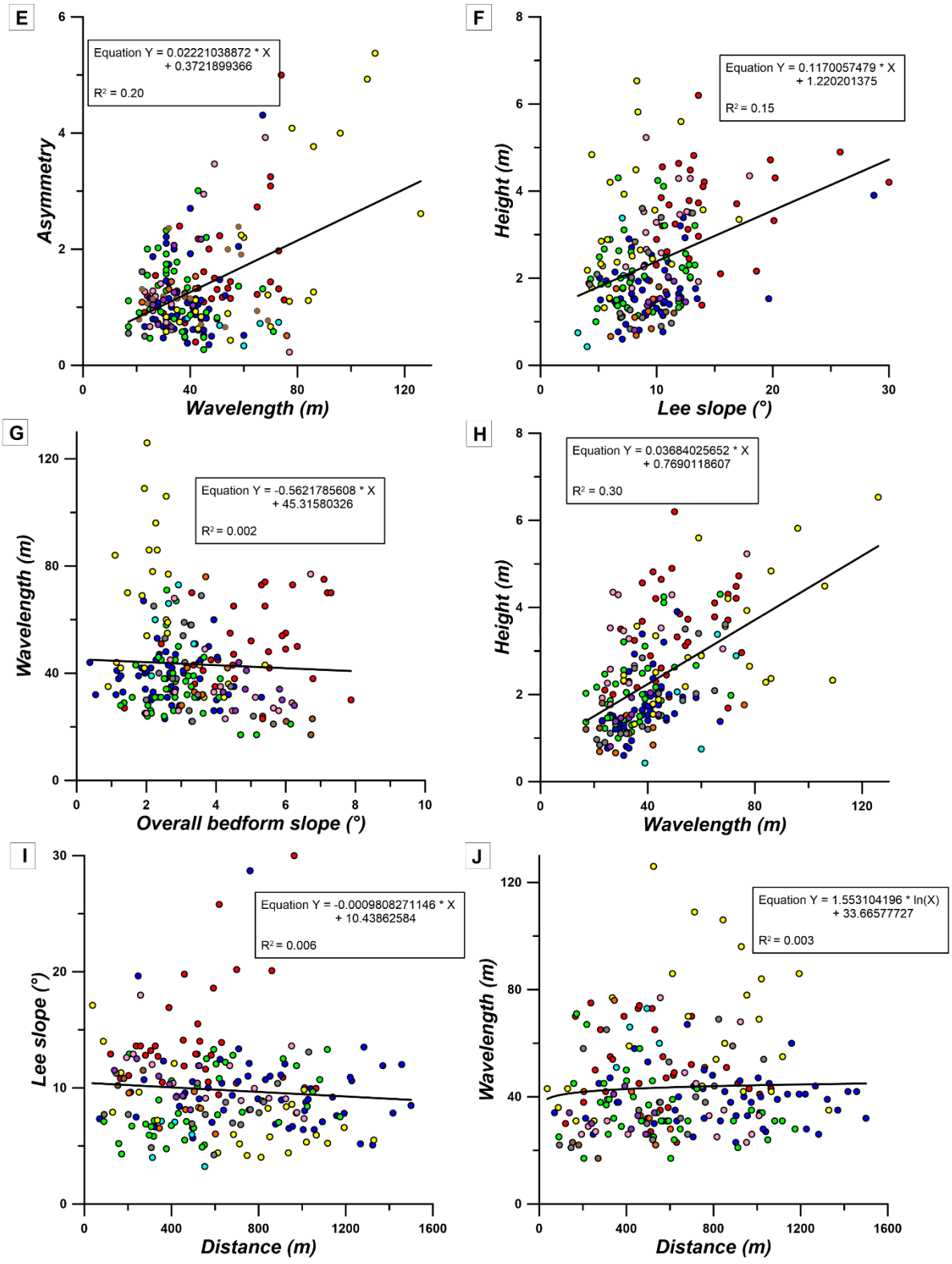
E
Equation Y = 0.02221038872 * X + 0.3721899366
R² = 0.20
Asymmetry
Wavelength (m)
F
Equation Y = 0.1170057479 * X + 1.220201375
R² = 0.15
Height (m)
Lee slope (°)
G
Equation Y = -0.5621785608 * X + 45.31580326
R² = 0.002
Wavelength (m)
Overall bedform slope (°)
H
Equation Y = 0.03684025652 * X + 0.7690118607
R² = 0.30
Height (m)
Wavelength (m)
I
Equation Y = -0.0009808271146 * X + 10.43862584
R² = 0.006
Lee slope (°)
Distance (m)
J
Equation Y = 1.553104196 * ln(X) + 33.66577727
R² = 0.003
Wavelength (m)
Distance (m)

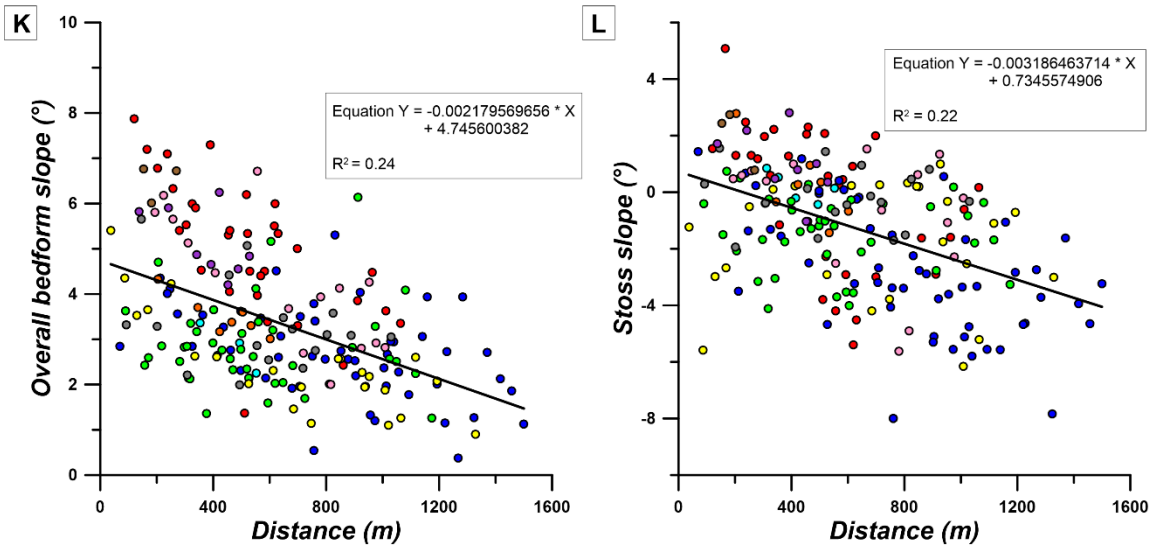

Figure 6.9. Scatter plots showing possible relationships between the main morphological parameters of the bedforms developed perpendicular to the coastline. Each colour represents a bedform fields as indicated in Suppl. Fig. 10.55 in Appendix.

6.2.7. SHELF GRAIN-SIZE DISTRIBUTION AND ITS RELATION WITH STREAM DISCHARGE AND LOCATION OF BEDFORMS

Interpolations of the mode grain-size (in ϕ) and of the finer sediment fraction (silt + clay) (Fig. 6.10) were obtained through the granulometric analyses of 397 sediment samples. The distribution of average grain-size show that the shelf can be differentiated in three main areas from west to east: (i) west of bedform field 1 coarse sands dominate; (ii) the area between bedform field 1 and bedform field 9, fine and very fine sand dominate and (iii) east of bedform field 9, medium to coarse sands are mostly found. When only the finer particles are considered, a similar pattern is found from west to east, although an additional area can be added (Fig. 6.11): (i) west of bedform field 1 the finer fraction only constitutes 1-10% of the whole grain-size distribution; (ii) the area between bedform field 1 and bedform field 7, the finer fraction often constitutes 40-60%, locally reaching 80% of the sediment, (iii) the area between bedform fields 7 and 9, the finer fraction constitutes 35%, and (iv) between bedform field 9 and 10 the finer fraction varies from 1-10% although in some areas offshore large hydrographic basins it may reach 40%.

When relating the sediment distribution with the shelf morphology, the location and area of the bedforms, the size of the hydrographic basins, and the volcano-stratigraphic units cropping out onshore it is possible to make a differentiation of the overall source to sink system (Figs. 6.10 and 6.11):

- SECTOR 1 is characterized by small hydrographic basins (5.5 ± 3 km^2 on average) eroding mostly material from the least weathered Upper Volcanic Complex, low shelf gradients (1,45° ± 1,1° on average), mostly coarse sands with small percentage of fines (< 0-10 %), and the presence of two major fields of type V bedforms.

- SECTOR 2 is fed by larger hydrographic basins than in sector 1 (8 ± 5 km^2 on average, if the largest hydrographic basin of Ribeira Brava, 41 km^2 is excluded). They erode formations from the Upper and Middle Volcanic Complexes and deliver sediment to a steeper shelf sector (3.8° ± 0.1° on average). Here, fine to very fine sands with high percentage of silt and clay are present (40-60%, locally reaching 70-80%) and the bedform fields (types I and II, III) are more numerous, occupy the largest areas and are mostly connected to streams mouths (types I and II).

- SECTOR 3 has even larger hydrographic basins than sector 2 (11 ± 6 km^2 on average, if one excludes the second largest hydrographic basin, Ribeira dos Socorridos) eroding material from the Upper and Middle Volcanic Complexes, shelf slopes are steeper than in sector 2 (6.4° ± 1.3° on average), shelf sediments are fine to very fine sands with small percentage of silt and clay (up to 35%, except off Ribeira dos Socorridos) and includes two bedform fields (one connected to streams onshore and the other not, i.e. types II-III), occupying small areas.

- SECTOR 4 comprises hydrographic basins with similar areas to sector 3 (10 ± 7 km^2 on average) mostly eroding material from the Upper Volcanic Complex, similar shelf slopes as in sector 3 (6.4° ± 0.8° on average), medium to coarse sands with very low percentage of fines (1-10%, locally reaching 30-40% off the largest hydrographic basin) and the two smallest bedform fields in term of area (types III - IV).

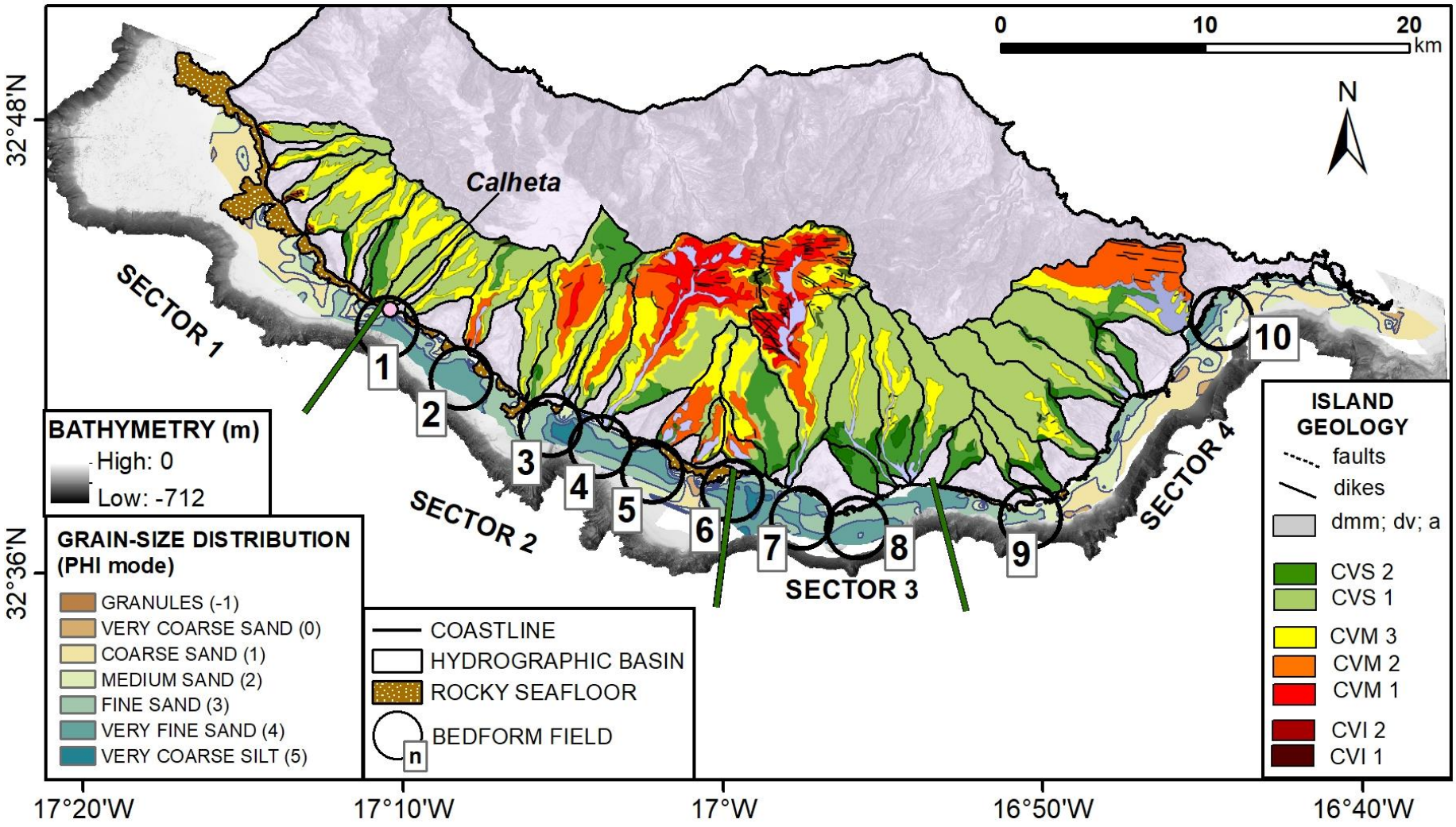

Figure 6. 10. Grain-size sediment distribution along the shelf and their relation to the size of hydrographic basins and respective outcropping volcano-stratigraphic units crossed by streams. Circles represent the bedform field's as in Fig. 6.1. Brown polygons delimit the nearshore rocky seafloor. In the geologic legend "dmm", "dv" and "a" represent mass wasting deposits, slope deposits and alluvium, respectively.

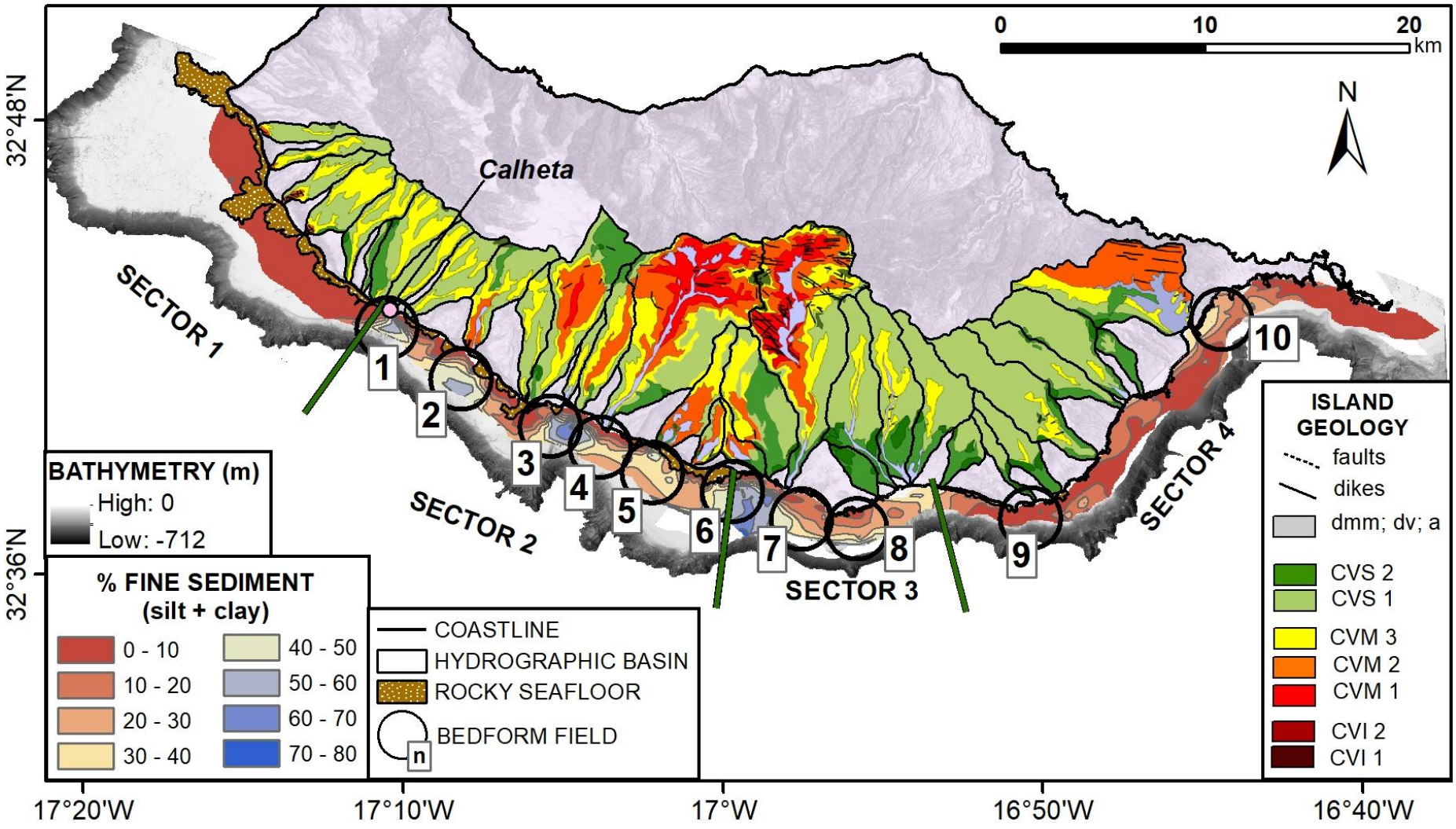

Figure 6.11. Fine sediment (percentage of silt + clay) distribution along the shelf and their relationship with the size of the feeding hydrographic basins and respective to the outcropping volcano-stratigraphic units crossed. Circles represent the bedform fields location as in Fig. 6.1. Brown polygons delimit the nearshore rocky seafloor.

6.2.8. COMPARISON BETWEEN MULTITEMPORAL DTMs

Seafloor changes between 2002 and 2019 covering the area of bedform fields 2, 3 and 4 are represented in Figs 6.12 and 6.13. On both figures it is possible to recognize wide areas of erosion (green to red) on the topset of the clinoform close to the rollover. These areas correspond to dredging sites for marine aggregates and some show circular features that are pits. The small circular areas in blue correspond to old pits that are now filled.

The zoom of Fig. 6.12 shows channels where, although deposition prevails over erosion, there is still the alternation between the two. There is no clear prevalence of one process over the other on the stoss and the lee sides; instead, both can occur on each bedform flank. Nevertheless, the data shows that waves migrate in the course of this period.

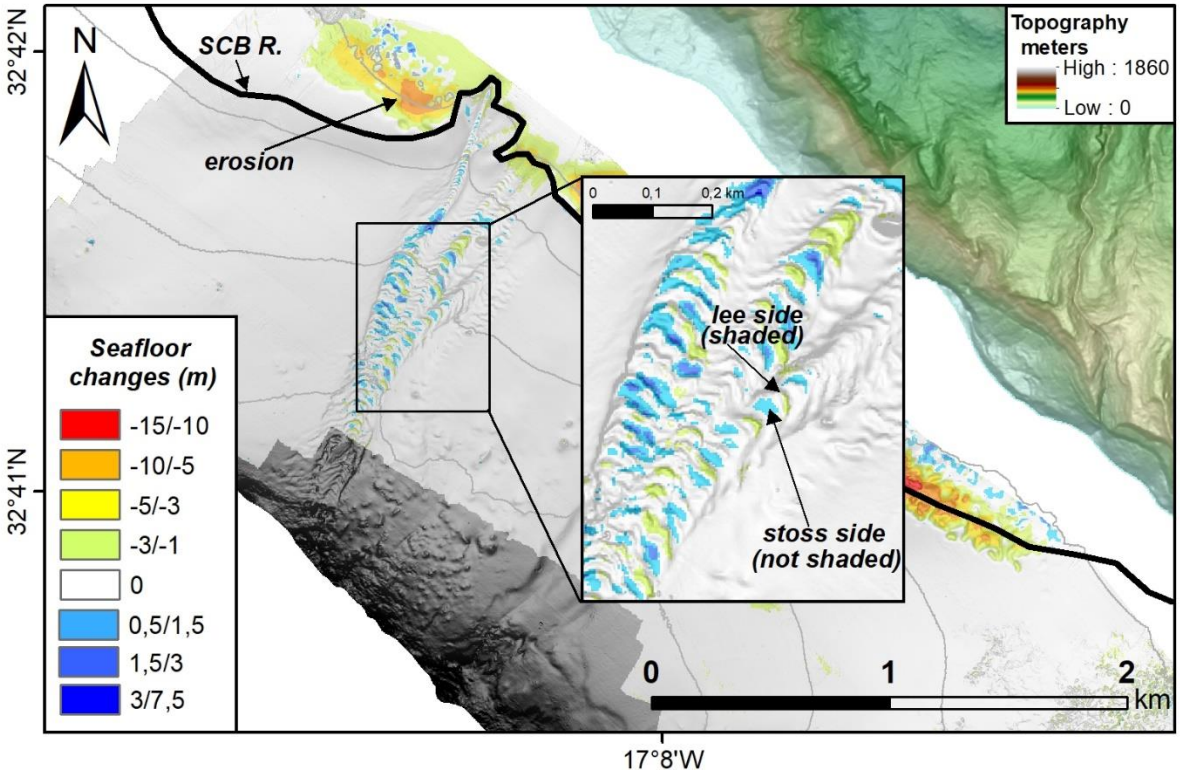

Figure 6.12. Seafloor changes between the 2002 and 2019 surveys (17 years) in bedform field 2 (location in Fig. 6.1). In blue tones are the areas subjected to deposition, and in light green to red, the areas subjected to erosion. The darker shaded relief is the bathymetry from 2019 while the lighter is the raster resulting from the changes between the examined bathymetries. Contours spaced every 25 meters. SCB R.: subaqueous clinoform body rollover.

No significant changes are observed on field 3 between the two surveys (Fig. 6.13), but on the west side of field 4 erosion prevails while on the east side slight erosion and deposition alternate. On the westernmost side of the area, a small-scale failure affecting the clinoform rollover generated a rounded scar and a deposit downslope, presenting bedforms with sinuous crests on its top. It is also possible to see headward erosion of the clinoform rollover in the area of the bedform field 4 and a migration of bedforms towards the shore (Suppl. Fig. 10.29 in the Appendix).

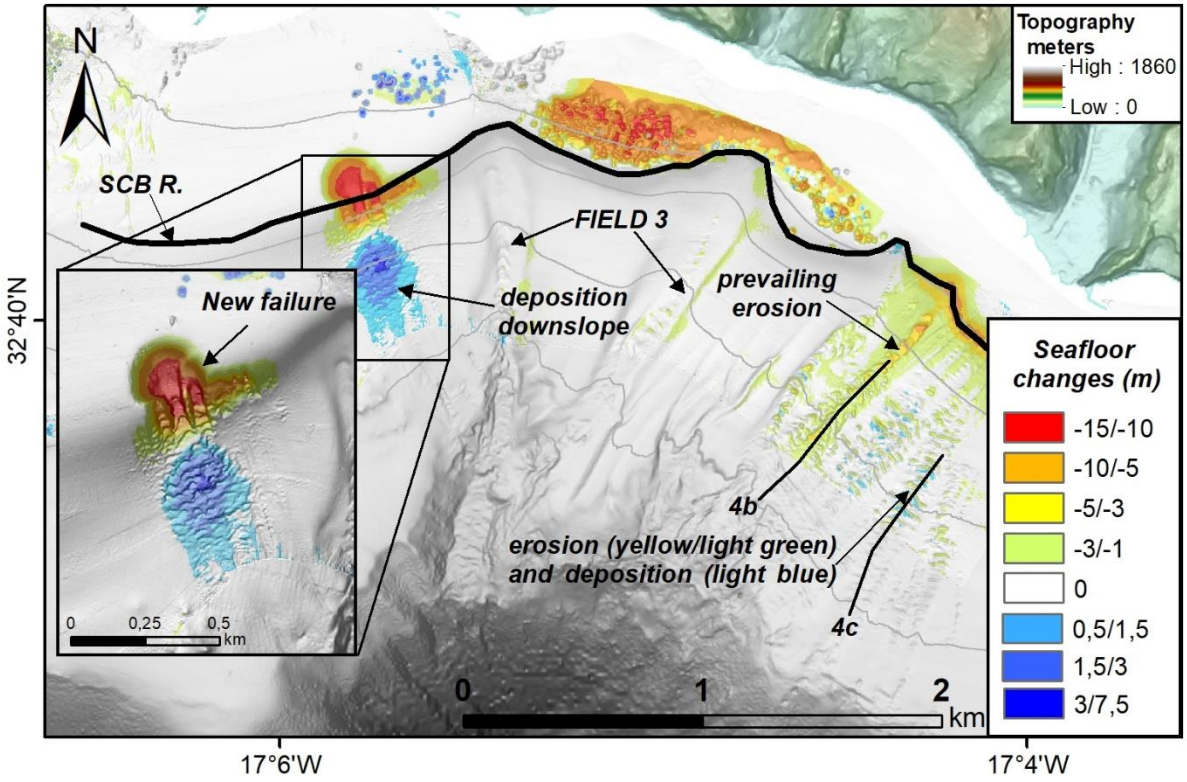

Figure 6.13. Seafloor changes between the 2002 and 2019 surveys (17 years) in bedform fields 3 and 4 (location in Fig. 6.1) linked to a large hydrographic basin (>40 km²). In blue tones are the areas subjected to deposition, and in light green to red, the areas subjected to erosion. Contours every 25 meters. SCB R.: subaqueous clinoform body rollover.

6.2.9. RECORD OF PRECIPITATION DATA

The precipitation dataset recorded in three weather-stations located on the southern side of Madeira Island shows that between 2000-2020, at least one intense precipitation event has occurred. In the record, there is at least one day per station (often on two or three stations) where precipitation exceeds the 95th percentile (Suppl. Table 10.2 in the Appendix). The number of days exceeding the 95th percentile in 2010 was the highest (11, 8, 6 days at Ponta do Pargo,

Lugar de Baixo and Funchal, respectively) when an extreme flash-flood event occurred on the 20th February 2010. During this extreme event, precipitation at Ponta do Pargo reached 94.7 mm/day while in the Funchal Observatory, 144.3 mm/day were registered. From the considered weather-stations which mostly cover the southwestern part of the island, other exceptional events were recorded in the three stations during 2006, 2009, 2012 and 2016. The weather-station of Funchal, which has a higher data record, also shows 6 days of extreme precipitation on 2001. 6 major events in 20 years, suggests 3.3 events per year.

6.3. DISCUSSION

6.3.1. WHICH PROCESSES CREATE TYPE I TO IV BEDFORMS: BOTTOM CURRENTS, SEDIMENT DENSITY FLOWS OR GRAVITY-DRIVEN PROCESSES?

In volcanic environments several processes have been proposed for the generation of bedforms similar to the above-described types I to IV: eruption-fed density flows, bottom currents, slope failures, and sediment density flows (Babonneau et al., 2013; Pope et al., 2018; Clare et al., 2018; Casalbore et al., 2021). Some bedforms can be related to large-magnitude silicic eruptions, which produce high-flux sustained pyroclastic density currents that enter the ocean and continue as submarine density flows (Pope et al., 2018). However, this mechanism is unlikely in the study area because, during the Holocene, Madeira volcanism is restricted to a few small basaltic eruptions and no caldera or silicic volcanic activity is known onshore or offshore.

A second hypothetical mechanism for the generation of bedforms are tidal and storm-driven longshore currents (Walgreen, et al., 2002). This might be the case of type V bedforms that are not parallel to the main shelf slope and have larger dimensions than the ones of Sectors 2-4 (that, instead, are perpendicular to the shelf slope and mostly found inside channels).

A third hypothesis is that bedforms could be formed by soft sediment deformation, creating extensional faults or creep folds (Lee et al., 2002; Wynn and Stow, 2002). These are normally found downslope of arcuate headwalls and are confined by well-defined lateral margins (Pope et al., 2018). The slope failure mechanism for type I and III bedforms are excluded because these are developed inside well-defined channels. However, types II and IV bedforms share the characteristics indicated by Pope et al. (2018) for slope failure products. In fact, in the bedform fields, failure scars are present followed by positive relief feature and the bedforms have their

wave-crest length increasing downslope with sinuous shape in plan-view. The 2019 DTM shows a new scar on the clinoform rollover and a deposit downslope with bedforms, which was absent in 2002 (Suppl. Fig. 10.28 in Appendix). This suggests that slope failures could form types II and IV bedforms, while types I and III are likely formed by channelized sediment density flows. However, bedforms are probably produced by a complex interaction of processes and features; for instance, creep folds could potentially provide the initial topography that allows sediment wave growth to occur (Wynn & Stow, 2002). This seem to be the case of bedform field 7 where, over the elevated topography of the fan-shaped feature, there are channels developing on both sides (7a and 7b in Fig. 6.6), suggesting the repeated occurrence of high-density sediment flows.

However, one main question remains: are the observed bedforms formed by subcritical density flows, and the sediment waves migrate in a downslope direction, or are they formed by supercritical density flows and correspond to antidunes or cyclic steps migrating upslope? Several studies have shown that density flows can be supercritical on slopes steeper than 0,07° to 0,6° (Slootman & Cartigny, 2020 and references therein). This slope range is well below the 3.9°-7.8° basement slopes where our shelf bedforms lie. In addition, according to Cartigny et al. (2011) and Symons et al. (2016), the plan-view curve of the bedforms is a good proxy to distinguish between supercritical density flows (antidunes and cyclic steps) and subcritical density flows (ripples and dunes). Supercritical bedforms migrate upslope and their crests are normally convex (or crescentic) downslope, while subcritical bedforms have convex upslope crests. This can be explained because the higher current velocities occur in the centre of the channel, which means that when wave crests curve downslope near the sides of a channel, the direction of migration is upslope and vice-versa. The majority of the observed bedforms have convex downslope wave crests, which supports their formation by supercritical density flows.

A further question is whether they are antidunes or cyclic steps? All the characteristics that have been measured indicate that they are more likely cyclic steps. Cyclic steps have normally steeper lee slopes than stoss slopes (Cartigny et al.,2011; Kostic, 2011), which is the case of the bedforms studied here. Stoss sides dip on average 2° and lee sides dip on average 10°. Because lee sides are steeper, flows accelerate and reach supercritical conditions favouring erosion on the lee sides. When the flow reaches the lee-stoss transition there is a step with a sudden slope decrease, which creates a hydraulic jump with simultaneous deceleration of the flow and passage to subcritical conditions favouring deposition on the stoss side. This mechanism promotes upslope migration of the bedforms. Antidunes also migrate upslope; the difference is

that in cyclic steps the bedforms evolve by alternation between supercritical and subcritical flows while on antidunes the flow is always supercritical (see subchapter 2.2.2 and references herein). Antidunes are relatively symmetrical (with similar stoss and lee sides dips) and flows decelerate when passing over stoss sides and tend to deposit sediments, accelerating again when reaching lee sides and eroding them (Slootman & Cartigny, 2020). In addition, antidunes are commonly ephemeral features going through cycles of build-up, oversteepening and destruction (Kostic et al., 2011; Slootman & Cartigny, 2020), while cyclic steps are prevailing bedforms in all submarine environments (Symons et al., 2016). All of this supports the likelihood of the shelf bedforms on Madeira being cyclic steps.

6.3.2. WHAT IS THE SOURCE OF THE SEDIMENT DENSITY FLOWS FORMING TYPES I AND III BEDFORMS?

The development of sediment density flows in subaqueous environment is relatively frequent since they can be triggered by different processes (Piper & Normak, 2009; Talling et al., 2013). Taking into account the subaerial and submarine characteristics of Madeira Island, two main types of triggering mechanisms can be attributed to bedform formation through density flows (Fig. 6.14):

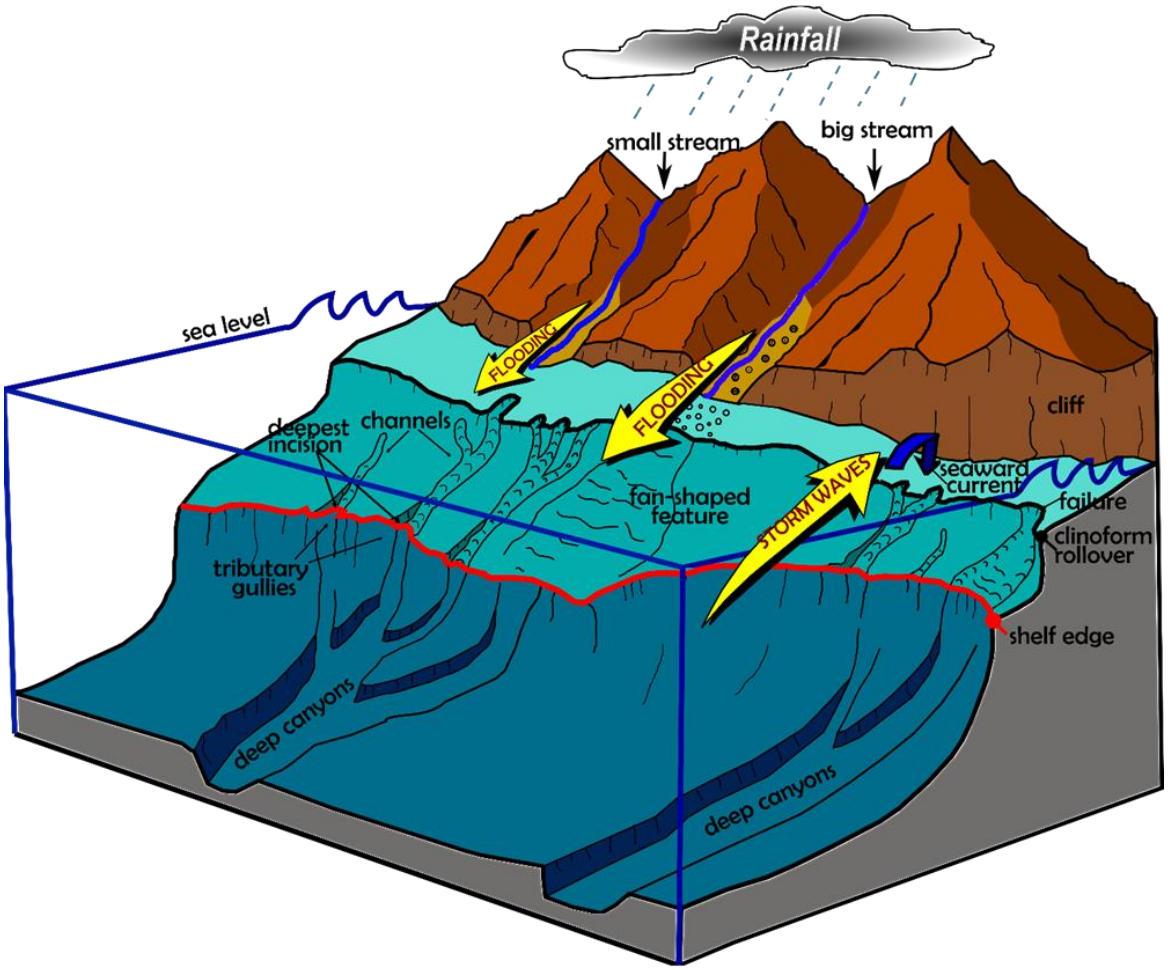

Figure 6. 14. Sketch showing the main trigger mechanisms of bedform formation through density flows. Blue arrow represents seaward downwelling currents.

1) The discharge of large amounts of sediment at stream mouths during flash floods creates a density contrast with the sea water forming hyperpycnal flows that may evolve into unconfined sediment density flows (e.g., Khripounoff et al., 2009) running down the shelf. According to Quartau et al. (2018), if these flows are able to cross the entire shelf, they could be responsible for the formation of gullies at the shelf edge and upper slopes. When these flows cross the shelf edge, in fact, they accelerate due to the increase in steepness (> 15° for the upper slope; < 6° at the shelf) producing erosion and starting to form gullies (Quartau et al., 2018). Gullies have dendritic patterns and evolve downslope to large canyon systems which may extend as far a 60-70 km from the shelf break. A recent study compiled sixteen events of intense precipitation that occurred in Madeira between 1945 and 2011 (Lopes et al., 2020), corresponding to a recurrence interval of 4.1 years. The precipitation data between 2000 to 2020, suggests a recurrence interval of 3.3 years. These events produced mass movements and flash floods in the streams that drain the southern slope of the island. Another study covering a longer period of episodic

flash flood events (1803-1998) indicates a recurrence period of 6.5 years (Quintal, 1999). A 22-year analysis of satellite data revealed that these events create river plumes contributing to favourable conditions for phytoplankton growth (Rosa et al., 2022). Although the cited study focused on the fine particles forming river plumes, certainly the denser ones can create hyperpycnal flows that interact with the seafloor. There are several worldwide examples of how hyperpycnal flows related to stream discharge promote slope failure of coastal sediments and development of bedforms (Babonneau et al. 2013, Normandeau et al., 2016; Bosman et al., 2017). The works of Babonneau et al. (2013) and Bosman et al. (2017) show very similar features with cyclic steps that develop at the head of channels that cross the shelf and feed canyon systems. This kind of mechanism is very clear for bedform fields 1 and 3 (Figs. 6.2, 6.4) but not in field 2 whose channel also reaches the shelf edge and shows bedforms but does not feed any canyon downslope. It has been also observed that channels have deeper incision near the shelf edge that decreases upslope with some channels never reaching the clinoform rollover (Figs 6.2, 6.4, 6.7). The headward erosion of these gullies starts to form channels that migrate upslope until they may capture the clinoform rollover. So, unconfined sediment density flows on the shelf end up confined inside channels. Some of these channels that have not yet reached the rollover already display incipient bedforms, but as soon as they capture the rollover the input of sediment must increase and so larger bedforms develop.

Some bedforms on top of fan-shaped features (bedform fields 4, 5 and 7) are also related to the occurrence of unconfined hyperpycnal flows at stream mouths. These fields occur offshore the largest hydrographic basins that likely supply higher amounts of sediment than what is supplied to fields 1 and 3. This causes a faster progradation of clinoforms, with steepening of the foreset and its consequent failure as seen in delta fronts (Normandeau et al., 2016). This has occurred on the western part of bedform field 3 sometime after 2002, since it is very clear on the 2019 bathymetry, and might be already present in the 2013 bathymetry that shows the downslope tip of a failure deposit (Suppl. Fig. 10.28 in Appendix). According to Bailey et al. (2021), turbidity currents can take place even when no catastrophic event, such as flash floods or large storm waves, has occurred. These authors monitored the occurrence of fourteen turbidity currents in the Monterey Canyon on an 18 months-time frame and observed that even minor external events are capable of triggering density flows via slope failure when the environment is preconditioned by sediment accumulation. This means that there is no need of an extreme event to happen for sediment density flows to be triggered. Sediments accumulate slowly on the clinoform rollover and, when a slope threshold is reached, it may fail triggering the flows.

2) Sediment density flows triggered by storm waves may be the result of sediment resuspension by wave-current interaction combined with offshore directed transport. On rocky cliff coastlines whose topography does not allow inundation by surges, storm setup can be balanced by downwelling currents, transporting sediment offshore (Babonneau et al., 2013; Meireles et al., 2013; Normandeau et al., 2020). Another possible cause for the occurrence of sediment density flows could be the shear stresses formed by wave-orbital motions that can result in sediment fluidization or liquefaction (Puig et al., 2004, 2014). In any case the steepness of the shelf would help accelerate the flows and sustain them along the shelf slope. Bedforms fields 6, 8, 9 and 10 are found offshore the clinoform rollover and frequently associated to failure of this feature. Where these sediment density flows transport more sediments, they tend to steepen further the clinoform foreset, which fails and promote the development of bedforms on top of the failed material. When no failure of the clinoform foreset occurs, these flows reach the shelf edge unconfined and tend to start gullies on the upper slope that migrate upslope the shelf as channels, where the bedforms form.

6.3.3 INFLUENCE OF THE HYDROGRAPHIC BASINS, SHELF MORPHOLOGY AND SEDIMENT GRAIN-SIZE ON THE BEDFORM GENERATION AND CHARACTERISTICS

The onshore and offshore morphologies and the grain size distribution of the shelf sediments clearly control not only how the bedforms are generated, but also their characteristics and, in our study, allowed defining four main areas on the shelf.

On sector 1 the only bedforms found are those oblique to the coastline. They are close to the rocky outcrops and probably result from the interaction between them and the wave-induced currents during energetic regimes coming mostly from W-SW, as their orientation and their presence only in this sector suggests. From their bathymetric profile, these bedforms seem to have steep lee-side and gentle stoss-side that it is characteristic of cyclic steps. However, the measurements and the observations are not enough to classify them as cyclic steps. The small hydrographic basins in this sector should prevent the formation of hyperpycnal flows that could generate sediment density flows. The low slope of the shelf (~1.5°) together with the coarser grain sizes of the sediment at the seabed might prevent sediment flows (triggered by storm waves) to reach supercritical conditions or, even if these conditions are reached, they are not able to transport medium to coarse sand and to form bedforms.

Sector 2 is where the majority of the bedform fields are located (fields 1 to 6). The bedforms have generally larger wave heights and wavelengths. These larger values can only be explained by higher fluxes of sediment density flows, since hyperpycnal flows formed during flash floods are likely more powerful than those triggered by storms. In addition, the shelf in sector 2 has finer sediments and these are more easily transported. With exception of field 6, probably formed by flows triggered by storms since no stream connection is observed, the remaining bedform fields appear to have been likely formed during flash-flood events. The presence of finer sediments on the shelf might also be related with the fact that the hydrographic basins are eroding older and more weathered lithologies (Figs. 6.10 and 6.11). Thus, finer sediments, larger hydrographic basins, and a relatively steep shelf (average 3.8°) when compared to sector 1, contribute to more numerous bedform fields, occupying larger areas of the shelf and having bigger dimensions.

Sector 3 only presents two main bedform fields (7 and 8). The average size of the hydrographic basins draining to sector 3 is higher than those in sector 2. However, hydrographic basins in sector 2 are more numerous (see Table 5.1 and Fig. 5.1A in chap. 5). The shelf is steeper on zone 3 (average 6.4°) and sediments here have the finest modes of the four sectors, but sector 2 has a higher percentage of fines (silt + clay) than sector 3. It is conceivable that the sediment carried by streams accumulates on SCBs in areas with steeper bathymetry and exposed to storm waves capable of suspending sediments (refer to Figure 5.16 in chap. 5). This accumulation may promote the development of sediment density flows, contributing to the formation of bedforms in field 7 and 8. However, the generated flows might be weaker, explaining the smaller bedforms (in terms of wave height and wavelength) found here.

Sector 4 has two bedform fields (9 and 10). This sector is very similar to sector 3 in terms of hydrographic basin sizes, but they are less productive in discharge rates (see Table 5.1 and Fig. 5.1A in chap. 5). This could be related to lower precipitation rates in this area (see chap. 7) and the fact that outcropping lithologies crossed by streams are mostly related to younger formations than in sectors 2 and 3, so they are less weathered (see Fig. 5.1B in chap. 5). The main difference is that sediment on the shelf is much coarser (the mode is medium sand) and has low percentages of fines (average 11%). The bedforms formed here have the smallest wave heights and wavelengths. In a similar way to sector 3, bedforms here may have been triggered by storm waves. They are only where the sediment is fine since the energetic regime here is low. Thus, the flows could be even weaker than in sector 3, resulting in smaller bedforms.

By comparing bathymetries obtained in two different years (2002 and 2019) it can be seen (Figs. 6.13 and 6.14) that there are different types of cyclic steps, i.e., presenting distinct combinations of deposition and erosion rates on stoss and lee sides. The bedforms in field 2 (likely triggered by hyperpycnal flows from a stream with a relatively small hydrographic basin, 9.75 km²) are partially depositional cyclic steps according to the aggradation-based classification scheme of Slootman and Cartigny (2020) because they show more depositional than erosional areas (Fig. 6.13). Differently, the bedforms in channel 4b (Fig. 6.14) are fully erosional cyclic steps, while the bedforms immediately to the east are only partially erosional because they show alternation of depositional with erosional areas (likely triggered by hyperpycnal flows from a stream with a large hydrographic basin, 41 km²). So, larger hydrographic basins tend to create stronger flows, which are more erosive than depositional or a mix between the two processes.

The bedforms also show some correlation between wave height and lee slopes (Fig. 6.9 F). According to Casalbore et al. (2014), steeper lee slopes increase the flow acceleration and erosion rates, which in turn increases the bedform height. According to Normandeau et al. (2016), steep stoss slopes also facilitate the acceleration of the flows contributing even more to the increase of the wave height of the bedforms. However, there is not any relation between wave height and stoss slope. Although a good relationship between aspect ratio and bedform slope exists as reported by Dietrich et al. (2016), the trend (also reported) that bedforms with smaller aspect ratio had coarser grain sizes is not seen here. Nonetheless, the bedforms on the steepest slopes (sector 4) were in fact formed by the coarsest sediment, although this is more likely linked to sediment sources than to other causes. Sector 4 has the smallest hydrographic basins which also cross younger lithologies that are only slightly weathered, thus producing fewer fine sediments. The only place where finer sediments exist in sector 4 is immediately west of bedform field 10 where a larger hydrographic basin includes older volcanic sequences, more weathered and dismantled.

6.3.4. HAZARD IMPLICATIONS

The results of this study show that the majority of the bedforms are likely formed by hyperpycnal flows and that bedforms monitored in multitemporal surveys moved between 2002 and 2013 and again between 2013 and 2019. This is clear evidence that bedforms are active and moving at least once every 6-11 years. Historical records also show that flash floods happen

every 4.1 to 6.5 years (Quintal, 1999; Lopes et al., 2020) and 2000-2020 precipitation data shows that powerful rainfall events occur at least once per year in the last 20 years. Thus, it is plausible that bedforms formed by hyperpycnal flows may move every year or at least more frequently than the multibeam surveys intervals (6-11 years). The bedforms formed during storm conditions may also move frequently since our analysis of threshold of motion show that, in the areas that feed them, the sediments can be always put in suspension during energetic events in the nearshore zone (see Fig. 5.15 in chap. 5). Probably not all storms can trigger sediment density flows, but it is often the cumulative effect of several storms that may trigger such events (Bailey et al., 2021). Finally, considering that atmospheric rivers are linked to extreme precipitation events in Madeira (Ramos et al., 2018) and that the frequency of these phenomena is expected to increase due to climate change (Ramos et al., 2016), bedforms associated to hyperpycnal flows will probably be more frequently formed.

Since these bedforms are formed by turbidity currents potentially triggered by different processes (flash floods, storms, sediment load accumulation in predisposed environment, etc.), it means that probably their occurrence is frequent. Turbidity currents are strong flows that can reach and overpass 120 cm s^{-1} (Khripounoff et al., 2003) transporting significant volume of sediment. Hazard implications related to bedforms formations are thus linked to damage of submarine infrastructures and ecological habitat stability. Turbidity currents can run for kilometres and are able to modify the seafloor morphology, compromising stability and integrity of submarine infrastructures such as telecommunication cables (Pope et al., 2018). Moreover, turbidity currents entrain large amounts of sediment, altering the seabed and resulting in ecological consequences in areas with sensitive ecosystems, potentially disturbing or damaging habitats (Harris, 2014).

6.4. CONCLUSIONS

The high-resolution DTMs of the southern shelf of Madeira Island allowed a detailed morphological and morphometrical analysis of the several bedform fields found. These features were formed by the combination of erosion, transport and depositional processes during sediment density flows triggered by different mechanisms. They were observed off stream mouths but also in areas without nearby streams. The majority of the bedforms occur within channels or on top of elevated fan-shaped features. The bedform fields offshore stream mouths were related to sediment density flows generated by hyperpycnal flows, while the remaining

fields were likely generated by sediment density flows triggered by storm waves. In general, the wave lengths and wave heights of the bedforms triggered by hyperpycnal flows are larger than those produced by storm waves, probably because the former flows are more intense. The bedforms inside channels seem to evolve in the following way: the channels start forming by erosion of the seafloor by unconfined sediment density flows at the shelf edge and migrate upslope; during the migration of the channels some bedforms already develop, but it is only when they reach the clinoform rollover that the failure of the latter contributes with further sediments to form larger bedforms. The bedforms on top of elevated fan-shaped features seem to develop in a different way: the failure of the foreset forms irregular deposits downslope which are the seed for the development of bedforms during the passage of subsequent flows.

Observed bedforms have varied wave heights and wave lengths, are generally asymmetric, with steeper lee sides and gentler stoss sides, and are crescentic downslope in plan-view. These characteristics and the fact that they form on shelf sectors with relatively high gradient suggest that they are cyclic steps and migrate upslope. The comparison between three different bathymetric surveys (2002, 2013, and 2019) show that the bedforms evolved during these periods. It has also shown different combinations of deposition and erosion on stoss and lee sides of bedforms. Bedforms related to larger hydrographic basins (hence larger flows) seem to be more erosional than depositional and vice-versa.

A relationship was found between bedform location/dimension and the onshore/offshore morphologies, which allowed to define four shelf sectors with different characteristics. These differences depend on the variable combinations of wave exposure, shelf morphology and sediment coverage outcropping lithologies and hydrographic basin contribution.

Finally, the analysis of historical data such as wave buoys, precipitation data, and records of flash floods allowed estimating the recurrence of these events. The bedforms formed during flash floods have a recurrence interval of 4.1 to 6.5 years, which agrees well with the bathymetric surveys that revealed movement of the sedimentary bodies in two-time windows of 7 and 11 years. The bedforms formed by storm waves are likely moving at least once every year based on the calculation of the threshold of motion for the sediment grain sizes found on the foresets of the clinoform rollovers. The above evidence shows that the southern insular shelf of Madeira Island is an active and dynamic environment, frequently subjected to erosive-depositional processes, which might be hazardous to infrastructure lying in the coastal area. This study allowed mapping and predicting the areas where anthropogenic infrastructures and

activities, such as telecommunication cables, marine aggregate dredging, and fish farming, may be endangered by sedimentary processes on the island shelf.

CHAPTER 7. THE CONTRIBUTION OF SEDIMENT SOURCES, SHELF MORPHOLOGY AND WAVE-INDUCED STRESS TO UNDERSTAND THE DISTRIBUTION OF DEPOSITIONAL AND EROSIONAL FEATURES ON THE SOUTHERN SHELF OF MADEIRA ISLAND

Studying the contribution of sediment sources, shelf morphologies and exposure to wave energy on the presence or absence of seafloor features is crucial for understanding the sedimentary dynamics on the submarine environment. To achieve this aim, two main features were analysed on the southern shelf of Madeira Island, namely subaqueous clinoform bodies (SCBs) and bedforms fields. Both features are the result of processes occurring during and/or are triggered by sea storms and rainy events (Chiocci & Romagnoli, 2004; Casalbore et al., 2017, Medri et al., 2023; Normandeau et al., 2016; Bailey et al., 2021; Lira et al., 2013; Provença et al., 2011).

Oceanic islands, such as Madeira, are periodically exposed to extreme waves which effects may be observed on the surrounding shelves (Meireles et al., 2013). Extreme precipitation in Madeira have historically caused catastrophic events on land and detailed descriptions only began to emerge around 1803 (Quintal, 1999). Usually, these storms are related to extreme rainfall and powerful debris/mud flows, but the impact of huge sediment supply to coastal areas has never been discussed in relation to the offshore morphologies.

Within this perspective, SCBs and bedforms are compared and related to the characteristics of the shelf, its exposure to extreme wave conditions, the average precipitation and the stream sediment production. Thus, in this chapter, the results presented in the previous chapters 5 and 6 are integrated to explore the influence of these external factors, providing an overview of how they can affect sediment formation, transport, and development of the morphologies observed on the southern shelf of Madeira.

7.1. RELATIONSHIP BETWEEN PRECIPITATION, SEDIMENT NATURE AND PRODUCTION

Streams in Madeira are characterized by torrential nature (Ribeiro, 1985) and their hydrographic basins have deep valleys formed by incision of rainwater (Miranda et al., 2018; Moura et al., 2019). In general, the erosive capacity of streams increases, as well as their flow rate, during and after intense precipitation (Singh, 1997).

Based on the characteristics of hydrographic basins of Madeira already introduced in chapters 5 (Fig. 5.1, Table 5.1) and 6 (Fig. 6.10 and 6.11), the correlation between average precipitation and sediment production is explored in relation to the nature of the sediment coverage on the shelf.

In sector 1, the hydrographic basin areas are small and most of them are characterized by lower annual average precipitation (Fig. 7.1) and lower sediment production relatively to the remaining sectors. Here, the contribution of cliff erosion and associated deposits is apparently more significant than stream discharge. This is evident from the higher cliffs and from the presence of coarser shelf sediments with low calcium carbonate contents (up to 20%) that increases at the shelf edge (see blue dots in Fig. 7.2). Additionally, the prevalence of coarser sediment may also stem from processes associated with the eastward transport of the finer fractions by longshore currents forming by refraction of the main wave regime coming from W-NW (Fortes et al., 2006; Rusu & Soares, 2012).

In sectors 2 and 3, the largest hydrographic basins of the south slope of the island, Ribeira Brava and Ribeira dos Socorridos, can be found. Most of the hydrographic basins in these sectors have larger areas compared to sector 1 and have higher annual average precipitation. In fact, these streams deliver more finer sediment to the shelf, explaining the predominantly high percentage of silt and clay in these sectors of the southern shelf (Fig. 7.1). The sediment is also characterized by low calcium carbonate content, highlighting that the terrigenous contribution is significant in this area (Fig. 7.2). In sectors 2 and 3, thus, the stream contribution is very significative. This is confirmed not only by the mode of the grain-size of the sediment covering these sectors (2.6 ϕ and 3 ϕ on average, respectively) but also from the lower percentage of calcium carbonate content (offshore streams mouths is between 0 and 5 %) compared to sector 1 (Fig. 7.2).

In sector 4, despite the hydrographic basin areas being similar to sector 3 and some even larger than sector 2, the sediment covering the shelf is on average coarser than the two previous sectors (1.4 ϕ). The finer sediment is restricted to the nearshore zone of the shelf and only offshore the outlet of larger hydrographic basins (Porto Cruz and Machico streams, see chap 5, Fig. 5.1) characterized by higher average precipitation (see purple colour in Fig. 7.1) and high estimated sediment production (see light green and yellow colours in Fig. 7.2). Moreover, in sector 4, streams have a lower maximum altitude and slope and lower annual precipitations in comparison to sectors 2 and 3, explaining the different estimated sediment production between

the sectors (Table 7.1). The coarser grain-size in sector 4 is likely related to high values of $CaCO_3$ content as shown in the graphs in Fig. 7.3 (i.e., higher shell content in the sediments). In fact, the graphs illustrate that in sectors 1 and 2 (southwestern), there is no correlation between sediment grain size and the $CaCO_3$ content of the sediments. Generally, in sectors 1 and 2, both coarser and finer sediments exhibit low percentage of $CaCO_3$ content in all the samples. Conversely, in sectors 3 and 4 (southeastern), there is a strong correlation between coarser sediments and high percentage of $CaCO_3$ in comparison to the previous sectors. This is probably due to wakes observed on the west and east leesides of the island formed by atmosphere-ocean interactions that cause upwelling and favour biological productivity (Caldeira & Sangrà, 2012; Alves et al., 2020, 2021; Caldeira et al., 2020). Another likely explanation for the increase of calcium carbonate content in sector 4 could be related to the wave energy. In sector 1, the terrigenous sediment is probably transported much further offshore (see red areas in Fig. 7.4) due to more exposition to higher waves. In fact, the sediment has more than 40-50 % of calcium carbonate content only at the shelf edge in this sector. In sector 4, although river erosion is higher than sector 1, it is more protected from waves (see fig. 5.15 in chap. 5), and the sediment is not transported longer distances offshore. Moreover, streams in sector 4 are incising younger and less erodible lithologies (except Machico stream, see Fig. 5.1B in chap. 5), which may contribute to a smaller volume of sediment reaching the shelf. In fact, the sediment in sector 4, composed of fine sand is only restricted to shallowest areas. Thus, a smaller terrigenous input increases the likelihood of having a proportionally higher percentage of bioclasts further offshore.

Nevertheless, it is essential to keep in mind that the calculations of sediment produced by each hydrographic basin (equation 4.11) is only one methodology among several others available in the literature and it might not correspond to the reality. In fact, it excludes the impacts of anthropic activity, variations in the annual precipitation, drainage capacity and slope of each hydrographic basin, as well as the lithologic characteristics of the formations in which the basin is installed. These factors are fundamental for better understanding the conditions of each hydrographic basin (Syvitski et al., 2003). Additionally, the erosion rate is also influenced by such factors as the degree of weathering and jointing, which weaken the lithologies, and by the presence of landslides or areas prone to mass wasting that, during intense or prolonged rainfall could lead to an increased sediment production (Lira et al., 2013). Consequently, the sediment production from the hydrographic basins draining the southern slope of Madeira might be underestimated. Based on mapped landslides, Lira et al. (2013) estimated volumes of displaced

sediment of 217.000-344.000 m^3 and 605.000-984.000 m^3 for the Funchal and Ribeira Brava basins, respectively. These values, that refer to a single day (although related to an extreme event), are three times higher than those obtained with the equation 4.11 for the entire year. However, such events are infrequent, and result from the combination of extreme rainfall events and long-lasting rainfall periods (Fragoso et al., 2012) but they have likely contributed to the creation of deposits ready to be mobilized by subsequent rainfall events (Lira et al., 2013).

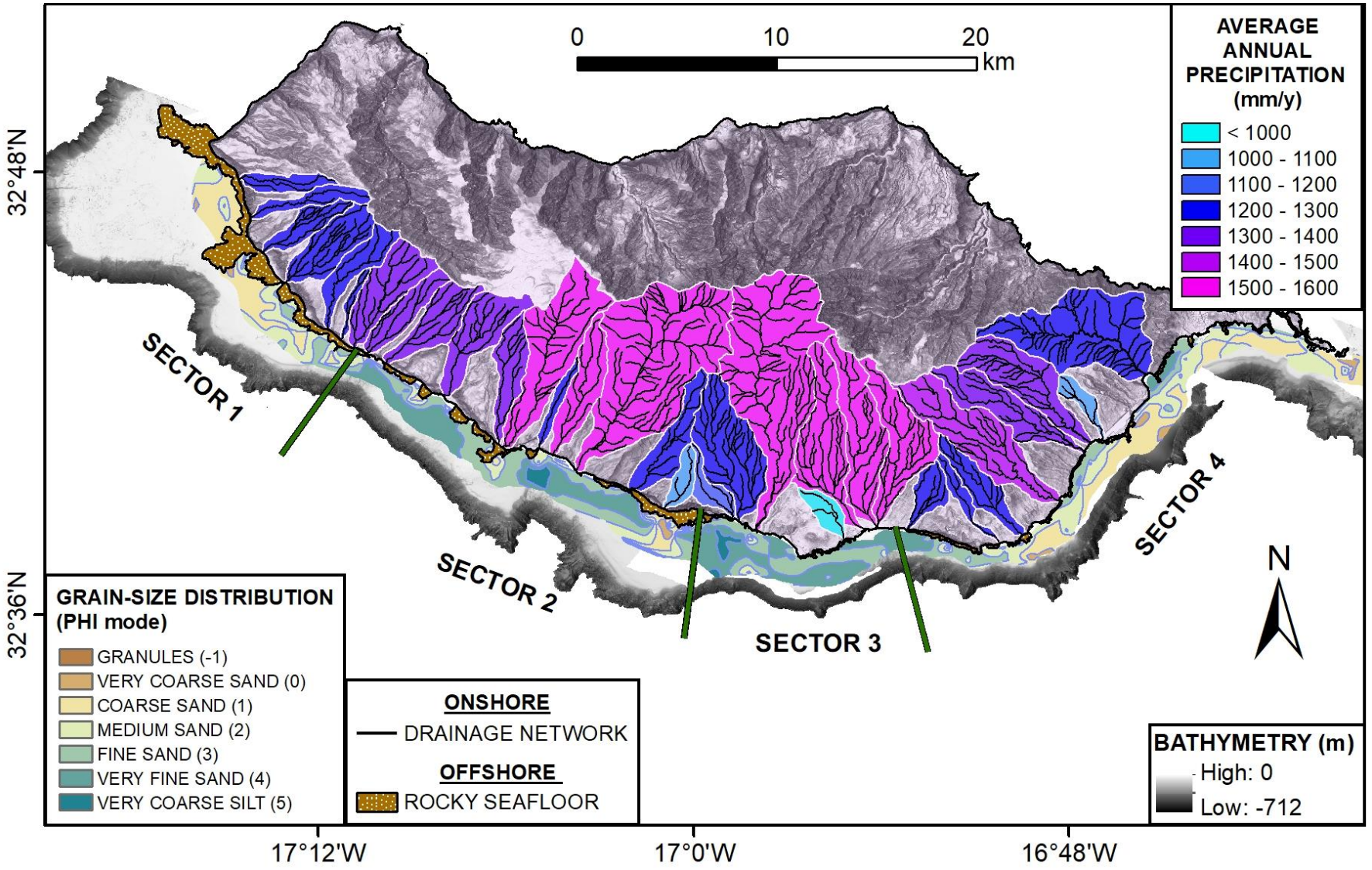

Figure 7. 1. Annual average precipitation in each hydrographic basin and relationship with the grain-size sediment distribution offshore. The average precipitation is based on data from the 1961-1990 period (Atlas do Ambiente, 1995). Brown polygons represent nearshore rocky seafloor.

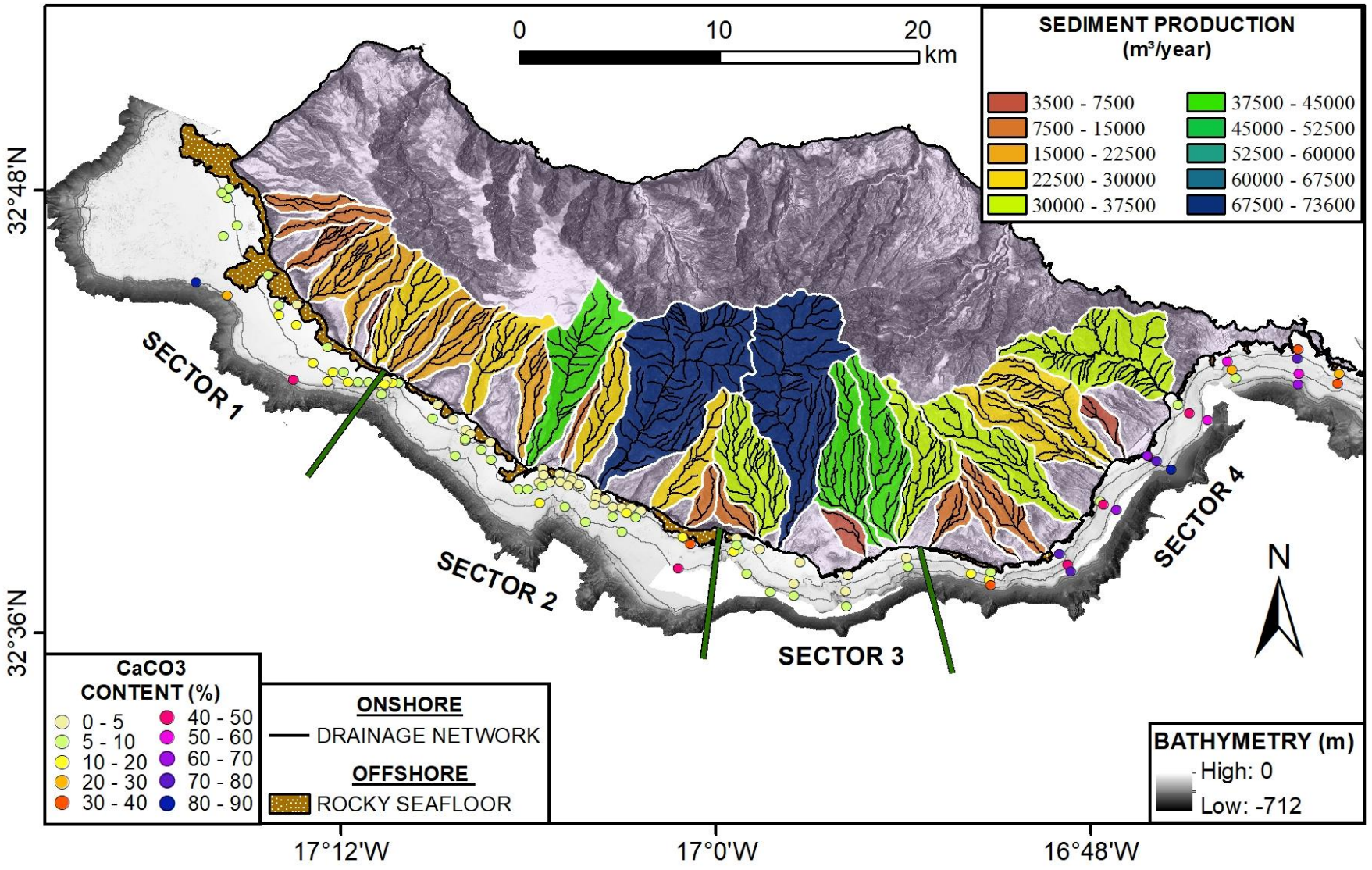

Figure 7. 2. Estimated sediment supply from each hydrographic basin (equation 4.11 in chap. 4) and calcium carbonate content in the sedimentary cover. Notice the higher percentage of calcium carbonate in the easternmost part of the shelf at shallower depths. Brown polygons represent nearshore rocky seafloor. Contours are spaced each 50 m.

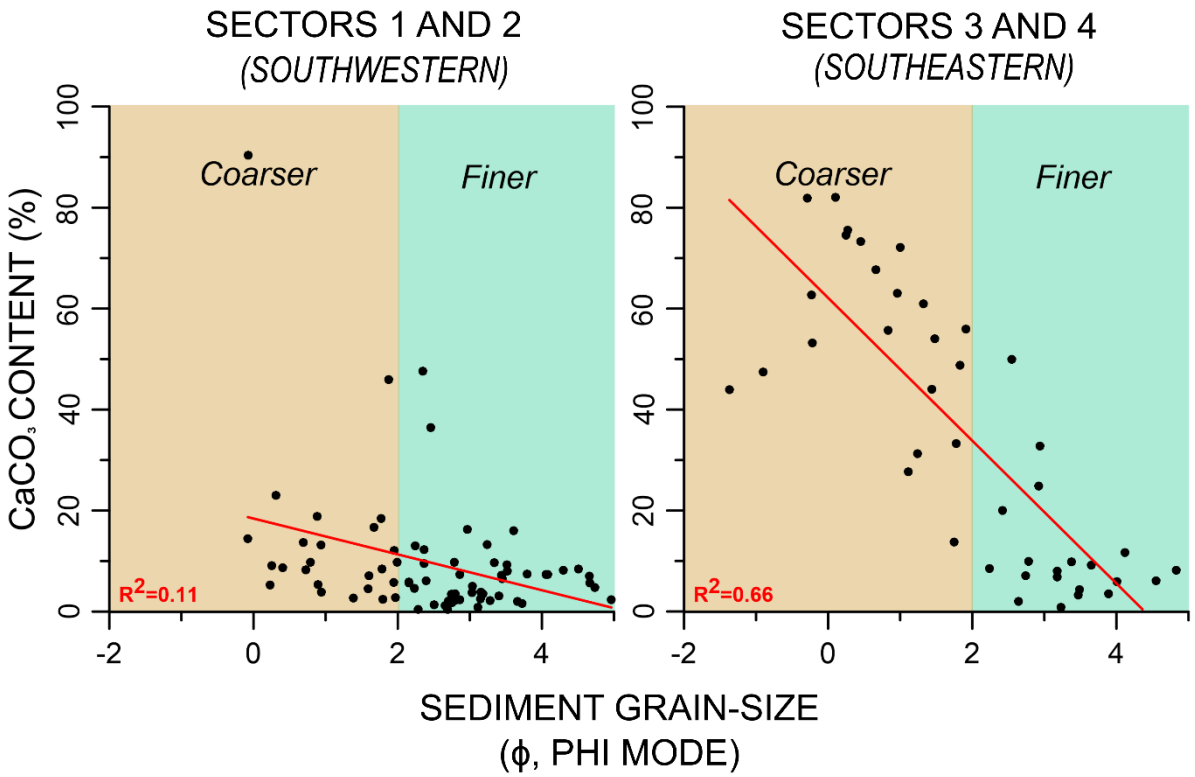

Figure 7. 3. Scatter plots and relationship between the $CaCO_3$ content (%) and the average sediment grain-size in different shelf sectors.

7.2. RELATIONSHIP BETWEEN SCBs AND BEDFORMS SPATIAL DISTRIBUTION VERSUS WAVE ENERGY AND RELATIVE INDUCED STRESS, SHELF MORPHOLOGY AND SEDIMENT SUPPLY

The interplay between onshore and offshore characteristics together with the meteorological external factors (i.e. sea storms and intense precipitations) control the characteristics of SCBs and the bedforms present on the seafloor of Madeira Island (Table 7.1). SCBs are fundamental for the development and evolution of bedforms fields since they provide sediment for their formation (see chap. 6).

Oblique bedforms predominantly occur in sector 1, characterized by higher wave energy (Fig. 7.3), a wide shelf, gentle gradients (approximately 1.5°), coarse sediment cover, and numerous rocky outcrops. Sector 1 is directly exposed to the impact of the primary wave regime coming from the west (Rusu et al., 2012). Here, the waves are notably higher and have the capacity to mobilize sediment over larger and deeper areas compared to sectors 2 and 3, which experience a lower energetic wave regime. It is thus possible that during storms coming mostly from W, the waves interact with the nearshore rocky outcrops, favouring the development of powerful

downwelling currents that form the bedforms oblique to the coastline. This would explain the orientation of these features and the reason why they are mostly only present in sector 1, where nearshore rocky seafloor mostly outcrops (see brown polygons in Figs. 7.1 and 7.2). Moreover, in sector 1, the hydrographic basins are small and are probably not able to produce large hyperpycnal flows. The development of hyperpycnal flows is probably one of the most important trigger mechanisms for the occurrence of turbidity currents that form the bedforms perpendicular to the coastline that we see on Madeira shelf (Talling et al., 2013; Symons et al., 2016; Slootman and Cartingy, 2020). Therefore, while sediment transport is primarily governed by cross-shore movement, as indicated by the presence of the SCBs at the nearshore part of sector 1, there is a secondary along-shore component that contributes to its eastward displacement. Their formation, linked to the wave-regime and the consequent interaction with rocky outcrops and consequent formation of currents, could explain their absence in 4, which is mostly protected from waves and where rocky outcrops are small (see Suppl. Fig. 10.51, in Appendix).

Bedforms perpendicular to the coastline are present in sectors 2, 3 and 4. They develop where the shelf is steeper (> 4°) and narrower and there are stream mouths with large hydrographic basins. In sectors 2 and 3, the wave energy is lower than in sector 1 but still significantly influences these sectors. It is possible that the wave energy coupled with stream discharge would favour the formation and evolution of density currents crossing the shelf. These density currents may arise not only due to downwelling currents (that form in response to coastal set-up) but also by riverine input and formation of hyperpicnal flows (Talling et al., 2013), where the two processes have a constructive interference. Bedform fields perpendicular to the coastline, in these sectors, form where there is a significant sedimentary fine fraction of terrigenous origin as previous discussed in sub-chap. 6.2.

However, it seems that high shelf gradients play an essential role in promoting the development of perpendicular sediment-density currents, shaping bedform fields even in areas where the wave regime is not particularly energetic (Bailey et al., 2021). In sector 4, the discharged sediment is stocked in small SCBs that stay nearshore (in comparison with sectors 2 and 3). The arrival of sediments that stay nearshore and do not advance further offshore makes the foresets very steep. This loading preconditions the area making it prone to landslides more frequently, triggering the formation of density currents and the development of bedform fields.

Table 7.1. Summary of onshore and offshore characteristics of each sector. The values with "*"do not include the largest hydrographic basins (Ribeira Brava and Ribeira dos Socorridos). The values with "†" are related to the larger SCBs observed in sector 4. CVS: Complexo Vulcânico Superior; CVM: Complexo Vulcânico Médio.

		SECTOR 1 (average ± st. dev.)	**SECTOR 2** (average ± st. dev.)	**SECTOR 3** (average ± st. dev.)	**SECTOR 4** (average ± st. dev.)
	ONSHORE				
Sediment supply	Average annual precipitation (mm/y)	1200 ± 200	1350 ± 250	1300 ± 300	1255 ± 245
	Hydrographic basins average area (km^2)	5.5 ± 3	8 ± 5*	11 ± 6*	10 ± 7
	Main outcropping units	CVS	CVM	CVM-CVS	CVS
	Estimated sediment production (m^3/y)	15554 ± 6117	21798 ± 10365*	26742 ± 16416*	19698 ± 11573
	OFFSHORE				
Shelf characteristics	Shelf slope (°)	1.45 ± 1.1	3.8 ± 0.1	6.4 ± 1.3	6.4 ± 0.8
	Min. and max. shelf width (km)	1.8 – 9.5	1.6 – 4.5	1.5 – 2.5	0.9 – 2.3
	Sediment grain-size (ϕ)	1 ± 0.5	2.6 ± 1	3 ± 0.3	1.4 ± 0.8
Wave exposure	Wave height (95^{th} percentile - m)	2.43 ± 0.36	1.24 ± 0.18	0.95 ± 0.20	0.72 ± 0.14
Resulting morphological features	SCBs thickness (m)	9 ± 6	15 ± 7	10 ± 4	11 ± 2 (†)
	SCBs rollover point depth (m)	60 ± 15	38 ± 5	27 ±4	22 ± 5
	Bedform fields perpendicular to the coastline	absent	present (6 fields)	present (2 fields)	present (2 fields)
	Bedform fields oblique to the coastline	present (abundant)	present (rare)	absent	absent

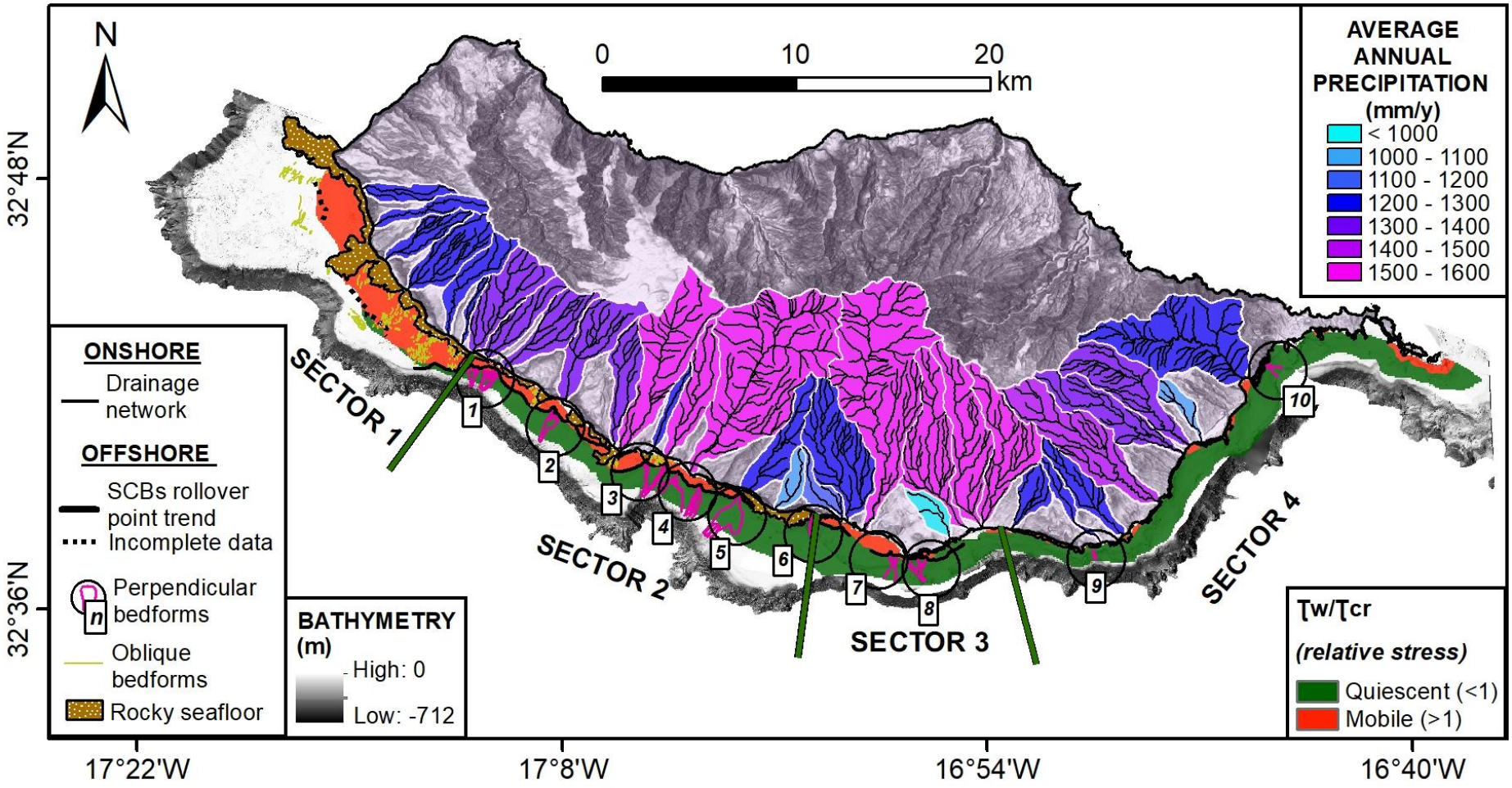

Figure 7. 4. Annual average precipitation of the hydrographic basins. Relation of SCBs rollover depth and bedforms distribution on the southern shelf versus wave-induced bed stress. Red areas indicate locations where sediment is suspended by waves, whereas green areas represent sites where sediment remains unaffected by wave action. Brown polygons represent nearshore rocky seafloor.

7.3. CONCLUSIONS

SCBs morphology and bedforms are important features that provide insights on the hydrodynamics impacting the Madeira southern shelf. Moreover, they develop and evolve in response to the characteristics of the depositional environment. On Madeira Island, the geophysical and sedimentological data coupled with modelling of the surrounding wave regime and the estimation of the fluvial sediment supply allowed highlighting not only the processes involved but also to understand how they interplay and shape the morphology of these depositional and erosive features.

The quantitative estimation of erosion due to river drainage and the average precipitation as well as observation of the height of cliffs allowed to qualitatively understand the contribution of sediment supply from the hydrographic basins to the coast and to infer the main sedimentary feeding process in each sector of the study area. Thus, the main sediment source feeding Madeira shelf is the erosion by torrential streams. The streams input is reinforced in sectors 1 and 2 by cliff dismantling and the resulting landslide deposits. The supplied sediment is transported from the nearshore to the offshore during high-wave energy conditions forming SCBs. Particularly, the streams contribute to their formation when extreme rainfall hits the island (Oliveira et al., 1999). In fact, the larger SCBs depocenters and the location of most bedform fields characterized by cyclic steps is concentrated in sectors 2 and 3 where the streams deliver more sediment and are characterized by higher annual average precipitation. When high precipitation occurs, the resulting floods can deliver huge quantity of sediment to the ocean. In these occasions, hyperpycnal flows drive the sediment transport cross shore, forming and evolving into density sediment currents at the SCB rollover creating the bedforms fields perpendicular to the shelf. However, these bedforms do not occur in the absence of favourable conditions. Although high shelf gradients drive and promote the formation of narrow SCBs depocenters with steeper foresets which are more prone to fail, bedforms tend to be rare in sector 4 because high stream discharge is missing, and wave energy is small to transport sediments offshore. Therefore, density currents are more difficult to form on sector 4.

CHAPTER 8. CONCLUSIONS AND FUTURE WORK

The outcomes of this Ph.D. project increased the knowledge about the erosional and depositional features present on the southern shelf of Madeira Island. Despite the availability of recent marine data, including multitemporal bathymetries, sparker seismic profiles, and sediment samples, they had not been thoroughly explored until now. Through the adoption of different software made available by Instituto Hidrográfico (e.g. DELPH and ArcGIS), the morphological and morphometric characteristics of these features were investigated. The elucidated findings can be summarized as follows:

- The seafloor of the southern shelf of Madeira presents two primary types of erosive and depositional features. These are bedform fields and subaqueous clinoform bodies (SCBs);
- These features are useful for better constrain the role of subaerial topography and geology, climate, sediment supply, the pre-existing bathymetry and wave regime driving their formation and evolution;
- Recent SCBs occur along the entire southern shelf displaying a great variability in terms of topset width, clinoform thickness and rollover point depth. This variability allowed defining the driving key factors at the local scale;
- The morphometric and morphological analysis of the bedforms revealed that they are probably cyclic steps, antidunes or transitional features between them. In any case, they are the result of turbidity currents as observed in other similar geological settings. These currents can be induced by several mechanisms, and proposals have been put forward based on the onshore characteristics and the occurrence of extreme events on the island;
- The spatial distribution of these erosional and depositional features coupled with the onshore elements allowed the division of the shelf into four sectors. They have different characteristics in terms of sediment supply, shelf morphology and hydrodynamics;
- Furthermore, their case study serves as a noteworthy example, providing valuable insights for comparisons with other oceanic volcanic islands in different settings. This contributes to increase our understanding of the intricate dynamics between land and ocean and their influence on marine morphologies.

Beyond the importance of this study for the scientific community, there is also a significant socio-economic contribution. This project holds particular relevance for the resident

populations. Firstly, as in other volcanic archipelagos, the shelf represents a shallow-water repository of sediment and habitats for biological communities. Knowing their characteristics is the base for defining measures that aim to safeguard and protect these areas but also for the sustainable use of their resources (for instance marine aggregates dredging activity). Moreover, Madeira is a volcanic island characterized by extreme events such as flash floods and cliff gravitative instability. These can trigger other processes including hyperpycnal flows and turbidity currents, which represent an actual hazard for marine infrastructures, such as telecommunication cables and aquaculture infrastructures on the shelf. Understanding where these hazards are more prone to take place is crucial for the management of the submarine territory.

Despite the findings of this study, the marine environment around Madeira Island still requires extensive exploration and study. The results can be further integrated, enhanced, and juxtaposed with additional research. In particular, further investigation can be conducted by integrating supplementary data such as to:

- Examine the morphological characteristics of the northern shelf to enhance the complete analysis of the submarine environment and facilitate meaningful comparisons between both sides of the island.
- Analyse the cores (which are already available) for the southern shelf that cuts recent SCBs to infer and better constrain age and sedimentary processes.
- Continuous monitoring of all bedform fields over time to gain a better understanding of their evolution and to quantify and qualify those present in the western part of the island, which have not been extensively surveyed.
- Measure seafloor currents over longer timespans to improve interpretation of how the studied features form and evolve.

REFERENCES

Alves, J.M.R., Tomé, R., Caldeira, R.M.A., Miranda, P.M.A., (2021). Asymmetric Ocean Response to Atmospheric Forcing in an Island Wake: A 35-Year High-Resolution Study. Front. Mar. Sci., 8, 62, 43-92. doi: 10.3389/fmars.2021.624392

Alves, J., Caldeira, R., Miranda, P., (2020). Dynamics and oceanic response of the Madeira tip-jets. Quart. Jour. of the Royal Meter. Soc. doi:10.1002/qj.3825.

Ainsworth, R.B., McArthur, J.B., Lang, S.C., and Vonk, A.J., (2020). Parameterizing parasequences: importance of shelf gradient, shoreline trajectory, sediment supply, and autoretreat. AAPG Bull., 104, 53–82.

Alexander, J., Bridge, J.S., Cheel, R.J., Leclair, S.F., (2001). Bedforms and associated sedimentary structures formed under supercritical water flows over aggrading sand beds. Sedim., 48, 133‑152.

Allen, J.R.L., (1982). Sedimentary structures, their character and physical basis. Develop. Sedimentol. 30A, 593, Elsevier, Amsterdam.

Ashley, G.M., (1990) Classification of large-scale subaqueous bedforms: A new look on an old problem. Jour. of Sedim. Petrol., 60, 160–172.

Burgess, P.M., Steel, R.J., Granjeon, D.I., 2008. Stratigraphic forward modeling of basin margin clinoform systems: Implications for controls on topset and shelf width and timing of formation of shelf-edge deltas. In: Recent Advances in Models of Siliciclastic Shallow-Marine Stratigraphy, 90, 35–45.

Babonneau, N., Delacourt, C., Cancouët, R., Sisavath, E., Bachèlery, P., Mazuel, A., Jorry, S. J., Deschamps, A., Ammann, J., Villeneuve, N., (2013). Direct sediment transfer from land to deep-sea: Insights into shallow multibeam bathymetry at La Réunion Island. Mar. Geol., 346, 47–57. doi.org/10.1016/j.margeo.2013.08.006.

Bailey, L. P., Clare, M. A., Rosenberger, K. J., Cartigny, M. J. B., Talling, P. J., Paull, C. K., Gwiazda, R., Parsons, D. R., Simmons, S. M., Xu, J., Haigh, I. D., Maier, K. L., McGann, M., Lundsten, E., (2021). Preconditioning by sediment accumulation can produce powerful turbidity currents without major external triggers. Earth and Planet. Sci. Lett., 562. doi.org/10.1016/j.epsl.2021.116845.

Baioni, D., (2011). Human activity and damaging landslides and floods on Madeira Island. Nat. Haz. and Eart. Syst. Scien., 11, 3035–3046. doi.org/10.5194/nhess-11-3035-2011.

Bintanja, R., Van de Wal R.S.W., Oerlemans, J., (2005). Modelled atmospheric temperatures and global sea levels the past million years. Nat., 437, 125-128.

Booij, N., Ris, R.C., Holthuijsen, L.H., (1999). A third-generation wave model for coastal regions. Part 1: Model description and validation, Jour. Geophys. Res., 104, 4, 7649-7666.

Bosman, A., Casalbore, D., Dominici, R., (2017). Cyclic Steps at the Head of Channelized Features Along the Calabrian Margin (Southern Tyrrhenian Sea, Italy). In J. Guillén, J. Acosta, F. L. Chiocci, A. Palanques (Eds.), Atlas of Bedforms in the Western Mediterranean, 29–233, Springer International Publishing.

Brum da Silveira, A., Madeira, J., Ramalho, R., (2014). Field Trip Guide "Geology of Madeira Island" Leader: António Brum da Silveira. In Geology.

Brum da Silveira, A., Madeira J., Ramalho, R., Fonseca, P., Rodrigues, C. and Prada, S., (2010c). Notıcia Explicativa da Carta Geologica da Ilha da Madeira na escala de 1:50000, technical report. Secr. Reg. do Ambiente e Recursos Naturais, Governo Reg. da Madeira, Funchal, Madeira Island.

Brum da Silveira, A., Madeira, J., Ramalho, R., Fonseca, P., Prada, S., (2010b). Carta Geológica da Região Autónoma da Madeira, na escala 1:50.000, folhas A e B. Edited by Secretaria Regional do Ambiente e Recursos Naturais, Madeira Regional Government: ISBN: 978-972-98405-1-7.

Brum da Silveira, A., Madeira, J., Ramalho, R., Fonseca, P., Prada, S., (2010a). Notícia explicativa da Carta Geológica da Região Autónoma da Madeira, na escala 1:50.000, folhas A e B. Edited by Secretaria Regional do Ambiente e Recursos Naturais, Madeira Regional Government: 47, ISBN: 978-972-98405-2-4.

Brum da Silveira, A., Madeira, J., Prada, S., Canha, S; Fonseca, F., Ramalho, R., (2006). Glacial landforms in Madeira Island (Portugal). 3° Congress of Geomorphology, October, 12th-14th, Funchal.

Caldeira, R.M.A., S. Groom, S., Miller, P., Pilgrim, D., Nezlind, N.P., (2020). Sea-surface signatures of the island mass effect phenomena around Madeira Island, Northeast Atlantic. Rem. Sens. of Environ., 80, 336– 360.

Caldeira, R.M.A., Sangrà, P., (2012). Complex geophysical wake flows Madeira Archipelago case study. Oc. Dyn., 62, 683–700.

Carling, P.A., Shvidchenko, A.B., (2002). A consideration of the dune: antidune transition in fine gravel. Sedimentol. 49, 1269–1282.

Carracedo, J.C., Troll, V.R., (2020). North-East Atlantic Islands: The Macaronesian Archipelagos. Eart. Syst. and Envir. Scienc., Encycl. Geol., 4, 674-699. doi:10.1016/b978-0-08-102908-4.00027-8.

Cartigny, M. J. B., Ventra, D., Postma, G., Van Den Berg, J. H., (2014). Morphodynamics and sedimentary structures of bedforms under supercritical-flow conditions: New insights from flume experiments. Sediment., 61, 3, 712–748. doi:10.1111/sed.12076.

Cartigny M.J.B., Postma G., H. van den Berg J., Mastbergen D. R., (2011). A comparative study of sediment waves and cyclic steps based on geometries, internal structures and numerical modeling. Mar. Geol., 280, 1-4, 40–56.

Casalbore, D., Clare, M. A., Pope, E. L., Quartau, R., Bosman, A., Chiocci, F. L., Romagnoli, C., Santos, R., (2021). Bedforms on the submarine flanks of insular volcanoes: New insights gained from high resolution seafloor surveys. Sediment., 68, 4, 1400-1438. doi.org/10.1111/sed.12725.

Casalbore, D., Romagnoli, C., Adami, C., Bosman, A., Falese, F., Ricchi, A., Chiocci, F.L., (2018). Submarine Depositional Terraces at Salina Island (Southern Tyrrhenian Sea) and Implications on the Late-Quaternary Evolution of the Insular Shelf. Geoscien., 8, 1, 20.

Casalbore, D., Bosman, A., Romagnoli, C., Chiocci, F.L., (2017). Small-Scale Bedforms Generated by Gravity Flows in the Aeolian Islands. In Atlas of Bedforms in the Western Mediterranean, 287–292. Springer International Publishing. doi.org/10.1007/978-3-319-33940-5_44

Casalbore, D., Bosman, A., Romagnoli, C., Chiocci, F.L., (2016). Morphological map of Salina offshore (Southern Tyrrhenian Sea). J. Maps 12, 5, 725-730. doi.org/10.1080/17445647.2015.1070300.

Casalbore, D.; Romagnoli, C.; Pimentel, A.; Quartau, R.; Casas, D.; Ercilla, G.; Hipolito, A.; Sposato, A.; Chiocci, F.L., (2015). Volcanic, tectonic andmass-wasting processes offshore Terceira Island (Azores) revealed by high-resolution seafloor mapping. Bull. Volcanol., 77.

Casalbore, D., Romagnoli, C., Bosman, A., Chiocci, F.L., (2014). Large-scale seafloor waveforms on the flanks of insular volcanoes (Aeolian Archipelago, Italy), with inferences about their origin. Mar. Geol., 355, 318-329.

Casalbore, D., Romagnoli, C., Chiocci, F.L., Frezza, V., (2010). Morpho-sedimentary characteristics of the volcaniclastic apron around Stromboli volcano (Italy). Mar. Geol., 269, 3–4, 132–148. doi.org/10.1016/j.margeo.2010.01.004.

Clare, M.A., Le Bas, T., Price, D.M., Hunt, J.E., Sear, D., Cartigny, M.J.B., Vellinga, A., Symons, W., Firth C., Cronin, S., (2018). Complex and cascading triggering of submarine landslides and turbidity currents at volcanic islands revealed from integration of high-resolution onshore and offshore surveys. Front. Earth Sci., 6, 223. doi: 10.3389/feart.2018.00223.

Cheel, R., (2016). Chapter 5: Bedforms and stratification under unidirectional flows [Figure 5.1]. spartan.ac.brocku.ca/~rcheel/teaching/sedimentology/

Chiocci, F. L., Romagnoli, C., Bosman, A., (2008). Morphologic resilience and depositional processes due to the rapid evolution of the submerged Sciara del Fuoco (Stromboli Island) after the December 2002 submarine slide and tsunami. Geomorphol., 100, 3–4, 356–365.

Chiocci, F.L., Romagnoli, C., (2004). Terrazzi deposizionali sommersi nelle Isole Eolie. Memorie Descrittive della Carta Geologica d' Italia, 58, 81–114.

Chow, V.T., (1959). Open-channel Hydraulics. McGraw- Hill Book, New York.

Dietrich, P., Ghienne, J.F., Normandeau, A., Lajeunesse, P., (2016). Upslope-migrating bedforms in a proglacial sandur delta: cyclic steps from river-derived underflows?. Jour. Sediment. Res., 86, 1, 112-122.

Fedele, J.J., Hoyal, D.C., Barnaal, Z., Tulenko, J., Awalt, S., (2016). Bedforms created by gravity flows. In: In: Budd, D., Hajek, E., Purkis, S. (Eds.), Autogenic Dynamics and Self-Organization in Sedimentary Systems, 106. SEPM Spec. Pub., 95–121.

Field, M.E. Roy, P.S., (1984). Offshore transport and sand-body formation: evidence from a steep, high energy shoreface, southeastern Australia. J. Sediment. Petrol., 54, 4, 1292–1302.

Fildani, A., Hubbard, S.M., Covault, J.A., Maier, K.L., Romans, B.W., Traer, M., Rowland, J.C., (2013). Erosion at inception of deep-sea channels. Mar. Petrol. Geol., 41, 48‑61.

Folk, R.L., (1974). Petrology of Sedimentary Rocks. Hemphill Publishing Co., Austin, Texas, 184.

Fortes, C., Coli, A.B., Neves, M.G., Capitao, R., (2006). Porto Santo Island: Offshore wave characterization and propagation. J. Coast. Res., 1600–1605.

Fragoso, M., Trigo, R.M., Pinto, J.G., Lopes, S., Lopes, A., Ulbrich, S., (2012). The 20 February 2010 Madeira flash-floods: synoptic analysis and extreme rainfall assessment. Nat. Hazards Earth Syst. Sci., 12, 715–730. doi: 10.5194/nhess-12-715-2012.

García-Ramos, D. A., Zuschin, M., (2018). High-frequency cycles of brachiopod shell beds on subaqueous delta-scale clinoforms (early Pliocene, south-east Spain). Sediment. doi:10.1111/sed.12541.

Geldmacher, J., Hoernle, K., Klügel, A., Van Den Bogaard, P., Duggen, S., (2006). A geochemical transect across a heterogeneous mantle upwelling: Implications for the evolution of the Madeira hotspot in space and time. Lithos 90: 131-144.

Geldmacher, J., Hoernle, K., (2000). The 72 Ma geochemical evolution of the Madeira hotspot (eastern North Atlantic): recycling of Paleozoic (?500 Ma) basaltic and gabbroic crust. Earth Planet. Sci. Lett., 183, 73-92.

Geldmacher, J., van den Bogaard, P., Hoernle, K., Schmincke, H.-U., (2000). The 40 Ar/ 39 Ar age dating of the Madeira Archipelago and hotspot track (eastern North Atlantic). In Geochem. Geophys. Geosyst., 1.

Goodfriend, G. A., Brigham-Grette, J., Miller, G. H., (1996). Enhanced Age Resolution of the Marine Quaternary Record in the Arctic Using Aspartic Acid Racemization Dating of Bivalve Shells. Quat. Resear., 45, 02, 176–187. doi:10.1006/qres.1996.0018.

Gonçalves, M., Martinho, P., Soares, C.G., (2020). Wave energy assessment based on a 33-year hindcast for the Canary Islands. Ren. En., 152, 259-269.

Hamilton, E.L. Bachman, R.T., (1982). Sound velocity and related properties of marine sediments. J. Acoust. Soc. Am., 72, 6, 1891-1904. doi:10.1121/1.388539.

Harris, P. T., (2014). Shelf and deep-sea sedimentary environments and physical benthic disturbance regimes: A review and synthesis. Mar. Geol., 353, 169–184. doi:10.1016/j.margeo.2014.03.023.

Hernández-Molina, F.J., Fernández-Salas, L.M., Lobo, F., Somoza, L., Díaz-del-Río, V., Alveirinho Dias, J.M., (2000). The infralittoral prograding wedge: a new large-scale progradational sedimentary body in shallow marine environments. Geo-Mar. Lett. 20, 109-117.

Hizzett, J.L., Hughes Clarke, J.E., Sumner, E.J., Cartigny, M.J.B., Talling, P.J., Clare, M.A., (2017). Which triggers produce the most erosive, frequent and longest runout turbidity currents on deltas? Geophys. Res. Lett. 45, 855‐863.

Hoffmann, G., Silver, E., Day, S.J., Driscoll, N., Orange, D., (2011). Deformation versus deposition of sediment waves in the Bismarck Sea, Papua New Guinea, in: Shipp, R.C., Weimer, P., Posamentier, H.W. (Eds.), Mass-Transport Deposits in Deepwater Settings. Sediment. Geol., 455-474.

Innocentini, S., Quartau, R., Casalbore D., Roque C., Vinhas, A., Santos, R., Rodrigues, A. (2022). Morpho-stratigraphic characterization of the southern shelf of Porto Santo Island (Madeira Archipelago): insights for small-scale instability processes and post-LGM sedimentary architecture. Mar. Geol., 444, 1-14.

Klügel, A; Schwarz, S.; Van Den Bogaard, P.; Hoernle, K.; Wohlgemuth-Ueberwasser, C.; Köster, J., (2009). Structure and evolution of the volcanic rift zone at Ponta de São Lourenço, Eastern Madeira. Bull. Volc., 71, 671–685.

Komar, P.D. Miller, M.C., (1973) The threshold of sediment movement under oscillatory water waves. J. Sed. Res., 43, 1101–1110.

Instituto do Ambiente, 1995a. Atlas Digital do Ambiente. Bacias Hidrográficas, ribeiras e levadas. Carta VII.2 - Recursos Hídricos superficiais. Região Autónoma da Madeira.

Instituto do Ambiente 1995b Atlas Digital do Ambiente. Temperatura média anual. Região Autónoma da Madeira.

Instituto Hidrográfico, (2007). Dinâmica Sedimentar da costa sul da ilha da Madeira (Cabo Girão à Ponta de S. Lourenço). REL.TF.GM.02/03. Instituto Hidrográfico, Lisboa, Portugal., 131.

Instituto Hidrográfico, (2003). Dinâmica Sedimentar da costa sul da ilha da Madeira. REL.TF.GM.02/03. Instituto Hidrográfico, Lisboa, Portugal., 161.

Instituto Hidrográfico, (2002). "Dinâmica sedimentar na costa sul da madeira jun 2002 - jul 2002". REL.TF.OC04/2002

Instituto Hidrográfico, (2001). "Roteiro da costa de portugal - Arquipélago da Madeira" (3ª edição), Lisboa.

Kennedy, J.F., (1963). The mechanics of dunes and antidunes in erodible-bed channels. J. Fluid Mech., 16, 521–544.

Kleinhans, M.G., (2001). The key role of fluvial dunes in transport and deposition of sand–gravel mixtures, a preliminary note. Sedim. Geol., 143, 7–13.

Khripounoff, A., Vangriesheim, A., Crassous, P., Etoubleau, J., (2009). High frequency of sediment gravity flow events in the Var submarine canyon (Mediterranean Sea). Mar. Geol., 263, 1-6.

Koller, D., Manica, R., Borges, A., Fedele, J., (2019). Experimental bedforms by saline density currents. Braz. J. Geol., 49. doi.org/10.1590/2317-4889201920180118.

Koller, D.K., Borges, A.L.D.O., Puhl, E., Manica, R., (2017). Prediction of the bedforms generated by density currents based on fluvial phase diagrams. Braz. J. Water Res. 22, 49. doi.org/10.1590/2318-0331.0217160021.

Koloseus, H.J., Davidian, J., (1966). Free surface instabilities correlations. U.S. Geol. Surv. Water-Sup. Pap., 1592-C, 72

Kostic, S., (2011). Modeling of submarine cyclic steps: Controls on their formation, migration, and architecture. Geosph., 7, 294-304.

Kostic, S., Sequeiros, O., Spinewine, B., Parker, G., (2010). Cyclic steps: a phenomenom of supercritical shallow flow from the high mountains to the bottom of the ocean. J. Hydr. Environ. Res., 3, 167‑172.

Lang, J., Le Heron, D.P., Van den Berg, J., and Winsemann, J., (2020). Bedforms and sedimentary structures related to supercritical flows in glacigenic settings. Sedim. doi.org/10.1111/sed.12776.

Leat, P.T., Tate, A.J., Tappin, D.R., Day, S.J., Owen, M.J., (2010). Growth and mass wasting of volcanic centers in the northern South Sandwich arc, South Atlantic, revealed by new multibeam mapping. Mar. Geol., 275, 110-126.

Lee, J.H., Syvitski, J.P.M., Parker, G., Orange, D., Locat, J., Hutton, E.W.H., Imran, J., (2002). Distinguishing sediment waves from slope failure deposits: field examples, including the "Humbolt slide" and modelling results. Mar. Geol., 192, 79-104.

Lira, C., Lousada, M., Falcão, A. P., Gonçalves, A. B., Heleno, S., Matias, M. P., Pereira, M. J., Pina, P., Sousa, A. J., de Oliveira, R. P., de Almeida, A. B. (2013). The 20 February 2010 Madeira Island flash-floods: VHR satellite imagery processing in support of landslide inventory and sediment budget assessment. Nat. Haz. and Earth Syst. Sci., 13, 3, 709–719. doi.org/10.5194/nhess-13-709-2013

López-Saavedra, M. Martí, J., (2023). Reviewing the multi-hazard concept. Application to volcanic islands. Eart. Sci. Rev., 236, 104-286.

Lopes, S., Fragoso, M., Lopes, A., (2020). Heavy Rainfall Events and Mass Movements in the Funchal Area (Madeira, Portugal): Spatial Analysis and Susceptibility Assessment. Atmosph., 11, 104.

Lucchi, F.; Lucchi F, Ricchi A, Romagnoli C, Casalbore D, Quartau R., (2019). Late-Quaternary paleo sea-level geomorphological tracers of opposite vertical movements at Salina volcanic island (Aeolian Arc). Ear. Surf. Proc. and Landf., 44, 2377-2395. doi: 10.1002/esp.4651

Madeira, J., Brum, A., Ramalho, R., Fonseca, P., Prada, S. (2007). Carta geológica da Madeira, 1–43.

Marti, J., Gropelli, G. Brum da Silveira, A. (2018) Volcanic Stratigraphy: a review. J. Volcanol. Geoth. Res., 357, 68-91. doi: 10.1016/j.jvolgeores.2018.04.006.

Masson, D.G., Le Bas, T.P., Grevemeyer, I., Weinrebe, W., (2008). Flank collapse and large-scale landsliding in the Cape Verde Islands, off West Africa. Geochem. Geophys. Geosyst., 9. doi:10.1029/2008GC001983.

Matos, C., Silveira, G., Matias, L., Caldeira, R., Ribeiro, M.L., Dias, N.A., Krüger, F., Bento dos Santos, T., (2015). Upper crustal structure of Madeira Island revealed from ambient noise tomography. Jour. Volc. Geoth. Res., 298, 136–145. doi.org/10.1016/j.jvolgeores.2015.03.017.

Mazuel, A., Sisavath, E., Babonneau, N., Jorry, S.J., Bachèlery, P., Delacourt, C., (2016). Turbidity current activity along the flanks of a volcanic edifice: The Mafate volcaniclastic complex, La Réunion Island, Indian Ocean. Sed. Geol., 335, 34-50.

Medri, E., Simms A.R., Kluesner, J., Johnson S.Y., Nishenko S.P, H. Gary Greene G., James E. Conrad, J.E. (2023). Subaqueous clinoforms created by sandy wave-supported gravity flows: Lessons from the Central California shelf. Mar.Geol., 456, 1-13.

Meireles, R. P., Quartau, R., Ramalho, R. S., Rebelo, A. C., Madeira, J., Zanon, V., Ávila, S. P. (2013). Depositional processes on oceanic island shelves - Evidence from storm-generated Neogene deposits from the mid-North Atlantic. Sediment., 60, 7, 1769–1785. doi.org/10.1111/sed.12055

Milankovitch, M., (1930). Mathematische Klimalehre und Astronomische Theorie der Klimaschwankungen. Handbuch der Klimatologie, Band I, Teil A. Gebruder Borntraeger, Berlin, 298.

Miranda, D. G., Camacho, R. F., Lousada, S., Castanho, R. A., (2018). Hydraulic studies and their influence for regional urban planning: a pratical approach to Funchal's rivers. Revista Brasileira de Planejamento e Desenvolvimento, Curitiba, 7, 1, 145-164. 10.3895/rbpd. v7n1.7179.

Mitchell, N. C. Zhao, Z., (2023). Effects of currents and waves on the morphologies of coastal sandy clinoforms: sediment mobility calculations based on current meter and wave data from Southern California, U.S.A. Jour. Sedim. Resear., 93, 7, 488-501.

Mitchell, N.C., Quartau, R., Madeira, J., (2012). Assessing tectonic movements in volcanic islands using near-shore marine geophysical data: South Pico Island, Azores. Bull. Volcanol., 74, 483‑496.

Mitchell, N.C., (2012). Modelling the rollovers of sandy clinoforms from the gravity effect on wave-agitated sand. J. Sediment. Res., 82, 464–468.

Mitchum, R. M. Jr., Vail, P.R., Sangree, J.B., (1977a, b). Seismic Stratigraphy and Global Changes of Sea Level, Part 6: Stratigraphic Interpretation of Seismic Reflection Patterns in Depositional Sequences. In: Seismic Stratigraphy — Applications to Hydrocarbon Exploration. Eds: Charles E. Payton. Am. Assoc. Petrol. Geol., 26, 53-62. doi.org/10.1306/M26490

Moura, A., Lousada, S., Castanho R. A. (2019). Canais Artificiais e a suaInfluênciaem Processos de Planeamento Urbano e Ordenamento Territorial. Revista Científica Monfragüe Desarrollo Resiliente – Scientific Journal., XII, 9, 183-199. ISSN 2340- 5457.

Nielsen, P. (1992) Coastal bottom boundary layers and sediment transport. In: Advanced Series on Ocean Engineering. 4. World Scientific, Singapore.

Normandeau, A., Bourgault, D., Neumeier, U., Lajeunesse, P., St-Onge, G., Gostiaux, L., Chavanne, C. (2020). Storm-induced turbidity currents on a sediment-starved shelf: Insight from direct monitoring and repeat seabed mapping of upslope migrating bedforms. Sediment., 67, 2, 1045–1068. doi.org/10.1111/sed.12673.

Normandeau, A., Lajeunesse, P., Poiré, A. G., Francus, P. (2016). Morphological expression of bedforms formed by supercritical sediment density flows on four fjord-lake deltas of the south-eastern Canadian Shield (Eastern Canada). Sediment., 63, 7, 2106–2129. doi.org/10.1111/sed.12298.

Omira, R., Baptista, M.A., Quartau, R., Ramalho, R.S., Kim, J., Ramalho, I., Rodrigues, A., (2022). How hazardous are tsunamis triggered by small-scale mass-wasting events on volcanic islands? New insights from Madeira – NE Atlantic. Earth Planet. Sci. Lett., 578, 117-333.

Parker, G., Izumi, N., (2000). Purely erosional cyclic and solitary steps created by flow over a cohesive bed. J. Fluid Mech., 419, 203‑238

Parker, G., (1996). Some speculations on the relation between channel morphology and channel-scale flow structures. In: Coherent Flow Structures in Open Channels. Eds P.J. Ashworths, S.J. Bennett, J.L. Best and S.J. McLelland. 423‑458. John Wiley Sons, New York.

Patruno, S. Helland-Hansenb, W. (2018). Clinoforms and clinoform systems: Review and dynamic classification scheme for shorelines, subaqueous deltas, shelf edges and continental margins. Eart.-Sci. Rev., 185, 202–233. doi: 10.1016/j.earscirev.2018.05.016.

Patruno, S., Hampson, G.J. Jackson, C.A.L. (2015). Quantitative characterisation of deltaic and subaqueous clinoforms. Eart.-Sci. Rev., 142, 79–119. doi: 10.1016/j.earscirev.2015.01.004.

Piper, D.J.W., Normark, W.R., (2009). Processes That Initiate Turbidity Currents and Their Influence on Turbidites: A Marine Geology Perspective. J. Sediment. Res., 79, 347-362.

Pope, E. L., Jutzeler, M., Cartigny, M. J. B., Shreeve, J., Talling, P. J., Wright, I. C., Wysoczanski, R. J. (2018). Origin of spectacular fields of submarine sediment waves around volcanic islands. Earth and Planet. Sci. Lett., 493, 12–24. doi.org/10.1016/j.epsl.2018.04.020.

Prada, S., Menezes de Sequeira, M., Figueira, C., da Silva, M.O., (2009). Fog precipitation and rainfall interception in the natural forests of Madeira Island (Portugal). Agricult. For. Meteor., 149, 1179-1187.

Prada, S.N., da Silva, M.O., Cruz, J.V., (2005). Groundwater behaviour in Madeira, volcanic island (Portugal). Hydrogeology Journal, 13, 5-6, 800–812. doi:10.1007/s10040-005-0448-3.

Prada, S.N., Fonseca, P., Rodrigues, C.; Madeira, J., Serralheiro, A., (2002) Relation between volcano-stratigraphic units and slope stability in Madeira Island: preliminary studies. Proceedings of the International Symposium of Rock Engineering for Mountainous Regions (EUROCK2002), Funchal, 25-28 Nov., 2002, 205-212.

Proença de Oliveira, R., Betâmio de Almeida, A., Sousa, J., Pereira, M. J., Portela, M. M., Coutinho, M. A., Ferreira, R., Lopes, S. (2011). A avaliação do risco de aluviões na ilha da Madeira. 1-20.

Puig, P., Ogston, A.S., Mullenbach, B.L., Nittrouer, C.A., Parsons, J.D., Sternberg, R.W., (2004). Storm-induced sediment gravity flows at the head of the Eel submarine canyon, northern California margin. J. Geophys. Res., 109. doi: 03010.01029/02003JC001918.

Puig, P., Palanques, A., Martín, J., (2014). Contemporary Sediment-Transport Processes in Submarine Canyons. Ann. Rev. Mar. Sci., 6, 53-77.

Quartau, R., Ramalho, R. S., Madeira, J., Santos, R., Rodrigues, A., Roque, C., Carrara, G., Brum da Silveira, A. (2018). Gravitational, erosional and depositional processes on volcanic ocean islands: Insights from the submarine morphology of Madeira Archipelago. Earth and Planet. Sci. Lett., 482, 288–299. doi.org/10.1016/j.epsl.2017.11.003

Quartau, R., Trenhaile, A.S., Ramalho, R.S., Mitchell, N. C. (2018). The role of subsidence in shelf widening around ocean island volcanoes: Insights from observed morphology and modeling. Earth and Planet. Sci. Lett., 498, 408–417. doi.org/10.1016/j.epsl.2018.07.007.

Quartau, R., Madeira, J., Mitchell, N.C., Tempera, F., Silva, P.F., Brandão, F., (2016). Reply to comment by Marques et al. on “The insular shelves of the Faial–Pico Ridge (Azores

archipelago): a morphological record of its evolution". Geochem. Geo-phys. Geosyst., 17, 633–641.

Quartau, R., Madeira, J., Mitchell, N.C., Tempera, F., Silva, P.F., Brandão, F. (2015). The insular shelves of the Faial-Pico Ridge (Azores archipelago): A morphological record of its evolution. Geochem., Geophys., Geosyst., 16, 5, 1401–1420. doi.org/10.1002/2015GC005733.

Quartau, R., Hipólito, A., Romagnoli, C., Casalbore, D., Madeira, J., Tempera, F., Roque, C., Chiocci, F.L., (2014). The morphology of insular shelves as a key for understanding the geological evolution of volcanic islands: Insights from Terceira Island (Azores). Geochem., Geophys., Geosyst., 15, 5, 1801–1826. doi.org/10.1002/2014GC005248.

Quartau, R., Tempera, F., Mitchell, N.C., Pinheiro, L.M., Duarte, H., Brito, P.O., Bates, C.R., Monteiro, J.H. (2012). Morphology of the Faial Island shelf (Azores): The interplay between volcanic, erosional, depositional, tectonic and mass-wasting processes. Geochem. Geophys. Geosyst., 13, 4. doi.org/10.1029/2011GC003987.

Quartau, R., Trenhaile, A.S., Mitchell, N.C., Tempera, F. (2010). Development of volcanic insular shelves: Insights from observations and modelling of Faial Island in the Azores Archipelago. Mar. Geol., 275, 1–4, 66–83. doi.org/10.1016/j.margeo.2010.04.008

Quintal, R., (1999). Aluviões da Madeira. Séculos XIX e XX. Territorium, 6, 31–48. doi.org/10.14195/1647-7723_6_4.

Ramalho, R.S., Brum da Silveira, A., Fonseca, P.E., Madeira, J., Cosca, M., Cachão, M., Fonseca, M.M., Prada, S.N., (2015). The emergence of volcanic oceanic islands on a slowmoving plate: The example of Madeira Island, NE Atlantic, Geochem. Geophys. Geosyst., 16, doi:10.1002/2014GC005657.

Ramalho, R.S., Quartau, R., Trenhaile, A.S., Mitchell, N.C., Woodroffe, C.D., Ávila, S. P., (2013). Coastal evolution on volcanic oceanic islands: A complex interplay between volcanism, erosion, sedimentation, sea-level change and biogenic production. Eart.-Sci. Rev., 127, 140–170. doi.org/10.1016/j.earscirev.2013.10.007.

Ramalho, R., Helffrich, G., Schmidt, D.N., Vance, D., (2010). Tracers of uplift and subsidence in the Cape Verde Archipelago. Journal of the Geological Society. Geolog. Soc. Lond., 167, 519-538.

Ramos, A.M., Trigo, R.M., Tomé, R., Liberato, M.L.R., (2018) Impacts of Atmospheric Rivers in Extreme Precipitation on the European Macaronesian Islands. Atmosph., 9, 325.

Ramos, A.M.; Tomé, R.; Trigo, R.M.; Liberato, M.L.R.; Pinto, J.G., (2016) Projected changes in atmospheric rivers affecting Europe in CMIP5 models. Geophys. Res. Lett, 43, 9315–9323

Ribeiro, O. (1985). A Ilha da Madeira até Meados do Século XX: Estudo Geográfico. (1°). Instituto de Cultura e Língua Portuguesa.

Ribeiro, M.L. Ramalho M., (2009). Uma visita geológica ao Arquipélago da Madeira. Principais locais geoturísticos. Laboratório Nac. Energia e Geologia e Dir. Reg. Comércio, Indústria e Energia da Madeira, 1-91.

Ricchi, A, Quartau, R., Ramalho, R., Romagnoli, C., Casalbore, D., Ventura da Cruz, J., Fradique, C., Vinhas, A., (2018). Marine terrace development on reefless volcanic islands: new insights from high-resolution geophysical data offshore Santa Maria Island (Azores Archipelago). Mar. Geol. 406, 42-56; doi.org/10.1016/j.margeo.2018.09.002

Robertson, J.M. Rouse, H., (1941) On the four regimes of open-channel flow. Civ. Eng. (N.Y.), 11, 169‑171.

Romagnoli, C., Casalbore, D., Ricchi, A., Lucchi, F., Quartau, R., Bosman, A., Tranne, C. A., Chiocci, F.L., (2018). Morpho-bathymetric and seismo-stratigraphic analysis of the insular shelf of Salina (Aeolian archipelago) to unveil its Late-Quaternary geological evolution. Mar. Geol., 395, 133–151.

Romagnoli, C., Jakobsson, S. P., (2015). Post-eruptive morphological evolution of island volcanoes: Surtsey as a modern case study. Geomorph., 250, 384–396. doi.org/10.1016/j.geomorph.2015.09.016.

Romagnoli, C. (2013). Characteristics and morphological evolution of the aeolian volcanoes from the study of submarine portions. Geol. Soc. Mem., 37(1), 13–26. doi.org/10.1144/M37.3

Rosa, A., Cardoso, C., Vieira, R., Faria, R., Oliveira, A.R., Navarro, G., Caldeira, R.M.A., (2022). Impact of Flash Flood Events on the Coastal Waters Around Madeira Island: The “Land Mass Effect”. Front. Mar. Sci., 8.

Rodrigues, A., Oliveira, A., Fonseca, R., Taborda, R., Cascalho, J., (2004). Sedimentary dynamics of the Southern Shelf of Madeira (Portugal). J. Coast. Res., 39.

Rusu, E., Guedes Soares, C. (2012). Wave energy pattern around the Madeira Islands. Ener., 45, 1, 771–785. doi.org/10.1016/j.energy.2012.07.013.

Rusu, L., (2022). The near future expected wave power in the coastal environment of the Iberian Peninsula. Ren. Ener., 195, 657-669.

Rusu, L., (2023). An evaluation of the synergy between the wave and wind energy along the west Iberian nearshore. Energy Conversion and Management: X, 20, 100453.

Santos, R., Quartau, R., Brum da Silveira, A., Ramalho, R., Rodrigues, A., (2019). Gravitational, erosional, sedimentary and volcanic processes on the submarine environment of Selvagens Islands (Madeira Archipelago, Portugal). Mar. Geol., 415, 105945.

Sequeiros, O., E. (2012). Estimating turbidity current conditions from channel morphology: a Froude number approach. Geophys. Res. Oc., 117, 1–19. doi.org/doi:10.1029/ 2011JC007201.

Silva, F.A., Meneses, C.A., (1978). Elucidário madeirense. Secretaria Regional de Educação e Cultura, Funchal, 4th edition.

Singh, V.P., (1997). Effect of spatial and temporal variability in rainfall and watershed characteristics on stream flow hydrograph. Hydrol. Process., 11, 1649-1669. doi.org/10.1002/(SICI)1099-1085(19971015)11:12<1649::AID-HYP495>3.0.CO;2-1.

Symons, W.O., Sumner, E.J., Talling, P.J., Cartigny, M.J.B., Clare, M.A., (2016). Large-scale sediment waves and scours on the modern seafloor and their implications for the prevalence of supercritical flows. Mar. Geol., 371, 130–148. doi:10.1016/j.margeo.2015.11.009.

Syvitski, J. P., Peckham, S. D., Hilberman, R., Mulder, T., (2003). Predicting the terrestrial flux of sediment to the global ocean: a planetary perspective. Sediment. Geol., 162, 1-2, 5–24. doi:10.1016/s0037-0738(03)00232-x.

Soulsby, R., (1997). Dynamics of Marine Sands: A Manual for Practical Applications. Thomas Telford, London.

Slootman, A., Cartigny, M. J. B. (2020). Cyclic steps: Review and aggradation-based classification. Eart. Sci. Rev., 201, 102-949. doi.org/10.1016/j.earscirev.2019.102949.

Slootman, A., De Boer, P. L., Cartigny, M. J. B., Samankassou, E., Moscariello, A. (2019). Evolution of a carbonate delta generated by gateway-funnelling of episodic currents. Sediment., 66, 1302–1340. doi:10.1111/sed.12585.

Spinewine, B., Sequeiros, O.E., Garcia, M.H., Beaubouef, R.T., Sun, T., Savoye, B. and Parker, G., (2009). Experiments on wedge-shaped deep-sea sedimentary deposits in minibasins and/or on channel levees emplaced by turbidity currents. Part II. Morphodynamic evolution of the wedge and of the associated bedforms. J. Sed. Res., 79, 608–628.

Sun, T., Parker, G., (2005). Transportational cyclic steps created by flow over an erodible bed. Part 2. Theory and numerical simulation. J. Hydraul. Res., 43, 502‑514.

Swenson, J.B., C. Paola, C., Pratson, L., Voller, V.R., Murray, A.B., (2005). Fluvial and marine controls on combined subaerial and subaqueous delta progradation: morphodynamic modeling of compound-clinoform development. J. Geophys. Res. Earth Surf., (F2),110.

Talling, P. J., Paull, C. K., Piper, D. J. W., (2013). How are subaqueous sediment density flows triggered, what is their internal structure and how does it evolve? Direct observations from monitoring of active flows. In Earth-Science Reviews, (125), 244–287. doi.org/10.1016/j.earscirev.2013.07.005

Teixeira, H.M.M., (2010). Caracterização Hidráulica, Hidrológica e de Transporte Sólido do Evento de 20 de Fevereiro de 2010 na Ribeira de São João – Ilha da Madeira. Civil Engineering Master degree thesis. University of Madeira, 175.

Trenhaile, A.S., (2000). Modeling the development of wave-cut shore platforms. Mar. Geol., 166, 1, 163–178.

Trenhaile, A.S., (2001). Modelling the Quaternary evolution of shore platforms and erosional continental shelves. Earth Surf. Process. Landf., 26, 10, 1103–1128.

Ulicny, D., Nichols, G., Waltham, D., (2002). Role of initial depth at basin margins in sequence architecture: field examples and computer models. Basin Research, 14(3), 347–360. doi:10.1046/j.1365-2117.2002.00183.x

Valente, E., (2020). Sedimentary dynamics on insular shelves of volcanic ocean islands: Insights from two marine cores of Faial shelf, Azores. MSc Thesis. Faculdade de Ciências da Universidade de Lisboa, 64.

Van Dijk, T.A.G.P., Best, J., Baas, A.C.W., (2020). Subaqueous and subaerial depositional bedforms, in: Alderton, D., Elias, S.A. (Eds.). Encyclopedia of Geology. Academic Press, Oxford, 771-786.

Verardo, J., Froelich, P., Mcintyre, A., (1990). Determination of organic carbon and nitrogen in marine sediments using the Carlo Erba NA-1500 analyzer. Env. Sci., 37, 1, 157-165. doi:10.1016/0198-0149(90)90034-S.

Walgreen, M., Calvete, D., de Swart, H.E., (2002). Growth of large-scale bed forms due to storm-driven and tidal currents: a model approach. Cont. She. Res., 22, 2777-2793.

Walsh, J.P., Nittrouer, C.A., Palinkas, C.M., Ogston, A.S., Sternberg, R.W., Brunskill, G.J., 2004. Clinoform mechanics in the Gulf of Papua, New Guinea. Cont. She. Res., 24, 2487-2510.

Wear, C. M., Stanley, D.J., Boula, J.E., (1974). Shelf break physiography between Wilmington and Norfolk canyons. Mar. Technol. Soc. J., 8, 4, 37-48.

West, L.M., Perillo, M.M., Olariu, C., Steel, R.J., (2019). Multi-event organization of deepwater sediments into bedforms: long-lived, large-scale antidunes preserved in deepwater slopes. Geol., 47, 5, 391‑394.

Wynn, R.B., Piper, D.J.W., Gee, M.J.R., (2002). Generation and migration of coarse-grained sediment waves in turbidity current channels and channel-lobe transition zones. Mar. Geol., 192, 59-78.

Wynn, R.B., Stow, D.A.V., (2002). Classification and characterisation of deep-water sediment waves. Mar. Geol., 192,1-3, 7-22. doi:10.1016/S0025-3227 (02)00547-9.

Wynn, R.B., Weaver, P.P.E., Ercilla, G., Stow, D.A.V., Masson, D.G., (2000b). Sedimentary processes in the Selvage sediment-wave field, NE Atlantic: new insights into the information of sediment waves by turbidity currents. Sedimentol., 47, 1181-1197.

Wynn, R.B., Masson, D.G., Stow, D.A.V., Weaver, P.P.E., (2000a). Turbidity current sediment waves on the submarine slopes of the western Canary Islands. Mar. Geol., 163, 185-198.

Yokokawa, M., Izumi, N., Naito, K., Parker, G., Yamada, T., Greve, R., (2016). Cyclic steps on ice. J. Geophys. Res. Earth, 121, 1023‑1048.

Zhang, J., Wonsuck, K., Olariu, C., Steel, R., (2019). Accommodation- versus supply-dominated systems for sediment partitioning to deep water. Geol., 47, 419–422. doi .org /10 .1130 /G45730.1ma

Zhao, Z., Mitchell, N.C., Quartau, R., Moreira, S., Rusu, L., Melo, C., Ávila, S.P., Das, D., Afonso, P., Pombo, J., Duarte, J., Rodrigues, A., (2022). Wave influenced deposition of carbonate-rich sediment on the insular shelf of Santa Maria Island, Azores. Sedimentol., 69, 1547-1572.

APPENDIX

10.1. SUPPLEMENTARY MATERIAL OF CHAPTER 5

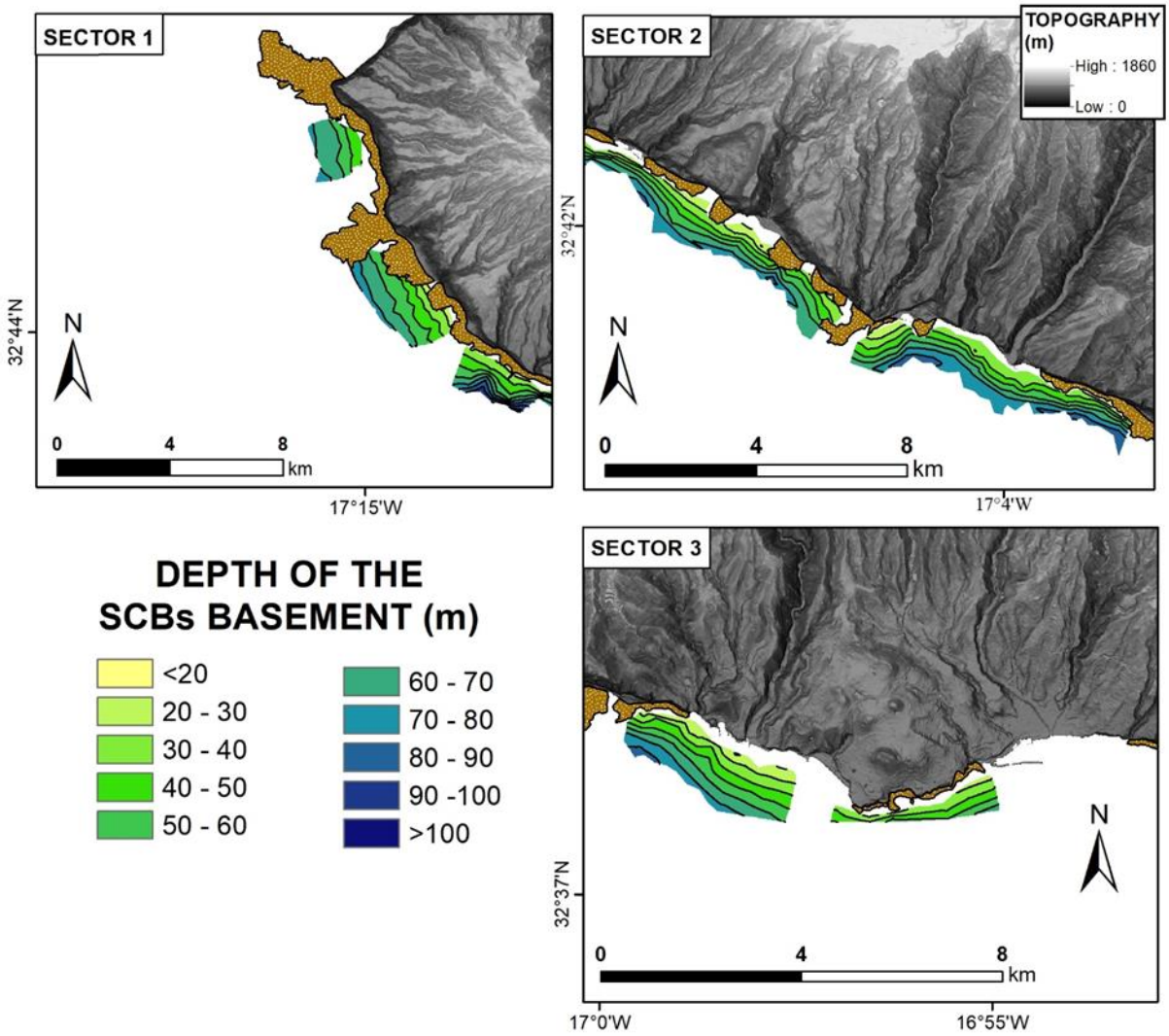

Supplementary Figure. 10.1. Depth distribution of the SCBs basal surface in sectors 1, 2 and 3. See squares in Fig. 5.3 in chap. 5 for the locations. Depth increases from yellow to blue colours. Brown polygons represent the nearshore rocky seafloor.

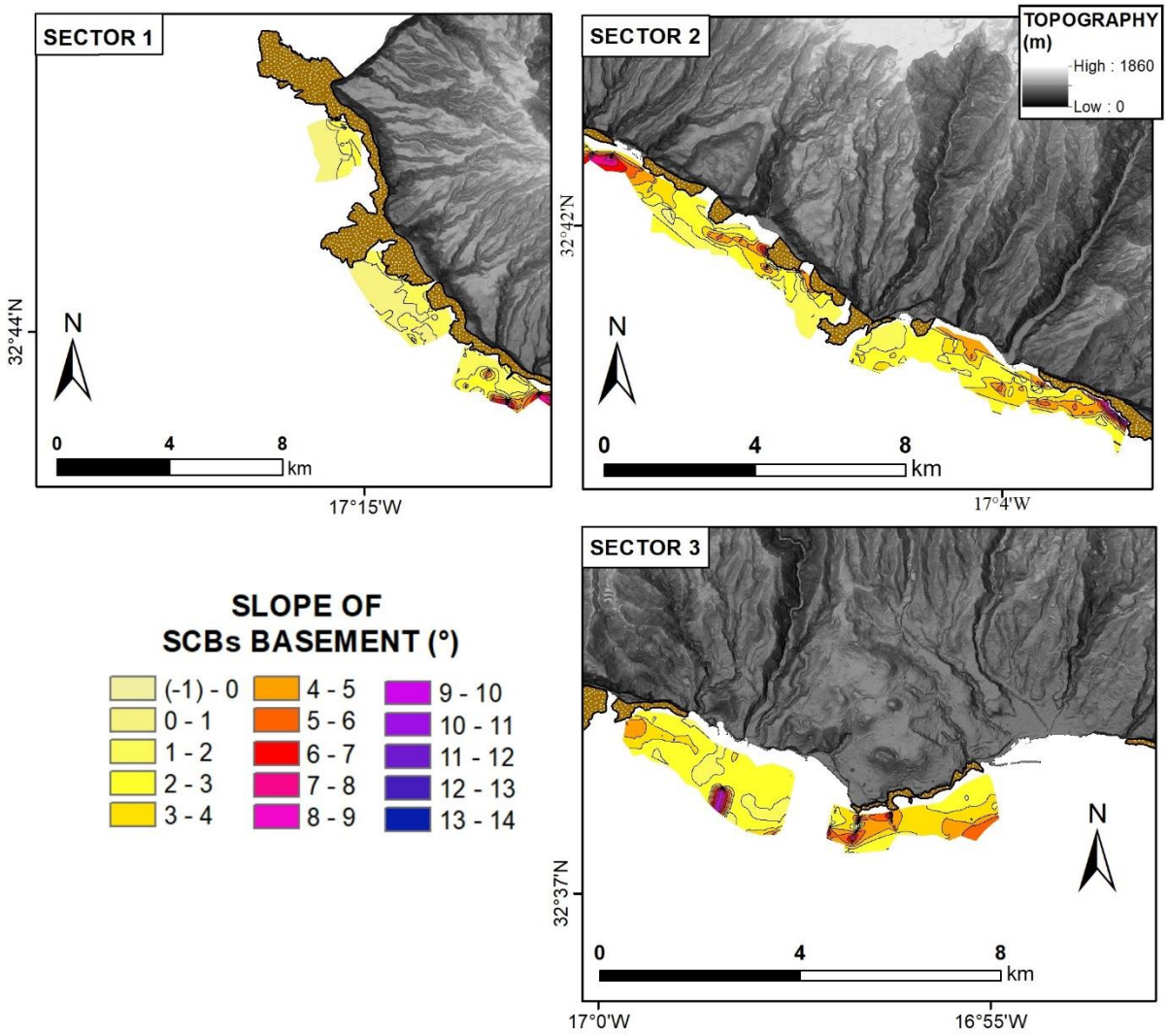

Supplementary Figure. 10.2. Slope distribution of the SCBs basal surface in sectors 1, 2 and 3. See squares in Fig. 5.3 in chap. 5 for the locations. Gradient increases from yellow to blue colours. Brown polygons represent the nearshore rocky seafloor.

10.2. SUPPLEMENTARY MATERIAL OF CHAPTER 6

Supplementary Table 10.1. Significant wave height and peak wave period derived from the Funchal Buoy for the period between January 1997 and December 2002 (from Instituto Hidrográfico).

H/T	3-4	4-5	5-6	6-7	7-8	8-9	9-10	10-11	11-12	12-13	13-14	14-15	15-16	16-17	17-18	18-19	%	Days
0-1	0.429	4.243	3.253	5.381	7.119	6.727	6.025	10.201	9.95	5.478	5.507	4.384	2.972	1.53	0	0.591	73.8	269
1-2	0	0.702	0.813	1.508	2.853	3.06	2.092	2.676	2.535	1.841	1.87	1.316	0.754	0.377	0	0.103	22.5	82
2-3	0	0	0.007	0.133	0.333	0.429	0.384	0.473	0.31	0.185	0.192	0.074	0.074	0.052	0	0.037	2.7	10
3-4	0	0	0	0	0.03	0.096	0.096	0.237	0.111	0.074	0.059	0.007	0.044	0.007	0	0.015	0.8	3
4-5	0	0	0	0	0	0	0.052	0.067	0.096	0.015	0	0	0.007	0.015	0	0	0.3	1
5-6	0	0	0	0	0	0	0	0	0	0	0	0	0	0	0	0	0	0
6-7	0	0	0	0	0	0	0	0	0	0	0	0	0	0	0	0	0	0
7-8	0	0	0	0	0	0	0	0	0	0	0	0	0	0	0	0	0	0
8-9	0	0	0	0	0	0	0	0	0	0	0	0	0	0	0	0	0	0
%	0.429	4.945	4.073	7.022	10.335	10.312	8.649	13.654	13.002	7.593	7.628	5.781	3.851	1.981	0	0.746	100	365

Supplementary Table 10.2. Extreme precipitation (90th and 95th percentiles) of the series 2000-2020 for three weather stations in Madeira Island.

	PONTA DO PARGO (32.81N/17.26W)	**LUGAR DE BAIXO (32.68N/17.09W)**	**FUNCHAL OBSERVATORY (32.64N/16.89W)**
% Precipitation data record	85	80	96
Value of extreme precipitation (mm - 95 percentile)	22.7	35.9	38.0
Days exceeding extreme precipitation (20 years)	49	35	40
Precipitation on 20th February 2010 (mm)	94.7	No data	144.3
Year	**Number of days with extreme precipitations (>95 percentile, October to March)**		
2000	0	0	1
2001	0	0	6
2002	0	1	2
2003	2	0	0
2004	1	0	1
2005	1	2	2
2006	2	3	3
2007	1	2	2
2008	4	2	0
2009	5	2	3
2010	11	8	6
2011	4	1	1
2012	4	4	2
2013	0	2	3
2014	3	1	1
2015	1	1	0
2016	3	4	3
2017	2	2	1
2018	3	0	2
2019	1	0	0
2020	1	0	1

BEDFORM FIELD 1

This bedform field encloses an area of about 1 km² (pink line in Fig. 6.2). It is composed of three main channels with headwalls at depths of about 20 m to 50 m that extend down to 152 m to 172 m. The channels have different shapes in plan-view and can incise the insular shelf by up to 40 m (see profile A-B on Supplementary Fig. 10.3). Onshore, the coast is dominated by three main stream outlets. The total area of these basins is about 25 km².

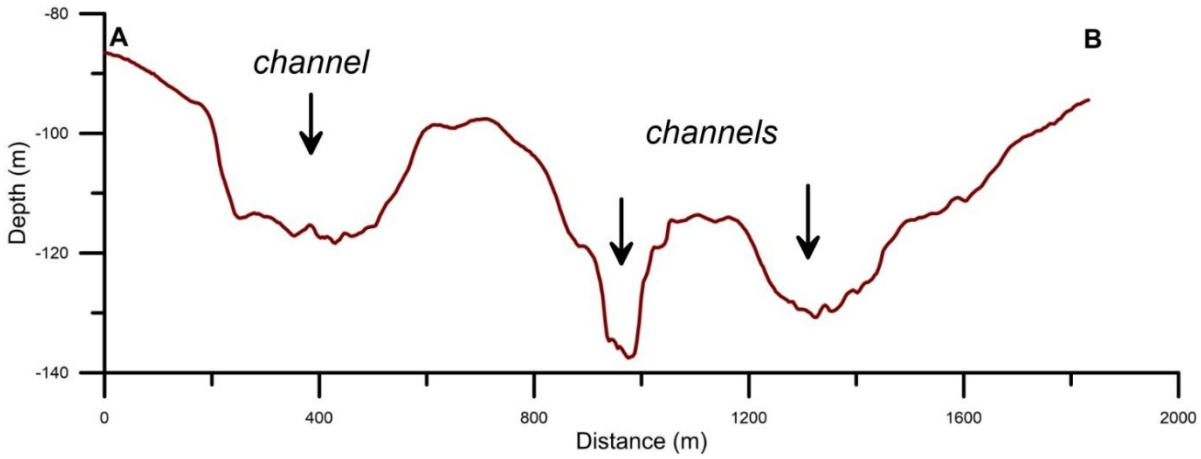

Supplementary Figure 10.3. Transversal cross-section A-B (location in Fig. 6.2) showing how deep the channels incise the shelf. Black arrows indicate the channels' thalweg.

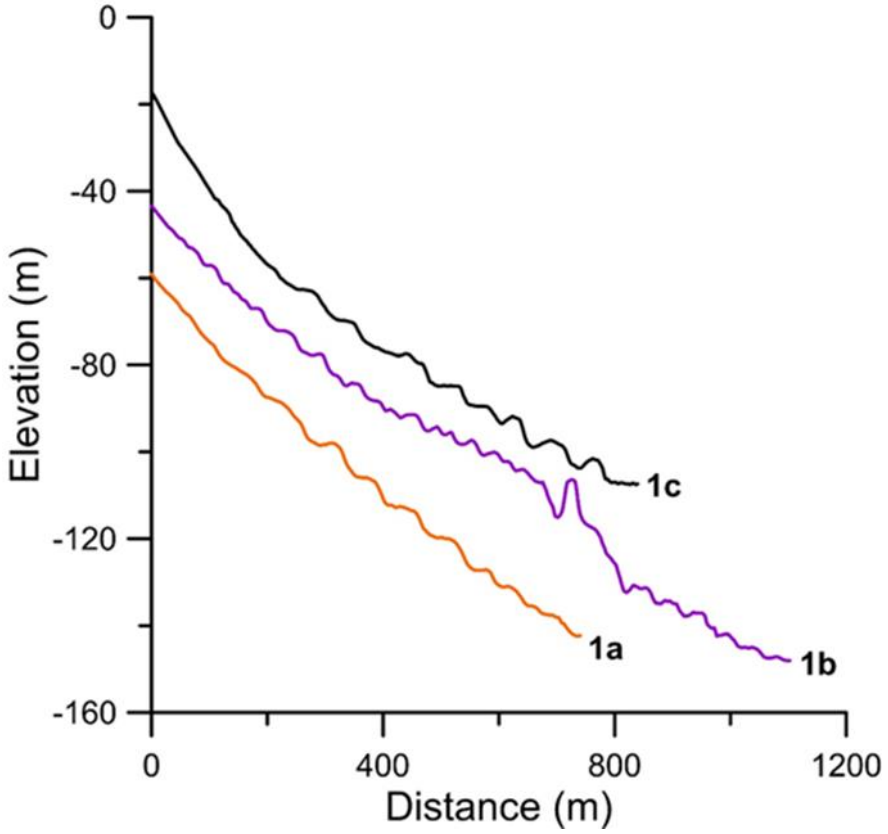

Supplementary Figure 10.4. Longitudinal bathymetric profiles of the bedforms (location on Fig. 6.2).

A summary of the morphometric data of the channels and bedforms is presented in Supplementary Table 10.3.

Supplementary Table 10.3. Morphometry of bedform field 1**.** "beg" = beginning; "mid" = middle; "end" = ending; "min" = minimum; "max" = maximum.

	Start depth (m)	**End depth (m)**	**Width (beg/mid/end) (m)**	**Length (m)**	**Plan-view pattern**	**Wave heights (min/max) (m)**	**Wavelengths (min/max) (m)**	**Wave crest depths (min/ max) (m)**	**Bedform shape in plan-view**	**General slope (min/max) (°)**	**Stoss-side length (min/max) (m)**	**Stoss-side slope (min/max) (°)**	**Lee-side length (min/ max) (m)**	**Lee-side slope (min/ max) (°)**
Channel 1a	34	157	587/409/189	1018	Dendritic upslope	1.94/6.73	48/81	83/138	Crescentic	5.87	26/50	-5.08/ -0.45	15.02/ 35.8	9.49/ 16.2
Channel 1b	20	170	595/328/70	1343	Dendritic upslope	1.38/6.20	23/51	57/145	Crescentic	4.94/3.77	9.4/33.5	-1.54/4.52	8.6/ 23	9.97/30
Channel 1c	21	165	120/185/135	1350	Linear	3.72/4.99	49/74	63/101	Crescentic	9/4.48	27/62	-2.35/8.02	26.8/ 12.4	10.5/ 28.7

In the area where the channels are incised, the shelf is narrower and the clinoform extension smaller (see Supplementary Fig. 10.5**Supplementary Figure 10.**). This is because the channels are often associated with a canyon system and its retrogressive erosion that extends to the headwalls of the channel. These alongshore variations are detailed on Supplementary Table**Supplementary Table** 10.4.

Supplementary Table 10.4. Dimensions and depths of the clinoform and shelf within and outside the bedform field**.**

	Distance to shore of clinoform rollover (m)	**Depth of clinoform rollover (m)**	**Shelf width (m)**	**Shelf break (m)**
Western area	1530	52	2720	-130
Bedform area	235	15	1570	-170
Eastern area	725	42	2490	-120

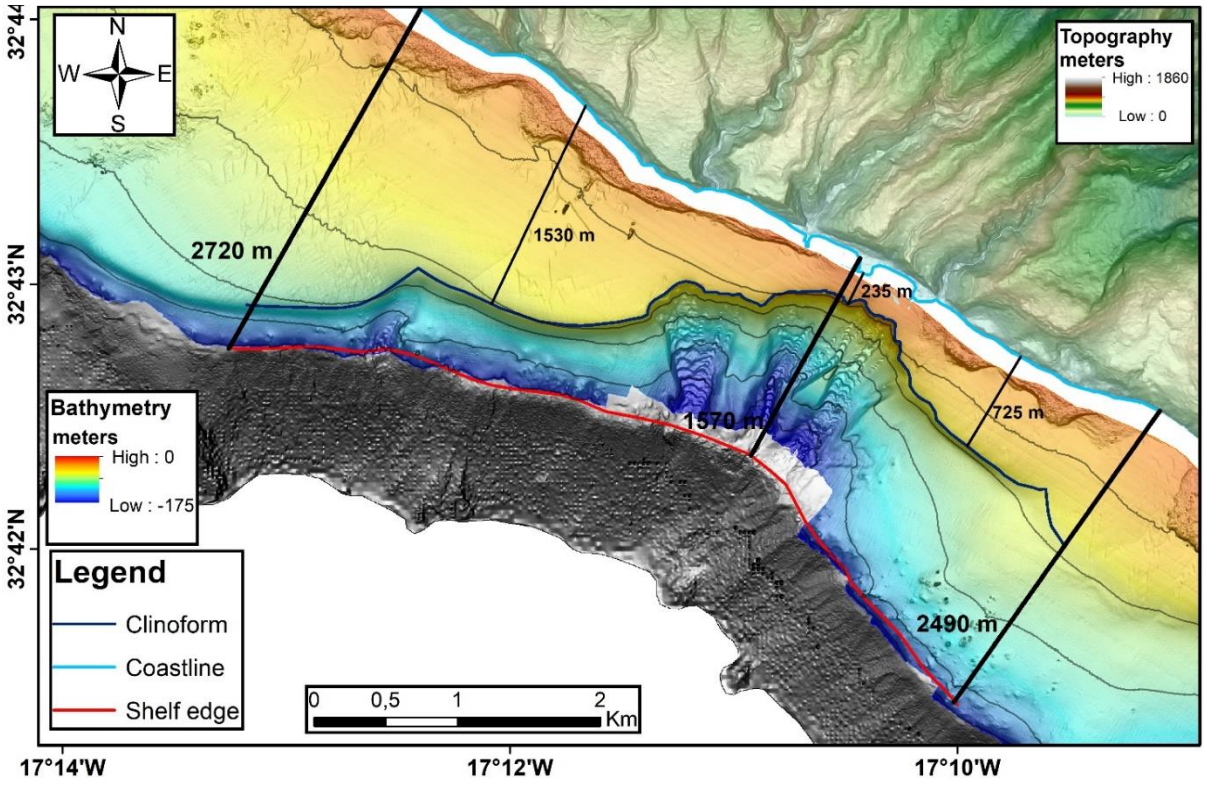

Supplementary Figure 10.5. Bathymetric map showing the retreat of both the clinoform bodies and the shelf break within the bedform field 1. Subaerial and submarine areas have the same legend as that of Fig. 6. Dark blue line represents the clinoform rollover and red line the shelf break. Black bold and thin straight lines and numbers next to them represent respectively the measured shelf width and clinoform rollover distance from the coastline.

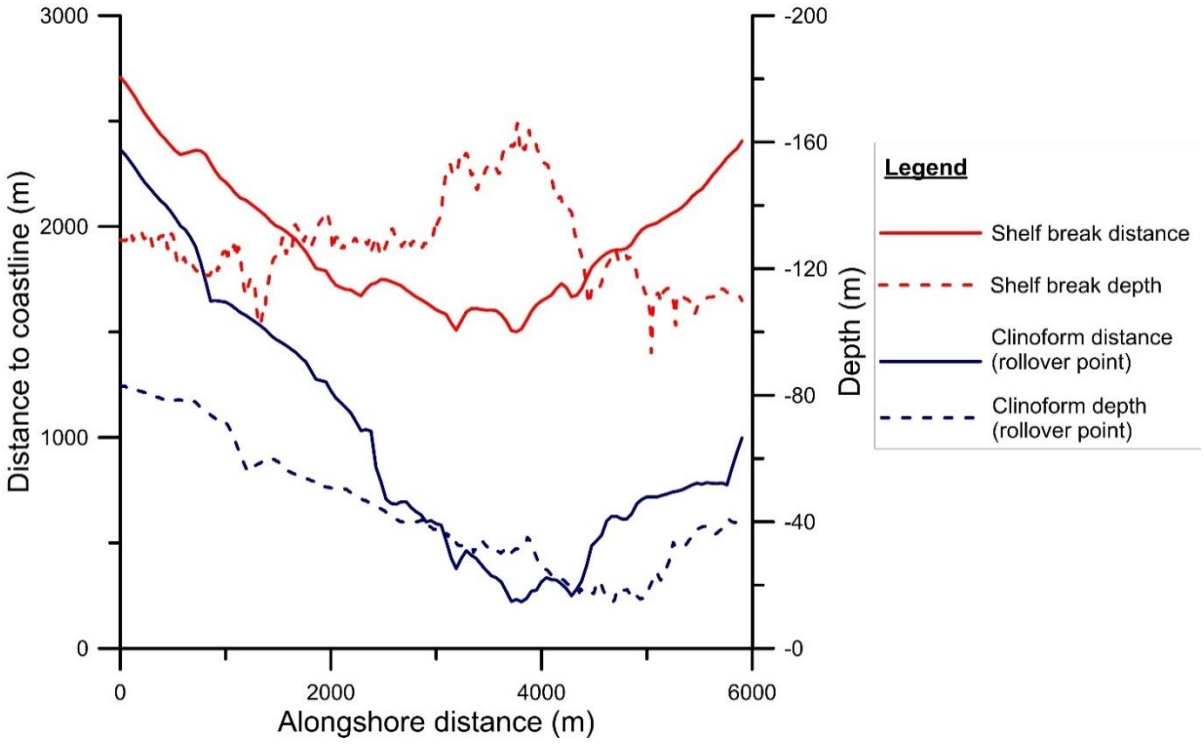

Supplementary Figure 10.6. Alongshore variations of the clinoform rollover and shelf break depths and their respective distances to the coast.

A multibeam bathymetric survey in 2013 allowed comparing the changes to the bedforms where they overlap (Supplementary Fig. 10.7).

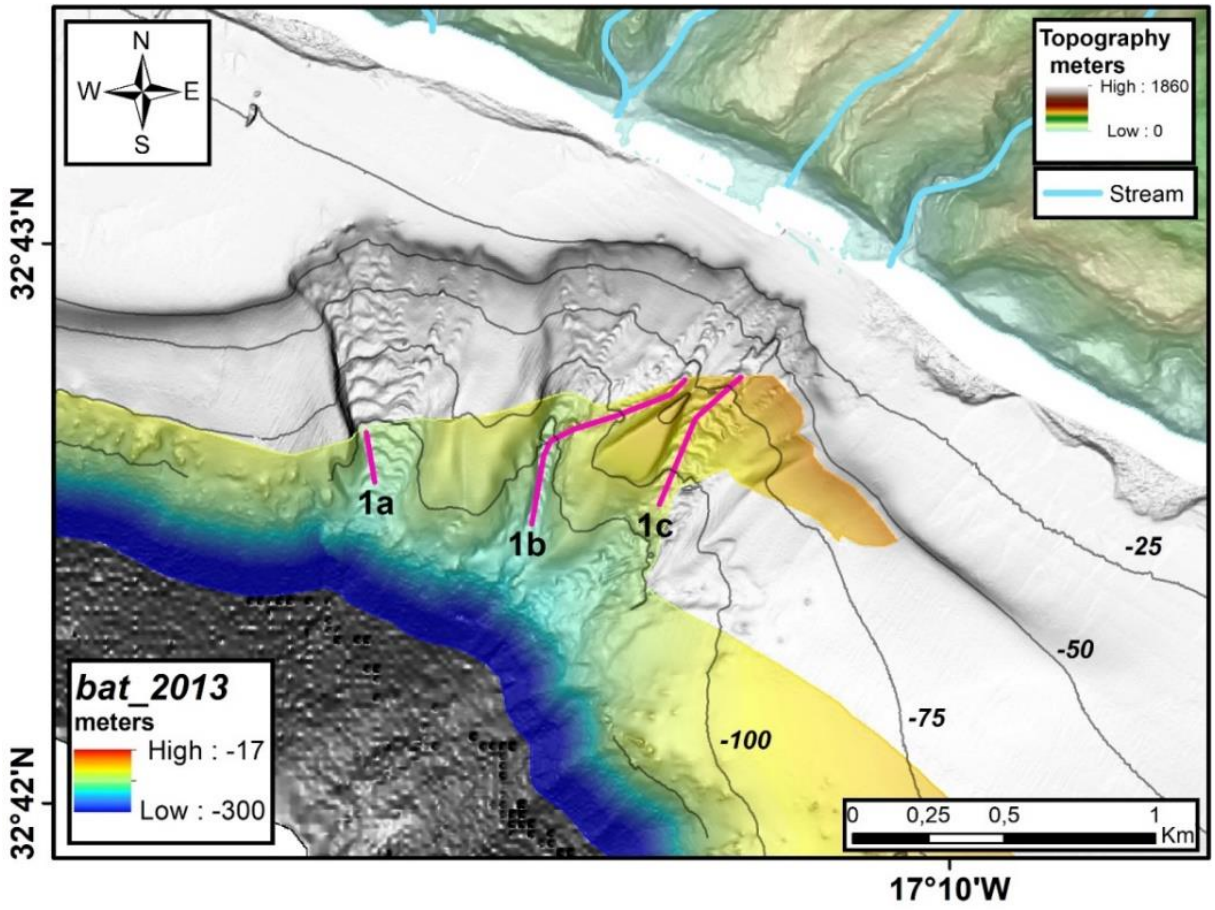

Supplementary Figure 10.7. 2013 bathymetry in color on top of the 2002 survey in hillshade grey. Pink lines represent the profiles of Fig. 6.2 where both bathymetries overlap.

A summary of the morphometric measurements of the channels and bedforms is presented in Supplementary Table 10.5.

Supplementary Table 10.5. Measurements of the main bedform parameters in 2013

	Wave height (min/max) (m)	**Wavelength (min/max) (m)**	**Wave Crest depth (min/max) (m)**	**Stoss-side length (min/max) (m)**	**Stoss-side slope (min/max) (°)**	**Lee-side length (min/max) (m)**	**Lee-side slope (min/max) (°)**
Profile 1a	1.14/4.40	31/72	83/138	26/50	-5.08/-0.45	15.02/35.8	9.49/16.2
Profile 1b	0.91/3.16	22/51	84/144	6.8/31.5	-0.31/4.33	10.5/19.7	6.79/10.5
Profile 1c	1.14/4.40	31/72	77/101	14.8/35.3	-0.15/3.85	13.6/31.7	6.53/16.4

The plot of the profiles from the 2002 and 2013 bathymetries shows a small upstream migration (not entirely evident along the entire profiles) with a prevailing deposition on the stoss-side and

erosion on the lee side. Only on the profile 1b and below -130 m there is deposition on both sides (Supplementary Fig. 10.8).

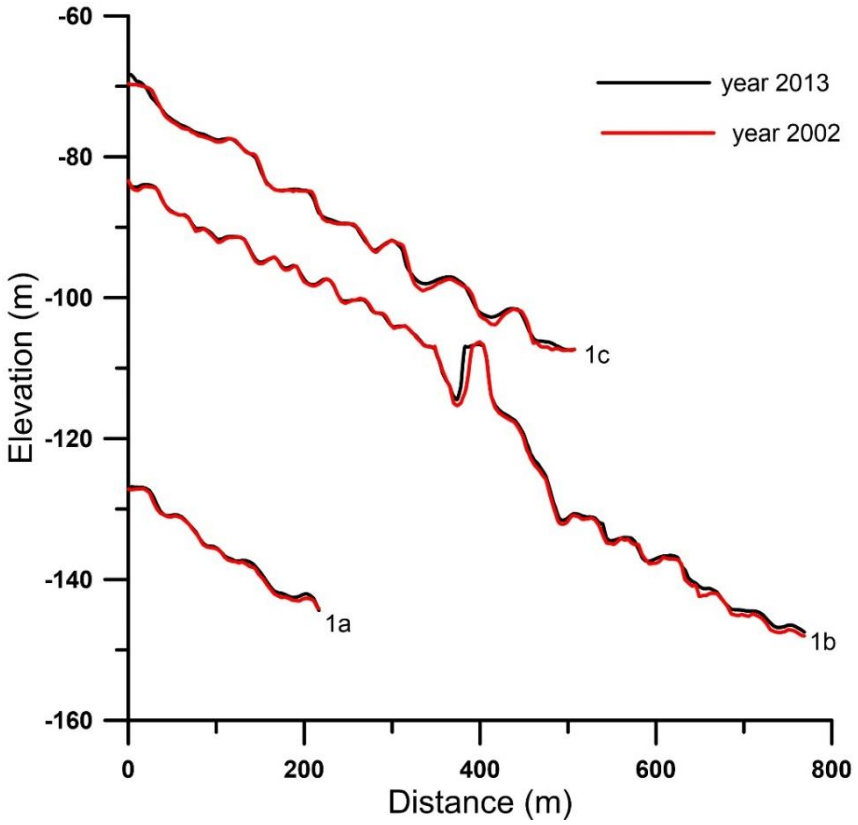

Supplementary Figure 10.8. Comparison of overlapping bathymetric profiles from the 2002 and 2013.

BEDFORM FIELD 2

Bedform field 2 is characterized by two channels (Supplementary Fig. 10.9), one with bedforms and the other without. The main channel is dendritic upwards and incises the shelf up to -10 m (Supplementary Fig. 10.10) and the bedforms occupy the entire channel area (~0.62 km²). The channels start at -26 m and end at -153 m; in plan-view the bedforms are crescentic upslope. Their morphological characteristics are presented in Supplementary Table 10.6 and the along-bedform profiles in Supplementary Fig. 10.11.

The shelf width (Supplementary Fig. 10.12) remains constant relatively to the area outside the channels, but the shelf break is deeper where the channels occur (Supplementary Fig. 10.13). The clinoform rollover is very incised where the channels lie but extends further offshore outside the channels. Onshore, there is one main stream outlet whose hydrographic basin covers an area of 12,75 km^2.

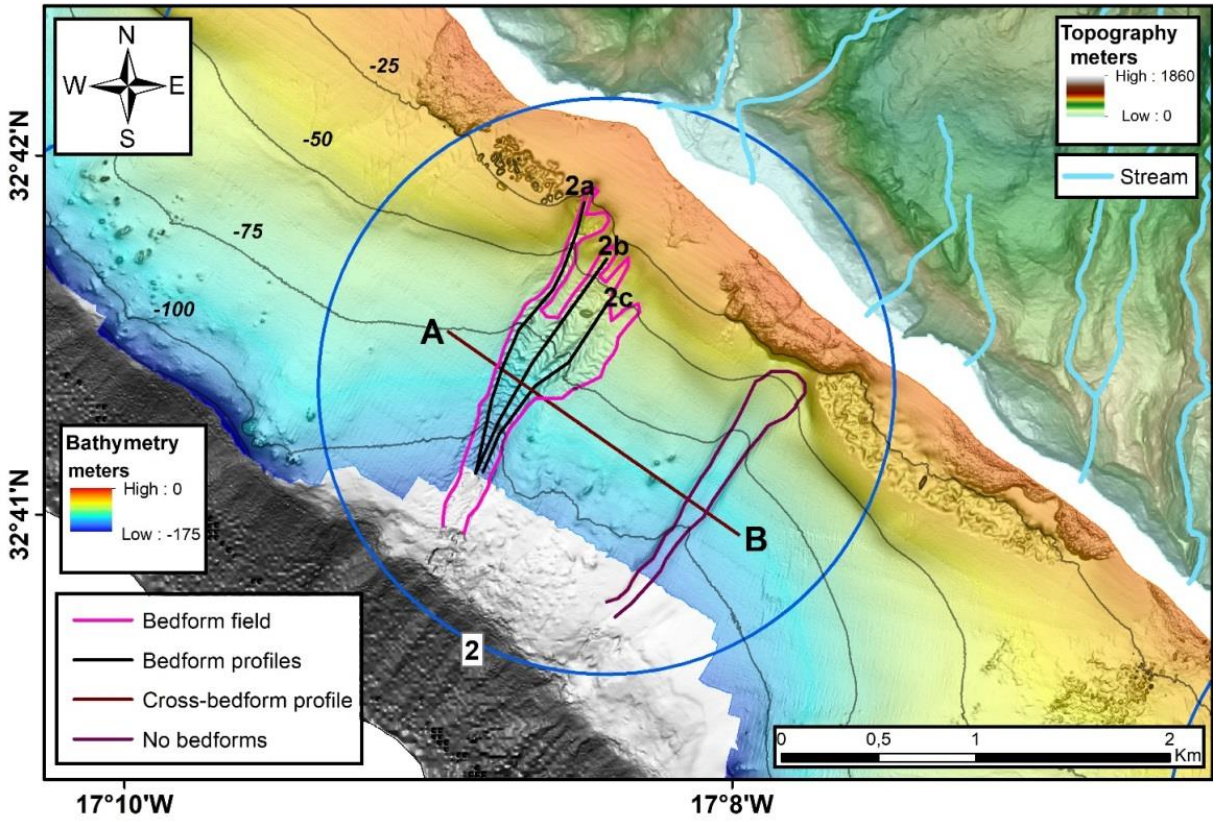

Supplementary Figure 10.9. Bedform field 2. Pink line delimits the channels with bedforms and purple line the one without bedforms. Brown line A-B is the cross-section profile along the bedforms (Supplementary Fig. 10.10). Black lines are the topographic profiles represented in Supplementary Fig 10.11; grey lines represent isobaths spaced every 25 m and.

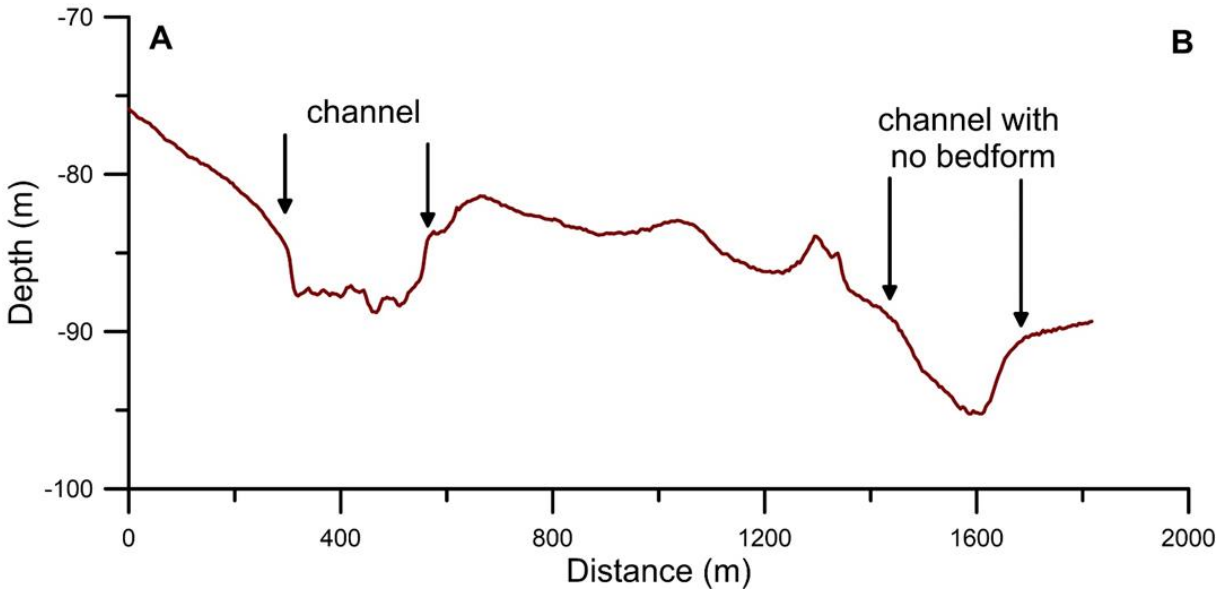

Supplementary Figure 10.10. Cross-section along the bedform field 2. Black arrows indicate the channels' lateral margins.

Supplementary Table 10.6. Morphometry of bedform field 2**.** "beg" = beginning; "mid" = middle; "end" = ending; "min" = minimum; "max" = maximum.

	Start depth (m)	End depth (m)	Width (beg/mid/ end) (m)	Length (m)	Plan-view shape	Wave height (min/max) (m)	Wavelength (min/max) (m)	Wave crest depth (min/max) (m)	Bedform shape in plan-view	General slope (°)	Stoss-side length (min/max) (m)	Stoss-side slope (min/max) (°)	Lee-side length (min/ max) (m)	Lee-side slope (min/ max) (°)
Channel with profiles 2a, 2b, 2c	26	153	478/474/167	1902	Dendritic upslope	0.6/3.39	23/67	47/108	Crescentic	2.40/ 3.60	8.06/50	-1.43/ 5.80	7.5/ 39.5	5.1/ 13.5
Channel without bedforms	41	153	243/117/91	1417	Linear	-	-	-	-	-	-	-	-	-

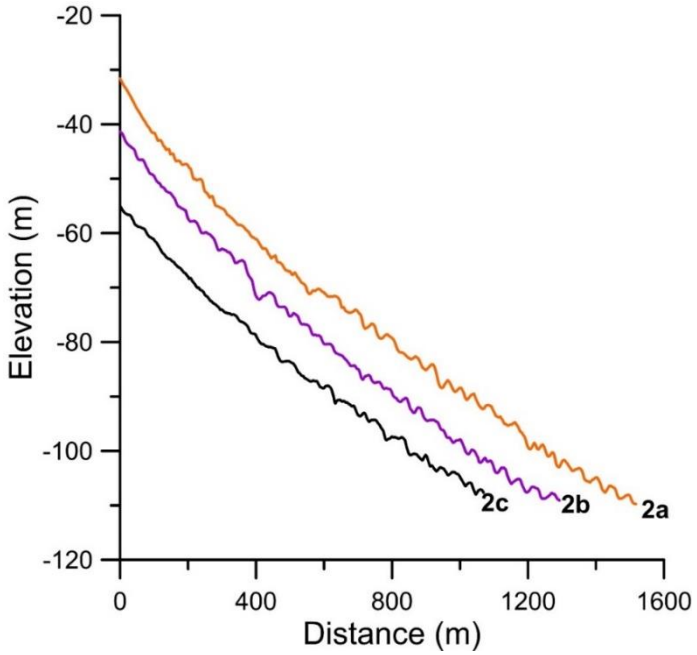

Supplementary Figure 10.11. Bathymetric profiles of the bedforms (location in Supplementary Fig. 10.9)

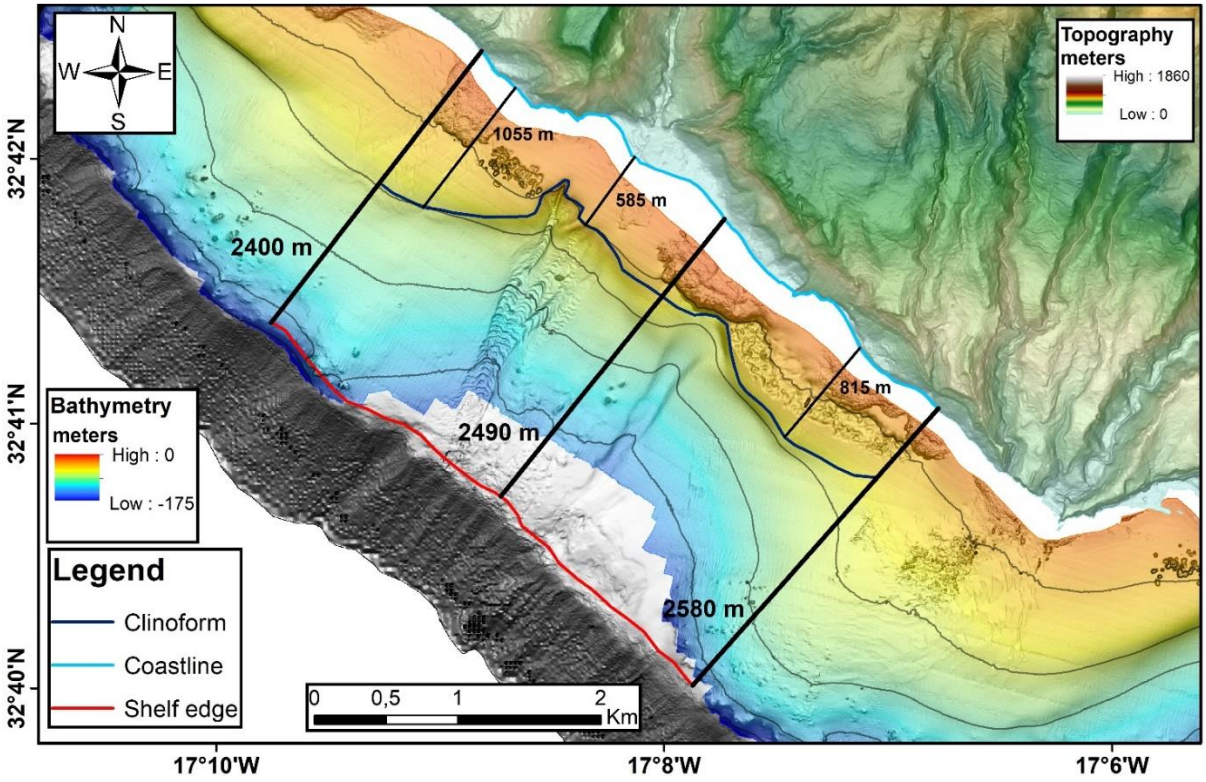

Supplementary Figure 10.12. A) Bathymetric map showing the retreat of the clinoform bodies within the bedform field 2. Subaerial and submarine areas have the same legend as that of Fig. 6.2. Blue line represents the clinoform rollover and red line the shelf break. Black bold and thin straight lines and numbers next to them represent respectively the measured shelf width and clinoform extension.

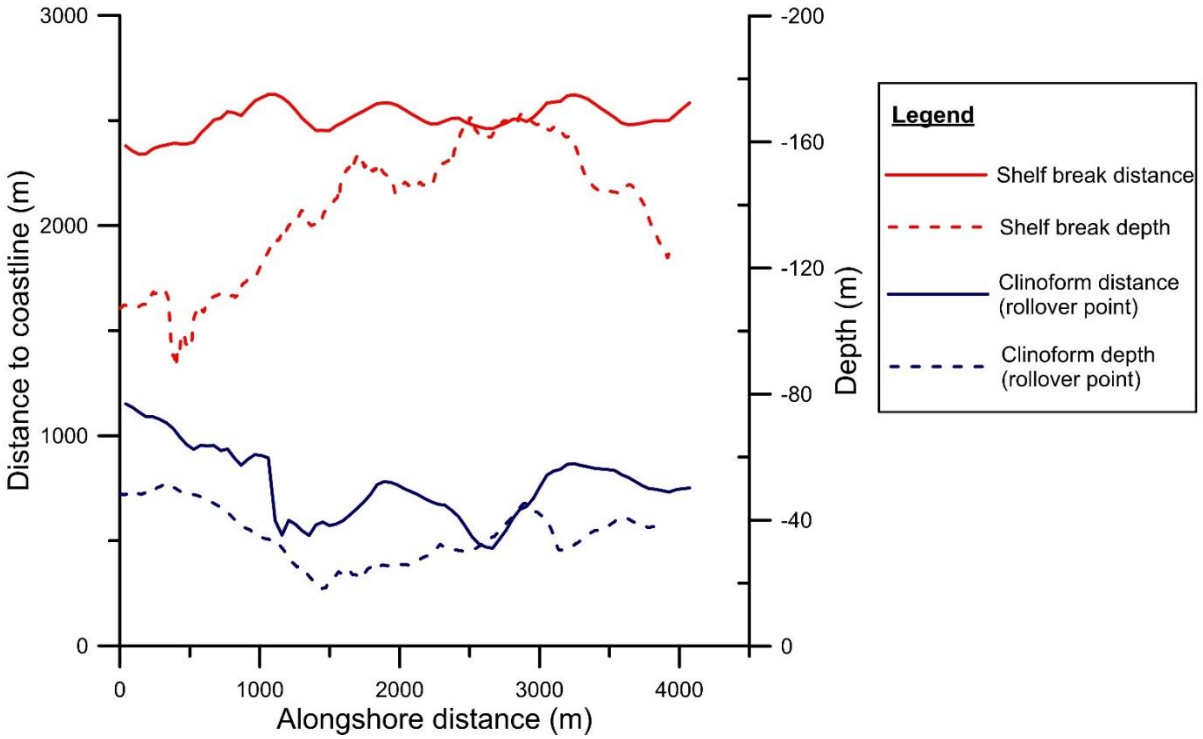

Supplementary Figure 10.13. Alongshore variations of the clinoform rollover and shelf break depths and their respective distances to the coast. A detail of these variations can be found in Supplementary Table 10.7.

Supplementary Table 10.7. Distance from the coastline and depths of the clinoforms rollover and shelf within and outside the bedform field.

	Distance to shore of clinoform rollover (m)	Depth of rollover (m)	Shelf width (m)	Shelf break (m)
Western area	1055	39	2400	-116
Bedform area	585	31	2490	-160
Eastern area	815	37	2580	-120

This area was surveyed in 2013 and 2019. The 2013 bathymetry only covers the deeper part of the bedform field (Supplementary Fig. 10.14). The overlapping profiles show that there was a general predominant deposition on the lee sides (Supplementary Fig. 10.15).

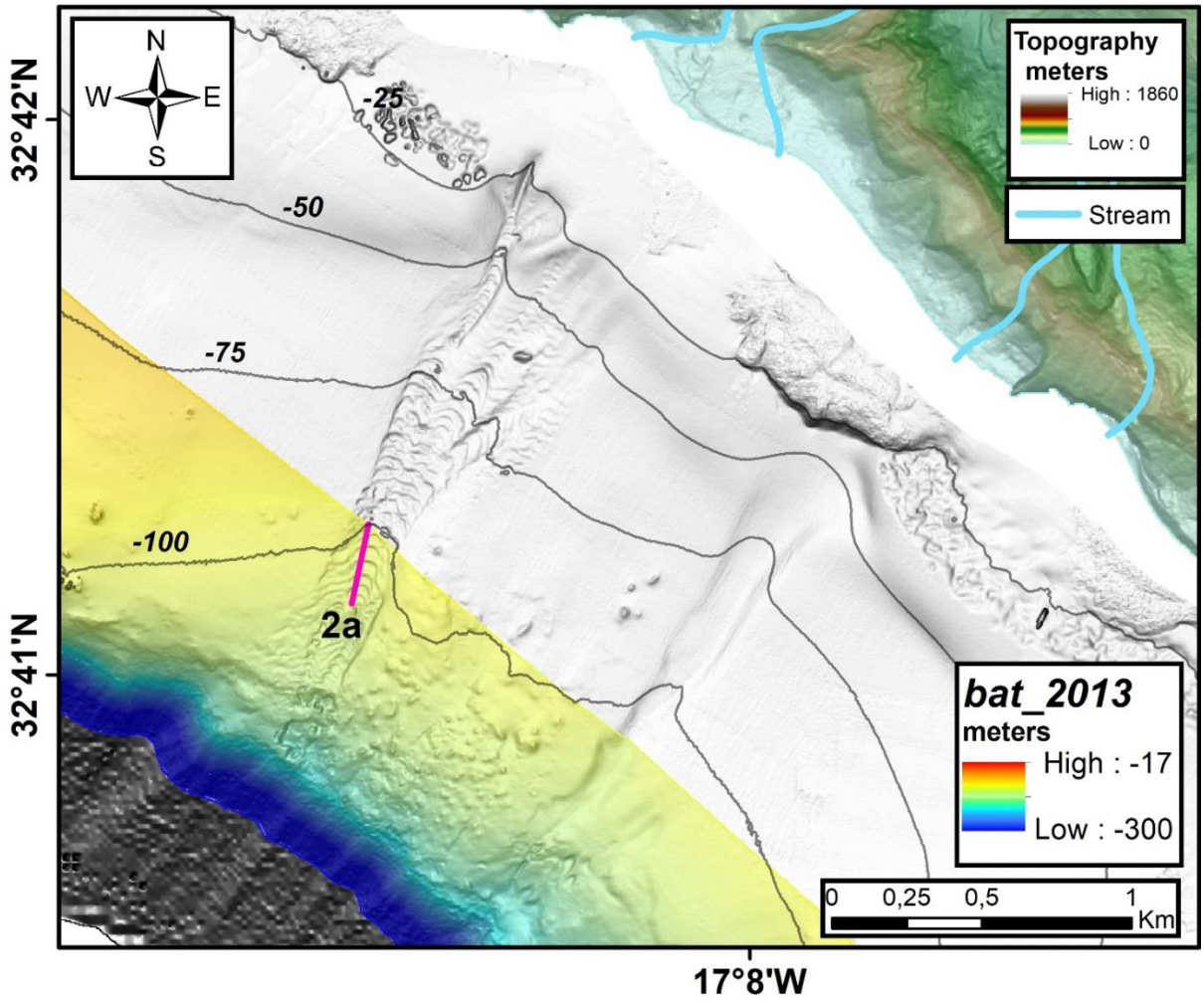

Supplementary Figure 10.14. 2013 bathymetry in color on top of the 2002 survey in hillshade grey. Pink line represents the profiles of Fig. 10.15 where both bathymetries overlap.

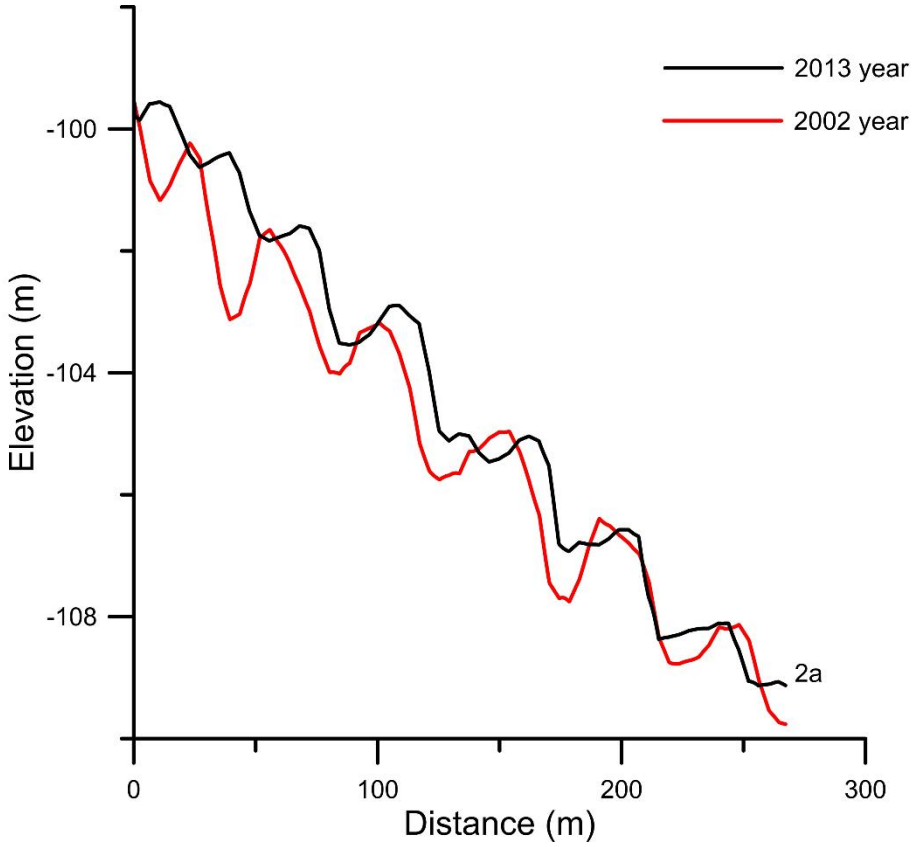

Supplementary Figure 10.15. Comparison of overlapping bathymetric profiles from the 2002 and 2013 surveys.

The profile was characterized from a morphometric point-view and a synthetic description is reported in Supplementary

Supplementary Table Table 10.8.

Supplementary Table 10.8. Measurements of the main bedform parameters in 2013.

	Wave height (min/max) (m)	**Wavelength (min/max) (m)**	**Wave Crest depth (min/max) (m)**	**Stoss-side length (min/max) (m)**	**Stoss-side slope (min/max) (°)**	**Lee-side length (min/max) (m)**	**Lee-side slope (min/max) (°)**
Profile 2a	1.77/3.04	22/45	99/106	8.2/28.7	0.58/3.65	11.5/18.2	5.81/14.73

The 2019 bathymetry shows that no significant change has occurred in the morphology of the area (Supplementary Fig. 10.16) over the last 17 years. The overlapping profiles show a general migration upstream (Supplementary Fig. 17) and the bedforms characteristics are presented in Supplementary Table 10.9.

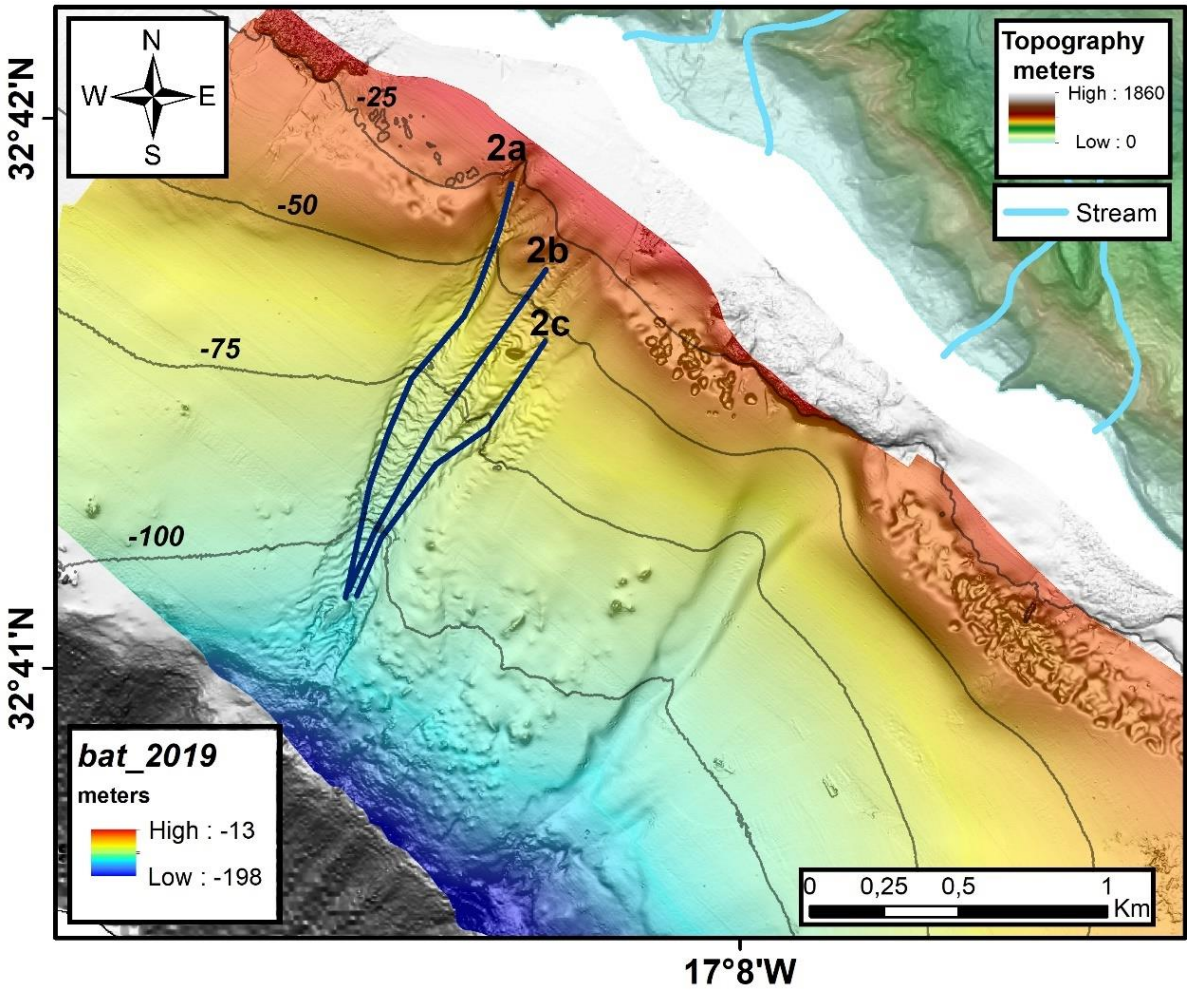

Supplementary Figure 10.16. Map of 2019 bathymetry in color on top of the 2002 survey in hillshade grey. Blue lines represent the profiles of Supplementary Figure 10.17 where both bathymetries overlap.

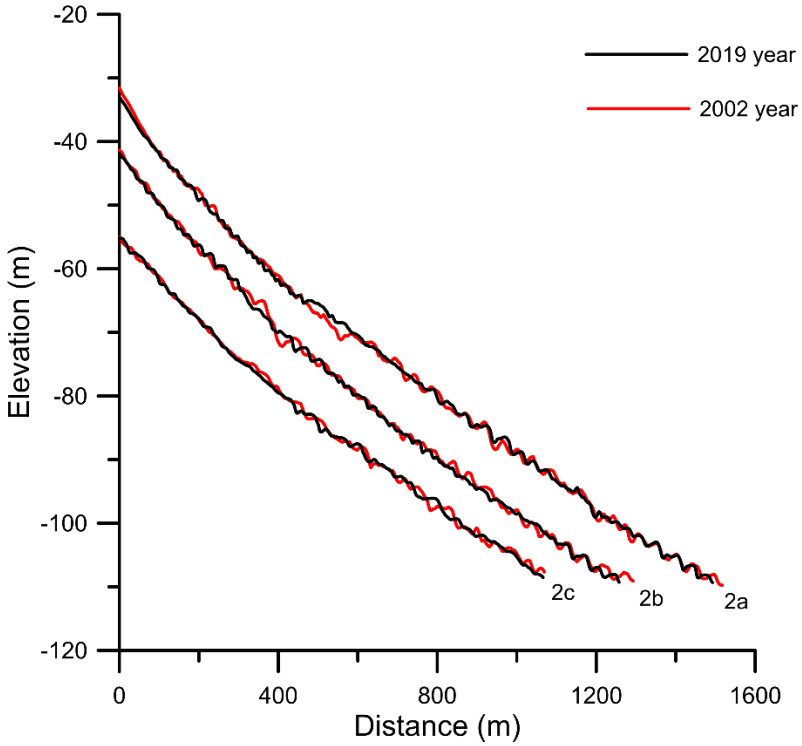

Supplementary Figure 10.17. Comparison of overlapping bathymetric profiles from the 2002 and 2019 surveys.

Supplementary Table 10.9. Measurements of the main bedform parameters in 2019.

	Wave height (min/max) (m)	**Wavelength (min/max) (m)**	**Wave Crest depth (min/max) (m)**	**Stoss-side length (min/max) (m)**	**Stoss-side slope (min/max) (°)**	**Lee-side length (min/max) (m)**	**Lee-side slope (min/max) (°)**
Profile 2a	1.50/3.09	26/44	46/106	9.3/30.3	-0.38/1.11	10.5/17.5	7.3/10.7
Profile 2b	2.09/2.70	24/47	46/104	9.9/26.6	-0.27/2.08	9.8/16.7	14.3/8.3
Profile 2c	0.96	29/77	57/104	15.8/40	-0.50/0.60	18.3/34.2	5.3/8.8

BEDFORM FIELDS 3, 4 AND 5

These fields comprise the largest bedform fields of the southern shelf of Madeira (Fig. 6.1).

Bedform field 3 has a total area of 0.60 km² (pink lines). It is composed of two channel branches that start at -29 m to -42 m and converge downslope near the shelf edge at -209 m. Onshore, there are three stream outlets belonging to hydrographic basins with a total area of 12.85 km^2.

Bedform field 4 is formed by an area elevated above the surrounding seafloor with a fan shape in the westernmost part and a channel to the east (Fig. 6.4). Both features show bedforms which cover an area of about 2 km^2. Onshore, one main stream discharges and the total hydrographic basin size is 45.55 km^2. The morphological properties of the bedforms fields 3 and 4 are expressed in Supplementary Table 10.10 and the profiles in Supplementary Fig. 10.18.

Supplementary Table 10.10. Morphometry of bedform fields 3 and 4. “beg” = beginning; “mid” = middle; “end” = ending; “min” = minimum; “max” = maximum.

	Start depth (m)	End depth (m)	Width (beg/mid/end) (m)	Length (m)	Plan-view pattern	Wave height (min/max) (m)	Wavelength (min/max) (m)	Wave crest depth (min/max) (m)	Bedform shape in plan-view	General slope (°)	Stoss-side length (min/max) (m)	Stoss-side slope (min/max) (°)	Lee-side length (min/max) (m)	Lee-side slope (min/max) (°)
profile 3 channel	42/ 33	209	1069/703/210	1878	Bifurcate upslope	0.43/3.38	39/73	83/95	Crescentic	2.86	15/30	-0.85/ 0.43	20/45	3.22/ 7.13
Profile 4a channel	29	166	140/118/85	1611	Dendritic downslope	1.37/4.3	25/67	66/90	Crescentic	2.70	7.01/40	-0.5/4.1	10.5/ 39.1	5.07/ 12.6
profile 4b channel	27	149	71/108/84	1577	Linear	1 / 2.6	25/45	72/82	11.3/19.8	1.19/ 3.05	11.3/19.8	1.19/3.05	11.7/ 28.4	4.76/ 11.9
Fan-shaped feature (profile 4c)	33	131	391/646/1012	1493	-	1.3/2.67	34/71	71/93	13.9/34.4	-0.74/ 0.98	13.9/34.4	-0.74/0.98	16.3/ 41.6	4.31/ 7.68

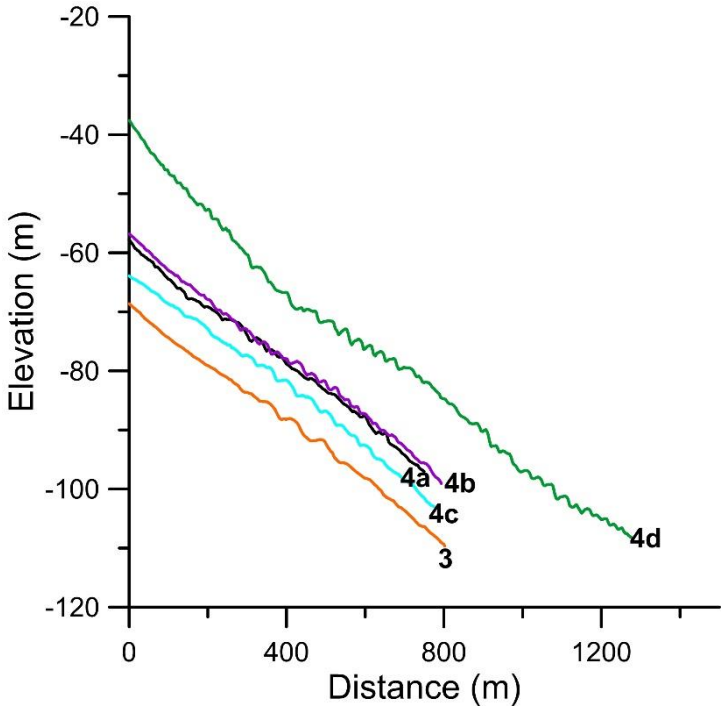

Supplementary Figure 10.18. Profiles within channelized structures in area 3 and 4 (location on Fig. 6.4 in chap. 6).

In Supplementary Fig. 10.19, it is visible that some channels are not much incised (max 10 m), but near the shelf edge the most western one shows an incision of up to 50-60 m (Supplementary Fig. 10.20).

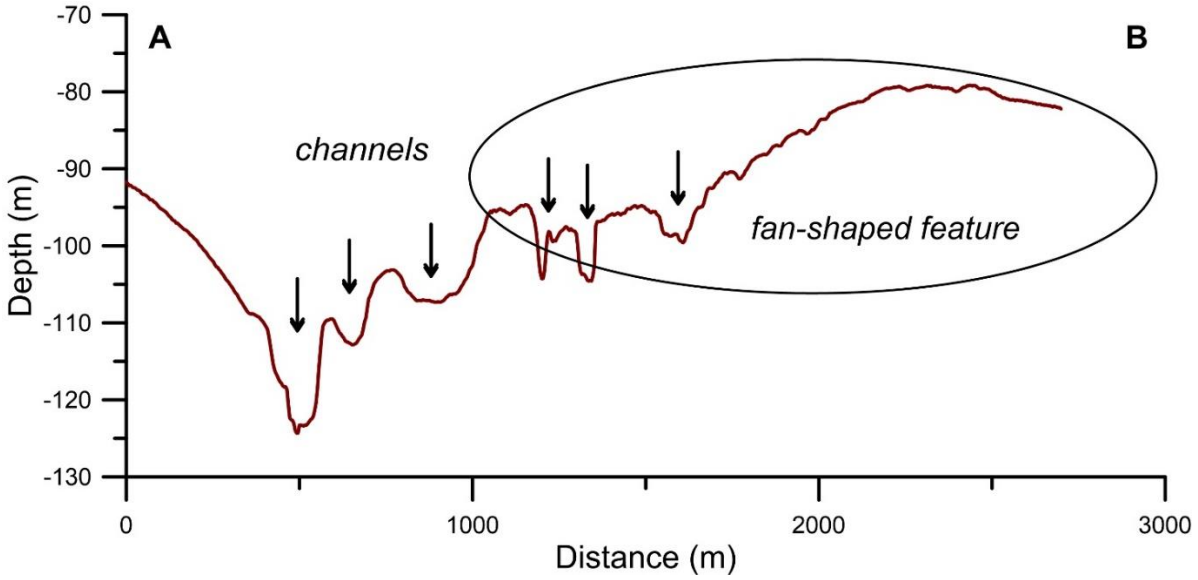

Supplementary Figure 10.19. Cross-section of bedform fields 3 and 4. Location of profiles in Fig. 6.4 in chap.6. Black arrows indicate the channels' thalweg.

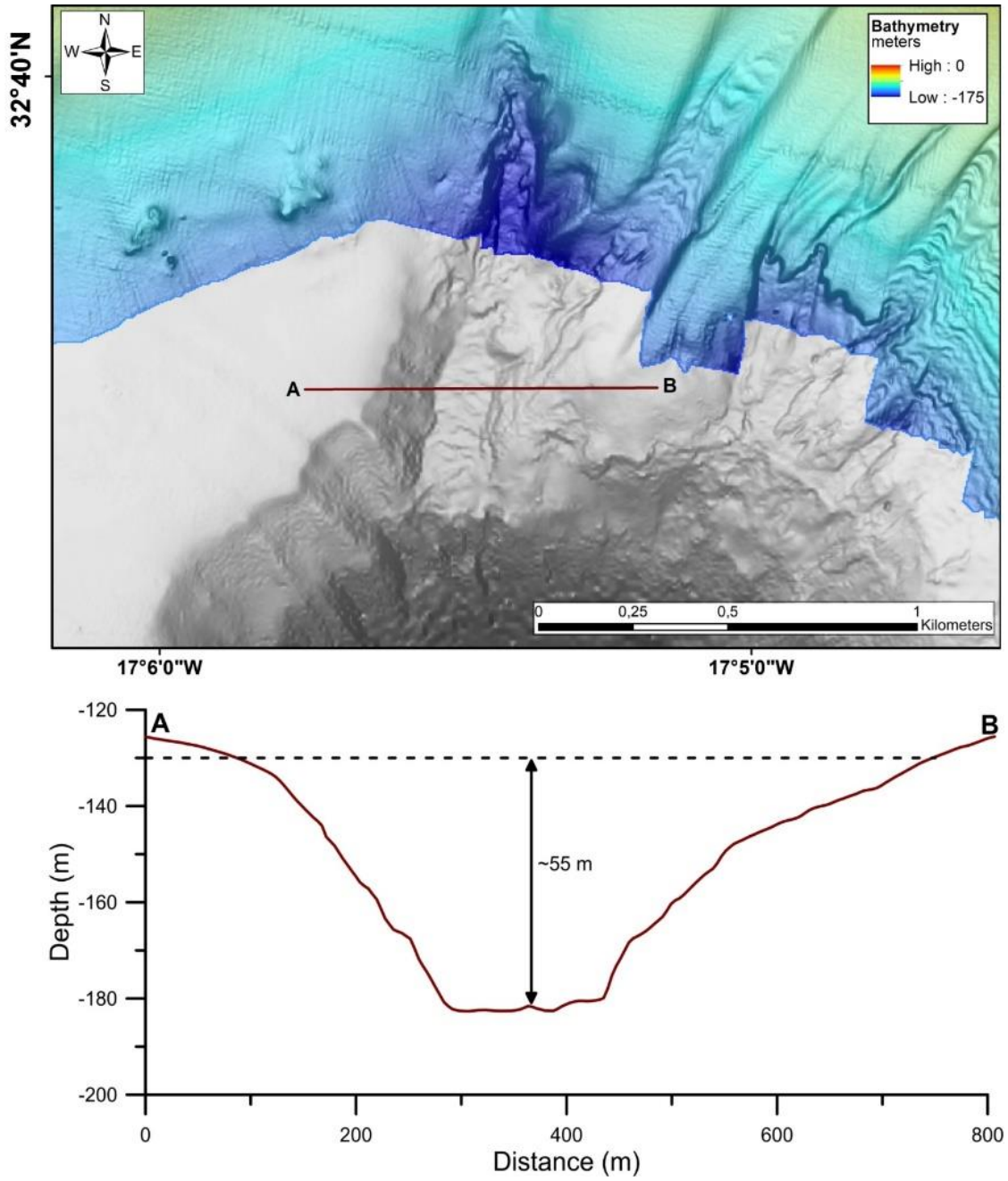

Supplementary Figure 10.20. Cross-section of the western channel in area 3.

The 5th bedform field covers ~1.99 km² (pink lines in Fig. 6.4 in chap.4) and has a fan shape that widens downslope. The headwall of this feature is also characterized by scars on the clinoform rollover. The characteristics of the bedforms are presented in Supplementary Table 10.11 and in the profiles in Supplementary Fig. 10.21. The area of the hydrographic basin that delivers sediments to this field is 7.73 km^2.

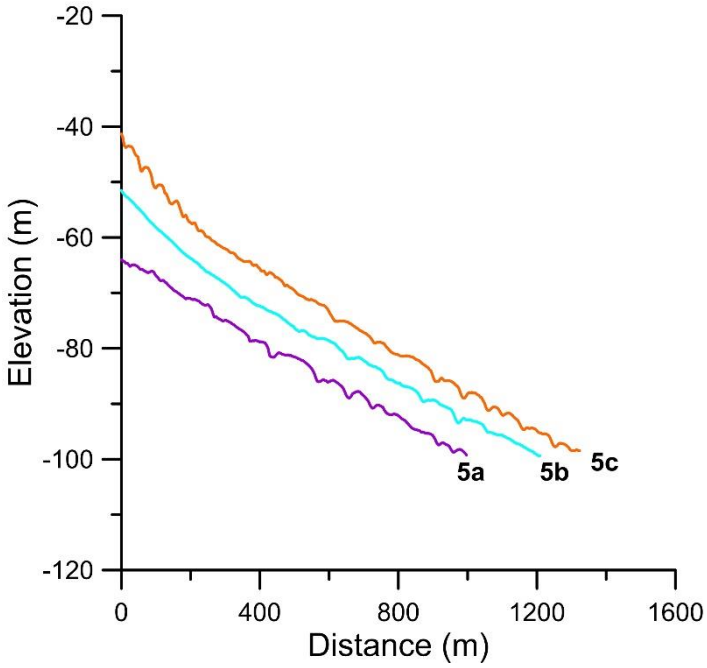

Supplementary Figure 10.21. Bathymetric profiles of bedforms in areas 4 and 5. Location of profiles in Fig. 6.4. in chap. 6.

Supplementary Table 10.11. Characteristics of channelized areas of fields 4 and 5. “beg” = beginning; “mid” = middle; “end” = ending; “min” = minimum; “max” = maximum.

	Start depth (m)	End depth (m)	Width (beg/mid/end) (m)	Length (m)	Plan-view pattern	Wave height (min/max) (m)	Wavelength (min/max) (m)	Wave crest depth (min/max) (m)	Plan view of bedform	General slope	Stoss-side length (min/max) (m)	Stoss-side slope (min/max) (°)	Lee-side length (min/max) (m)	Lee-side slope (min/max) (°)
Channel 4d	29	127	54/365/462	1753	Dendritic downslope	1.13/4.24	17/46	52/103	Crescentic	3	9.96/32.8	-0.18/ 3.70	8.97/ 23.9	7.18/ 13.9
Fan-shaped feature with profiles 5a-5b-5c	27	148	26/956/482	3012	Funnel downslope	1.32/4.49	35/109	43/97	Sinuous	3.90/2.06	15.4/94	-0.33/ 6.15	15.4/ 28.9	4.04/ 17.1

There are two main channels where profile 4d is located (incision not deeper than 5-6 m) separated by a wide depressed area towards the East without bedforms (Supplementary Fig. 10.22).

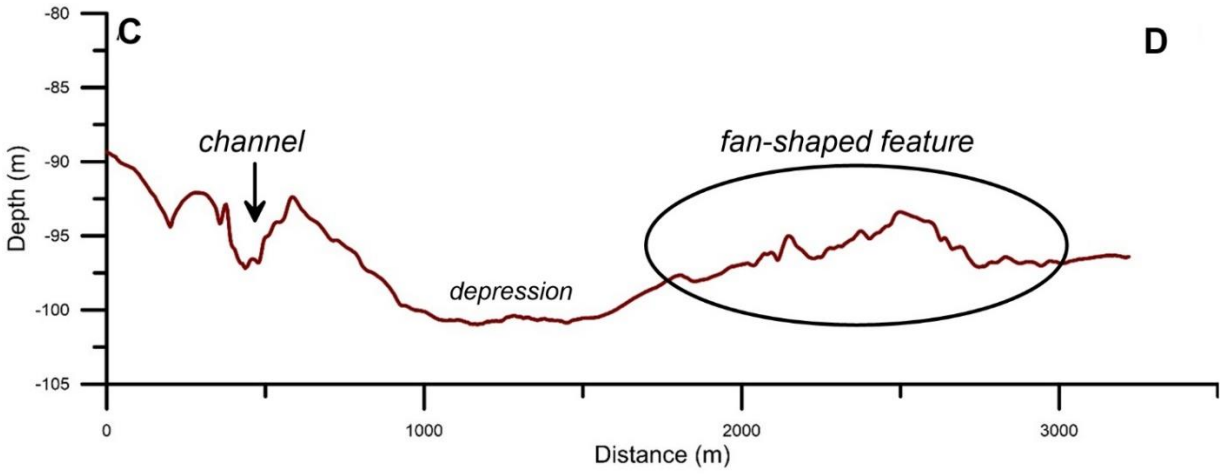

Supplementary Figure 10.22. Section across bedforms 4d and 5. Location in Fig. 6.4. The black arrow represents the channel's thalweg.

In these three areas, the alongshore morphology of the shelf changes significantly (Supplementary Fig. 10.23). The width of the shelf decreases where the bedforms of area 3 are located relatively to the west and one of the channels is very deep (~55 m). The shelf widens to the east where bedforms of areas 4 and 5 are located (Supplementary Fig. 10.24). Nevertheless, the clinoform bodies which cover the shallower areas of the shelf show a relatively constant width, being narrower only where the headwalls of channels are present (Supplementary Fig. 10.24). The shelf morphological variations are presented in Supplementary Table 10.12.

Supplementary Table 10.12. Dimensions and depths of the clinoforms and shelf within and outside the bedform field.

	Distance to shore of clinoform rollover (m)	**Depth of rollover point (m)**	**Shelf width (m)**	**Shelf break (m)**
West of area 3	1065	46	2800	-201
Bedform area 3	460	32	2320	-210
Bedform area 4	640	33	2080	-131
Bedform area 5	190	19	3260	-214
East of area 5	720	49	4120	-200

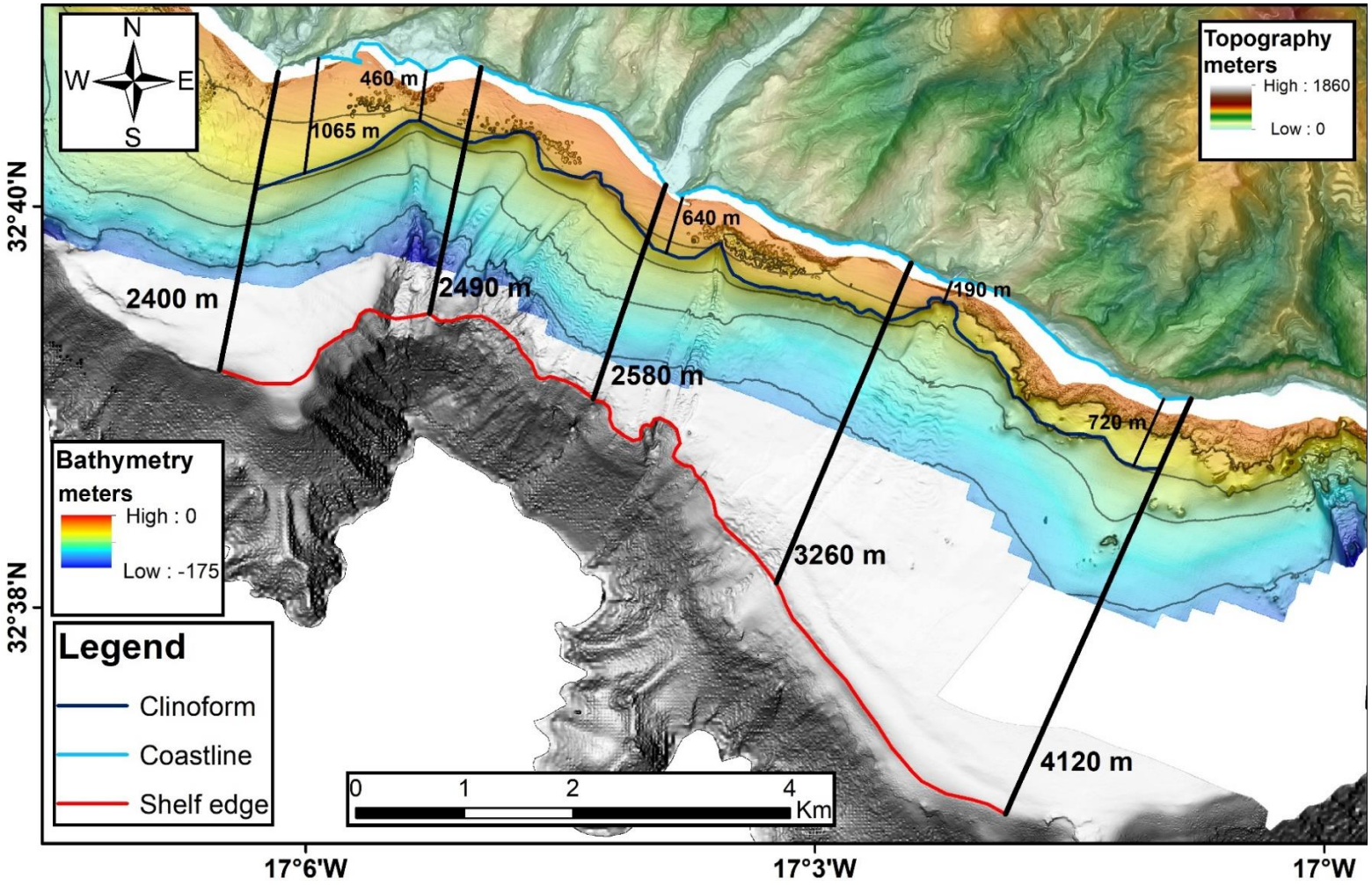

Supplementary Figure 10.23. A) Bathymetric map showing the retreat of the clinoform bodies and shelf width within the bedform fields 3, 4, 5. Subaerial and submarine areas have the same legend as that of Fig. 6.1 in chap. 6. Dark blue line represents the clinoform rollover and red line the shelf break. Black bold and thin straight lines and numbers next to them represent respectively the measured shelf width and clinoform extensions.

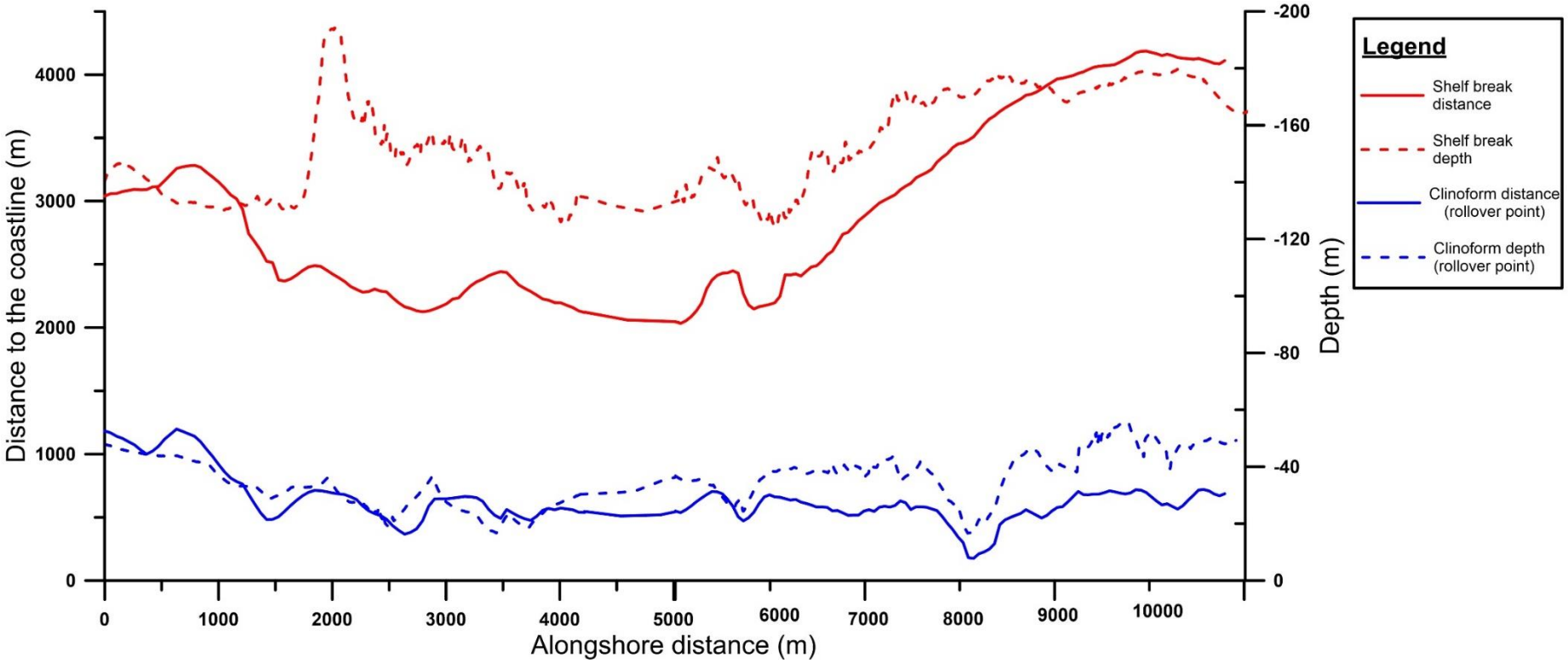

Supplementary Figure 10.24. Alongshore variation of the clinoform rollover and shelf break depths and their respective distances from the coastline of the bedform fields 3, 4 and 5. A detail of these variations can be found in Supplementary Table 10.9.

The 2013 multibeam bathymetric survey covers the area below -70 m in fields 3, 4 and 5. The overlapped area is presented in Supplementary Fig. 10.25.

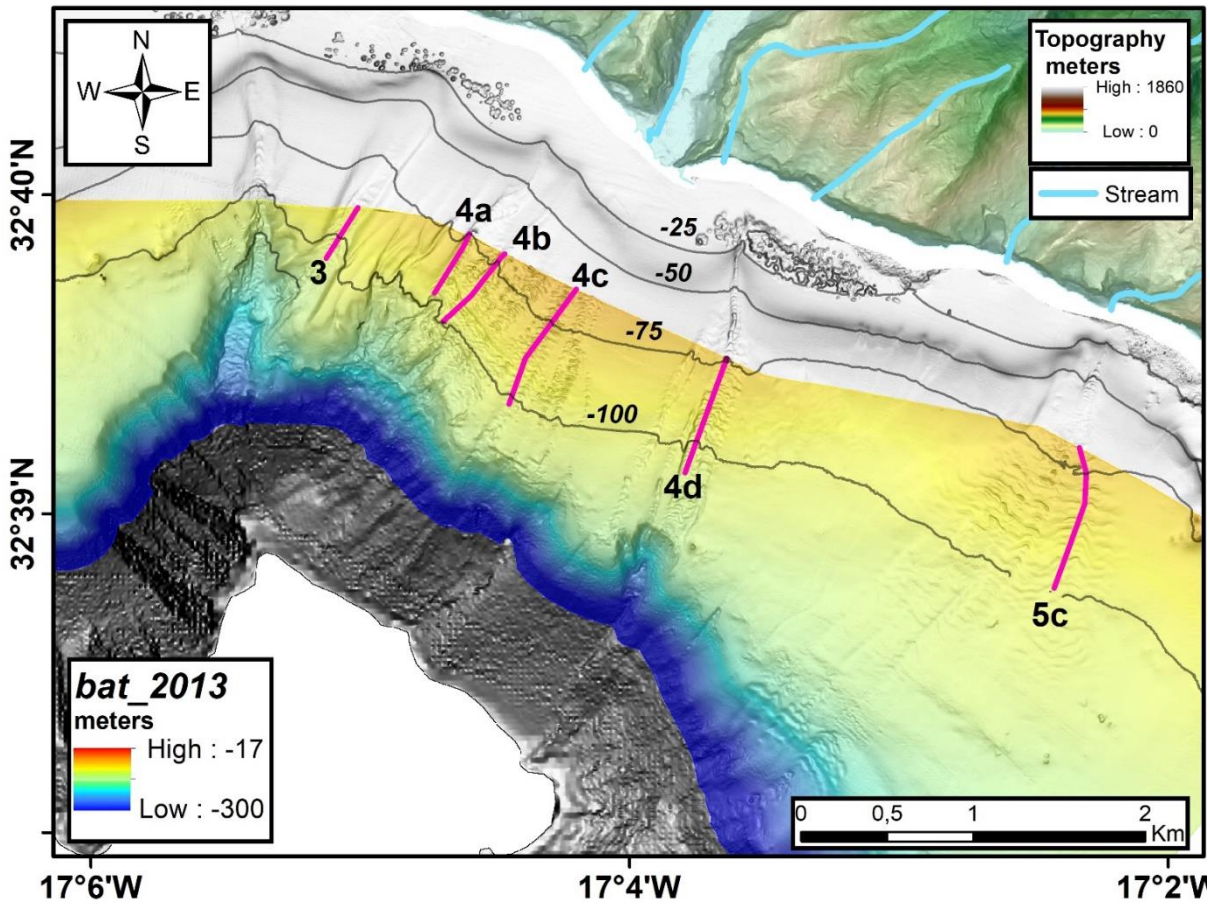

Supplementary Figure 10.25. Bathymetry from 2013 in color on top of the bathymetry from 2014 survey in hillshade grey. Pink lines represent the profiles of Fig. 6.4 where both bathymetries overlap.

The comparison of the 2002 and 2013 profiles of fields 3 and 4 shows generally an onshore bedform migration (Supplementary Fig. 10.26, with the exception of profile 4b that shows erosion while the 4d shows a general offshore migration above -80 m and onshore migration below -80. A resume of the bedform measurements is presented in Supplementary Table 10.13.

Supplementary Table 10.13. Measurements of main bedform parameters in 2013

	Wave heights (min/max) (m)	Wavelengths (min/max) (m)	Wave Crest depth (min/max) (m)	Stoss-side length (min/max) (m)	Stoss-side slope (min/max) (°)	Lee-side length (min/max) (m)	Lee-side slope (min/max) (°)
Profile 3	0.95/2.03	59/69	91/95	12.5/59.7	-0.56/2.05	42/44	3.06/4.99
Profile 4a	0.73/1.80	24/45	75/92	10.3/14.2	-0.21/9.5	10.9/30	4.25/10.7
Profile 4b	1.21/1.86	35/48	76/83	12.2/29.4	-0.6/2.4	20.2/23.1	4.62/6.97
Profile 4c	1.34/2.63	23/39	66/94	8.34/15.5	4.08/8.27	11.9/29.2	6.38/13.65
Profile 4d	0.58/2.01	17/45	75/106	8.2/26.3	-0.37/3.88	7.5/21.3	6.02/17.2

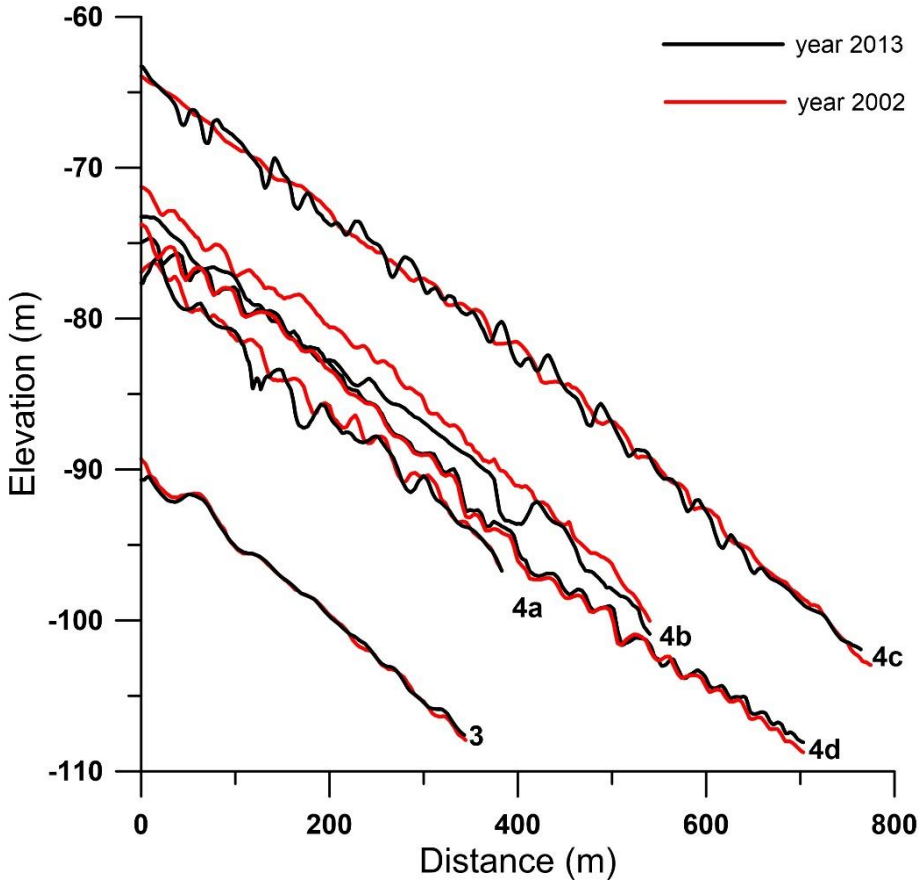

Supplementary Figure 10.26. Comparison of overlapping profiles from 2002-2013 bathymetries.

The overlapped profile 5c shows deposition along the entire profile (Supplementary Fig. 10.27). A resume of the bedform measurements is presented in Supplementary Table 10.14.

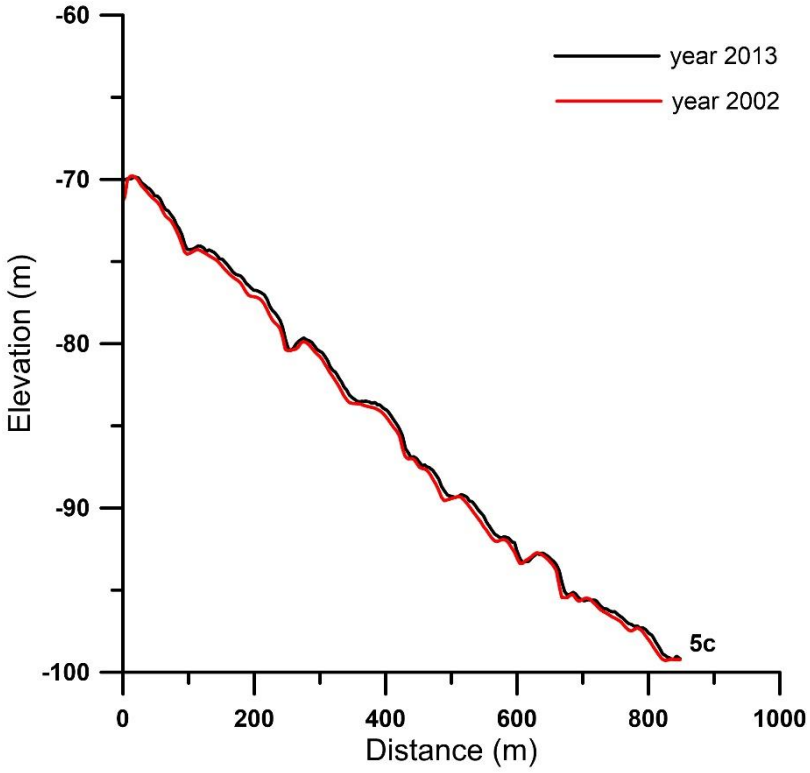

Supplementary Figure 10.27. Comparison of overlapping profiles from 2002 and 2013 bathymetries.

Supplementary Table 10.14. Measurements of main bedform parameters in 2013.

	Wave height (min/max) (m)	**Wavelength (min/max) (m)**	**Wave Crest depth (min/max) (m)**	**Stoss-side length (min/max) (m)**	**Stoss-side slope (min/max) (°)**	**Lee-side length (min/max) (m)**	**Lee-side slope (min/max) (°)**
Profile 5c	0.78/1.96	48/95	69/97	9.2/40.3	-0.64/7.79	23.1/80.7	3.32/10.3

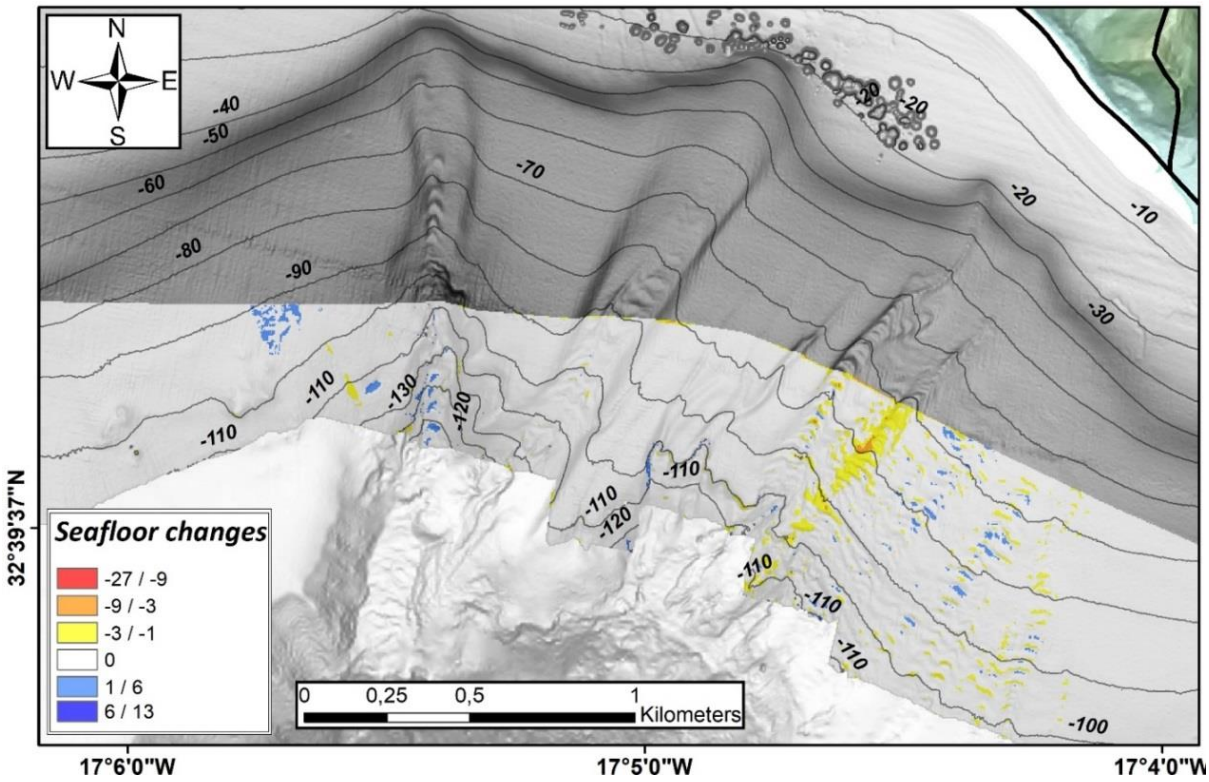

Supplementary Figure 10.28. Seafloor changes observed between 2002 and 2013.

The comparison between the 2002 and 2013 (Supplementary Fig. 10.28) bathymetries shows mostly deposition on bedform field 3, an area of erosion where channel 4 b is located and alternation of erosion and deposition on the area of profile 4c (Fig. 6.13 in chap. 6). The 2019 bathymetry shows that a new failure of the clinoform rollover has happened west of channel 3 and the formation of a new bedform zone downslope occurred (arrow in Supplementary Fig. 10.29).

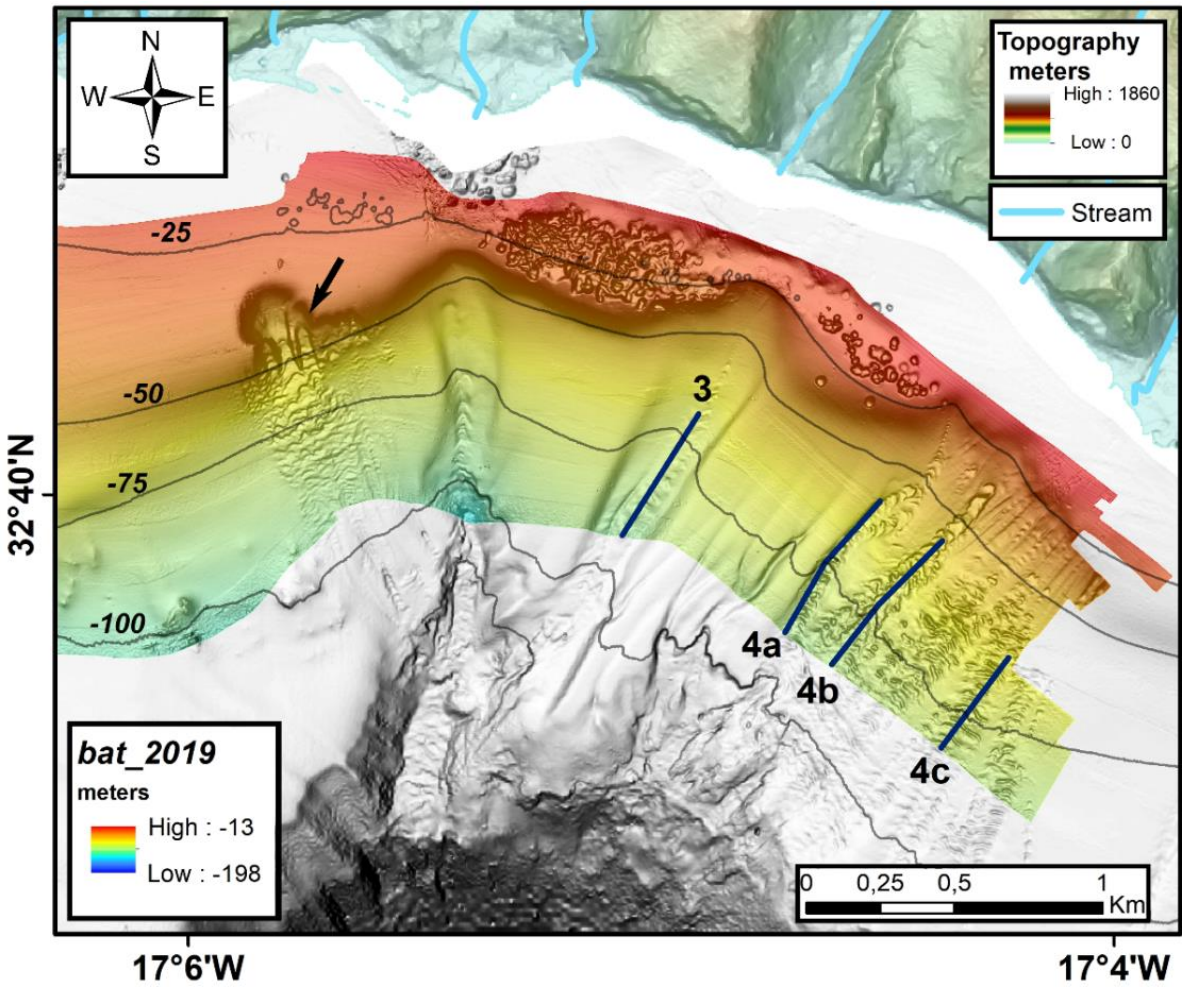

Supplementary Figure 10.30. The 2019 bathymetry in colour on top of the 2002 survey in hillshade grey. Blue lines represent the profiles of Fig. 6.4 in chap. 6 where both bathymetries overlap. Black arrow points out to a clinoform rollover failure that formed bedforms downslope.

The plots of 2002-2019 bedforms shows a general erosion of the channels and it is difficult to see the migration direction (Supplementary Fig. 10.30)

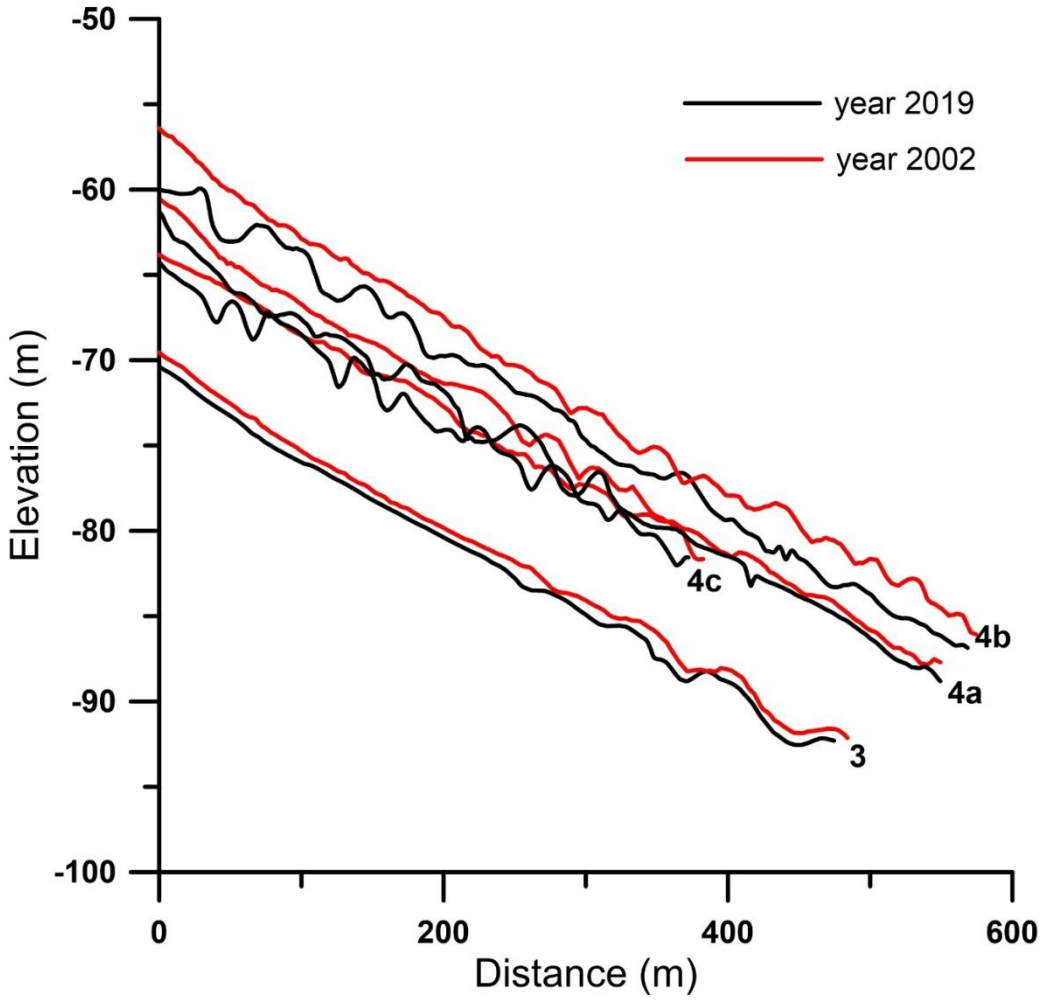

Supplementary Figure 10.30. Comparison of overlapping profiles from the 2002 and 2019 bathymetries.

The bedform characteristics of the 2019 bathymetry are described on Supplementary Table 10.15.

Supplementary Table 10.15. Measurements of the bedform parameters in 2019.

	Wave height (min/max) (m)	**Wavelength (min/max) (m)**	**Wave Crest depth (min/max) (m)**	**Stoss-side length (min/max) (m)**	**Stoss-side slope (min/max) (°)**	**Lee-side length (min/max) (m)**	**Lee-side slope (min/max) (°)**
Profile 3	1.60/2.6	34/60	85/88	14.9/14.1	-0.21/1.2	16.4/46.2	5.85/6.80
Profile 4a	1.35/3.23	33/58	63/85	13.3/28.7	0.20/5.99	14.5/33.9	3.88/11.6
Profile 4b	1.05/2.79	26/37	62/76	8.81/15.8	-0.76/4.59	14.9/28.2	5.65/10
Profile 4c	1.12/2.53	23/60	66/76	6.4/15.4	5.86/10	11.6/47	6.14/16.4

Looking at the three different bathymetries, from 2002 to 2019, headward erosion of the clinoform rollover of channels 3, 4a and 4b (arrows on Supplementary Fig. 10.31) and failure of the clinoform west of channel 3 (arrow south of ellipse) occurred. The failure must have happened between 2002 and 2013 because the downslope deposits are already visible on the 2013 bathymetry (Supplementary Fig. 10.31). The ellipse also points out for an area that was being dredged in 2002 and in 2019. There, the seabed was fully recovered showing that sedimentation on that area prevails (Fig. 6.13).

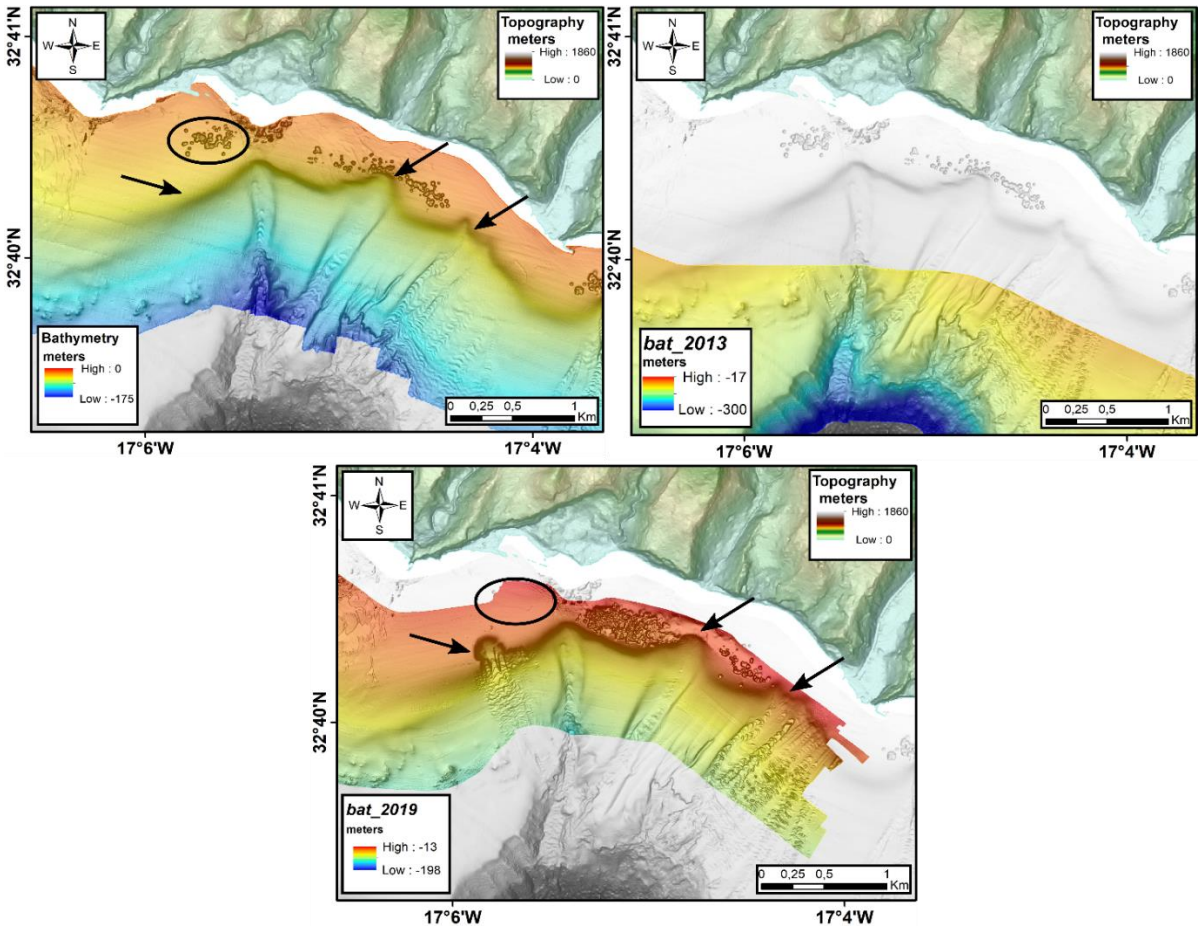

Supplementary Figure 10.31. Three different time lapses (2002-2013-2019) showing the headward erosion of channels, the failure of a clinoform rollover and filling of the dredging pit holes.

BEDFORM FIELD 6

Bedform field 6 has an area of 0.62 km² (Supplementary Fig. 10.32). This area was not completely covered by the multibeam survey and due to this, the measurements reported miss the entire bedform extension. The eastern channel is small, but the western one is deeper than 25 m (Supplementary Fig. 10.33).

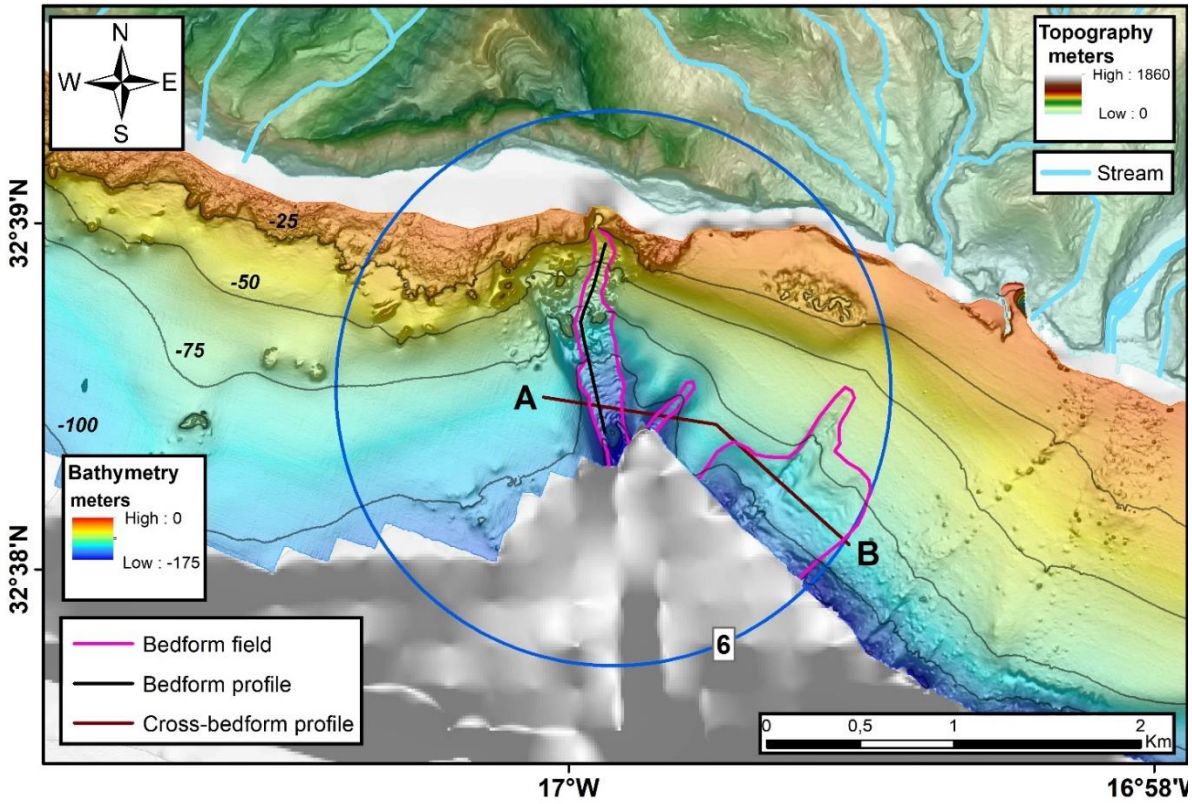

Supplementary Figure 10.32. Bedform field 6. Rose line delimits the channels with bedforms. Brown line A-B represents the cross-section profile along the bedforms in Supplementary Fig. 10.33 and black line is the topographic profile represented in Supplementary Fig. 10.34. Grey lines represent isobaths every 25 m. Subaerial and submarine areas have the same legend as that of Fig. 6.1.

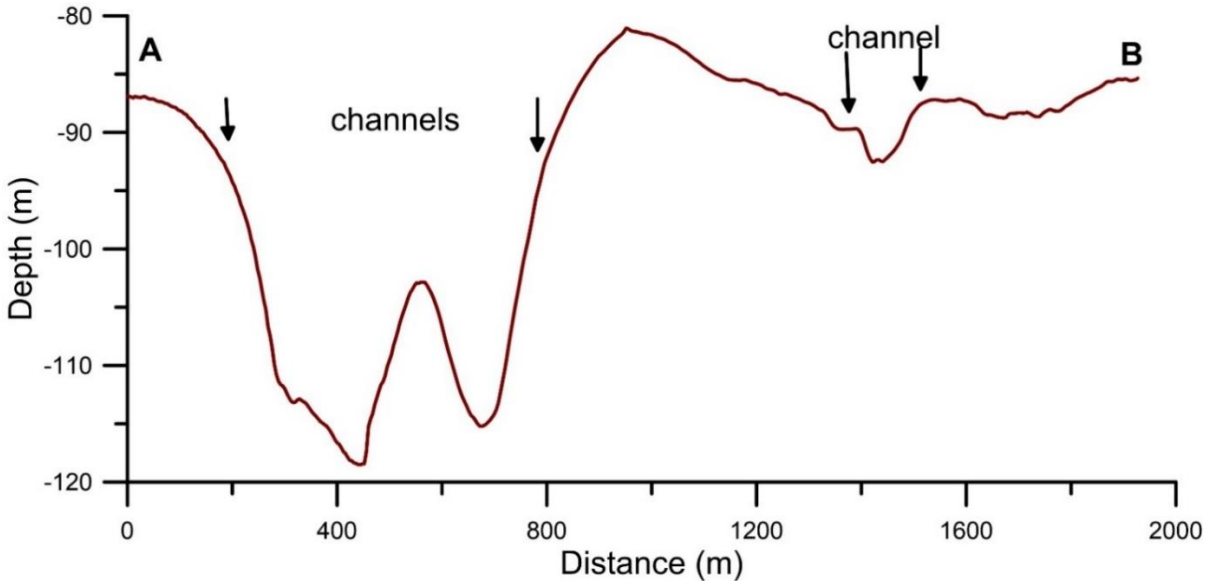

Supplementary Figure 10.33. Cross-section of the bedform field 6. Location in Supplementary Fig. 10.32. Black arrows represent the lateral margins of the channels.

The morphological parameters of the bedforms are presented in Supplementary Table 10.16 and the profile in Supplementary Fig. 10.33

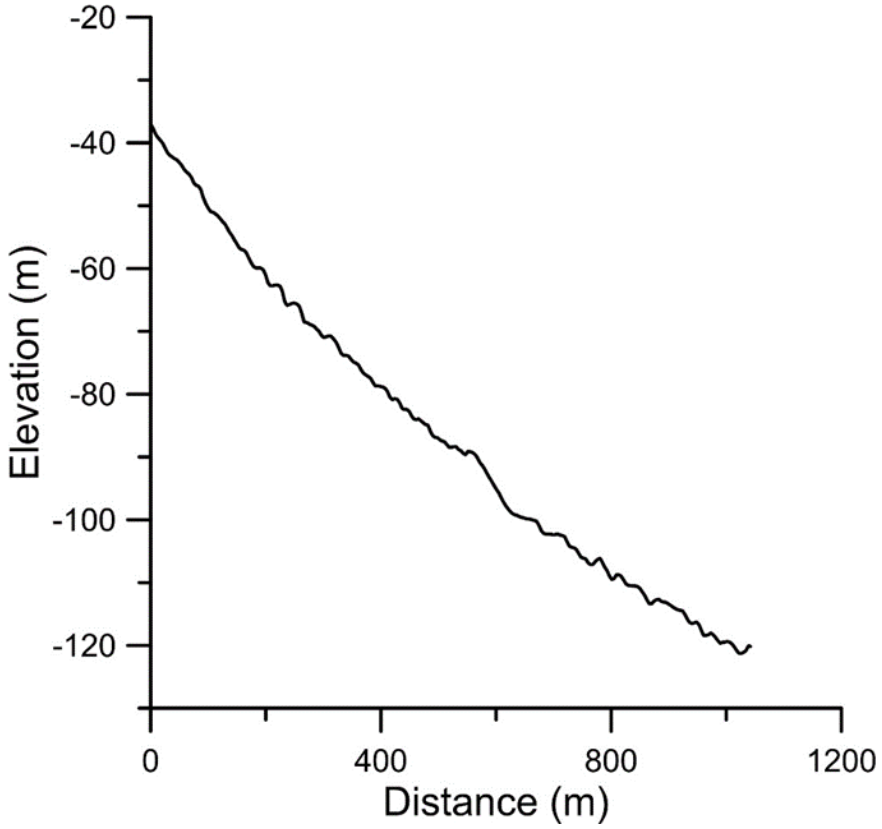

Supplementary Figure 10.34. Bathymetric profile of bedforms in area 6. Location of profile in Supplementary Fig. 10.32**.**

Supplementary Table 10.16. Morphometry of bedform field 6. “beg” = beginning; “mid” = middle; “end” = ending; “min” = minimum; “max” = maximum.

	Start depth (m)	End depth (m)	Width (beg/mid/end) (m)	Length (m)	Plan-view pattern	Wave height (min/max) (m)	Wavelength (min/max) (m)	Wave crest depth (min/max) (m)	Bedform shape in plan-view	General slope	Stoss-side length (min/max) (m)	Stoss-side slope (min/max) (°)	Lee-side length (min/max) (m)	Lee-side slope (min/max) (°)
Profile 6 channel	29	134	84/187/135	1250	Linear	1.77/5.23	23/77	60/118	Crescentic	4.82/3.65	12.9/51	-1.34/ 5.62	11.3/ 64	7.35/ 12.9
Channel	96	124	52/51/55	242	Linear	-	-	-	-	-	-	-	-	-
Channel	58	110	31/87/84	908	Linear	-	-	-	-	-	-	-	-	-

The nearshore part of bedform field 6 shows the presence of rocky outcrops that are likely the product of cliff failure; some rocky blocks have fallen into the channel (Supplementary Fig. 10.35). A low-resolution bathymetry from EMODNET allowed the analysis of the shelf width and depth of shelf break, as well as clinoform extension and rollover depth (Supplementary Figs. 10.35 and 10.36). It is possible to see the clinoform rollover retreat where the channels incise the shelf.

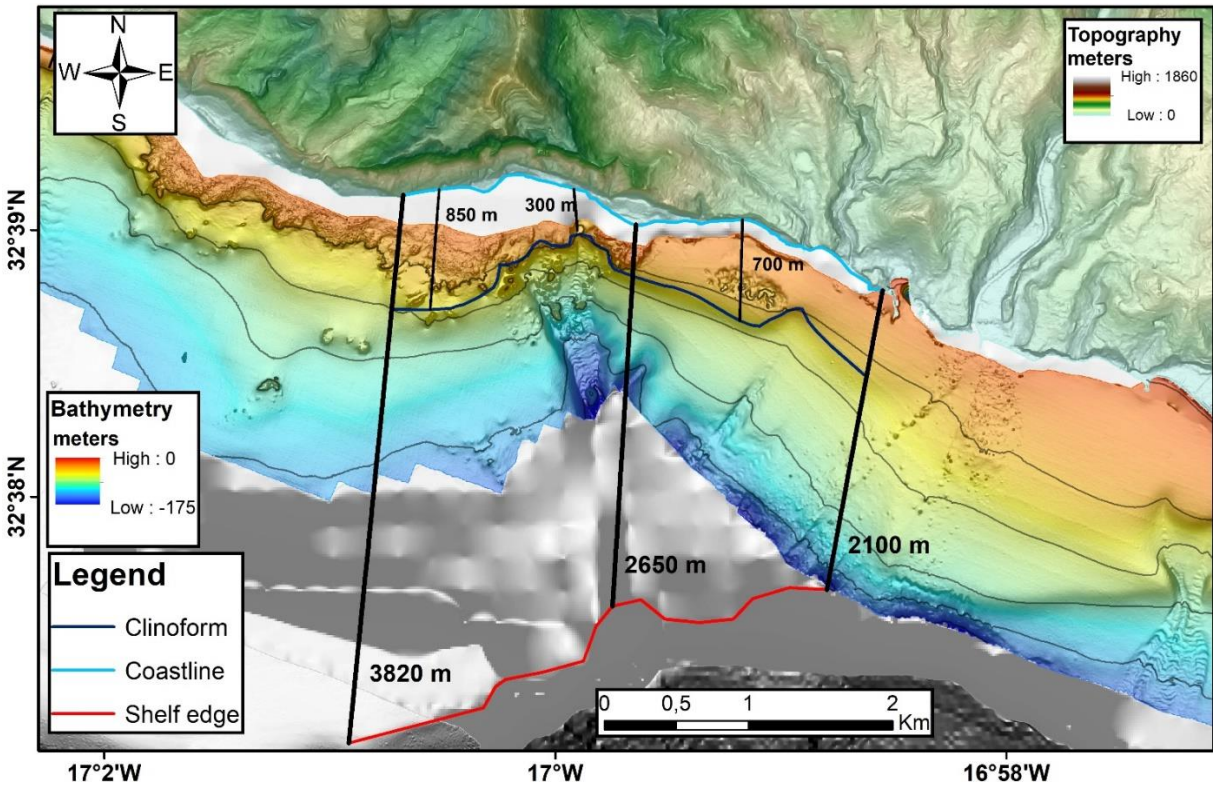

Supplementary Figure 10.35. Bathymetric map showing the retreat of the clinoform bodies and shelf width within the bedform field 6. Subaerial and submarine areas have the same legend as in Fig. 6.4. Dark blue line represents the clinoform rollover and red line the shelf break. Black bold and thin straight lines and numbers next to them represent respectively the measured shelf width and clinoform extensions.

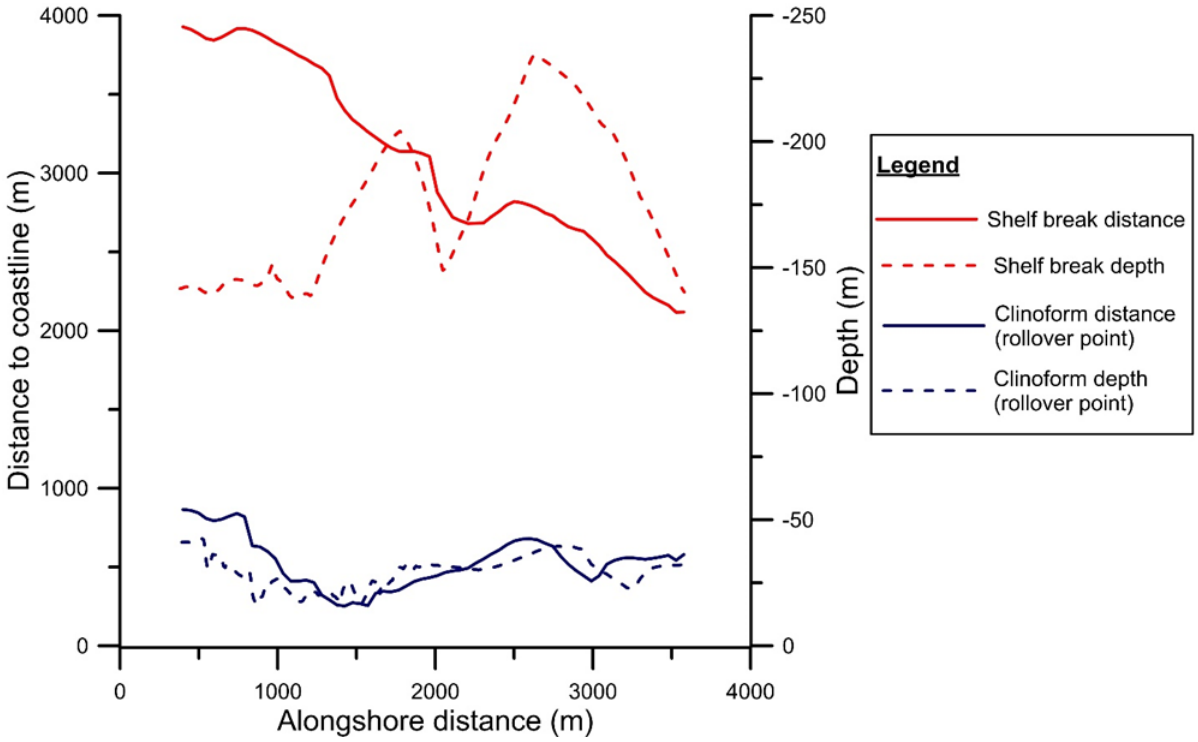

Supplementary Figure 10.36. Alongshore variation of the clinoform rollover and shelf break depths and their respective distances to the coast. A detail of these variations can be found in Supplementary Table 10.17.

Supplementary Table 10.17. Dimensions and depths of the clinoforms and shelf within and outside the bedform field.

	Distance to shore of clinoform rollover (m)	Depth of rollover (m)	Shelf width (m)	Shelf break (m)
Western area	850	40	3820	-151
Bedform area	300	36	2750	-212
Eastern area	700	32	2100	-130

BEDFORM FIELDS 7 AND 8

The bedform field 7 has an area of 0.58 km² (rose line in Supplementary Fig. 10.37). It is composed of a fan-shaped elevation, downslope a clinoform rollover failure. Onshore, the nearest hydrographic basin area is about 43 km^2.

Bedform field 8 occurs offshore a lava delta (arrow in Supplementary Fig. 10.37) and is dominated by a channelized feature that covers an area of 0.54 km². The channel is dendritic upslope and linear and narrow at its offshore end, incising the seafloor ~40 m (Supplementary Fig. 10.38).

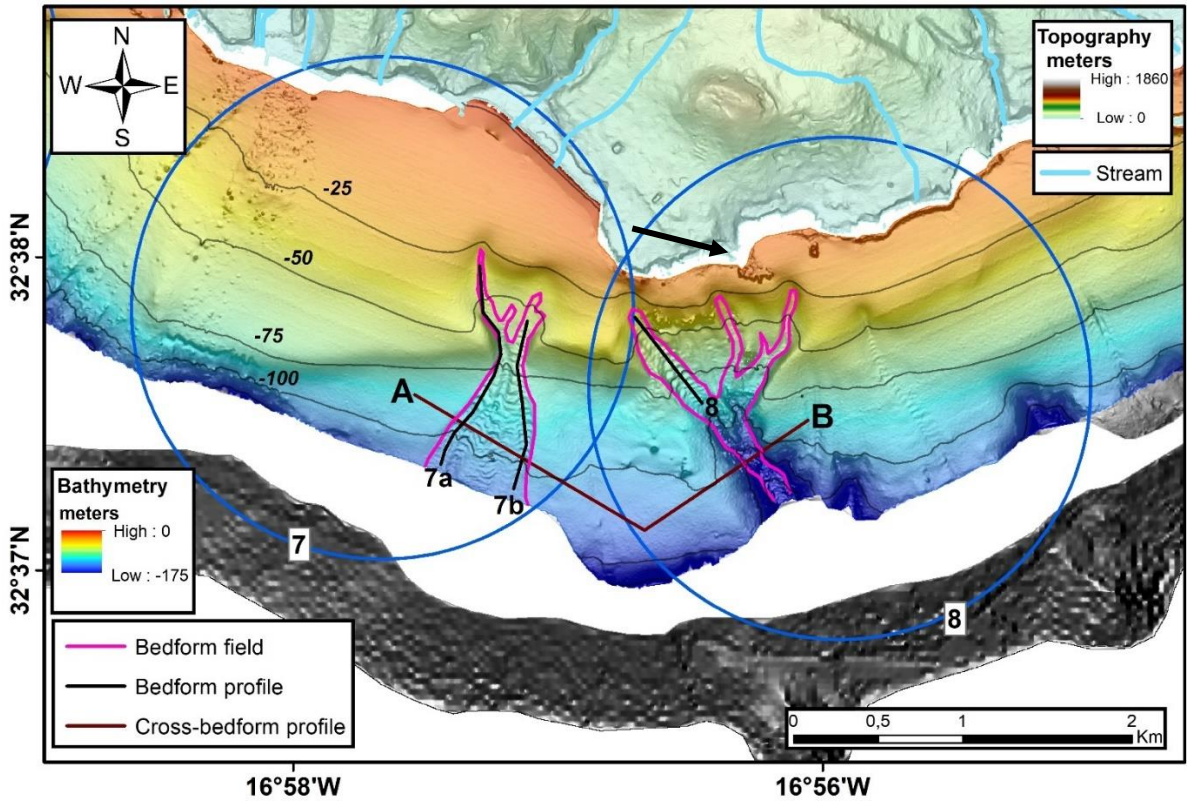

Supplementary Figure 10.37. Bedform fields 7 and 8. Pink line delimits the channels with bedforms. Brown line A-B represents the transversal profile along the bedforms in Supplementary Fig. 10.38 and black lines are the longitudinal profiles represented in Supplementary Fig. 10.39. Grey lines represent isobaths every 25 m. Subaerial and submarine areas have the same legend as that of Fig. 6.4. Black arrow indicates lava delta. Black lines in the shelf represent isobaths every 25 m.

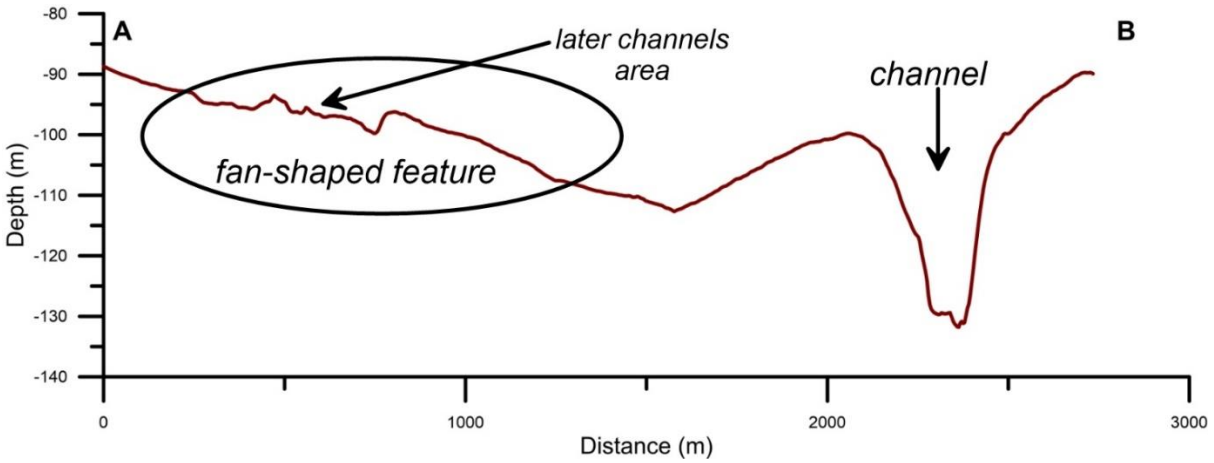

Supplementary Figure 10.38. Cross-section of the bedform fields 7 and 8. Locations in Supplementary Fig. 10.36. On the left, the arrow denotes the fan-shaped feature area affected by later channels incision. On the right, the black arrow indicates the main channel's thalweg.

The morphological parameters of the bedforms are presented in Supplementary Table 10.18 and their longitudinal profiles are in Supplementary Fig. 10.39.

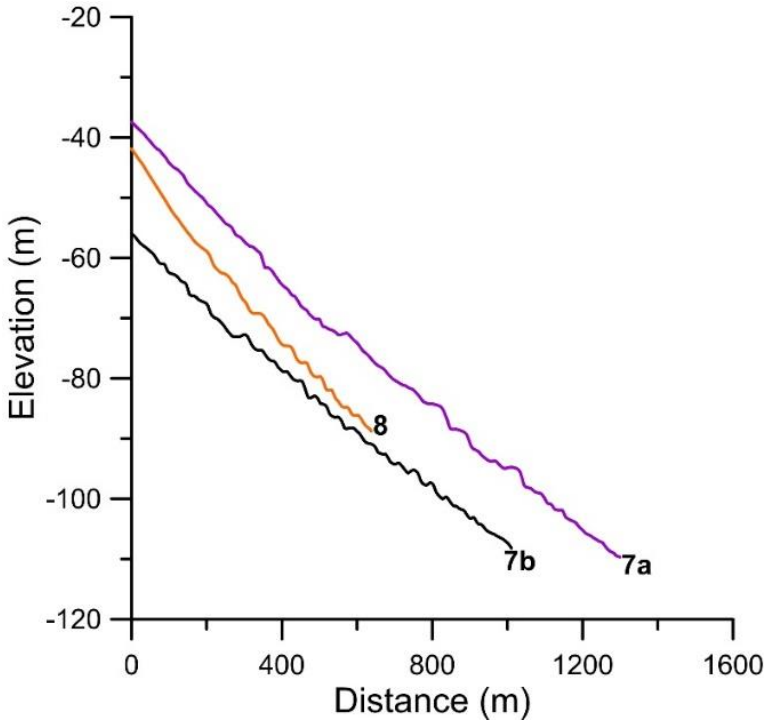

Supplementary Figure 10.39. Bathymetric profiles of bedforms on areas 7 and 8. Location in Supplementary Fig. 10.37.

Supplementary Table 10.18. Morphometry of bedform fields 7 and 8. “beg” = beginning; “mid” = middle; “end” = ending; “min” = minimum; “max” = maximum.

	Start depth (m)	End depth (m)	Width (beg/mid/ end) (m)	Length (m)	Plan-view pattern	Wave height (min/max) (m)	Wavelength (min/max) (m)	Wave crest depth (min/ max) (m)	Bedform shape in plan-view	General slope (°)	Stoss-side length (min/ max) (m)	Stoss-side slope (min/ max) (°)	Lee-side length (min/ max) (m)	Lee-side slope (min/ max) (°)
Fan-shaped feature with 7a and 7b profiles	34	112	387/148/548	1419	Fan-shaped downslope	0.65/2.84	21/65	61/97	Crescentic and sinuous	2.88	9.45/44.9	-1.51/ 4.04	11.2/ 31.5	4.24/ 11.26
Channel with profile 8	28	160	919/177/106	1469	Dendritic upslope	0.66/1.76	22/76	59/86	Crescentic	3.84	11.8/25.2	-2.78/ 1.44	11.3/ 49.2	6.04/ 9.68

The 2002 bathymetry does not reach below -175 m (Supplementary Fig. 10.40), so a low-resolution bathymetry from the EMODNET database was used to define the shelf break. The clinoform bodies have varied rollover distances to the coast; they are more developed at the west and less at the east (Supplementary Fig. 10.40). The nearest distance of the rollover to the coast is 175 m from the coast and it corresponds to the headwall of the erosive channel 8. The depth of the rollovers is variable, between 75 m to 15 m, being shallowest where the channels have developed their headwalls. East of the field 8, it appears that incipient channels are forming at the shelf edge and migrate upslope until they eventually capture the clinoform rollover (arrows in Supplementary Fig. 10.40).

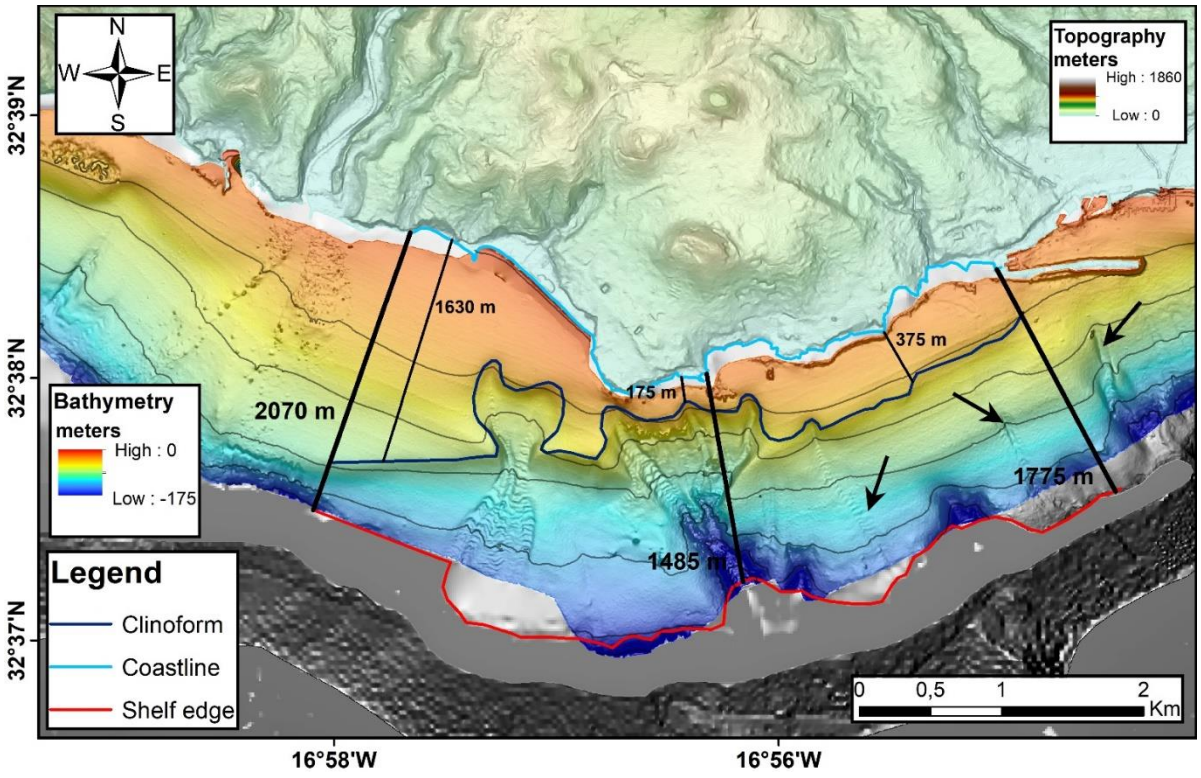

Supplementary Figure 10.40. Bathymetric map showing the retreat of the clinoform bodies and shelf width within the bedform fields 7 and 8. Subaerial and submarine areas have the same legend as in Fig. 6.1. Dark blue line represents the clinoform rollover and red line the shelf break. Black bold and thin straight lines and numbers next to them represent respectively the measured shelf width and clinoform extensions.

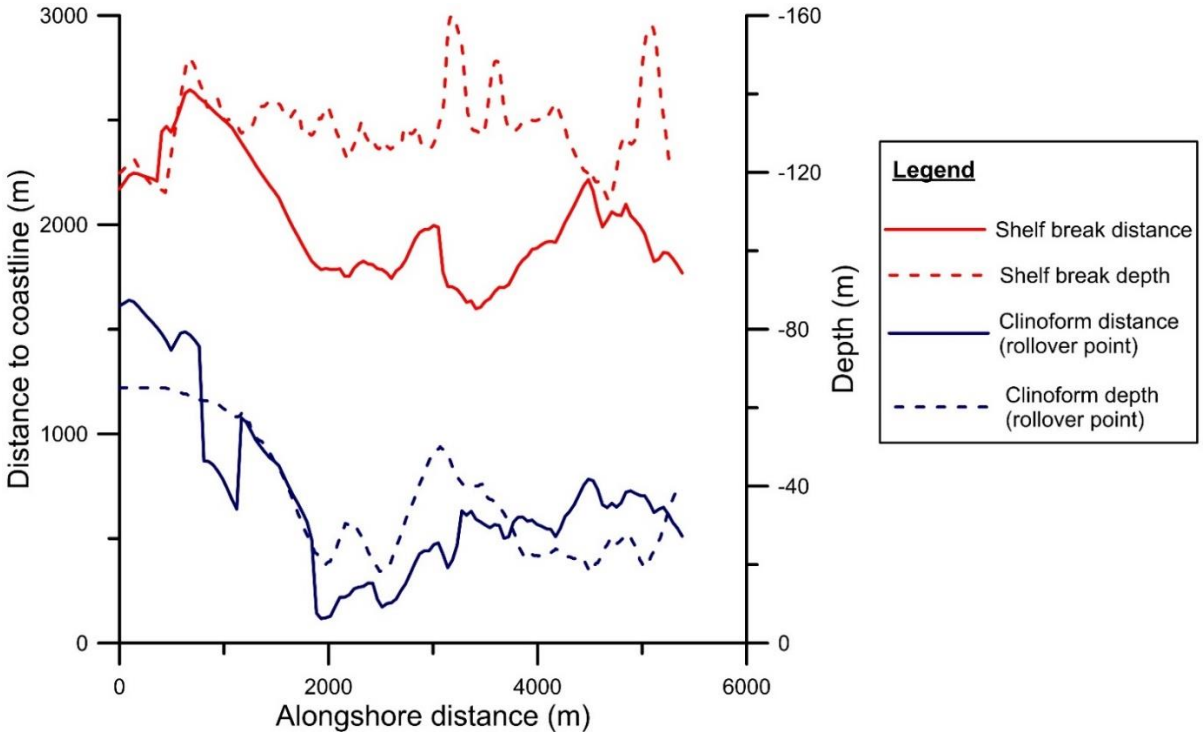

Supplementary Figure 10.41. Alongshore variation of the clinoform rollover and shelf break depths and their respective distances to the coast. A detail of these variations can be found in Supplementary Table 10.17.

Supplementary Table 10.17 synthesizes the shelf and clinoform morphologies. The absence of recent bathymetric data precludes the evaluation of the evolution of these features.

Supplementary Table 10.17. Dimensions and depths of the clinoforms and shelf within and outside the bedform field.

	Distance to shore of clinoform rollover (m)	**Depth of rollover (m)**	**Shelf width (m)**	**Shelf break (m)**
Western area	1630	70	2070	-112
Bedform areas	175	19	1485	-157
Eastern area	375	30	1775	-114

BEDFORM FIELD 9

Bedform field 9 is the smallest and it is located where the southern shelf is narrower. It is only 0.03 km² in area (pink line in Supplementary Fig. 10.42). There are two channels cutting the shelf but only the left one of them has bedforms (Supplementary Fig. 10.43). Onshore, tall cliffs are present and there are no stream outlets. The bedforms are very small in size and their main properties are shown in Supplementary Table 10.18.

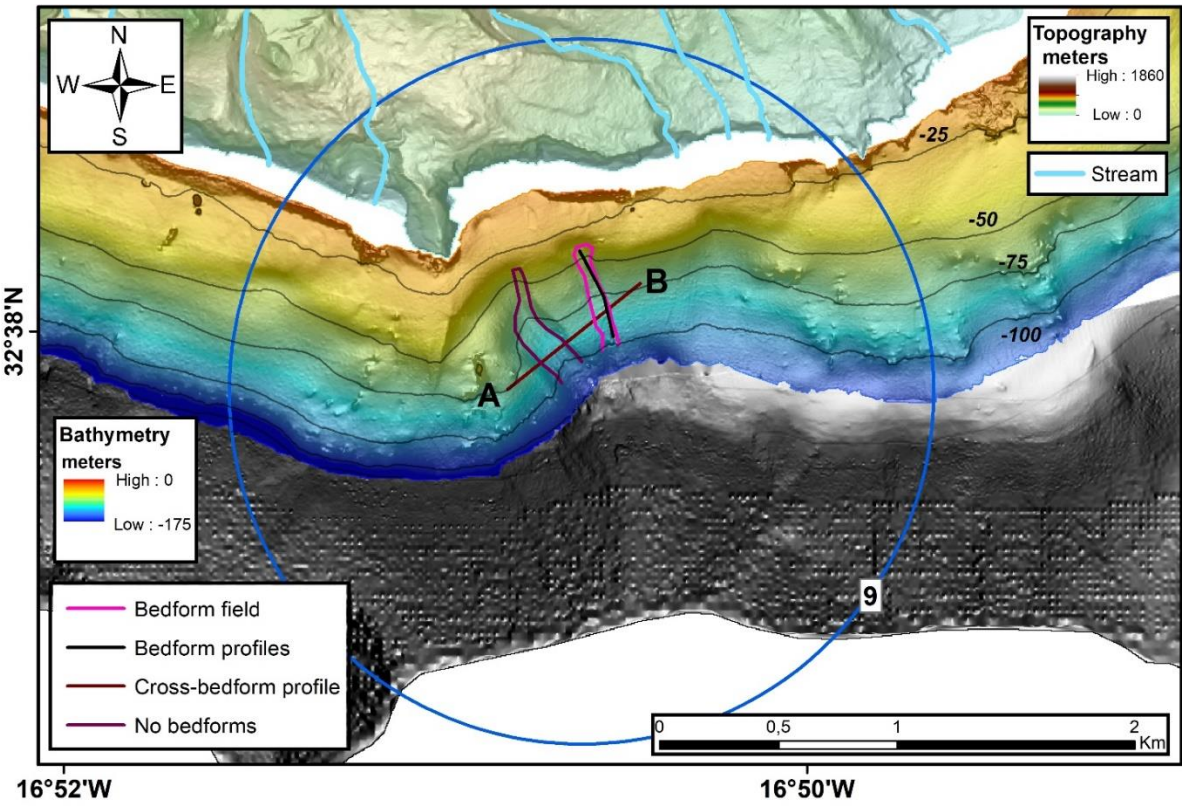

Supplementary Figure 10.42. Bedform field 9. Pink line delimits the channel with bedforms. Brown line A-B represents the transversal profile across the bedforms in Supplementary Fig. 10.43 and black line is the longitudinal profile represented in Supplementary Fig. 10.44. Grey lines represent isobaths every 25 m. Subaerial and submarine areas have the same legend as in Fig. 6.1.

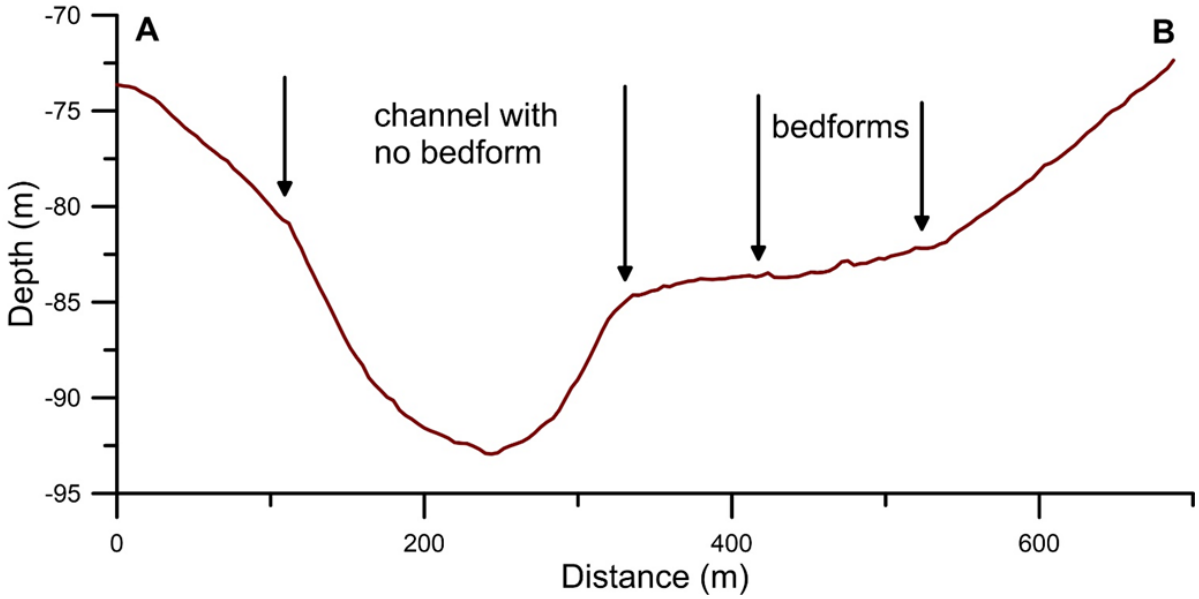

Supplementary Figure 10.43. Cross-section of bedform 9. Location in Supplementary Fig. 10.42. Black arrows represent the lateral margins of the channels. On the left, the channel does not show bedforms, on the right the channel shows bedforms.

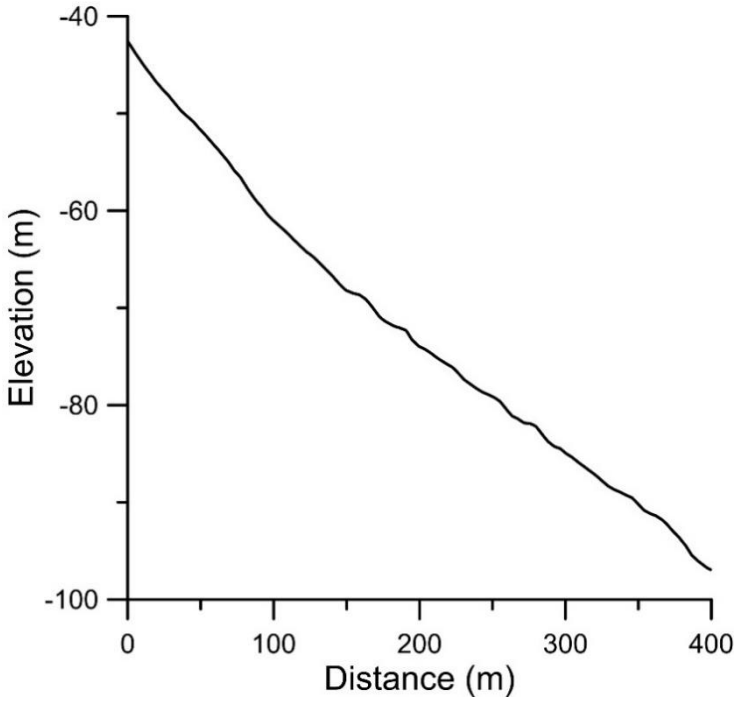

Supplementary Figure 10.44. Bathymetric profile of bedforms on area 9.

Supplementary Table 10.18. Morphometry of bedform field 9. “beg” = beginning; “mid” = middle; “end” = ending; “min” = minimum; “max” = maximum.

	Start depth (m)	End depth (m)	Width (beg/mid/end) (m)	Length (m)	Plan-view pattern	Wave height (min/max) (m)	Wavelength (min/max) (m)	Wave crest depth (min/max) (m)	Bedform shape in plan-view	General slope (°)	Stoss-side length (min/max) (m)	Stoss-side slope (min/max) (°)	Lee-side length (min/max) (m)	Lee-side slope (min/max) (°)
Channel without bedforms	45	120	42/130/121	600	Linear	-	-	-	-	-	-	-	-	-
Channel with profile	38	117	56/72/88	552	Linear	1.20/1.81	17/23	68/81	Crescentic	6.40	14.9/5.7	-2.44/ -0.78	16.1/ 9.1	10.2/ 10.8

In this sector, the shelf width is very narrow when compared to the other areas. In Supplementary Figs. 10.45 and 10.46, the shelf width and depth of the shelf break, as well as the clinoform extension and rollover depth are described.

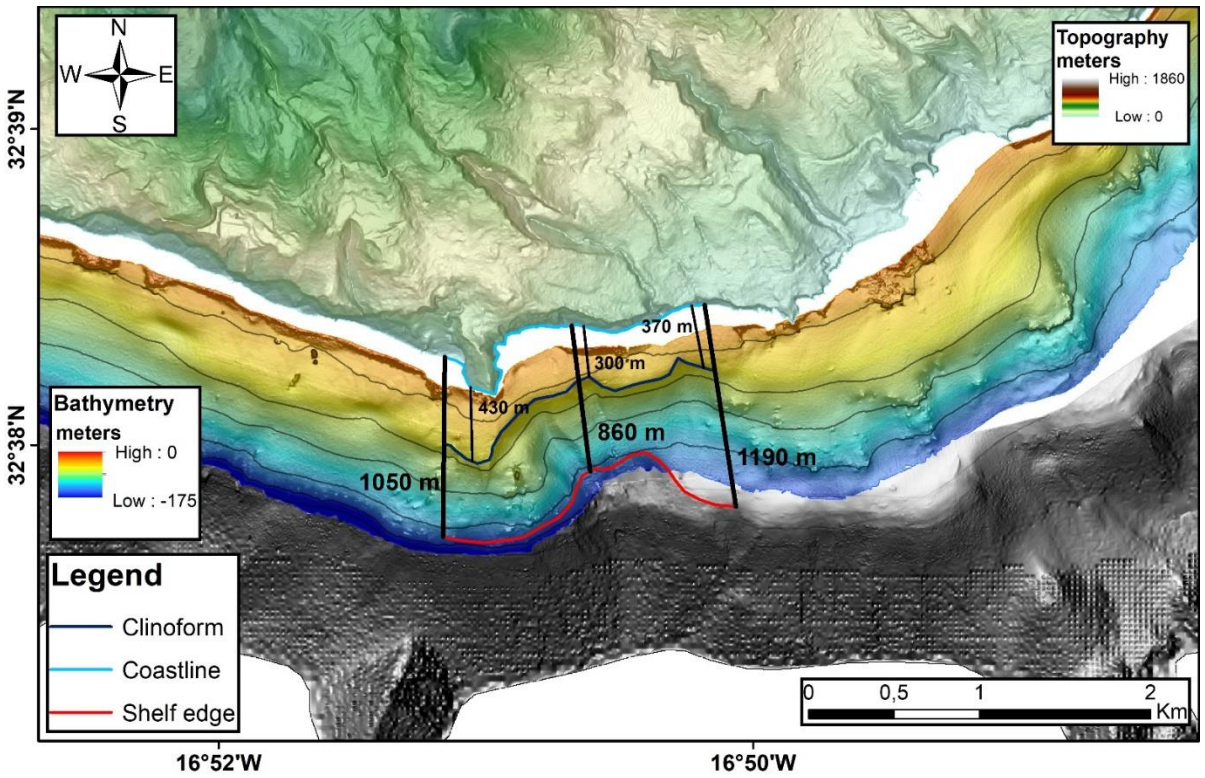

Supplementary Figure 10.45. Bathymetric map showing the retreat of the clinoform bodies and shelf width within the bedform field 9. Subaerial and submarine areas have the same legend as in Fig. 6.1. Dark blue line represents the clinoform rollover and red line the shelf break. Black bold and thin straight lines and numbers next to them represent respectively the measured shelf width and clinoform extension.

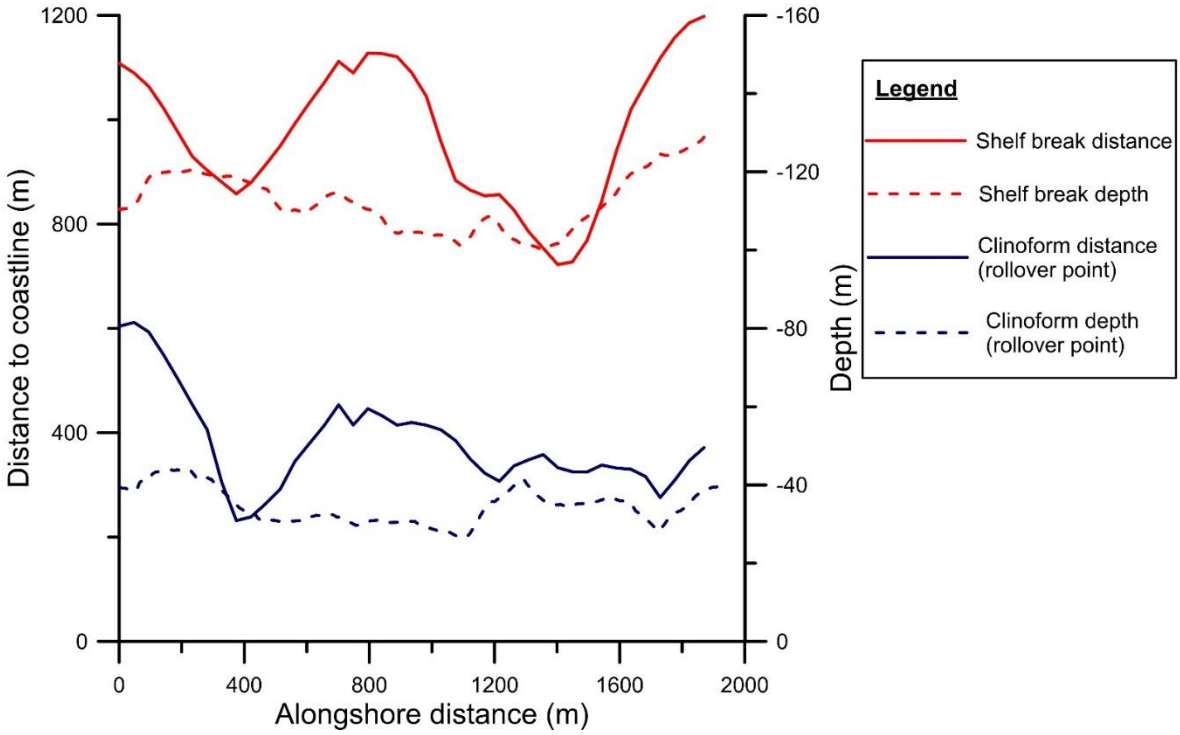

Supplementary Figure 10.46. Alongshore variation of the clinoform rollover and shelf break depth and their respective distances to the coast. A detail of these variations can be found in Supplementary Table 10.19.

Supplementary Table 10.19. Dimensions and depths of the clinoforms and shelf within and outside the bedform field.

	Distance to shore of clinoform rollover (m)	Depth of rollover point (m)	Shelf width (m)	Shelf break (m)
Western area	430	38	1050	-110
Bedform area	300	29	860	-115
Eastern area	370	40	1190	-131

BEDFORM FIELD 10

The bedform field 10 (Supplementary Fig. 10.47) covers a surface of 0.23 km² and it is characterized by the presence of a fan-shaped feature, elevated above the surrounding area. The area becomes larger downslope and has well defined bedforms (Supplementary 10.48 and 10.48) which characteristics are expressed in Supplementary Table 10.20. Onshore, there are tall cliffs and very small streams.

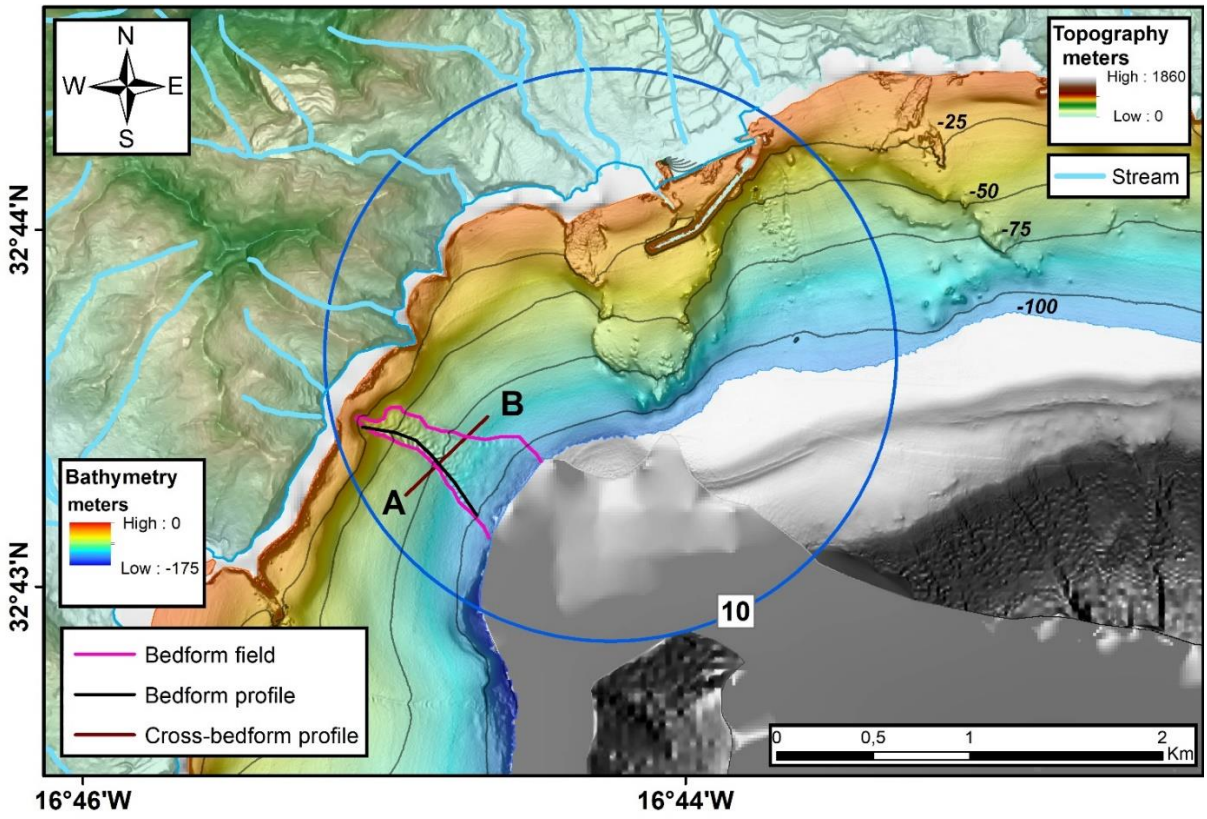

Supplementary Figure 10.47. Bedform field 10. Pink line delimits the area with bedforms. Brown line A-B represents the transversal profile along the bedforms in Supplementary Fig. 10.48 and black line is the longitudinal profile represented in Supplementary Fig. 10.49. Grey lines represent isobaths every 25 m. Subaerial and submarine areas have the same legend as that of Figure 6.1.

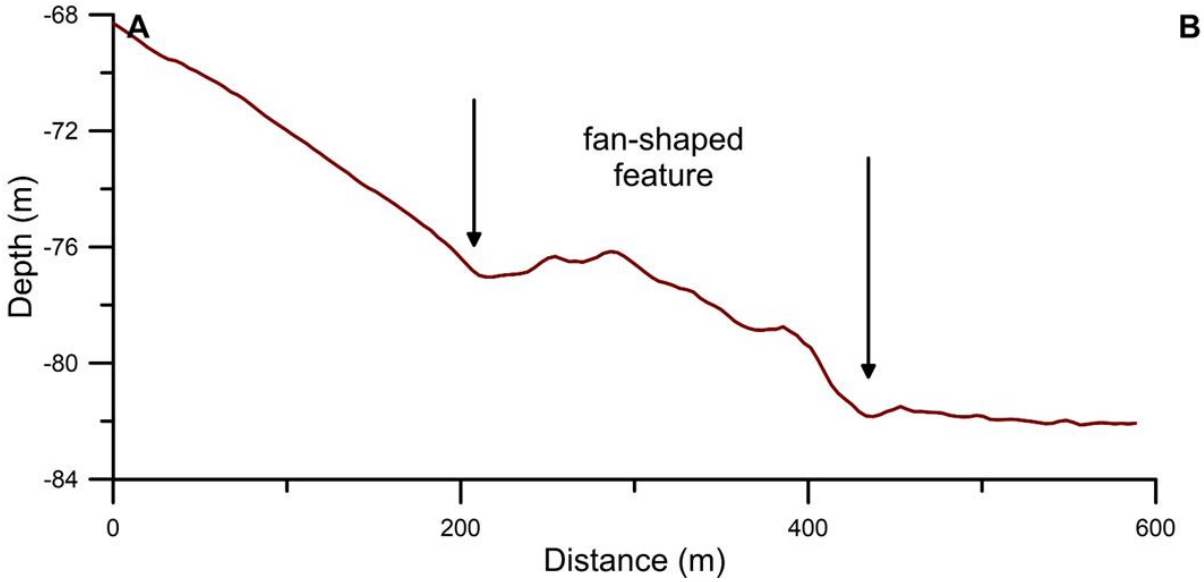

Supplementary Figure 10.48. Cross-section of bedform 10. Location in Supplementary Fig. 10.47. Black arrows delimit the fan-shaped feature.

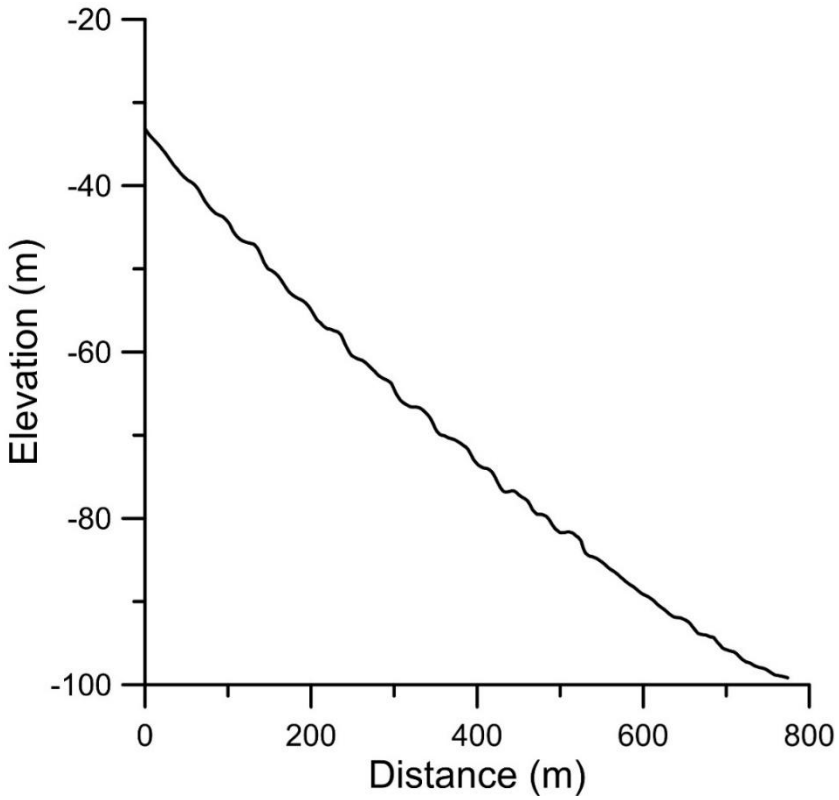

Supplementary Figure 10.49. Bathymetric profile of bedforms on area 10. Location in Supplementary Fig. 10.47.

Supplementary Table 10.20. Morphometry of bedform field 10. “beg” = beginning; “mid” = middle; “end” = ending; “min” = minimum; “max” = maximum.

	Start depth (m)	End depth (m)	Width (beg/mid/end) (m)	Length (m)	Plan-view pattern	Wave height (min/ max) (m)	Wavelength (min/max) (m)	Wave crest depth (min/max) (m)	Bedform shape in plan-view	General slope	Stoss-side length (min/ max) (m)	Stoss-side slope (min/max) (°)	Lee-side length (min/max) (m)	Lee-side slope (min/max) (°)
fan-shaped feature	24	102	171/191/473	881	Fan-shaped downslope	0.81/2.04	26/44	47/82	Sinuous	4.90	11.4/ 32.6	-2.81/ 1.03	10.8/ 19.9	8.01/ 12.5

There is no deep multibeam bathymetry of this area (Supplementary Fig. 10.50), so the low resolution from EMODNET is used to define the shelf break. The clinoform bodies are very small and reach a maximum extent of 405 m from the coastline. The rollover of the clinoform is narrower and shallower at the headwall of this bedform field.

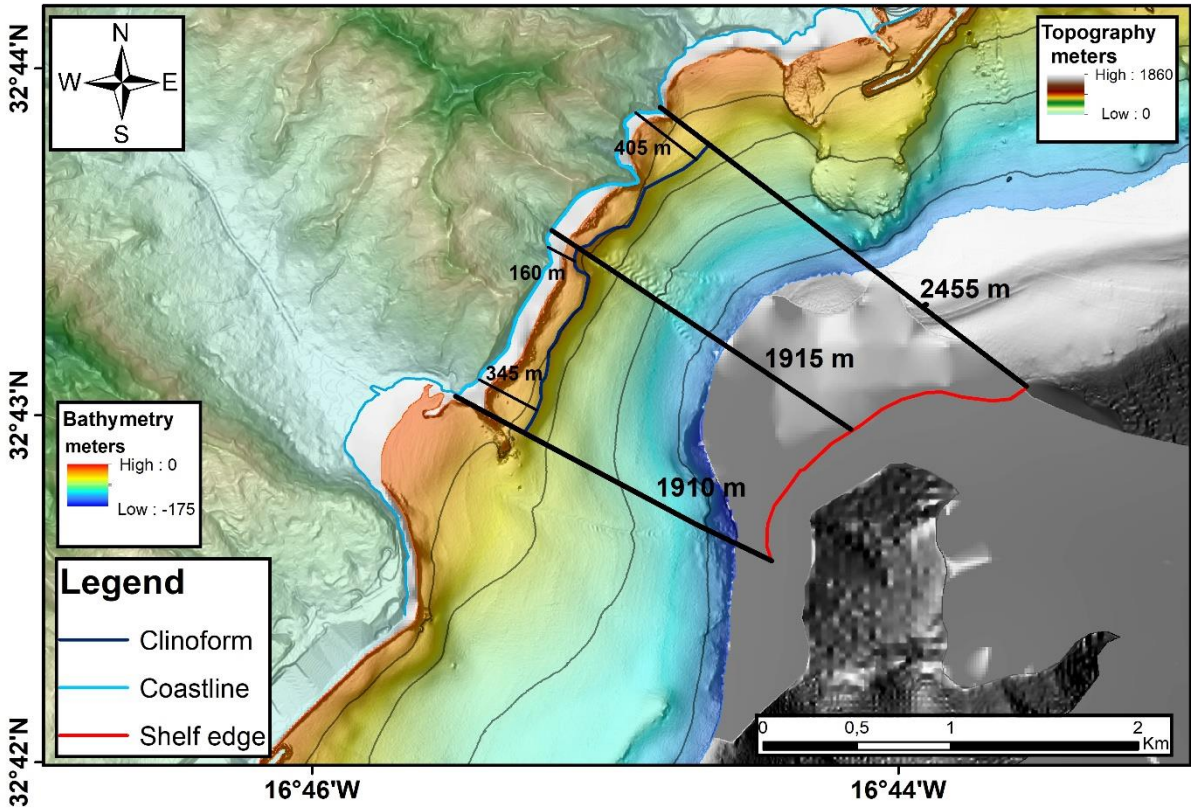

Supplementary Figure 10.50. A) Bathymetric map showing the retreat of the clinoform bodies and shelf width within the bedform field 10. Subaerial and submarine areas have the same legend as in Fig. 6.1. Dark blue line represents the clinoform rollover and red line the shelf break. Black bold and thin straight lines and numbers next to them represent respectively the measured shelf width and clinoform extension.

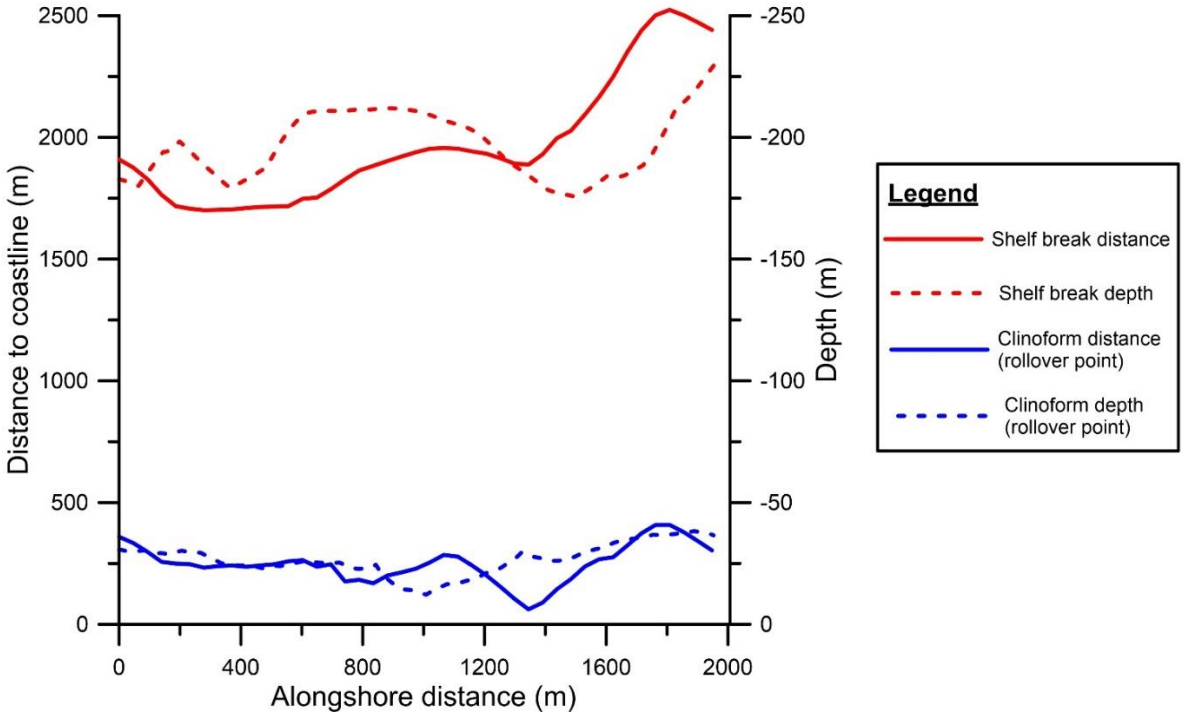

Supplementary Figure 10.51. Alongshore variation of the clinoform rollover and shelf break depth and their respective distances to the coast. A detail of these variations can be found in Supplementary Table 10.21.

Supplementary Table 10.21. Dimensions and depths of the clinoforms and shelf within and outside the bedform field.

	Distance to shore of clinoform rollover (m)	**Depth of rollover (m)**	**Shelf width (m)**	**Shelf break (m)**
Western area	345	31	1910	-118
Bedform area	160	13	1915	-112
Eastern area	405	27	2455	-127

BEDFORMS OBLIQUE TO THE COASTLINE

A different type of bedforms was found (red squares in Figure 6.1 and Supplementary Figs. 10.52 and 10.53) mainly in the southwestern part of the shelf (Sector 1 in Fig. 6.18), where the slope is gentler (up to 3°) and the shelf is covered by coarser sediments. They are oriented obliquely to the coastline and in plan-view their crests appear relatively straight. They do not show as clear step-train paths, they are rather discontinuous and irregular. Their profiles are shown in Supplementary Fig. 10.54 and their characteristics are described in Supplementary Table 10.22. and can be compared with the measurements of perpendicular bedform fields in Fig. 10.55 A-G.

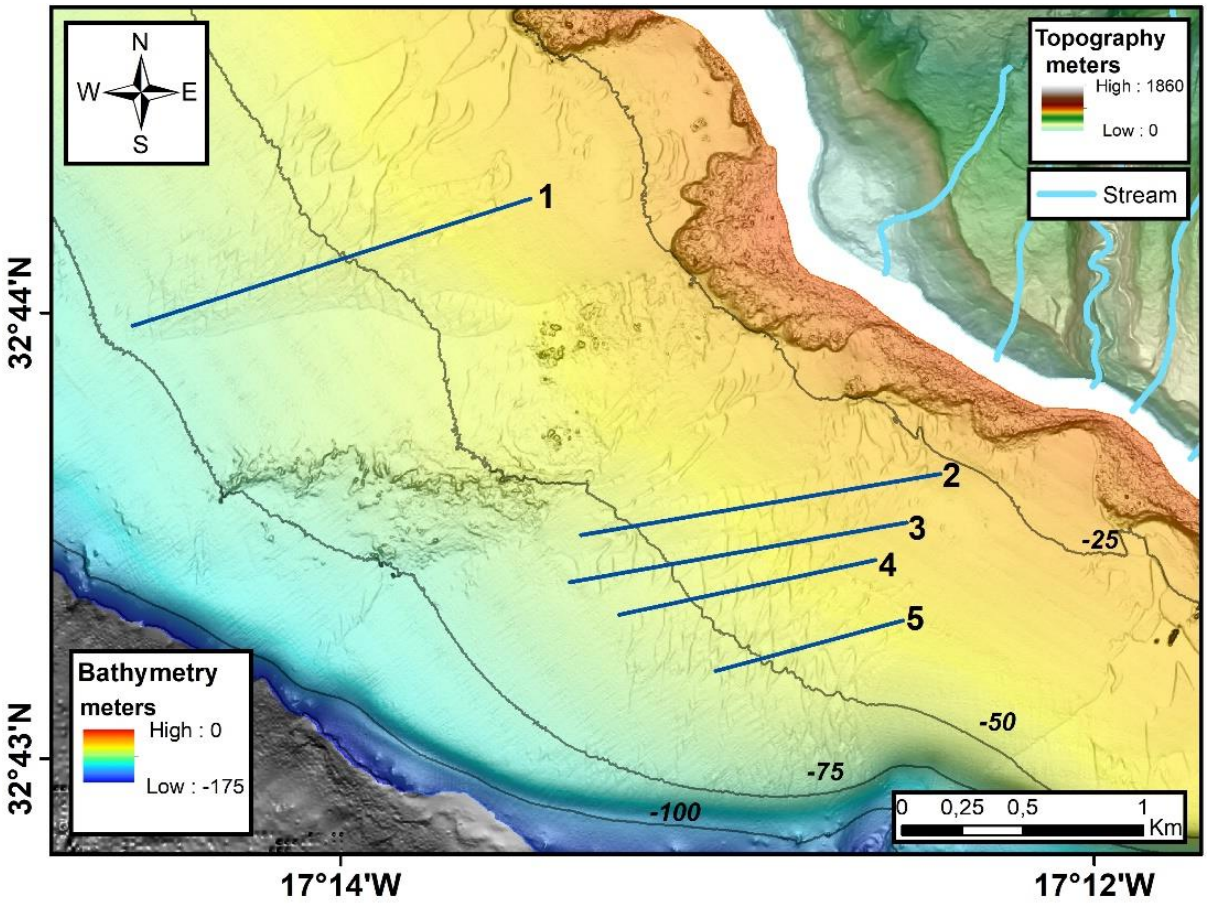

Supplementary Figure 10.52. Bedform field B (red square in Fig. 6.1). Blue lines represent the bathymetric profiles in Supplementary Fig. 10.54.

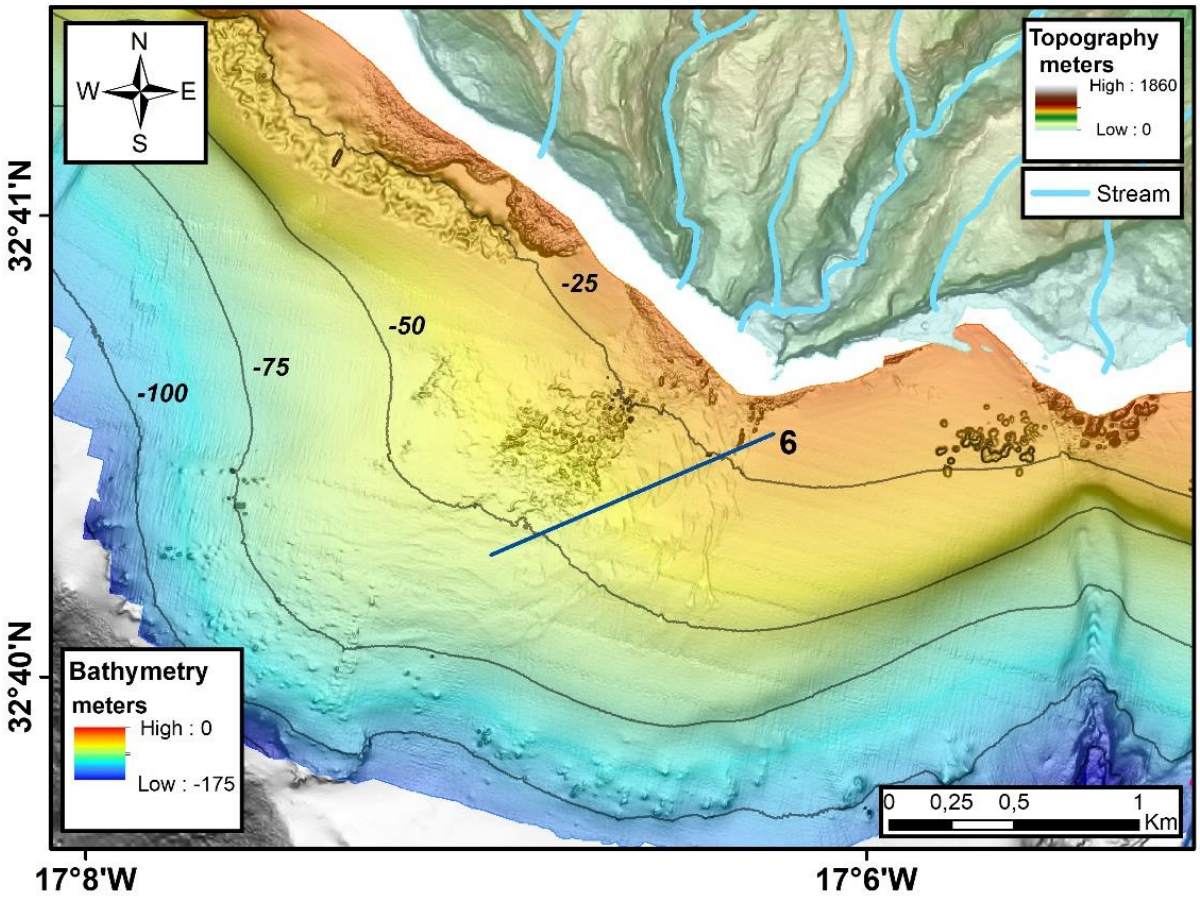

Supplementary Figure 10.53. Bedform field D (red square in Fig. 6.1). Blue lines represent the bathymetric profiles in Supplementary Fig. 10.54.

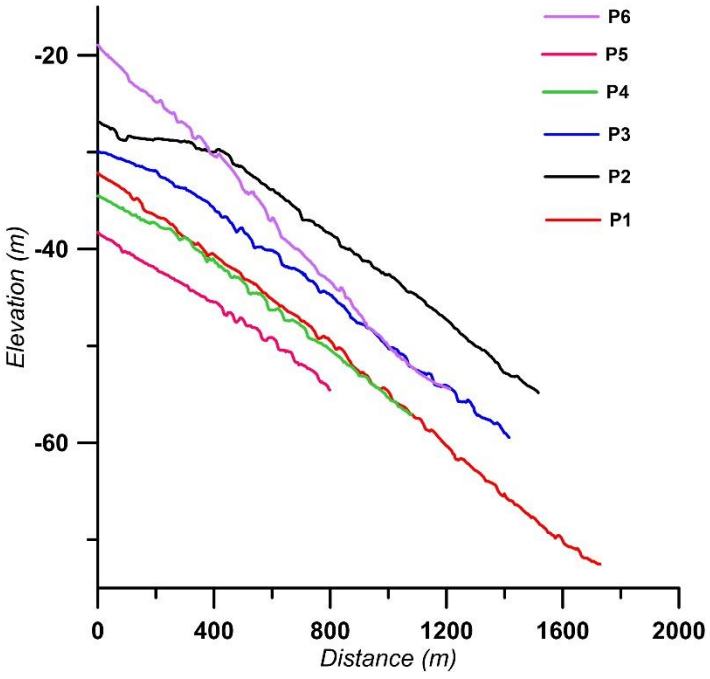

Supplementary Figure 10.54. Bathymetric profiles whose location are in Supplementary Figs 10.52 and 10.53.

Supplementary Table 10.22. Morphometry of the dunes observed on the southern shelf of Madeira Island according to the profiles.

	Wave height (min/max) (m)	Wavelength (min/max) (m)	Wave Crest depth (min/max) (m)	Stoss-side length (min/max) (m)	Stoss-side slope (min/max) (°)	Lee-side length (min/max) (m)	Lee-side slope (min/max) (°)
Profile 1	1.3/6.3	41/111	36/71	14/55	-0.26/0.54	10/58	2.36/6.35
Profile 2	2.3/4.7	40/68	29/41	16.4/24.6	-1.97/0.27	17.6/50	2.06/2.84
Profile 3	3.3/6.6	45/112	36/55	15.3/31.8	-1.69/0.42	20/72.4	1.95/5.67
Profile 4	2.5/7.6	35/80	37/53	19.2/39	-0.11/0.31	9.3/33.4	2.44/6.4
Profile 5	1.9/6.5	27/60	45/54	11.5/40.3	-2.4/3.7	9.7/24.1	3.1/6.47
Profile 6	1.9/4.8	30/92	24/36	10.4/29.3	-3.7/2.63	10.4/81.3	4.3/5.7

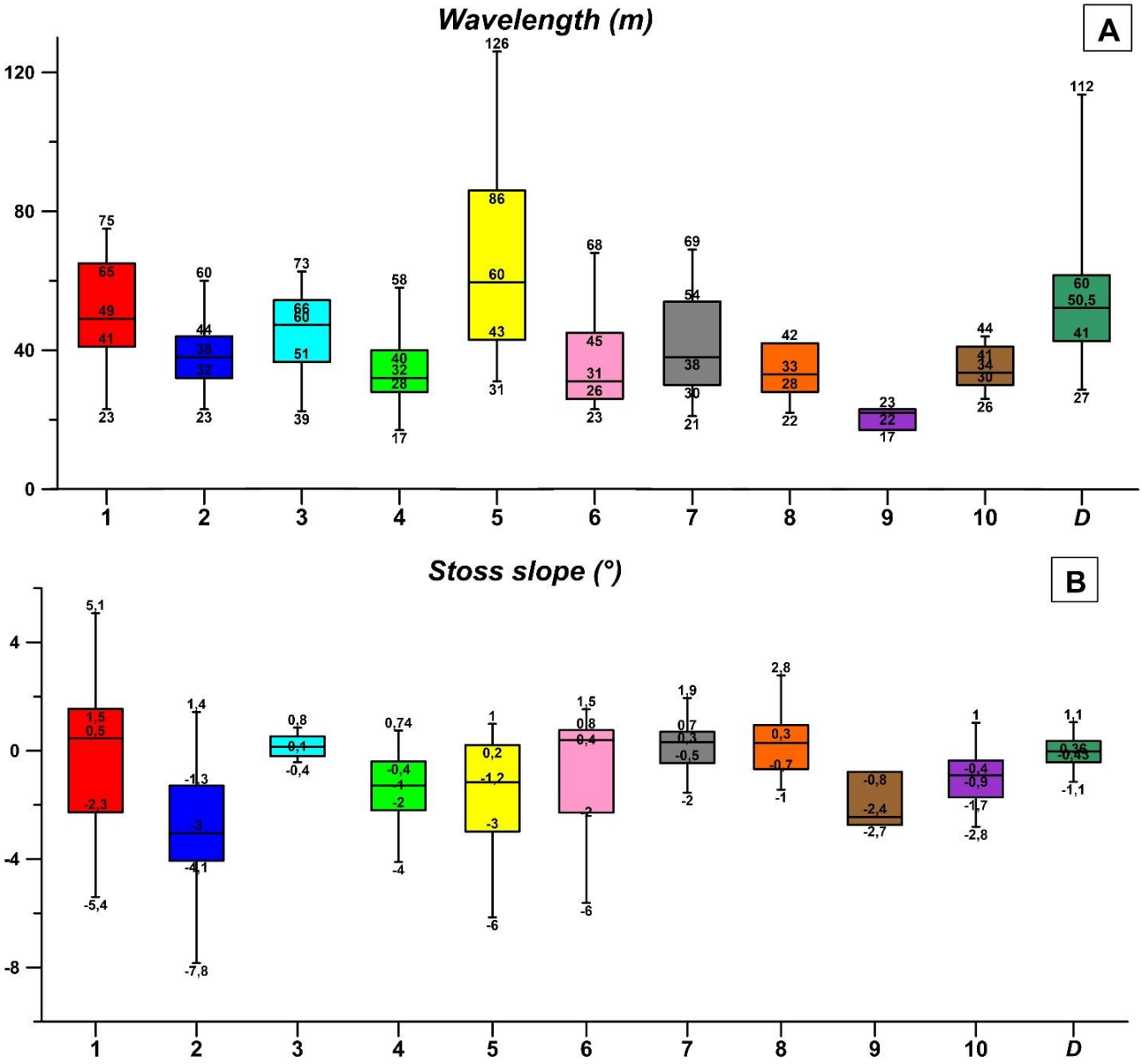

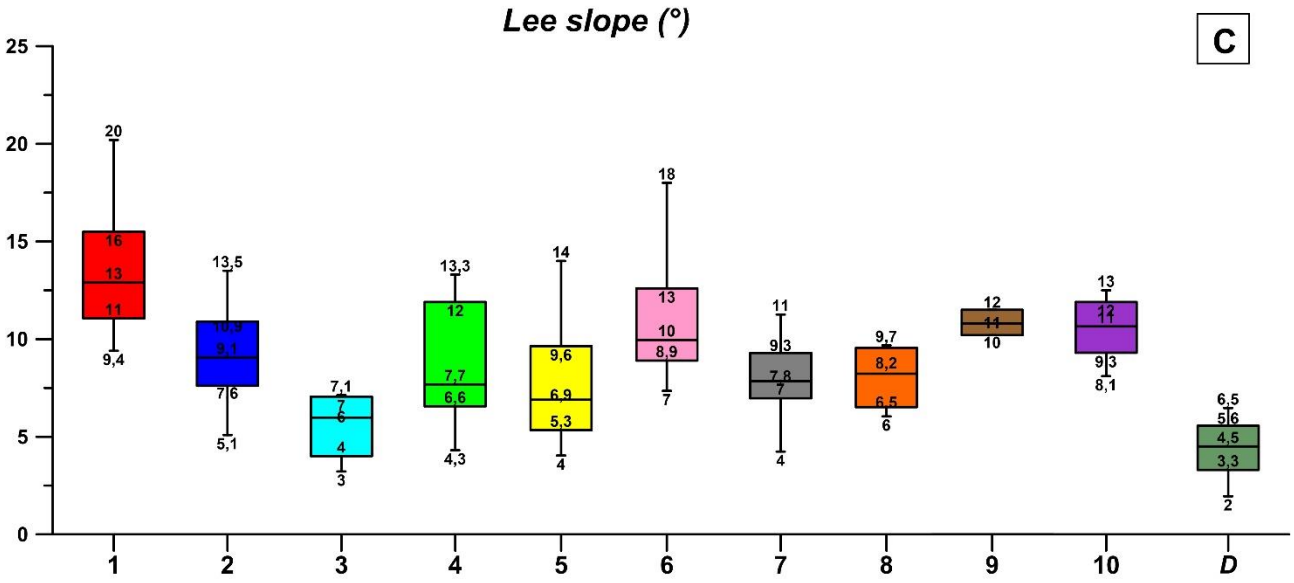
Lee slope (°)
C
25
20
15
10
5
0
1
2
3
4
5
6
7
8
9
10
D

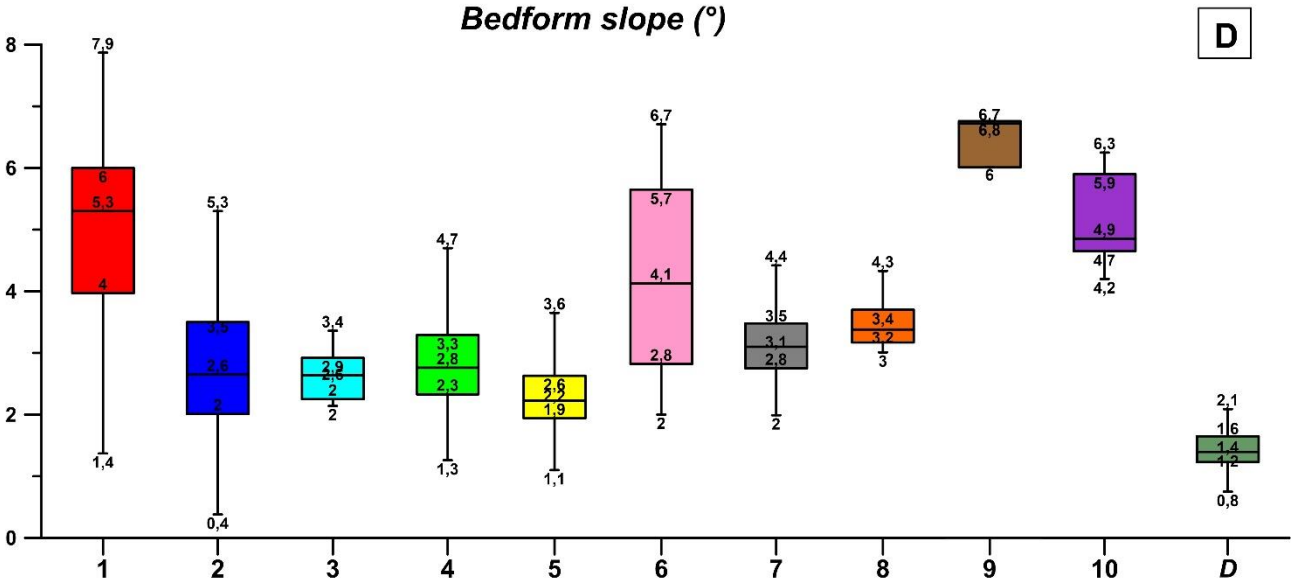
Bedform slope (°)
D
8
6
4
2
0
1
2
3
4
5
6
7
8
9
10
D

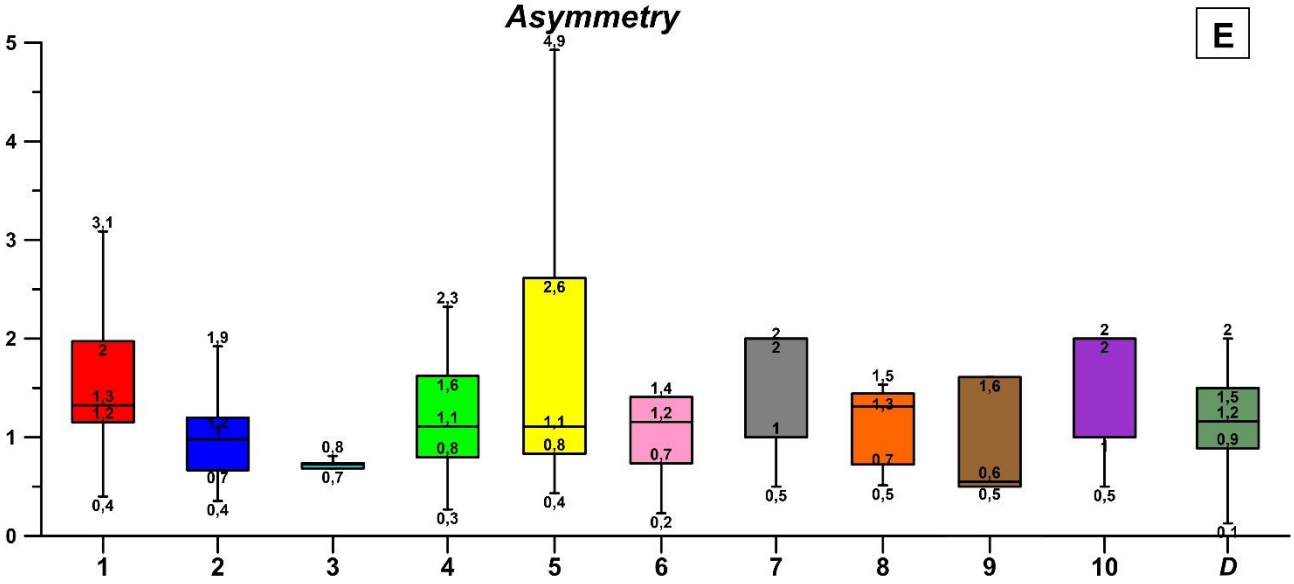
Asymmetry
E
5
4
3
2
1
0
1
2
3
4
5
6
7
8
9
10
D

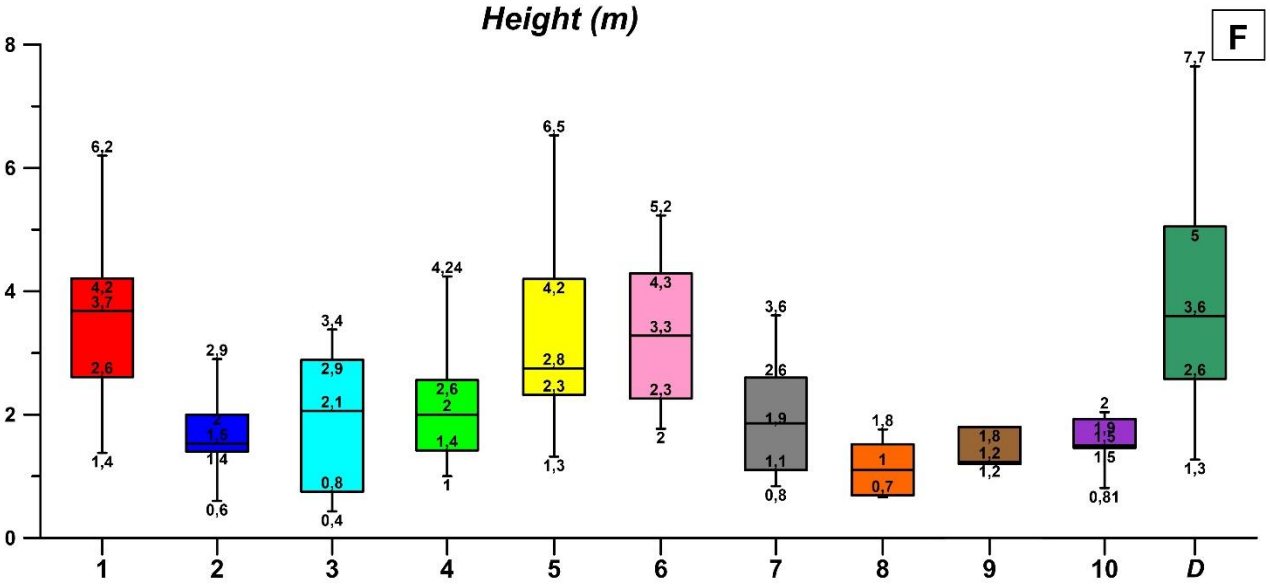

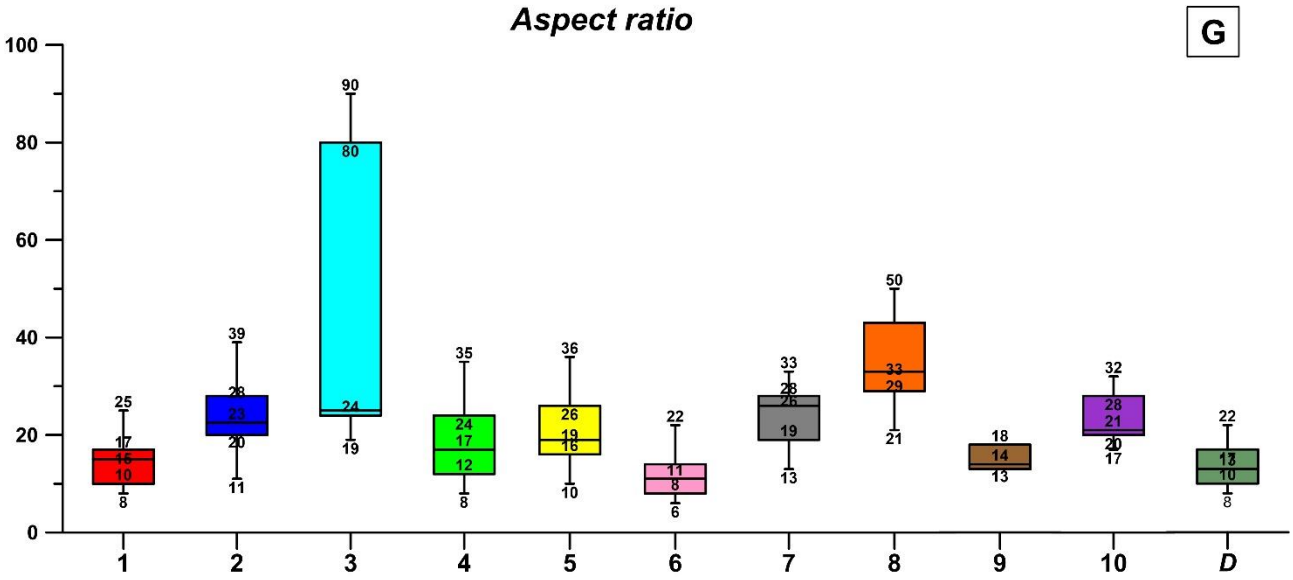

Supplementary Figure 10.55. A-F) Box plots of the main parameters (y-axis) measured for each bedform field (x-axis). D represents the bedforms oblique to the coastline.